AD 688924

THEORY OF COMBUSTION INSTABILITY IN LIQUID PROPELLANT ROCKET MOTORS

LUIGI CROCCO AND SIN-I CHENG

Published for and on behalf of
THE ADVISORY GROUP FOR
AERONAUTICAL RESEARCH AND DEVELOPMENT
NORTH ATLANTIC TREATY ORGANIZATION
by
BUTTERWORTHS SCIENTIFIC PUBLICATIONS
1956

DDC
JUN 20 1968

Best
Available
Copy

AGARDOGRAPH No. 8

THEORY OF COMBUSTION INSTABILITY IN LIQUID PROPELLANT ROCKET MOTORS

JUN 23 1969

This document has been approved for public release and sale; its distribution is unlimited.

BUTTERWORTHS PUBLICATIONS LTD.
88 KINGSWAY, LONDON, W.C.2

AFRICA: BUTTERWORTH & CO. (AFRICA) LTD.
DURBAN: 33/35 Beach Grove

AUSTRALIA: BUTTERWORTH & CO. (AUSTRALIA) LTD.
SYDNEY: 8 O'Connell Street
MELBOURNE: 430 Bourke Street
BRISBANE: 240 Queen Street

CANADA: BUTTERWORTH & CO. (CANADA) LTD.
TORONTO: 1367 Danforth Avenue

NEW ZEALAND: BUTTERWORTH & CO. (AUSTRALIA) LTD.
WELLINGTON: 49/51 Ballance Street
AUCKLAND: 35 High Street

Set in Monotype Baskerville type
Printed in Northern Ireland at The Universities Press, Belfast

FOREWORD

THE authors would like to express their appreciation for the encouragement, support and interest of the United States Air Force in making possible the preparation of this monograph as a national contribution to N.A.T.O.

The theoretical work mentioned here stems from a broader interest in the phenomena associated with combustion instability in liquid propellant rocket motors, which forms the basis for a research programme presently being carried out at Princeton University under the sponsorship of the Bureau of Aeronautics, United States Navy.

LUIGI CROCCO
SIN-I CHENG

CONTENTS

1

GENERAL CONSIDERATIONS

1.01. Statement of the Problem

Experimental observations show that the combustion in a rocket combustion chamber operating with liquid propellants is never perfectly smooth. Even when the introduction of the propellants through the injectors and the exhaust of the burnt gases through the nozzle are carefully designed, in order to obtain steady conditions, a certain amount of non-steadiness is always present, as is deduced from observation of the pressure recorded at any location in the chamber. Similar fluctuations of temperature, velocity, composition, etc., can also be assumed, even in the absence of direct indications. It is impossible to decide at present how much of this non-steadiness is due to pure fluid dynamic causes generating turbulence, and how much to the combustion processes themselves. What is certain is that an extremely turbulent condition is always present in the chamber, and is probably the cause for the intensity of the noise produced by the rocket operation, in accordance with theory[1]. The amplitude of the fluctuations is different for different motors and, in the same motor, for different operating conditions, When the fluctuations are small, the combustion is said to be smooth, and when they are large it is said to be rough; but these terms have no precise definition.

The results of combustion roughness on the operation of the rocket can be very different. In certain cases a considerable amount of roughness does not prevent successful operation and practical use of the rocket. In others very detrimental effects are produced, such as severe vibrations or interference with the controls and safety devices, mechanical failure of parts of the rocket or of the accessory systems, and finally, thermal failure (burn out) of some part of the internal rocket walls. It is the occurrence of these detrimental effects, and their importance in determining the life and the operating characteristics of a rocket system, that makes it necessary to gain some understanding of the underlying processes. A possible line of attack would be to describe in detail the phenomenological aspects of the question, trying to systematize the experimental information in order to derive general results. Leaving the detailed description following this inductive approach to another monograph of this series[2], we shall use a more deductive one. In other words, we shall make use of our present knowledge of the combustion process, even if only qualitative, with the following objectives:

(*a*) to establish a rational explanation for the existence of a detrimental and of a non-detrimental type of rough combustion

(*b*) to distinguish a number of mechanisms which may be responsible for the appearance of the detrimental type

(*c*) to give for some of these mechanisms plausible quantitative formulations

(*d*) to analyse in detail the results of the theoretical developments.

Item *a* of our programme is discussed briefly on a purely qualitative basis in Sections 1.02 to 1.05. Sections 1.06 to 1.10 deal with item *b* suggesting and

discussing qualitatively a few basic mechanisms without entering into any analytical development. In Section 1.11 a quantitative relationship is established as a working tool for the theoretical treatment of the different mechanisms (item *c*). The rest of the monograph is entirely devoted to the development of the theory and discussion of results (item *d*).

1.02. The Combustion Process

In order to be able to understand the reasons for the different behaviour of the combustion process in different cases it is necessary to discuss briefly how, in fact, combustion of one or two liquid propellants takes place. The process starts with the injection of the propellants, brought through an appropriate feeding system from the tanks to the injector, where a pressure excess exists with respect to the chamber pressure. The purpose of the injector is to make use of the pressure drop through the injection ports for the conditioning of the propellants for combustion. The requirements are different for different categories of propellants. In monopropellant systems the decomposition of the propellant is produced only by the contact with high temperature gases produced previously. It is therefore necessary to obtain:

(*1*) a large surface of contact between the liquid and the gases

(*2*) a convenient proportion between the mass of the propellant and the mass of the hot gases surrounding it

(*3*) a good renewal of the hot gases to activate surface exchanges.

Requirement *1* is satisfied through good atomization of the liquid, requirement *2* through proper dispersion of the droplets in the gaseous mass, and requirement *3* through positive recirculation of the hot gases in the atomization region.

In bipropellant systems a necessary prerequisite for any chemical reaction to take place is the mixing of the two propellants. Therefore one must obtain from the injection system:

(*4*) a fast, as uniform as possible, mixing between the two propellants.

The fulfilment of this requirement would be virtually sufficient for self-reacting propellants (hypergolic propellants or monopropellant and liquid catalyser). For non-hypergolic propellants, however, mixing is not a sufficient condition and combustion must again, as for the monopropellant case, be activated by exchanges with the hot gases; thus the injector has still to fulfil the requirements from *1* to *3* in addition to requirement *4*. The same is likely to be true for most of the systems using hypergolic propellants. Only during ignition do such systems generally rely on the reactivity of the propellants alone, and once ignition is obtained such systems operate substantially as other bipropellant systems, though in improved conditions. There are of course other important requirements of the injection system, but they have no direct connection with the combustion process.

If we follow an element of propellant (monopropellant case), or two elements of propellants destined to react together later (bipropellant case), from the moment of injection into the combustion chamber to the total conversion into the final products of combustion, the element will describe a more or less complicated path during which processes such as atomization, heating, vaporization, diffusion and turbulent mixing, and chemical reactions take place in an intricate way. The chemical reactions are generally important

only in the last stages, after the propellants have been properly conditioned. The evolution of the substance from the initial conditions of the propellants to the final conditions of the burnt gases is gradual. A quantitative description of the evolution would require a detailed knowledge of all the intermediate processes. This is impossible at present. However, an approximate description can be obtained, based on the consideration that the most important changes are produced by the chemical reactions and therefore only toward the end of the evolution. The well known exponential effect of temperature on the rates of reaction will tend to accentuate this effect in the

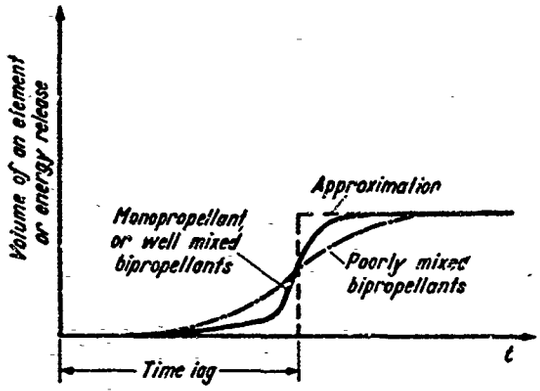

Figure 1. Schematic diagram of energy release or volume of an element versus time

monopropellant or in the well mixed bipropellant system, while the effect will be less sharp if mixing is still incomplete in the last stages of the evolution. Therefore if we were able to plot a certain representative quantity like energy release, or volume of the element, versus the time elapsed from the injection instant, the result would appear as shown by *Figure 1.*

1.03. Time Lag and Space Lag

The approximation to be taken is now evident. It consists of replacing the gradual evolution by a discontinuous process, in which the element does not produce any appreciable energy release or volume increase up to a certain time, whereupon it is suddenly transformed into the final products of reaction. In this way the impossible task of describing the combustion process through the quantitative knowledge of its intermediate history is made much simpler because the only quantity one needs to know for the timewise description of the combustion is the time elapsed between the injection and the sudden conversion into hot gases, that is the *time lag.*

If one is interested in the spacewise description of the combustion the time lag must be replaced by a space lag, a vectorial quantity indicating the location of the chamber where the sudden transformation of the element considered into hot gases takes place. Of course the space lag can be related to the time lag if the vectorial velocities of the elements are known during the time lag itself. It is clear, however, that the lack of indication about these velocities can be completely replaced by the independent knowledge of both time lag and space lag, the two quantities being, in principle, susceptible of

separate experimental determination. A very convenient consequence of the approximation introduced is that the propellant elements are present in the chamber either in the liquid form, with negligible volume and negligible contribution to the properties of the gases filling the chamber, or in the form of final products of complete combustion. It follows that the chamber can be considered to be filled only with burnt gases, through which liquid droplets are travelling without affecting the properties of the gases to any appreciable extent.

How closely this approximation represents the actual situation depends probably on the particular case under consideration. If in the case considered the propellants stay mainly in liquid form during most of the time lag, and vapours or other intermediate gaseous products have a very short lifetime and give place nearly immediately to the combustion products, then the approximation can be quite good. In the opposite case, when the propellants are vaporized early and remain in gaseous form during most of the time lag, the assumption that the gases present in the chamber are only the final product of combustion may introduce noticeable errors in the evaluation of the mean properties of the gases filling the chamber. Nevertheless, the fact that at present there is no way of predicting quantitatively the real process of evolution, makes it necessary to accept also in this case the approximate description of the process. Generally, the frequencies of longitudinal oscillations measured in efficiently operating rockets are below the so-called organ-pipe frequencies computed from the sound velocity in the burnt gases. This fact has been interpreted as a proof that the temperature of the gases decreases considerably, when going from the nozzle to the injector end. However, it will be shown in Chapter 3 that considerable departures from the organ-pipe frequencies toward lower values are produced by the simple presence of a de Laval nozzle. These departures may justify the observed decrease in frequency without having to accept a decrease in mean temperature of the gases in efficient rockets.

We are now able to describe quantitatively the whole process of combustion in a combustion chamber by specifying the proper time lag and the space lag of every element of propellant injected at any location of the injector. Generally these two quantities are different for different elements and they can be spread in a smaller or larger range; the case in which one or the other quantity has the same value for all elements must be considered only as an ideal limiting case. In agreement with the approximation we have just discussed, the combustion chamber is filled only with the final product of combustion and the presence of liquid propellants on their way from the injection point to the location corresponding to the space lag can be ignored except for the small correction of momentum exchanges as will be clear later. If we neglect this momentum exchange, the points where the sudden conversion of the propellants into combustion gases is effected, can be considered (in the aerodynamic sense) as sources of hot gases. It is clear that the flow properties in the combustion chamber are determined by the distribution and intensity of these sources. If we assumed, for instance, that the injection rates were independent of time, and that time and space lags were constant too, the resulting intensity of the sources would also be independent of time. This would result in a steady flow in the combustion chamber and

among other quantities, the local pressure would be perfectly constant. But we have already mentioned the fact that such a perfectly smooth combustion does not exist in practice. Therefore one of the aforesaid assumptions must be wrong. That is, the injection rate or the time lag or the space lag (or more than one quantity at one time) must be non-steady.

1.04. Rough Combustion and Unstable Combustion

In fact, the above conclusion is not too surprising. Suppose for a moment the injection rates are constant, a condition which can ideally be obtained by appropriate design of the feeding and injection systems. The physico-chemical processes taking place during the time lag proceed at rates which are more or less affected by such factors as pressure, temperature of the gases and of the liquids, relative velocities and so on. If these factors are changed, the rates change too and the time lag with them, faster rates resulting in shorter time lags. If the factors undergo fluctuations around a mean value, the time lag for each propellant element is also a fluctuating quantity. When, at a certain location, the time lag is, for instance, increasing, the result is a dilution in time of the combustion process and hence a decreased burning rate. On the contrary the burning rate is increased when the time lag is decreasing. Therefore fluctuations of the rate-affecting factors result in fluctuations of the burning rates, or in our simplified combustion model, in fluctuations of the strength of the sources of hot gases, even with constant injection rates. It is evident now that if we relieve this last restriction, the variations of the injection rate will introduce additional fluctuations in the burning rates or the strength of the sources.

On the other hand, the system consisting of the gases in the chamber, the propellant in the feeding system, and the mechanical parts of the chamber and of the feeding system, is capable of non-steady effects even in the absence of non-steady effects in the process of combustion. Processes such as the oscillations of the gases in the chamber, the liquids in the feeding system, or the mechanical parts, can always be produced if properly excited. These processes are generally distinguished by a characteristic time which corresponds to the period, if the process is periodic, and to some kind of relaxation time if the process is aperiodic.

Now two conditions are possible:

(*1*) None of these processes is excited; the fluctuations in the chamber are maintained by some internal effect related to the fluid dynamics of the system, such as, for instance, some kind of flow instability of boundary layers or shear flows, producing fluctuations of the same general character as in ordinary turbulent flows. In this eventuality, the correlation between fluctuations at two different locations or instants vanishes as soon as the space or time interval is not too small. Practically, the fluctuations at one point or instant are independent of those at different points or instants and therefore have a random character. As a result the integrated effect of the fluctuations on a finite extension of surface or time has a tendency to vanish and therefore no additional mechanical or thermal load is to be expected on the rocket and on the accessory systems, even when the fluctuations have considerable amplitudes. This case corresponds therefore to the non-detrimental type of rough combustion.

(2) One of the non-steady processes of the system is excited. As a result of the excitation of this process, that can be called the *coordinating process*, organized oscillations of some of the rate-affecting factors or of the injection rates are present, which in turn result in organized oscillations of the burning rates (or the source strengths). These provide the necessary exciting force for the maintenance of the coordinating process itself. It is to be observed that the effect produced on the burning rate by the instantaneous departure of one of the physical factors from its mean value is not felt immediately, but is displaced in time and space due to the existence of the time and the space lags. The behaviour of such a system must present analogies to the behaviour of the closed loop systems with time delay considered in servo control treatment. We know that these systems can be stable or unstable depending on the specific conditions of the case under consideration. The fundamental character of an unstable system is such that supposing initially the system is running smoothly (which is ideally possible from a static point of view), any small disturbance applied, say, to the pressure distribution in the chamber, has a tendency to amplify. Actually, its amplitude would grow without limits if non-linear effects were not present to limit the amplitude to a finite value. Therefore a necessary condition for the excitement and maintenance of the coordinating process is the instability of the system and it is proper to attribute to case *2* the name of *unstable combustion*. On the other hand, the condition of case *1* can be called stable no matter how large the random fluctuations of the physical factors are, because applied disturbances have a tendency to die without being able to excite any coordinating process. It must be observed that the causes that produce the random fluctuations are present also in unstable conditions. Therefore in unstable combustion random fluctuations are superposed on the oscillations corresponding to the coordinating process. Thus the fundamental difference between unstable and rough (but stable) combustion resides in the presence of these organized oscillations, and in the fact that, because of the organizing effect of the coordinating process, a well defined correlation is established between the fluctuations at two different points or instants, no matter how large the space or time interval is. When these organized oscillations are present the integrated effect on a finite surface or period can be different from zero with the result that increases in pressure forces, mechanical vibration levels, and thermal loads are to be expected. Thus we reach the important conclusion that the detrimental type of rough combustion can be identified with unstable combustion.

In general, because of the self-amplifying character of small oscillations in unstable combustion, the amplitude of the pressure fluctuations is expected to be larger than those in cases of stable rough combustion. However, this is not necessarily true, and one can very well conceive an unstable condition where strong non-linear effects limit the amplitude at a lower level than that of other cases with stable but very rough combustion. It is therefore clear that the level of pressure fluctuations is not an objective index for the discrimination between stable and unstable combustion, and therefore between safe and dangerous conditions. A more objective basis is found in the presence of periodic oscillations with well defined frequencies, or, in the case when the roughness of combustion makes it difficult to

detect such periodic oscillations if their amplitude is not very large, in the determination of the correlation between pressures measured at different points.

1.05. Non-linear Effects

In the preceding discussion we have characterized the unstable combustion by the property that small disturbances are self-amplifying. This is what, in analogy to other unstable systems, can be called *linear instability*, because for very small disturbances all the effects are proportional to their causes and the equations describing the system are of a linear type. However, one must observe that if combustion is linearly unstable, small initial disturbances are soon amplified to such an extent that important non-linear effects may appear. Among such effects we mention for example the fact that certain rates depend exponentially on temperature with the consequence that the mean rate is larger than the rate corresponding to the mean temperature. Another important non-linear effect is the generation of shock waves from the coalescence of compression waves in the combustion chamber. An important result of the presence of non-linear effects is that a system, stable against small disturbances, may become unstable when the amplitude of the disturbance is increased above a certain limit. Below this limit any disturbance would die out with time; but above this limit self-maintained oscillations are produced. This is what, in analogy to other systems, is called *non-linear instability*. Its possibility is interesting for rocket operation because if the non-linear limit is not too low it is possible to avoid this kind of combustion instability just through careful protection against functional or accidental disturbances.

One possible mechanism for non-linear instability can be conceived to consist of a direct action of shock waves on the rates of chemical reactions. If it is assumed, in accordance with some experimental indications[3,4], that a shock wave produces an effect, on chemical processes, larger than the combined effects of the pressure and temperature increases through the shock wave itself, then the interaction between fluctuations in the chamber and burning rates is emphasized when shock waves appear. The result of this assumption is that a system presenting stable combustion for small disturbances may become unstable when the disturbance is large enough to generate shock waves.

Though it is recognized that non-linear effects can be important, the fact that their physical essence is still obscure and that their analytical treatment involves great difficulties makes it necessary for the moment to discount non-linearities in developing a theory. Therefore in the following we shall consider only linear effects, which can be treated through the method of small perturbations. This means that the treatment will be strictly applicable only to cases where the effects of instability are not so strong as to produce large amplitude oscillations. In other words, the theory can be applied mainly to conditions of incipient instability and therefore to the determination of stability limits. As an *a posteriori* justification we observe that linear treatment actually predicts the possibility of unstable combustion in the observed ranges of frequency and that there seems to be a general qualitative agreement between the theoretical predictions on stability limits and many experimental observations.

1.06. Mechanisms of Unstable Combustion: Chugging

In order to illustrate the considerations of Section 1.05 and to formulate a quantitative treatment in a few representative cases, it is necessary to specify closer plausible mechanisms for the production of self-maintained oscillations in a rocket. Let us consider a rocket in steady state operation. By steady state we do not indicate here the absence of any fluctuations in the physical quantities, but merely the steadiness of the average quantities; and in effect we know from the discussion of the last sections that stable operation with steady values of the average quantities is possible even with rough combustion because the integrated effect of the random fluctuations on large areas or volumes is zero. Suppose now that we produce artificially a sudden increase of pressure in the combustion chamber, corresponding to an excess of gas content of the chamber with respect to the steady state content. Suppose also that the feeding system is designed in such a way as to be insensitive to chamber pressure variations and that the time lag is unaffected by pressure. As a particular case, the time lag could be negligibly small. This means that both the injection rate and the burning rate will keep the same value they had before the application of the disturbance. It is clear that the balance between burning rate and exhaust rate is disturbed, the latter now being too large. The excess of gas content must therefore decrease with time and the pressure excess with it, until eventually they both vanish and the steady state condition is re-established. The actual process of adjustment is complicated by the presence of waves travelling back and forth in the combustion chamber, which introduce non-uniformities in pressure and other physical quantities. However, for ordinary rockets, with the exception of the extreme case of a throatless motor, the change in chamber pressure during the total time of propagation back and forth of a wave is contained in narrow limits. As a consequence, the amount of non-uniformity of the physical quantities at any given instant is small, and one obtains a sufficiently accurate description of the process by neglecting the propagation time of the waves and assuming uniform conditions in the chamber. The problem can be solved simply, and results in an exponential decay of the disturbance with time, distinguished by a characteristic time constant or chamber relaxation time. For conventional systems the chamber relaxation time is generally between one thousandth and one hundredth of a second, the wave propagation time being generally several times smaller.

Let us next consider, as a second example, a simple monopropellant rocket with feeding system consisting of a constant pressure tank, an injector, and a connecting pipe. Suppose, for the sake of simplicity, that at every instant the exhaust rate is exactly equal to the burning rate and to the injection rate (these assumptions being correct only for zero time lag and zero chamber relaxation time). In steady state the pressure drop from the tank to the chamber must be sufficient to provide the proper injection rate. Suppose now a sudden increase of the flow in the feeding system is produced artificially and the rates of injection, burning and exhaust also increase instantaneously as postulated. The chamber pressure therefore also undergoes an instantaneous increase and the pressure drop a decrease, which is not compatible with the increased injection rate. Thus when the system is

left to itself, the flow rate and the chamber pressure must gradually decrease until eventually the steady state conditions are restored. Again the process is complicated by the presence of waves moving back and forth in the propellant lines, which results in non-uniform flow rates along the lines. However, if the variation of the flow rate during the total time for propagation of a wave back and forth in the line is relatively small, the mean process of adjustment is described with sufficient accuracy by neglecting the wave motion and assuming that the flow rate at every instant is uniform at all sections, so that the propellant moves as a single incompressible slug. With this approximation, sufficiently correct in many cases, the mean process is again found to be an exponential decay of the flow rate excess (at least for perturbations small enough to preserve the linearity), distinguished by a characteristic time constant, or *line relaxation time*.

For conventional feeding systems the line relaxation time is generally of the same order as the chamber relaxation time. However, it can vary independently of the latter and its magnitude can lie in a wider range. Of course the assumptions of these two examples are not very realistic. However, the results give an idea of the behaviour of more complicated systems in the ideal case of vanishing time lag.

In all cases an artificially applied disturbance must decay with time, aperiodically or periodically. An exception may be provided by servo-controlled feeding systems; in this case the flow system may be destabilized by the presence of the servo control, and the amplification of small disturbances may be the result. With the exclusion of this case, all rocket systems would be stable if the time lags were zero. Despite the fact that the decay of disturbance is not in general given by a simple exponential factor, it is possible to derive for this ideal case an approximate rate of decay or relaxation time. This is of the same order as the larger of the previously defined chamber relaxation and line relaxation times, and therefore much longer than the propagation time of waves in the chamber, and often also of the wave propagation time in the propellant lines. Thus, if the condition is also satisfied in the general case, the process of decay can be analysed neglecting the two types of wave motion. The order of magnitude of the relaxation time for conventional systems is between a few milliseconds and a few hundredths of a second, while the wave propagation time in the chamber is generally of the order of one millisecond or less. The wave propagation time in the lines can vary in a wider range. It is also difficult to define a wave propagation time in complicated feeding systems because of the heterogeneity of the lines. Generally it is of the order of a few milliseconds.

What is the result of introducing a finite combustion time lag? The answer is the same as for other types of systems: the time lag has a destabilizing effect. Thus if one increases the magnitude of the time lag, a system with aperiodic decay of disturbances will become oscillatory and damped; and eventually the damping rate can change its sign and the system can become unstable. That this final condition is possible can be shown on a purely qualitative basis through the following reasoning. Suppose a system with a constant pressure supply is working in oscillatory conditions, so that the chamber pressure oscillates around the mean value.

As a result the pressure drop also oscillates, going through a minimum when the chamber pressure is maximum and vice versa. The injection rate will also be affected with a certain delay, of the order of the line relaxation time, and the burning rate will follow the injection rate with a delay equal to the time lag, supposed, for simplicity, to be the same for all propellant elements. Thus the time phase between the minimum of the burning rate and the maximum of the chamber pressure is approximately equal to the sum of the line relaxation time and the combustion time lag.

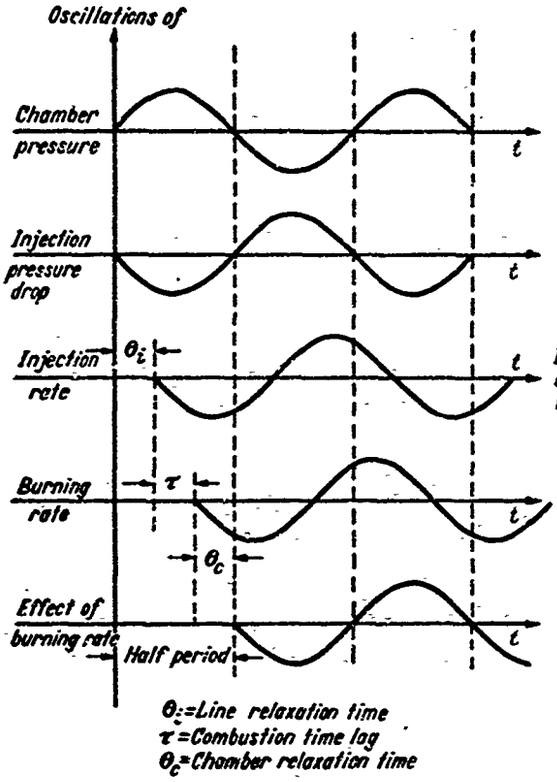

Figure 2. Schematic diagram of the various oscillating quantities versus time with constant time lag

On the other hand, the effect of burning rate oscillations is felt in the chamber with a delay of the order of the chamber relaxation time. Therefore if the sum of the two relaxation times and the combustion time lag is approximately equal to a half period of oscillation, the decreased contribution of combustion to the chamber pressure resulting from a maximum in the chamber pressure will be felt when the chamber pressure goes through a minimum and vice versa. The conditions for self-amplification of the oscillations are thus created. *Figure 2* shows schematically the relative situation of the oscillations of the various quantities in accordance with the foregoing discussion.

From this approximate consideration, not only is an unstable situation seen to be possible, but also an approximate condition for instability is obtained. This approximate condition of instability is that the sum of

the relaxation time of the system plus the combustion time lag must be of the order of half a period of oscillation. We shall see in Chapter 2 that a more accurate quantitative expression of this *time condition* is essential in the theory of unstable combustion.

We have now demonstrated the first mechanism for unstable combustion, in which the coordinating process consists of the relaxation process of the system, through oscillations of the injection rate and therefore of the burning rate. This mechanism is not only practically important because it occurs frequently, but is also historically important because it was the first to be recognized as possible in 1942 by von Kármán and his group, and also the first to be subject to analytical treatment[5–7]. The corresponding range of frequencies can be estimated from the time condition. If the time lag is small, compared with the system relaxation time, the system is stable. Therefore, in order to have unstable combustion, the time lag must be at least of the same order as the system relaxation time. In which case, from the time condition, we see that the period of the oscillation must be around four times the time lag; and both are of the order of the relaxation time. If, on the other hand, the relaxation time is small compared with the time lag, the period of oscillation is approximately double the time lag and both are larger than the relaxation time. Supposing that the time lag is around 5 msec (which gives the correct order of magnitude), the resulting frequencies are of the order of 50–100 c/s. Combustion instability with frequencies of this order is generally called, in the language of rocket engineering, chugging, or low frequency instability.

1.07. Another Mechanism for Chugging

An alternative mechanism for the production of chugging[8], independent of the injection process, is based on the fact, already discussed in Section 1.04, that the time lag under oscillating conditions is also an oscillating quantity. Suppose that the essential factors affecting the rates of the processes during the time lag are the pressure and the temperature, and that the temperature oscillations are correlated with the pressure oscillations. Since it is certain that in steady state an increase in pressure produces a decrease in time lag, the same will be true for non-steady conditions. That is, the time lag is shorter than its mean value when the pressure (averaged during the time lag itself) is above its mean value, and vice versa. The way of averaging the pressures during the time lag will be discussed later; but on purely qualitative grounds, we can say that if the pressure is oscillating, the time lag goes through a minimum when the pressure is around a maximum during the time lag and vice versa. This is illustrated in *Figure 3*, where, again, the same time lag is assumed for all propellant elements. If the injection rate is constant, and the time lag is close to a minimum or a maximum, the conditions will be close to those obtained for constant time lag, and therefore the departure of the burning rate from its mean value will be zero. On the other hand, if the time lag is increasing or decreasing, there is a dilution or concentration of combustion. Therefore the burning rate goes through a maximum when the rate of decrease of the time lag is a maximum, and through a minimum when the rate of increase is a maximum. Thus the resulting burning rate oscillations must lag a quarter period behind the

time lag oscillations, as shown in *Figure 3.* Finally the effect produced on the chamber pressure by the oscillations of the burning rate is felt with a delay of the order of the chamber relaxation time. If this effect is in phase with the chamber pressure oscillations, as in *Figure 3*, the most favourable conditions for self-amplification are created. Again, the time condition can be expressed in a similar way to the one discussed before, and if the time lag is given the same value of a few milliseconds, the resulting range of frequencies is the same as before.

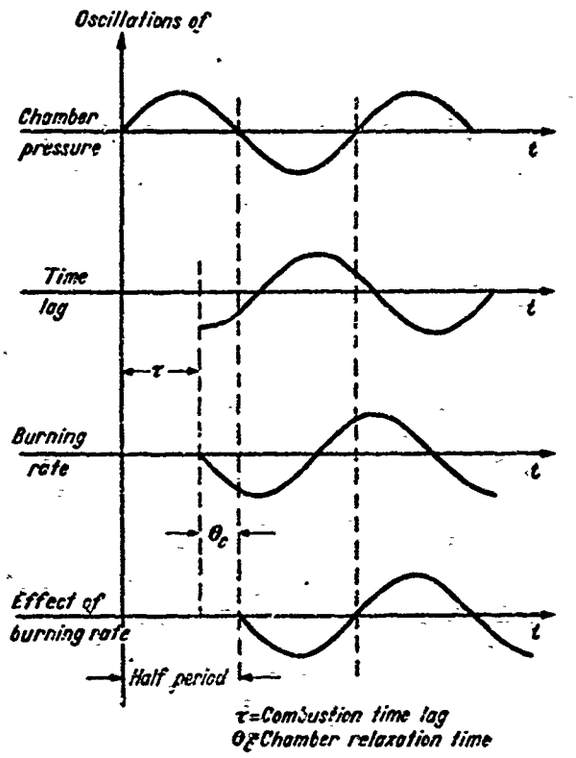

Figure 3. Schematic diagram of the various oscillating quantities versus time with variable time lag

We consider that chugging can be produced independently of the feeding system characteristics. The coordinating process for this type of instability, that has been called *intrinsic instability*, resides in the chamber relaxation process through the action of the oscillations of the physical factors on the burning rate. The mechanisms described thus far, for the production of instability, are distinct; however, since they are characterized by comparable frequency conditions they can also be present simultaneously, each one reinforcing the other. It is to be expected, for instance, that a chamber intrinsically unstable cannot be stabilized by the presence of a conventional feeding system. However, through the appropriate use of servo controls in the feeding system, one can think of producing stabilizing effects, a possibility suggested by H. S. Tsien[9]. All these questions will be subjected to analysis in the following chapter, where the instability limits resulting from both types of coordinating processes are determined, and Tsien's idea

of servo stabilization is shown possible. It must, however, be observed that in order to provide an effective control of this type, mechanical servo controls must be made to work in the range of frequencies characterizing chugging, that is, with mechanical time lags of the order of one hundredth of a second at most, much shorter than ordinary mechanical lags, which are around one tenth of a second. F. E. MARBLE[10] has suggested that servo stabilization can be obtained with a frequency of the servo control equal to a subharmonic of the unstable frequency.

Of course, as we have already noticed, servo controls can be destabilizing as well as stabilizing. The corresponding range of frequency for ordinary servo controls, with time lags around one tenth of a second, results in oscillations of frequencies below 10 c/s, and therefore is likely to be well distinct from chugging, and practically unaffected by the combustion phenomenon. For this reason, we think that this type of instability must be considered separately from chugging.

The same practical independence between the instabilities originated by the two types of coordinating processes, discussed in this and in the preceding section, is to be expected in the following case. We have thus far supposed that the time lags responsible for the two types are of the same magnitude. However, in Section 1.11 we shall discuss the possibility that only one part of the total lag is dependent on the physical factors in the chamber. The remaining portion of the time lag is then practically unaffected by changes of the physical factors. If this possibility is accepted, then considering again the case of intrinsic stability (without variations of the injection rate) we see immediately that the portion of the time lag which is unaffected by changing conditions has no effect on the stability; and that only the variable part of the time lag is important. Therefore the period of the oscillations for intrinsic instability can be much smaller than that for a feeding system type of instability. If the magnitudes are sufficiently different from each other (as for instance if the variable part of the time lag were of one or two thousandths compared with a total time lag of five thousandths) then the interaction between the two processes can become practically negligible. At the same time the frequency of intrinsic instability would increase, and become closer to the frequency characteristic of wave motion in the lines and in the chamber. The assumption of neglecting wave motion effects becomes more questionable. As a matter of fact above a certain frequency the wave motion can become essential, as will be discussed in the next sections.

For this reason, and with the purpose of avoiding too complicated computations we have confined the analytical treatment of Chapter 2 to the case when all of the time lag is affected by the physical factors. The effects of the coordinating process discussed in this section and its interaction with the feeding system in exciting instability are magnified by this assumption. The analytical results must therefore be considered only as representative of this limiting case.

1.08. MECHANISMS OF UNSTABLE COMBUSTION: SCREAMING

Hitherto, in discussing low frequency instability we have never specified the location of the chamber where particular elements of propellant burn. Our discussion has only dealt with the time lags, but not with the space

lags. In other words, for the analysis of chugging it is not necessary to know the source distribution in the chamber, but only the integrated value of all sources. This simplification is a direct consequence of the assumption that the wave propagation time in the chamber is negligible, so that the effect of the burning taking place at a given location is immediately transmitted throughout the chamber no matter where it happens. This is the reason why the only condition given for the appearance of instability is a time condition.

It is evident that this simplification is no longer possible when the wave propagation time cannot be neglected with respect to the period of the oscillations. In this case, contrary to the assumption of Sections 1.06 and 1.07, the local variation of physical factors during the wave propagation time can be large, with the result that non-uniformities of pressure, temperature, etc. are present at fixed instants in the chamber. As a consequence of the non-uniformity of the rate-affecting factors, the effect of their variation on the rates of burning (and on the source strengths) depends on the location in the chamber where the propellants were when the rate began to be affected and the location where combustion takes place. It is therefore necessary to know, in the high frequency case, the spatial distribution of combustion.

Let us consider a definite location in the chamber and the propellants burning at this location in a system with fixed injection rates. And for simplicity, let us suppose that the propellants have been at this location during all of the time lag instead of moving. Then we see that we have, locally, the same situation we have discussed for the whole chamber in the case of intrinsic instability. Thus if a pressure oscillation with a definite frequency is present at the location considered, oscillations in the burning rate are produced. With a simple construction like the one of *Figure 3*, it is immediately found that if the time lag is very short compared with the period, the oscillations of the burning rate are in quadrature with those of the pressure and therefore the system is stable. But if the time lag (which is supposed to be the same for all propellant elements) is equal to a half period, and the effects of pressure on the rate of the processes are uniformly distributed during the time lag, then the two oscillations are in phase, so that the optimum conditions for self-amplification and instability are created.

Thus far the frequency of the oscillations has been taken arbitrarily. However, it is clear that the effect of the establishment of the self-amplification conditions is maximum if the chamber is close to resonant conditions, that is, if the frequency is close to the frequency of one of the natural modes of oscillation of the gases in the chamber considered without effects of combustion. The time condition for this case is therefore that the time lag must be close to the half period of one of the natural modes. Naturally, as in the case of intrinsic instability, if only one part of the time lag is affected by variation of the physical factors, only that part of the time lag must satisfy this time condition. The constant part of the time lag does not influence the phenomenon, because we have assumed here that the rate of injection is unaffected by pressure oscillations. However, the same result must be true in the more general case of a feeding system sensitive to pressure

variations, provided the frequency is sufficiently large so that the period is much shorter than the line relaxation time, and provided that the wave motion is not excited in the propellant lines. (We shall return to the last question in Section 1.10.) In fact, in both cases, the injection rates are practically unaffected by pressure oscillations, and the time condition remains approximately the same, that is, the time lag must be close to a half period. This condition can be made more general when we consider the possibility that more than one period is contained in the duration of the time lag. From a simple graphical construction like the one of *Figure 3*, one finds that, supposing again for simplicity that the rates are affected uniformly for the duration of the time lag (more exactly for the variable part of the time lag), the pressure oscillation is in phase with the burning rate oscillation if the time lag is 3, 5, 7 etc. times the half period. Therefore a more general statement of the time condition is that the time lag must be an odd multiple of the half period of one of the natural modes.

A brief qualitative discussion about the natural modes is necessary here. As in Section 1.03 the chamber can be supposed approximately to be filled with products of complete combustion, and the presence of unburnt propellants can be disregarded in first approximation. However, even with this simple assumption, the gas is not in the same condition as in a closed chamber without outflow, and therefore the characteristics of the natural modes cannot be the same as in the corresponding problem of acoustics. The difference is twofold. First, there is an average flow of the gases superposed on the oscillations; second, and more important, the gases are discharged from the chamber through a de Laval nozzle. The consequences of the first difference are not too important, provided the maximum flow Mach number in the chamber is sufficiently below unity, a condition generally satisfied in rocket motors (with the exception of the throatless motor). However, the presence of a sonic nozzle may have considerable effects on the behaviour of the chamber if the frequencies are high. In effect it can be shown quantitatively (Appendix B) and understood qualitatively that if the frequency of the oscillation is very low, then the quasi-steady flow through the nozzle follows approximately the laws of steady flow so that, for instance, the Mach number at the nozzle entrance stays constant (being determined by the area ratio of the nozzle).

In these conditions the nozzle can be replaced by the condition of constant Mach number at its entrance, and again for low subsonic values of the Mach number the behaviour of the chamber does not differ substantially from the acoustic case. These conditions are approximately satisfied in the lower part of the range of frequencies characterizing chugging. But already in the higher part considerable departures can be obtained. And since the departure increases with increasing frequency, the acoustical approximation, for the frequencies proper of the natural modes, becomes unreliable. In other words, the propagation of waves along the nozzle and their reflection in the subsonic part modify the reaction of the nozzle to oscillating conditions by changing the phase between pressure and velocity oscillation, with the result that work is necessary to maintain the oscillations, even if the dissipative damping forces are negligible. Therefore, due to the outflow

of gases, even in the absence of damping forces, a continuous supply of work is necessary to maintain the oscillations, while in the corresponding acoustical case no energy is needed. Despite this essential difference, however, the nature and frequencies of the natural modes are not substantially affected, so that we can make use of the predictions of acoustical theory in order to complete the picture. This can be done very easily for cylindrical chambers (which is the most common case) where longitudinal and transverse (radial and angular) modes can be distinguished, the former, with gas properties uniform on each circular section of the cylinder, and the latter, uniform on each line parallel to the axis. Also, combinations of longitudinal and transverse modes are possible; actually they are particularly important in a rocket chamber, since a purely transverse mode cannot be generated, due to the presence of the nozzle and to the backward reflection of longitudinal waves when a transverse wave is present. This effect also constitutes a difference from the purely acoustical case in a closed cylindrical chamber terminated by plane walls.

A general feature of all modes, purely longitudinal or combined, is the presence of nodal surfaces on which the pressure does not oscillate. In the case of the rockets, these nodal surfaces take a particular importance, because it is clear that if the combustion processes (or the sources) are concentrated in the vicinity of a nodal surface, then the corresponding mode cannot become unstable because it cannot generate the amount of work necessary to maintain the oscillation. On the contrary, the larger the fraction of the combustion concentrated in the vicinity of what we may call the antinodal regions (where the amplitude of pressure oscillations is large), the larger will be the variations of the burning rates in these regions and that of the amount of work generated, and therefore the larger the tendency toward instability. It is evident, therefore, that the largest probability for the appearance of instability of a given mode is for the ideal case of combustion concentrated on the surface where the amplitude of pressure oscillations is maximum. For purely longitudinal modes this means combustion concentrated on the antinodal sections of the given mode. It is clear now that for the appearance of this type of instability, it is necessary to satisfy not only a time condition, concerning the time lags, but also a *space condition* concerning the distribution of the combustion. The presence of a time and a space requirement has been known for a long time in the problem of *singing flames*[10a] which presents some analogies to screaming in rockets, although it is based on a different coordinating process. If both conditions are fulfilled, a kind of instability is created, characterized by a frequency close to the frequency of one of the natural modes, in which the coordinating process resides in the natural process of oscillation through its action on the burning rates. In rocket language it is recognized as *high frequency instability*, or *screaming*. This mechanism for production of high frequency instability has been suggested by L. Crocco[8] and studied in detail by L. Crocco and Sin-I Cheng[11, 12] in the case of purely longitudinal oscillations. The treatment is partly reproduced and generalized in Chapter 3 of this monograph. The more complicated case of combined longitudinal and transverse modes has not yet been treated analytically; this case is of practical interest and is worth attempting at a future date.

1.09. Effect on Stability of Spreading the Combustion

In the discussions of the preceding sections, the time lag has been assumed to be uniform for all propellant elements. Also, we have concluded that high frequency instability of a given mode is most likely to appear when combustion is concentrated on the antinodal surfaces. The ideal case, where these two conditions are satisfied together, that is, where the combustion is concentrated both in time and space, is the most unstable case, because the time and space conditions are fulfilled in the most definite way. In other words, in this case, all of the combustion process can be used in generating, through oscillations, the maximum amount of work to overcome the stabilizing forces. This result is true for both screaming and chugging; in the latter case, the timewise concentration alone is effective.

If, however, the combustion is spread timewise and/or spacewise, even if the time and space conditions are in-average-satisfied, only those fractions of the combustion processes which are close to individually fulfilling the conditions will produce work. The further away the individual fractions are from satisfying these conditions, the less work they will generate and ultimately instead of producing they will absorb work and become stabilizing.

We conclude that for a given average value of the time lag, the larger the range of time lags for the individual fractions of propellants, the more stable is the combustion process, for both chugging and screaming. For screaming, starting from the ideal case of combustion concentrated in the antinodal region of a given mode, an unstable combustion can become stable by spreading the combustion away from the antinodal region. Of course, the opposite can be true for another mode, for which initially the combustion is concentrated in a nodal region, and for which the combustion can switch from stable to unstable conditions when it spreads toward the antinodal regions. If all the possible modes are considered together, the nodal regions practically fill all the chamber, so that the most favourable distribution for a given mode can be unfavourable for other modes. *A priori*, the best overall situation is likely to be obtained when the combustion is uniformly distributed in the chamber, and the time lags are also spread over the widest possible range. In this case there will be a convenient balance of stabilizing and destabilizing fractions for each mode. However, the possibility must be kept in mind that certain modes can be more detrimental than others; and also that the damping effect due to the presence of the nozzle, well established for longitudinal modes, might not be as strong for transverse modes. In this case, some distributions other than uniform might be more advantageous in having a larger stabilizing effect on the more detrimental or the less damped modes.

The quantitative study of the effect of spreading the combustion timewise or spacewise is given in Section 2.08 for chugging, and in Section 3.05 and the following for screaming, in the case of longitudinal oscillations.

1.10. Other Mechanisms for Unstable Combustion

One can imagine several other coordinating processes which might produce instability. Vortex shedding with determined frequencies[13], flow fluctuations in the injectors[14], and in the spray of two impinging jets[15], combustion

phenomena in ıdies, oscillatory chemical kinetics, flow phenomena in nozzles, and so on, may be distinguished by character stic times different from either the relaxation times or the period of the natural modes. Therefore, they may be able to produce unstable conditions with frequencies different from those of chugging and screaming. However, too little is known about these processes, and any attempt to formulate, even qualitatively, a mechanism based on them would merely represent a guess without substantial value.

One interesting mechanism, related to the discussion of the preceding sections, is the coordinating process of the wave motion in the propellant lines and the consequent oscillation of the injection rate. This oscillation produces a delayed oscillation in the burning rate and therefore in the chamber pressure and the pressure at the injection port. The oscillation of pressure at the injection port finally closes the loop, by providing the necessary driving force for the maintenance of the oscillations in the lines, provided that the proper time condition is satisfied. The frequency distinguishing this type of instability from other types is determined by the wave propagation time in the lines, and of course this frequency can vary in a wide range. Hence instability can be produced with frequencies intermediate between those of chugging and screaming. A particularly interesting situation arises, however, when the frequency due to wave propagation in the lines, falls in the same range as chugging or screaming frequencies, in which case the two types of instability will reinforce each other and particularly bad conditions are to be expected.

The difficulty in developing an analytical treatment of these effects, is that generally the propellant lines cannot be represented realistically by a simple connecting pipe of constant cross section between the tank or the pumping system and the injector ports. The injector passages are generally quite complicated and the lines are interrupted by valves of several types necessary for starting and shut-off. As a consequence of this fact, and the fact that different parts of th internal walls have different elastic constants, the oscillatory characteristics of the system are quite complex and it is difficult to estimate a length on which to base a fundamental frequency. As a result of this complicated situation a theory has not yet been developed for this kind of instability. Only a rudimentary consideration of the effect of wave propagation in feed lines on low frequency oscillation has been presented[16]. In principle, an analytical treatment should be possible and it seems that efforts in this direction should be worthwhile.

We have already noticed that particularly strong effects are to be expected when the frequency, characteristic of the propellant lines, coincides with one of the screaming frequencies. Now we can add that it is sufficient that this condition be satisfied for only one of the characteristic frequencies of the feeding system, and that due to the complicated design, it is very likely that some frequencies fall in the range of screaming frequencies no matter how long the entire lines may be. In particular, due to the fact that the sound velocity is of the same order in the propellants and in the burnt gases, it is possible to have direct resonance between the propellant side and the gas side of certain types of injectors in a direction parallel to the injector face.

An interesting suggestion for a coordinating mechanism in bipropellant systems, which would produce frequencies in a range intermediate between chugging and screaming is the following. In oscillating conditions, the energy content of the products of combustion can also oscillate because of oscillations in the mixture ratio. Thus the temperature of the products, taken at the mean pressure, will oscillate too, and so will the entropy. The entropy excess or deficiency moves with the products until it reaches the nozzle, where it produces pressure waves travelling back to the injectors. A closed loop is thus determined because the pressure oscillations at the injector may entertain the mixture ratio oscillations. A theory based on this mechanism has not yet been developed, but a rough calculation shows that the proper frequencies should be higher than for chugging and lower than for screaming. This mechanism is substantially the same as that suggested by K. BERMAN and S. H. CHENEY, Jr[16a] to explain some of the phenomena they have observed. It should be noticed, however, that Berman and Cheney stress the dependence of this effect on the presence of shock waves and discontinuities of temperature. In the opinion of the present authors these non-linear phenomena are not essential for the mechanism.

An analogous mechanism could operate on monopropellant systems, where the necessary entropy oscillations would result only from the oscillation of the pressure of combustion.

1.11. EQUATIONS FOR THE TIME LAG AND THE SPACE LAG

An analytical treatment of the phenomena qualitatively discussed in the preceding sections requires that each individual process of the phenomenon be given a quantitative formulation. Within the approximation of the assumptions of Section 1.03, we have already seen how the phenomenon of combustion can be conveniently represented through a suitable distribution of sources in steady state operation, after which the problem is practically reduced to a problem of fluid dynamics.

The same would be true for non-steady conditions, if the strength of the sources were unaffected. However, the opposite case is true. It is necessary, therefore, to know quantitatively how the source distribution, both in time and space, is determined by the physical factors; in other words, how time and space lags depend on the time and space history of the physical factors themselves.

Among the physical factors that are likely to have the largest influence, are the pressure and temperature of the gases and the relative velocities between the propellants and the gases. If one knew the details of the processes taking place during the time lag, it would be possible to express the rates of these processes at each point along the path of the propellants as a function of the aforesaid physical factors, which are supposed to be known at every instant and location. But we do not know the details of either the processes or their rates; moreover, it is doubtful if the values of such factors as temperature and relative velocities, as computed for our combustion model, would represent consistently the actual values which determine the rates, because the presence of vapour or other intermediate substances, even if it does not substantially affect the fluid dynamics of the burnt gases, probably has an important effect on the rate of the processes. For

this reason, it is better not to describe separately the effects of the different physical factors, but to make the simplifying assumption instead, that the rate of the processes can be correlated with the values of the local pressure. This does not mean that the other factors are assumed to exert negligible influence on the rates, but merely that their variations, and therefore their effects, are correlated to those of the pressure. Mathematically this can be expressed as follows[9]. The rate of the processes at a given location and time are a function $f(p, T, Z \ldots)$ of pressure, temperature, and any other physical factor Z. If starting from a certain steady condition, where the local values of these factors are $\bar{p}$, $\bar{T}$, $\bar{Z}$ we apply small perturbations p', T', Z', the new process rate will be

$$f(p, T, Z \ldots) = f(\bar{p}, \bar{T}, \bar{Z} \ldots) + p' \frac{\overline{\partial f}}{\partial p} + T' \frac{\overline{\partial f}}{\partial T} + Z' \frac{\overline{\partial f}}{\partial Z} + \ldots$$

where the partial derivatives are computed at $p = \bar{p}$, $T = \bar{T}$, $Z = \bar{Z}$ etc. If we assume that T and Z are correlated to p, so that $T = T(p)$ and $Z = Z(p)$ we can write $T' = p' \left(\frac{dT}{dp}\right)_{p=\bar{p}}$, $Z' = p' \left(\frac{dZ}{dp}\right)_{p=\bar{p}}$ so that the preceding expression becomes

$$f(p, T, Z \ldots) = f(\bar{p}, \bar{T}, \bar{Z} \ldots) \left[1 + p' \frac{1}{\bar{f}} \overline{\left(\frac{\partial f}{\partial p} + \frac{dT}{dp}\frac{\partial f}{\partial T} + \frac{dZ}{dp}\frac{\partial f}{\partial Z} + \ldots\right)}\right]$$

where the barred quantity has to be evaluated at $p = \bar{p}$, $T = \bar{T}$, $Z = \bar{Z}$.

Let us write

$$n = \frac{\bar{p}}{\bar{f}} \overline{\left(\frac{\partial f}{\partial p} + \frac{dT}{dp}\frac{\partial f}{\partial T} + \frac{dZ}{dp}\frac{\partial f}{\partial Z} + \ldots\right)} \qquad \ldots.(1.11.01)$$

and let us call n the 'interaction index'.

Then the instantaneous rate is given by

$$f(p, T, Z \ldots) = f(\bar{p}, \bar{T}, \bar{Z} \ldots)\left[1 + n\frac{p'}{\bar{p}}\right] \qquad \ldots.(1.11.02)$$

which is exactly the same as if f was assumed to depend only on p and to be proportional to p^n. Thus in the assumption that the physical factors are correlated we can disregard the explicit effects of all the factors except that of the pressure and represent the relation between the rate and the instantaneous local pressure as

$$f \sim p^n \qquad \ldots.(1.11.03)$$

Then variations are related by equation (1.11.02). To illustrate the idea with some examples let us consider the case in which the variations of state are isentropic, so that

$$\frac{\overline{dT}}{dp} = \frac{\gamma - 1}{\gamma}\frac{\bar{T}}{\bar{p}}$$

and assume a heat transfer process from the gases to the droplets following the law

$$f \sim p^m(T - T_s)$$

T_s being the temperature of the droplets and m an exponent close to unity.

We obtain from equation (1.11.01)

$$n = m + \frac{\gamma - 1}{\gamma} \frac{T}{T - T_p} \simeq m + \frac{\gamma - 1}{\gamma}$$

if $T_p \ll T$. Therefore the interaction index is likely to be slightly larger than m, but still close to unity. On the other hand, for a chemical process, we can assume for the rate a temperature dependence of the Arrhenius type

$$f \sim p^m \exp(-A/RT_r)$$

where A represents an overall activation energy, and T_r the effective temperature in the reacting zone, different from T. Assuming again an isentropic relation between T_r and p we find

$$n = m + [(\gamma - 1)/\gamma]\,[A/RT_r]$$

and we see that the interaction index can, in this case, be considerably greater than m if T_r is in the proper range, so that even if m is of the order of unity, as seems to be likely for most of the practical combustion processes, n may take values considerably larger. The purpose of these two examples is not to suggest the possibility of a precise determination of the index of interaction, because we do not have sufficient information, but merely to show that for processes which are likely to be present and important in rocket combustion, the index of interaction can be around unity and larger. They show also that among the physical factors affecting the variations of the rates, the pressure is probably the most important one because, for the processes considered, m is likely to be an essential fraction of n. This justifies to a certain extent the choice of the pressure as the single physical factor with respect to which the interaction index is defined, instead of, for instance, the temperature. It must be noticed, however, that the two influences (or more than two) could in principle be separated if we knew more about the processes involved.

The fact that the pressure alone has an important influence on the processes is also supported by some experimental results. It is known that the minimum volume (or minimum L^*), compatible with an efficient operation of rockets, decreases with increasing pressure, and that in certain cases its variation is roughly inversely proportional to the pressure. Since L^* is a measure of the residence time, and the minimum residence time is proportional to the time lag, it is concluded that in certain cases, the time lag can be roughly inversely proportional to the pressure, and therefore the rates of the processes leading to combustion are directly proportional to the pressure. Since the temperature of the burnt gases can be assumed to be practically unaffected by changes in the pressure level, this is purely a pressure effect. This deduction is substantiated by recent, more direct preliminary measurements of the time lag[17]. Such a marked effect of the pressure on the burning rate is not proper only of the combustion in rockets. Even in ordinary laminar flames the fact that flame velocities are only very slightly affected by pressure[18] indicates a mass burning rate nearly proportional to pressure. Similarly the self-ignition lag of fuels injected in atomized or vaporized form into a hot air stream has been found to vary approximately as the inverse of the pressure[19].

Equations (1.11.02) or (1.11.03) apply to a particular phase of the processes taking place during the time lag. Of course we cannot expect that all of these processes are equally affected by variations in the physical factors. For instance such processes as atomization or mixing, that constitute a necessary pre-requisite for the other processes, are likely to be practically unaffected by the physical conditions in the chamber and to depend substantially only on the injector configuration. Thus if we could follow in detail the history of a particular element of propellant on its path, we would find that the interaction index changes along the path, starting with negligible values immediately after injection, then increasing gradually while the processes sensitive to physical conditions begin taking over, and finally staying around unity for the rest of the time lag. Again, it is not possible to describe the process in detail with our present knowledge of the combustion processes in rockets. However, we can replace it with a plausible schematic process, which is apparent after the previous quantitative considerations. We can assume that the index of interaction is zero for a certain portion of the time lag, τ_i, that we shall call the insensitive time lag, and discontinuously becomes equal to a value n (of order unity) for the rest of the time lag, τ, which will be called the sensitive time lag. The total time lag τ_t is the sum of the two

$$\tau_t = \tau_i + \tau \qquad \ldots.(1.11.04)$$

Since the mixing process, which is essential in bipropellant rockets, is absent in monopropellant rockets (with thermal ignition, not with catalytic ignition), we can reasonably predict that τ_i will be relatively larger for bipropellants, and smaller for monopropellants where the only delay, prior to the thermal or chemical activation, is due to the time it takes to atomize and disperse the propellant through the burnt gases. In both cases we can expect a large influence of the injector configuration on τ_i. By definition τ_i is unaffected by variation of the physical factors, so that

$$\tau_i = \bar{\tau}_i \qquad \ldots.(1.11.05)$$

at each instant. On the contrary τ varies because the rate of the processes that determine its duration changes with the physical factors. The quantitative relation between τ and the physical factors can be derived as follows. The transformation into burnt gases takes place only when the preparatory processes have accumulated up to a well determined level, E_a. This can be expressed for an element which burns at the instant t by the relation

$$\int_{t-\tau}^{t} \mathrm{f}(t')\, \mathrm{d}t' = E_a \qquad \ldots.(1.11.06)$$

the integral being evaluated following the motion of the given element from the instant $t' = t - \tau$, when the rates began to be affected by the physical factors, to the instant of combustion $t' = t$.

The rate $\mathrm{f}(t')$ must be computed using the instantaneous values of the physical factors at each instant t' at the location where the element was at that instant. Let us denote the spatial coordinates of the position of the element at instant t' by $x_i(t')$. Then

$$\mathrm{f}(t') = \mathrm{f}\{p[x_i(t'), t')],\ T[x_i(t'), t'], \ldots\} \qquad \ldots.(1.11.07)$$

In steady state equation (1.11.06) gives

$$\int_{t-\bar{\tau}}^{t} \bar{\mathrm{f}}\,(t')\,\mathrm{d}t' = E_a \qquad \ldots.(1.11.08)$$

where the variation of $\bar{\mathrm{f}}$ is now due only to the possible spatial non-uniformity of the physical factors

$$\bar{\mathrm{f}}(t') = \bar{\mathrm{f}}\,\{\bar{p}[x_i(t')], T[x_i(t')] \ldots\}$$

If the velocities of the liquid droplets and the gases in the rocket chamber are small compared with the sound velocity (which is generally true, except for throatless motors) the steady state values of physical factors such as pressure and temperature are practically uniform in the chamber, $\bar{p}$ = constant, $\bar{T}$ = constant (see Chapter 3). In this case, neglecting the action of other physical factors, we can write equation (1.11.08) in the form

$$\bar{\mathrm{f}} \,.\, \bar{\tau} = \mathrm{f}\,(\bar{p}, \bar{T}, \ldots) \,.\, \bar{\tau} = E_a$$

Let us again assume that $p = \bar{p} + p'$, $T = \bar{T} + T'$, the perturbations p', T', being small compared with $\bar{p}$, $\bar{T}$, ... ; we can write $\tau = \bar{\tau} + \tau'$ and we can also expect τ' to be small with respect to $\bar{\tau}$. Equations (1.11.06) and (1.11.08) can be written as

$$\int_{t-\bar{\tau}}^{t} \mathrm{f}\,(t')\,\mathrm{d}t' + \int_{t-\tau}^{t-\bar{\tau}} \mathrm{f}\,(t')\,\mathrm{d}t' = E_a = \int_{t-\bar{\tau}}^{t} \bar{\mathrm{f}}\,(t')\,\mathrm{d}t' \quad \ldots.(1.11.09)$$

Now since τ' is a small quantity we can write after neglecting higher order terms

$$\int_{t-\tau}^{t-\bar{\tau}} \mathrm{f}(t')\,\mathrm{d}t' \simeq \tau'\ \mathrm{f}\,(t-\bar{\tau}) \simeq \tau' \,.\, \bar{\mathrm{f}}\,(t-\bar{\tau}) \quad \ldots.(1.11.10)$$

Using equations (1.11.02) and (1.11.10) and again neglecting higher order quantities, equation (1.11.09) becomes

$$\tau - \bar{\tau} = \tau' = -\frac{n}{\bar{\mathrm{f}}\,(t-\bar{\tau})} \int_{t-\bar{\tau}}^{t} \frac{\bar{\mathrm{f}}\,(t')}{\bar{p}(t')}\, p(t')\,\mathrm{d}t' \quad \ldots.(1.11.11)$$

When the steady state conditions are practically uniform in the chamber, $\bar{p}$ = constant, and $\bar{\mathrm{f}}\,(t')$ = constant = $\bar{\mathrm{f}}\,(t-\bar{\tau})$, so that

$$\tau - \bar{\tau} = -\frac{n}{\bar{p}} \int_{t-\bar{\tau}}^{t} p'(t')\,\mathrm{d}t' \qquad \ldots.(1.11.12)$$

Differentiation of equation (1.11.12) with respect to t gives

$$\frac{\mathrm{d}\tau}{\mathrm{d}t} = -n\frac{p'(t) - p'(t-\bar{\tau})}{\bar{p}} \qquad \ldots.(1.11.13)$$

The corresponding expression for the non-uniform case can be found by differentiating equation (1.11.11).

In general the perturbation p' is a function of space and time so that

$$p'(t) = p'[x_i(t), t]$$
$$p'(t-\bar{\tau}) = p'[x_i(t-\bar{\tau}), t-\bar{\tau}] \qquad \ldots.(1.11.14)$$

However, as already observed in Section 1.08, if p' changes so slowly that its change during the wave propagation time can be neglected (low frequency case), p' is practically uniform at every instant throughout the combustion chamber. In this case the space dependence disappears from the relation (1.11.14) and equation (1.11.13) reduces to its simplest form, suitable for the case of chugging.

The quantity $d\tau/dt$ plays an important role in the theory of stability because it is closely related to the perturbations of the burning rate of a given element.

Consider the total rate $\dot{m}_i(t)$ of injection of propellant at a given instant t, and consider a small fraction of this rate, $\delta\dot{m}_i(t)$, having at this instant a total time lag $\tau_t(t)$; the value of τ_t being generally different for different fractions and variable with time for each fraction. For the fraction under consideration the amount injected between t and $t + dt$ is $\delta\dot{m}_i(t)\,dt$. This amount burns between $t + \tau_t$ and $t + \tau_t + dt + d\tau_t$, that is, in the interval $dt + d\tau_t$, with the so far undetermined average burning rate $\delta\dot{m}_b(t + \tau_t)$. Therefore we have

$$\delta\dot{m}_i(t)\,dt = \delta\dot{m}_b(t + \tau_t)\,.\,(dt + d\tau_t)$$

If instead of giving the instant of injection and the τ_t pertaining to this instant, we assign the instant of combustion and consider the value of τ_t corresponding to this instant, the preceding equation can be written, after division by dt, as

$$\delta\dot{m}_b(t) = \delta\dot{m}_i(t - \tau_t)\,[1 - d\tau/dt] \qquad \ldots.(1.11.15)$$

where $d\tau_t/dt$ has been replaced by the identical quantity $d\tau/dt$. In the steady state τ is constant and

$$\delta\bar{\dot{m}}_b = \delta\bar{\dot{m}}_i \qquad \ldots.(1.11.16)$$

Subtracting (1.11.16) from (1.11.15) we find the relations between the perturbations

$$[\delta\dot{m}_b(t) - \delta\bar{\dot{m}}_b] = [(\delta\dot{m}_i(t - \bar{\tau}_t) - \delta\bar{\dot{m}}_i) - (d\tau/dt)\delta\dot{m}_i(t - \bar{\tau}_t) \qquad \ldots.(1.11.17)$$

In writing this equation τ_t has been replaced by $\bar{\tau}_t$ because the corresponding perturbation $\tau_t - \bar{\tau}_t$ introduces only higher order terms.

The equation (1.11.17) holds in general for any $d\tau/dt$. In particular, if the derivations of this section are used, $d\tau/dt$ is given by equation (1.11.13). The corresponding more elaborate formula for the non-uniform case can be obtained from equation (1.11.11).

If the injection rate is fixed, $\delta\dot{m}_i = \delta\bar{\dot{m}}_i$, equations (1.11.15) and (1.11.16) can be written simply as

$$\delta\dot{m}_b = \delta\bar{\dot{m}}_b(1 - d\tau/dt) \qquad \ldots.(1.11.18)$$

All the equations that have been derived so far can be written in terms of the space variable instead of the time variable, when the vector velocity of the unburnt propellant element along its path is known. These equations can be formulated for general three-dimensional flow in the combustion chamber. We shall treat in Chapter 3 only the case of one-dimensional flow in connection with the stability of the purely longitudinal modes of high frequency oscillations which is the only one treated in this monograph.

2

CHUGGING ANALYSIS (LOW FREQUENCY INSTABILITY)

List of Symbols

Superscript *	indicates that the quantity is dimensional
Superscript ′	indicates a small perturbation
Subscripts $_r$ and $_i$	indicate respectively the real part and the imaginary part of the quantity, if not otherwise stated
Subscripts $_o$ and $_f$	refer to oxidizer line and fuel line respectively
$\bar{\quad}$	bar over a quantity indicates mean or steady state value
M_g	mass of burnt gas in combustion chamber
$\dot{m}_b$	rate of burnt gas generation or burning rate in combustion chamber
$\dot{m}_e$	rate of burnt gas ejection out of combustion chamber
$\dot{m}_i$	rate of injection of propellant into combustion chamber
$\bar{m} = \bar{m}_b$	steady state mass flow rate, the reference mass flow rate
μ_b	fractional burning rate perturbation
μ_e	fractional variation of burnt gas ejection
μ_i	fractional variation of propellant injection
p	pressure of gas in combustion chamber or local flow pressure at stations indicated by the subscript
T_g	temperature of gas in combustion chamber
t	dimensional time
$\theta_g = \bar{M}_g/\bar{m}$	mean gas residence time in the chamber based on the mass $\bar{M}_g$ of burnt gas in the combustion chamber
z	dimensionless time t/θ_g or $t/\theta_r = t/\theta_g(1+b)$
b	coefficient of $\mathrm{d}/\mathrm{d}z$ in the transfer function N_n of the rocket nozzle as defined in equation (2.01.08)
$\theta_r = \theta_g(1+b)$	corrected gas residence time or relaxation time for chamber–nozzle combination used as reference time
$\tau_l^* = \tau_i^* + \tau^*$	dimensional total time lag from instant of injection to instant of combustion of a given propellant element
τ_i^*	dimensional insensitive part of total time lag
τ^*	dimensional sensitive part of total time lag
$\tau_l = \tau_i + \tau = \tau_l^*/\theta_r$	dimensionless total time lag
$\tau_i = \tau_i^*/\theta_r$	dimensionless insensitive part of the total time lag
$\tau = \tau^*/\theta_r$	dimensionless sensitive part of the total time lag
δ	critical values of the dimensionless sensitive time lag corresponding to neutral oscillations
δ_i	critical value of insensitive time lag
n	pressure index of interaction between combustion processes and oscillations in the combustion chamber defined in equation (1.11.01)
φ	fractional pressure perturbation

γ	specific heat ratio c_p/c_v or adiabatic index of burnt gas
α_n	specific admittance ratio of neutral acoustical disturbances in de Laval nozzle = ratio of local fractional velocity variation to local fractional density variation at the entrance of the nozzle
$N_n\left(\frac{\mathrm{d}}{\mathrm{d}\bar{z}}\right)$	transfer function of mass flow through rocket nozzle defined as the ratio of fractional mass flow rate variation to fractional variation of the impressed pressure
$F\,(\mathrm{d}/\mathrm{d}\bar{z})$	transfer function of feedback circuit for servo stabilization
C_l	flow capacitance of feed line
C_c	control capacitance of feedback circuit
D	constant of feed pump characteristics
χ	equivalent spring constant of line capacitance
y	position of the equivalent concentrated capacitance C_l downstream of feed pump as fraction of feed line length
A	effective area of feed line
A_i	effective area of injector nozzle
P	pressure drop parameter of the feeding system
E	elasticity parameter of the feeding system
J	inertia parameter of the feeding system
Λ^*	dimensional amplification coefficient
Ω^*	dimensional angular frequency
$\Lambda = \Lambda^*\theta_r$	dimensionless amplification coefficient
$\Omega = \Omega^*\theta_r$	dimensionless angular frequency
$s = \Lambda + i\Omega$	a complex quantity which is the Laplace transformation variable and is the root of the characteristic equation for oscillations with exponential time dependence
ω	dimensionless critical angular frequency of neutral oscillation
Ψ	flow reactance of feed line
Φ	flow susceptance of feed line
h	integers including zero indicating successive higher unstable ranges of the values of the sensitive time lag = integral numbers of oscillation periods contained in the sensitive time lag
$r = \dot{m}_o/\dot{m}_f$	mixture ratio or ratio of mass flow rate of oxidizer to that of fuel
$H = \frac{1}{2}(\bar{r}-1)/(\bar{r}+1)$	a parameter of steady state mixture ratio
$K = \frac{1}{2}\frac{\bar{r}}{\bar{T}_g}\frac{\mathrm{d}\bar{T}_g}{\mathrm{d}\bar{r}}$	a parameter representing the sensitivity of the adiabatic flame temperature to mixture ratio variation
V	combustion chamber volume
$n_{\min}$	minimum value of n compatible with unstable oscillations in a given system
$N = N_r + i\omega N_i$	overall transfer function of feeding system defined as μ_i/φ
$R + iS$	$= N \exp(-i\omega\delta_i)$
$\mathrm{f}(\bar{\tau})$	fractional amount of propellant elements having sensitive time lag $\leqslant \bar{\tau}$ with $\mathrm{f}(\bar{\tau}_{\min}) = 0$ and $\mathrm{f}(\bar{\tau}_{\max}) = 1$

C	magnification factor due to the effect of spreading the sensitive time lag defined in equation (2.08.06)
$\bar{\tau}_e$	effective sensitive time lag defined in equation (2.08.06)
δ_e	critical value of $\bar{\tau}_e$ for neutral oscillation

2.01. Equation of the Combustion Chamber

The actual situation in the combustion chamber is too complicated and obscure to allow analytical treatment. However, in agreement with the discussion of Section 1.03 a satisfactory working model is obtained by neglecting the presence of the unburnt propellant elements until, after the time lag has elapsed, they are suddenly transformed into completely burnt gases. The flow of the burnt gases in the chamber can be considered as the flow of an ideal gas with distributed sources and determined by the laws of conservation of mass, momentum and energy. Additional simplifications are obtained if we assume that the Mach numbers up to the nozzle entrance are sufficiently below unity so that, in steady state, the pressure and the temperature of the gases are practically constant throughout the chamber. Moreover, in the range of low frequencies pertaining to chugging, the propagation of the pressure waves can be supposed to be practically instantaneous. Thus, as already noticed, the following assumptions, fundamental for chugging, can be made:

(*a*) The gas pressure is practically uniform throughout the combustion chamber at every instant and oscillates about the mean or steady state value as a whole. Another simplifying assumption concerns the temperatures of the gases. First, we can suppose that at the instant of generation, the burnt gases have the same temperature irrespective of the particular conditions of combustion. This means that in the case of a monopropellant rocket we neglect the effects of differences in heat transferred to the propellants before combustion and the variation of dissociation with pressure; moreover, in the bipropellant case, we assume constant mixture ratio (this assumption is dropped in Section 2.07). Once the burnt gases are generated they undergo changes in pressure and therefore in temperature. In order to compute these changes, we should know at every instant for each fraction of burnt gases the pressure under which they were generated. With some simplifying assumptions, this can be done, and has been done in Section 2.10, showing that under these assumptions the effects of these temperature variations are of secondary importance. The effect would completely vanish if the adiabatic index γ were taken as unity; and the actual values of γ for rocket gases are not far from unity. Therefore in order to simplify the analysis and bring out the main features of chugging we can neglect all temperature changes and make the following assumption:

(*b*) the temperature of the gases in the chamber is practically constant and uniform irrespective of the pressure oscillations.

A last simplifying assumption concerns the time lag, about which we shall make the assumption that

(*c*) the time lag is uniform, that is, it has the same value for all propellant elements.

As already noticed in Section 1.03, this must be considered only as an ideal case, and the corresponding assumption will be dropped in Section

2.09. Assumption *c* can be made with respect to both the insensitive and the sensitive time lags, and hence for the total time lag; or only for the sensitive time lag, when the insensitive time lag does not enter into the picture. It should be noted that this assumption does not imply that all elements have the same space lag because their velocities can be widely different.

The simplifications arising from these assumptions are as follows: Assumption *a* replaces completely the momentum equation, which therefore does not need to be considered. Similarly assumption *b* takes the place of the energy equation; moreover, with this assumption we do not need to know the spacewise distribution of combustion. Also the timewise distribution of combustion can be ignored with the introduction of assumption *c*.

With these assumptions, the dynamics of the gas system in the combustion chamber is essentially governed by the balance of mass, that is, the rate of burnt gas generation $\dot{m}_b(t)$ must be equal to the sum of the rate of ejection $\dot{m}_e(t)$ of the gas out of the combustion chamber through the nozzle and of the rate $\frac{d}{dt} M_g$ at which mass is being accumulated in the combustion chamber itself, i.e.

$$\dot{m}_b(t) = \dot{m}_e(t) + \frac{d}{dt} M_g(t) \qquad \ldots.(2.01.01)$$

Since the combustion chamber volume is constant and the gas temperature is assumed to be independent of gas pressure, $M_g(t)$ is proportional to the chamber pressure $p(t)$. Thus the mass accumulation term becomes $\bar{M}_g \cdot \frac{d}{dt}\left[\frac{p(t)}{\bar{p}}\right]$. Introducing the following fractional variations of gas pressure, burning rate and ejection rate over their respective steady state values,

$$\varphi = \frac{p - \bar{p}}{\bar{p}}\,; \qquad \mu_b = \frac{\dot{m}_b(t) - \bar{m}}{\bar{m}}\,; \qquad \mu_e = \frac{\dot{m}_e(t) - \bar{m}}{\bar{m}} \qquad \ldots.(2.01.02)$$

we can rewrite equation (2.01.01) as

$$\theta_g \, d\varphi/dt + \mu_e(t) = \mu_b(t) \qquad \ldots.(2.01.03)$$

where $\theta_g = \bar{M}_g/\bar{m}$ represents the gas residence time, that is, the time an average burnt gas element will spend in the combustion chamber in steady operation before it enters the nozzle. In accordance with Section 1.05, the fractional variations defined in equation (2.01.02) will be assumed small in the following treatment, and their products or powers will be neglected as higher order small quantities. Equation (2.01.03) clearly indicates that θ_g is the proper characteristic time which can be used to reduce equation (2.01.03) into dimensionless form. If μ_b vanishes and μ_e is equal to φ as will be clear later, equation (2.01.03) shows that θ_g represents the chamber relaxation time. The average gas residence time is therefore one of the fundamental constants characterizing the dynamics of the burnt gas

in the combustion chamber in problems of low frequency combustion stability. D. F. GUNDER and D. R. FRIANT[5] neglected the mass accumulation term. As a result, they failed to notice the importance of this residence time. In terms of the 'characteristic length' L^* and the 'characteristic exhaust velocity' c^* that are more conventionally used in the field of rocket engineering, this average gas residence time is easily shown to be

$$\theta_g = \frac{L^* c^*}{RT_g} = \frac{1}{\gamma}\left(\frac{2}{\gamma+1}\right)^{-\frac{\gamma+1}{\gamma-1}} \cdot \frac{L^*}{c^*}$$

where γ is the ratio of the mean specific heats of the combustion gas. It should be noted that the total residence time of a propellant element in the chamber in steady state is bigger than the gas residence time by the total time lag $\tau_t^* = \tau_i^* + \tau^*$ that elapses before the propellant is transformed into hot gas. For convenience, dimensionless time and dimensionless total, sensitive and insensitive, time lags are defined as

$$z = t/\theta_g; \quad \tau = \tau^*/\theta_g, \quad \tau_i = \tau_i^*/\theta_g, \quad \tau_t = \tau_i + \tau \quad \ldots.(2.01.04)$$

Let us now consider the fractional variation μ_b of burnt gas generation which, as already noticed, is complicated by the variation of the time lag. At instant t, the propellant elements injected after the interval $t - \tau_t^*$ have not yet burned. Hence, considering the total amount burnt from the beginning of the operation, $t = 0$, to the instant t we can write

$$\int_0^t \dot{m}_b(t')\,dt' = \int_0^{t-\tau_t^*} \dot{m}_i(t')\,dt'$$

where $\dot{m}_i(t')$ is the rate of injection of propellants into the chamber at the instant t' and $\dot{m}_b(t')$ is the rate of burnt gas generation at the instant t'. Differentiating with respect to t, we again obtain equation (1.11.15)

$$\dot{m}_b(t) = (1 - d\tau_t^*/dt) \cdot \dot{m}_i(t - \tau_t^*) \quad \ldots.(2.01.05)$$

The first factor of the right-hand side can be obtained from equation (1.11.13), and can be expressed in dimensionless form as

$$1 - \frac{d\tau_t^*}{dt} = 1 - \frac{d\tau^*}{dt} = 1 + n[\varphi(t) - \varphi(t - \bar{\tau}^*)] \quad \ldots(2.01.06)$$

Introducing in equation (2.01.05) the fractional variations $\mu_b = (\dot{m}_b - \bar{m})/\bar{m}$ and $\mu_i = (\dot{m}_i - \bar{m})/\bar{m}$ and $1 - d\tau^*/dt$ from equation (2.01.06) we obtain after linearization

$$\mu_b(z) = \mu_i(z - \bar{\tau}_t) + n[\varphi(z) - \varphi(z - \bar{\tau})] \quad \ldots.(2.01.07)$$

where the dimensionless time has been introduced.

Next we consider the fractional variation μ_e of gas ejection. The mass-outflow from the combustion chamber through a given de Laval nozzle with supersonic exit in steady state operation is directly proportional to the chamber pressure and inversely proportional to the square root of chamber temperature. For the case of very low frequency oscillations

the flow through the nozzle may be considered as quasi-steady in the first approximation; that is, $\dot{m}_e \sim p/\sqrt{T_g}$ where p and T_g are the instantaneous gas pressure and gas temperature in the combustion chamber. The quasi-steady assumption gives, for a small isentropic oscillation, $\mu_e = \frac{p'}{p} - \frac{1}{2}\frac{T'}{T} = \frac{\gamma+1}{2\gamma}\varphi$ and the ratio between the fractional variations of the flow rate and of the pressure, that is, the nozzle transfer function, is given by $\mu_e/\varphi = (\gamma+1)/2\gamma$. When T_g is assumed to be constant $\dot{m}_e \sim p$, the quasi-steady argument gives $\mu_e = \varphi$ and the transfer function for the nozzle $\mu_e/\varphi = 1$. The quasi-steady assumption is, however, not quite correct, especially when the length of the subsonic portion of the nozzle is not too small. A better approximation can be obtained by applying non-steady one-dimensional analysis to the flow in the nozzle (refs. [24] and [25] and Appendix B). In this one-dimensional analysis, the ratio of small fractional oscillations of the velocity to small fractional oscillations of the gas density at the nozzle entrance can be determined. Extending the accepted terminology of acoustics, this quantity will be called the specific *admittance ratio*. The admittance ratio for the particular case of isentropic flow in a nozzle with linear steady state velocity distribution in the subsonic part has been calculated for the whole range of frequencies. For low frequency oscillations and general velocity distribution the specific admittance ratio α can be represented approximately by

$$\alpha = \frac{\gamma-1}{2} + ik\Omega^* \qquad \ldots.(2.01.08)$$

where Ω^* is the angular frequency of the oscillations, and k is a proportionality constant depending on the nozzle geometry. For isentropic flow the nozzle transfer function is

$$N_n = \frac{\mu_e}{\varphi} = \frac{1+\alpha}{\gamma} = \frac{\gamma+1}{2\gamma} + i\frac{k}{\gamma}\Omega^*$$

For ordinary configurations and frequencies in the chugging range, the imaginary part of this expression does not substantially exceed a value of 0·20. We see, therefore, that the modulus of the transfer function in chugging conditions is never appreciably different from $(\gamma+1)/2\gamma$ which is the quasi-steady value; but the phase can be quite significant. These results were obtained for isentropic flow. In order to be consistent with the assumption b of this section we modify the expression for N_n so that for zero frequency the transfer function is unity. Using the dimensionless angular frequency Ω instead of Ω^* we therefore write

$$N_n = 1 + ib\Omega \qquad \ldots.(2.01.09)$$

where $b = \Omega^* k/\Omega\gamma$ is a function of the nozzle geometry which can be computed explicitly from equation (B.60). Finally we observe that the analysis of the flow in the nozzle has been based on the assumption of purely harmonic oscillations; that is, the previous expression for N_n refers to neutral oscillations. For near-neutral oscillations and frequencies in the

chugging range, we shall write the nozzle transfer function in operational form as follows

$$\frac{\mu_e}{\varphi} = N_n = \left(1 + b\,\frac{\mathrm{d}}{\mathrm{d}z}\right) \qquad \ldots.(2.01.10)$$

For neutral oscillations equation (2.01.10) reproduces the previous results.

Introducing equations (2.01.07) and (2.01.10) into equation (2.01.03), we obtain a linear equation of mass conservation in dimensionless form for the two fractional perturbations φ and μ_i including approximately the effect of non-steadiness of the nozzle flow.

$$(1+b)\,\frac{\mathrm{d}\varphi(z)}{\mathrm{d}z} + \varphi(z) = \mu_i(z-\bar{\tau}_t) + n[\varphi(z) - \varphi(z-\bar{\tau})] \quad \ldots.(2.01.11)$$

This is the fundamental equation that governs the dynamics of gas flow in the combustion chamber under the assumptions mentioned previously. Equation (2.01.11) differs from a linear ordinary differential equation of first order by the presence of the dependent variables with retarded arguments $(z-\bar{\tau})$ and $(z-\bar{\tau}_t)$. The insensitive time lag enters only in the variation of the injection rate μ_i. The characteristics of intrinsic stability where the rate of injection of the propellant is constant, are therefore not affected by the value of the insensitive time lag. If, on the contrary, the injection rate is affected by the pressure oscillations, the insensitive time lag will have an effect on combustion instability. The case where $n = 0$ (no sensitive time lag $\bar{\tau}$) and μ_i variable, has been considered by D. F. GUNDER and D. R. FRIANT[5], M. YACHTER and WALDINGER[6], and M. SUMMERFIELD[7]. The concept of sensitive time lag was introduced by L. CROCCO[8], who also showed theoretically the possibility of unstable combustion even with constant injection rate and gave it the name of 'intrinsic instability'. Several special cases with $n \neq 0$, and μ_i variable have been analysed by L. CROCCO[8] and H. S. TSIEN[9]. The generalization including the phase lead component of the nozzle transfer function is due to SIN-I CHENG[20], who showed that all the results of previous investigations concerning chugging cases can be easily modified to include the effect of the non-steadiness of the nozzle flow without introducing any complication.

The relation between μ_i and φ is determined by the dynamics of the feeding system. Therefore to complete the formulation for the analysis of chugging we need an investigation into the dynamics of the feeding system.

2.02. EQUATION OF THE FEEDING SYSTEM, MONOPROPELLANT CASE

There are several types of more or less complicated feeding systems. Here, we shall consider systems where the pressurization is obtained by the use of pumps powered by a servo-controlled motor. Such systems are the most extensively used today in large thrust units, and they can include, as particular cases, systems where the pressurization is due to gas pressure, as is common in small units.

If the response of the servo-controlled motor is not very fast, as is the case ordinarily, and if the inertia of the moving parts is not too small, one can, for frequencies in the chugging range, suppose that the pumps are driven at constant speed. Despite the great simplification achieved through this

assumption, the dynamics of the feeding system is still quite complicated. The propellants and the supply lines are not completely rigid but possess a certain amount of elasticity, which can be represented by a distributed capacitance responding to pressure variations. Gas bubbles or parts with less rigidity (like plastic seals) may introduce larger concentrated capacitances. The distributed line capacitance and the inertia of the propellant result in a finite speed of propagation of pressure disturbances in the lines. As already observed in Section 1.10, the analysis of the system with the consideration of the wave processes in the lines is made practically impossible by the presence of valves, bends and other connections. However,

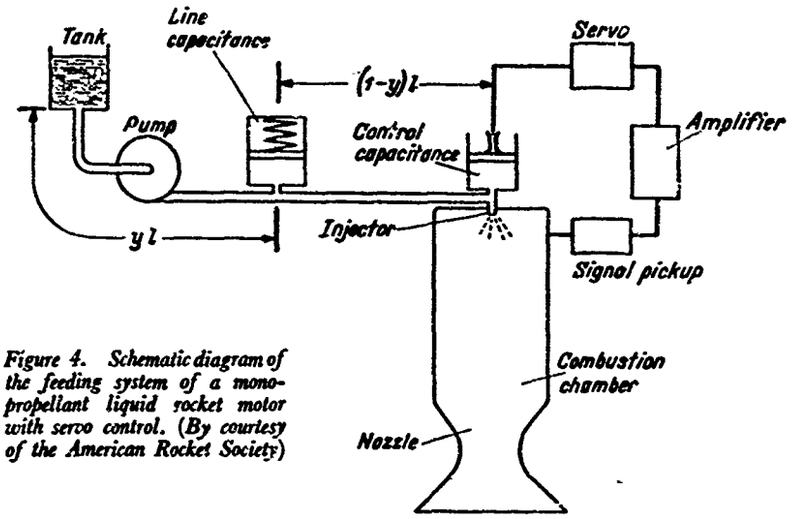

Figure 4. Schematic diagram of the feeding system of a monopropellant liquid rocket motor with servo control. (By courtesy of the American Rocket Society)

the wave processes can be disregarded if we make the assumption that the corresponding characteristic frequencies are sufficiently higher than the chugging frequency. In this case, we can represent a monopropellant system schematically as shown in *Figure 4*. The elasticity of the propellants and of the line and the possible presence of gas bubbles and other concentrated capacitances can be approximated by a single equivalent spring loaded capacity C_l located at a distance yl downstream of the tank outlet, where l is the entire length* of the feed line joining the tank to the injector. The location of the pump is unimportant provided it is close enough to the tank. A variable capacitance C_c controlled by feedback servo is introduced right next to the injector with a view toward the possibility of controlling the combustion instability in the combustion chamber. The servo is activated by the signals picked up in the combustion chamber.

For small perturbations the fractional variation of the flow rate over its steady state value is proportional to the fractional variation of delivery pressure p_0 downstream of the pump

$$\frac{p_0 - \bar{p}_0}{\bar{p}_0} = -D\frac{\dot{m}_0 - \bar{m}_0}{\bar{m}_0} \qquad \ldots.(2.02.01)$$

* If the lines are not of constant cross section, l and yl must be considered as equivalent lengths and calculated as shown, for example, in references [5] and [6].

If, instead of the absolute delivery pressure, p_0 were the relative head of the pump with respect to the tank conditions the proportionality constant $-D$ would coincide with the slope of the performance curve of the pump for constant speed, with the relative values of the relative head plotted against the relative values of the flow rate, both being unity at the steady-state operation point where the slope is measured. In this case, D would represent a characteristic constant of the pump at the design point. With the actual meaning of p_0, D depends somewhat on the tank conditions, but again it is a constant for fixed tank pressure. When $D = 0$, the flow rate can change while the delivery pressure stays constant, so that $D = 0$ represents the case of gas-pressurization; when $D = \infty$, the flow rate is constant despite changes in line pressure, a condition which is characteristic of a constant rate pump or of any other constant rate system, such as can be obtained with *cavitating Venturis*[32]. Intermediate values of D correspond to different types of pumps or different operating points for the same pump. For conventional centrifugal pumps, D is of the order of unity.

The capacity C_l of the equivalent line capacitance varies with the line pressure p_1. The equivalent spring constant χ of the capacitance is defined as the change in volume of the feed line produced by unit pressure rise in the line. Considering the propellant as incompressible, the difference of the flow rates upstream and downstream of the capacitance is given as

$$\dot{m}_0 - \dot{m}_1 = \rho_0 \chi \frac{dp_1}{dt} \qquad \ldots.(2.02.02)$$

where ρ_0 is the density of the propellant.

The instantaneous pressure drop in the feed line is due to the inertia of the propellant and to the frictional loss. Both can be easily taken into account[5, 7]. However, since it is desirable to reduce the number of parameters in a general treatment like the present one, and since the dynamic head in the feed line is usually much smaller than the pressure drop across the entire feeding system, the frictional loss is neglected and the pressure drop in the line in unsteady operation is assumed to be due to the acceleration of the flow only. Thus, for the feed line upstream of the equivalent line capacitance, we have

$$p_0 - p_1 = \frac{\gamma l}{A} \frac{d\dot{m}_0}{dt} \qquad \ldots.(2.02.03)$$

where A is the cross sectional area of the feed line*. Similarly, between the line capacitance and the control capacitance, we have

$$p_1 - p_2 = \frac{(1-\gamma)l}{A} \frac{d\dot{m}_1}{dt} \qquad \ldots.(2.02.04)$$

---

* If the lines are not of constant cross section, A is the equivalent sectional area used in the determination of the equivalent lengths l and γl.

where p_2 is the pressure at the control capacitance immediately upstream of the injector. The pressure drop across the injector is

$$p_2 - p = \tfrac{1}{2}\dot{m}_i^2/\rho_0 A_i^2 \qquad \ldots.(2.02.05)$$

where A_i is the effective orifice area of the injector. The inertia in the injector passage can be taken into account in the inertia of the line by a suitable increase of l. It is assumed that the injector walls are rigid enough so that A_i is not affected by pressure variations. For steady state operation,

$$\bar{p}_0 - \bar{p} = \Delta\bar{p} = \tfrac{1}{2}\bar{m}^2/\rho_0 A_i^2 \qquad \ldots.(2.02.06)$$

In unsteady state operation, $\dot{m}_i$ differs from $\dot{m}_1$ by the rate of accumulation of propellant in the control capacitance C_c

$$\dot{m}_1 - \dot{m}_i = \mathrm{d}C_c/\mathrm{d}t \qquad \ldots.(2.02.07)$$

The rate of variation of the control capacitance depends on the design of the feedback circuit. The signal that is picked up from the combustion chamber is assumed to be the pressure variation in the chamber. Discussion of the detailed design of the feedback circuit and the difficulties of practical realization is beyond the scope of the present treatment. We shall therefore specify only the overall feedback transfer function of the entire circuit without inquiring how and if it can be obtained in practice. The characteristics of an ordinary feedback circuit can usually be described by a linear algebraic relation between the input φ, the output C_c and their time derivatives with constant coefficients. Thus we can usually define the transfer function of the feedback circuit in dimensionless operational form as

$$F\left(\frac{\mathrm{d}}{\mathrm{d}z}\right) = \frac{C_c}{\bar{m}\theta_g}\Big/\varphi \qquad \ldots.(2.02.08)$$

where $F\,(\mathrm{d}/\mathrm{d}z)$ is the ratio of two polynomials of the differential operator $\mathrm{d}/\mathrm{d}z$.

Equations (2.02.01)–(2.02.08) describe completely the dynamics of the feeding system. These eight equations enable us to eliminate the following seven quantities $\dot{m}_0$, $\dot{m}_1$, p_0, p_1, p_2, A_i and C_c, to obtain a single relation between chamber pressure p and injection rate $\dot{m}_i$ which describes the overall behaviour of the feeding system. It is convenient to reduce all these equations into dimensionless form; and we find that when this is done four dimensionless parameters D, P, E, and J are sufficient in characterizing the overall system dynamics for low frequency oscillations, where

$$P = \frac{\bar{p}}{2\Delta\bar{p}}, \qquad E = \frac{2\Delta\bar{p}\rho_0\chi}{\bar{m}\theta_g}, \qquad J = \frac{l\bar{m}}{2\Delta\bar{p}A\theta_g} \qquad \ldots.(2.02.09)$$

and D is the constant of the feed pump; P is the pressure drop parameter, a relative measure of the pressure drop across the injector; E is the elasticity parameter, a ratio of the rate of mass accumulation in the line capacitance due to a characteristic rate of pressure change $2\Delta\bar{p}/\theta_g$ to the mean mass flow rate in the system; and J is the inertia parameter, a ratio of the time required to accelerate a given mass element from rest to the state of motion in the feed line under the pressure $2\Delta\bar{p}$ to the characteristic time of the system, that is, the gas residence time.

The dimensionless equation of the feeding system dynamics relating φ and μ_i is obtained as

$$\left\{P\left[1+DE(P+\tfrac{1}{2})\frac{d}{dz}+JEy\frac{d^2}{dz^2}\right]\right.$$
$$+\left[D(P+\tfrac{1}{2})\frac{d}{dz}+J\frac{d^2}{dz^2}+DJE(1-y)(P+\tfrac{1}{2})\frac{d^3}{dz^3}\right.$$
$$\left.+J^2Ey(1-y)\frac{d^4}{dz^4}\right]F\left(\frac{d}{dz}\right)\Bigg\}\varphi$$
$$+\left\{[1+D(P+\tfrac{1}{2})]+[DE(P+\tfrac{1}{2})+J]\frac{d}{dz}\right.$$
$$+[DJE(1-y)(P+\tfrac{1}{2})+JEy]\frac{d^2}{dz^2}$$
$$\left.+J^2Ey(1-y)\frac{d^3}{dz^3}\right\}\mu_i=0 \qquad \ldots\ldots(2.02.10)$$

Equation (2.02.10) essentially defines the overall transfer function μ_i/φ of the entire feeding system through the four characteristic dimensionless constants J, E, D, P, and the constants defining the feedback servo system. If the feed line does not contain gas bubbles or any other concentrated capacitance, the equivalent line capacitance should be located, in the present assumption of uniform cross section, half way between the pump outlet and the injector; that is, if the pump is placed at the outlet from the tank, $y=\frac{1}{2}$. This is the case formulated by H. S. TSIEN[9]. If there is a gas pocket of considerable size in the feed line, the capacitance C_i should be located in the immediate neighbourhood of the pocket. Despite the simplifying assumptions, equation (2.02.10) is still quite involved algebraically, and does not allow a general analytical discussion. Only two special cases, one with constant rate of supply, $D=\infty$, and the other with constant feed pressure, $D=0$, have been studied analytically by L. CROCCO[8]. However, the discussion of particular systems with given values of the constants can be made without difficulty using the complete equation (2.02.10).

2.03. General Considerations on the System of Equations. Intrinsic Instability

Equation (2.02.10) should be solved simultaneously with equation (2.01.11) for μ_i and φ. It is interesting to note that, in equation (2.01.11), the nozzle constant b can be very easily absorbed by a change of the characteristic time from θ_g to $\theta_r=\theta_g(1+b)$. The resulting equation in terms of the new dimensionless time $z'=z/(1+b)$ is identical in form with equation (2.01.11) after putting $b=0$. The overall transfer function μ_i/φ of the feeding system as defined by equation (2.02.10) can be obtained as a combination of y, P, D, $E\frac{d}{dz}$, $J\frac{d}{dz}$, and the expression $\frac{d}{dz}F\left(\frac{d}{dz}\right)=\frac{dC_e}{dt}\Big/\bar{m}\varphi$ relative to the feedback control circuit; these quantities are independent of the change of characteristic time. Therefore, for a given feeding system with

a given feedback control circuit, if any, the transfer function μ_i/φ is independent of the choice of the characteristic time, as can be physically expected. The dynamics of the burnt gas in the combustion chamber for systems with different exhaust nozzles is therefore governed by the same equation (2.02.10) and by the equation obtained from (2.01.11)

$$\frac{d\varphi(z)}{dz} + \varphi(z) = \mu_i(z - \bar{\tau}_i) + n[\varphi(z) - \varphi(z - \bar{\tau})] \quad \ldots.(2.03.01)$$

with the new dimensionless time variable $z = t/\theta_r$. All the dimensionless parameters like E, J, Ω and τ are of course defined in terms of the new characteristic time θ_r. For simplicity in writing, the prime, which is used to distinguish between the dimensionless time expressed in terms of the uncorrected reference time and the new corrected reference time is henceforth dropped with the understanding that if b is not zero, the characteristic time is $\theta_r = \theta_g(1 + b)$ instead of θ_g.

The phase lead component of the transfer function of the nozzle is due to the inertia of the gas in the subsonic portion of the nozzle which increases the capacity of the combustion chamber in storing burnt gas in response to increasing chamber pressure. In other words, a certain effective part of the volume of the subsonic portion of the nozzle should be added to the chamber volume in evaluating the gas residence time or the relaxation time of the chamber–nozzle combination. If the nozzle is very short so that the nozzle volume is negligibly small, it is expected that the assumption of quasi-steady flow in the nozzle should be valid and little correction on the gas residence time need be made.

Since both equations (2.02.10) and (2.03.01) are linear, the equation for $\varphi(z)$ after the elimination of μ_i is linear with constant coefficients but involves $\varphi(z - \bar{\tau}_i)$ and $\varphi(z - \bar{\tau})$ in addition to $\varphi(z)$. The presence of the retarded variable changes the analytical nature of the equation considerably as compared to that of an ordinary linear differential equation. The fact that there are two retarded functions with two different lags $\bar{\tau}_i$ and $\bar{\tau}$ is analytically a matter of minor importance but it makes the calculation and the presentation of the results much more involved. For this reason and because of the uncertainty of our knowledge of these time lags, the two have been assumed to be equal, that is, all the processes are sensitive throughout the time lag. As discussed in Section 1.11, this assumption is justifiable for the monopropellant case. It is clear that this restriction on the values of the time lags is not needed when $\bar{\tau}_i$ does not appear in the equations, as for instance in the simplest case of intrinsic instability to be treated in this section, or in the more complicated case of screaming. Thus, for the general treatment of chugging, we assume $\bar{\tau}_i = 0$ and $\bar{\tau}_c = \bar{\tau}$ unless otherwise stated.

The analytical nature and the methods of solution of the equation of the type

$$L_1\left(\frac{d}{dz}\right)\cdot[\varphi(z)] = L_2\left(\frac{d}{dz}\right)\cdot[\varphi(z - \bar{\tau})] \quad \ldots.(2.03.02)$$

as a general form of the eliminant of equations (2.03.01) and (2.02.10) is discussed in Appendix A. Since equation (2.03.02) is a linear equation

with constant coefficients, the solution of this equation is a linear combination of an infinite number of particular solutions of the type exp (sz) where s is a complex quantity with its imaginary part representing the angular frequency of the particular mode of oscillatory solution and the real part representing the amplification coefficient of this mode. The infinite number of values of s are defined as the roots of the following characteristic equation

$$L_1(s) = e^{-s\bar{\tau}} L_2(s) \qquad \ldots . (2.03.03)$$

A given oscillatory mode is stable, neutral or unstable depending upon whether the real part of s is less than, equal to or greater than zero, and a sufficient condition for the system to be stable is that the characteristic equation (2.03.03) has no root in the right half of the complex s plane. We shall begin the discussion with several simple ideal cases with a view to the fact that the influence on instability of certain important parameters like the time lag and the pressure index n of interaction of the combustion processes and chamber oscillations should qualitatively be the same for simple conditions as for cases involving complicated feeding systems.

The simplest case in which the injection rate is assumed to be independent of the pressure oscillations in the combustion chamber will first be considered. This fundamental case must be considered only as an ideal limit, though it can be approached with the use of a displacement pump or of a cavitating Venturi and with a careful design of rigid feed lines. For this case, $\mu_1 = 0$ and equation (2.03.01) becomes

$$\left[\frac{d}{dz} + (1 - n)\right]\varphi(z) = -n\varphi(z - \bar{\tau}) \qquad \ldots . (2.03.04)$$

so that the characteristic equation (2.03.03) becomes

$$s + 1 - n + ne^{-s\bar{\tau}} = 0 \qquad \ldots . (2.03.05)$$

Let $s = \Lambda + i\Omega$ and separate the real and imaginary parts of equation (2.03.05). We have

$$\left.\begin{aligned} \Lambda + (1 - n) + n\, e^{-\Lambda\bar{\tau}} \cos \Omega\bar{\tau} = 0 \\ \Omega - n\, e^{-\Lambda\bar{\tau}} \sin \Omega\bar{\tau} = 0 \end{aligned}\right\} \qquad \ldots . (2.03.06)$$

The quantity $\Omega\bar{\tau}$ is the angular displacement of the oscillation during the time lag, the ratio of $\Omega\bar{\tau}$ to 2π is therefore the ratio of the time lag $\bar{\tau}$ to the period of oscillation T.

$$\frac{\Omega\bar{\tau}}{2\pi} = \frac{\bar{\Omega}^*\bar{\tau}^*}{2\pi} = \frac{\bar{\tau}}{T} \qquad \ldots . (2.03.07)$$

From equation (2.03.06) it can be obtained that

$$\begin{aligned} f(\bar{\tau}, n) &= n\bar{\tau}\, e^{(1-n)\bar{\tau}} \\ &= \frac{\Omega\bar{\tau}}{\sin \Omega\bar{\tau}} \exp\left[-\frac{\Omega\bar{\tau}}{\tan \Omega\bar{\tau}}\right] = h(\Omega\bar{\tau}) \end{aligned} \qquad \ldots . (2.03.08)$$

which can be solved graphically for any set of given values n and $\bar{\tau}$. Both

f and h are universal functions and have been calculated[8] as shown in *Figure 5.* f $(\bar{\tau}, n)$ is plotted against $\bar{\tau}$ for several values of n on the left-hand side; and h $(\Omega, \bar{\tau})$ is plotted against $\Omega\bar{\tau}/2\pi$ on the right-hand side. The value of f $(\bar{\tau}, n)$ is read for given values of $\bar{\tau}$ and n. A horizontal line is drawn to cut the curves of h $(\Omega, \bar{\tau})$. At the intersections, the values of $\Omega\bar{\tau}/2\pi$ can be read and Ω calculated. Λ can be determined from the second of equations (2.03.06) as

$$e^{\Lambda\bar{\tau}} = n\bar{\tau}\frac{\sin\Omega\bar{\tau}}{\Omega\bar{\tau}} = \frac{n\bar{\tau}}{K(\Omega\bar{\tau})} \qquad \ldots\ldots(2.03.09)$$

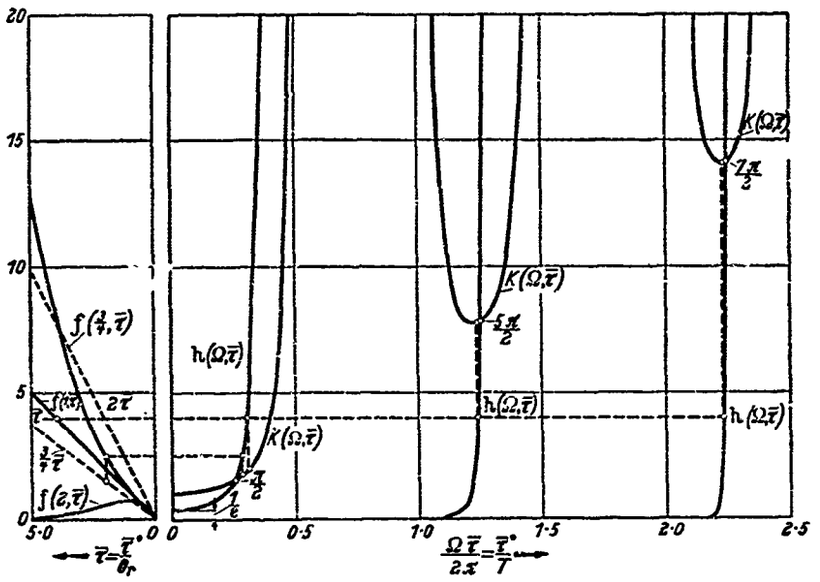

Figure 5. Graphical determination of eigenvalues $\Lambda + i\Omega$ of equation (2.03.06)
(By courtesy of the American Rocket Society)

The dotted straight lines in the left-hand side curves are $n\bar{\tau}$ for different values of n. $K(\Omega, \bar{\tau}) = \Omega\bar{\tau}/\sin\Omega\bar{\tau}$ is plotted in the right-hand side curves. The solution is stable, neutral or unstable depending upon $K(\Omega, \bar{\tau}) \gtrless n\bar{\tau}$.

An examination of the graphical solution leads to the following qualitative conclusions:

(*i*) For a given system ($\bar{\tau}$ and n given) there is an infinite number of oscillatory modes corresponding to increasing values of Ω not exactly in harmonic ratio. If the value of $\bar{\tau}$ is too small, the fundamental oscillating mode may be absent.

(*ii*) For a given system, $K(\Omega, \bar{\tau})$ increases with higher modes of oscillation while h $(\Omega, \bar{\tau})$, f $(n, \bar{\tau})$ and $n\bar{\tau}$ are all constants. If the jth mode is stable, all the modes higher than the jth are stable. Therefore, the necessary and sufficient condition for intrinsic stability is that the fundamental mode shall be stable.

(*iii*) For sufficiently small $\bar{\tau}$ all modes are stable regardless of the value of n.

The complete solution of equations (2.03.06) is only of academic interest. It is more in the line of small perturbation theory to determine the stability boundary of such ideal systems. Putting $\Lambda = 0$, equations (2.03.06) are compatible only when $\bar{\tau}$ takes some well determined values δ, that we call critical values, corresponding to neutral oscillations. Then the

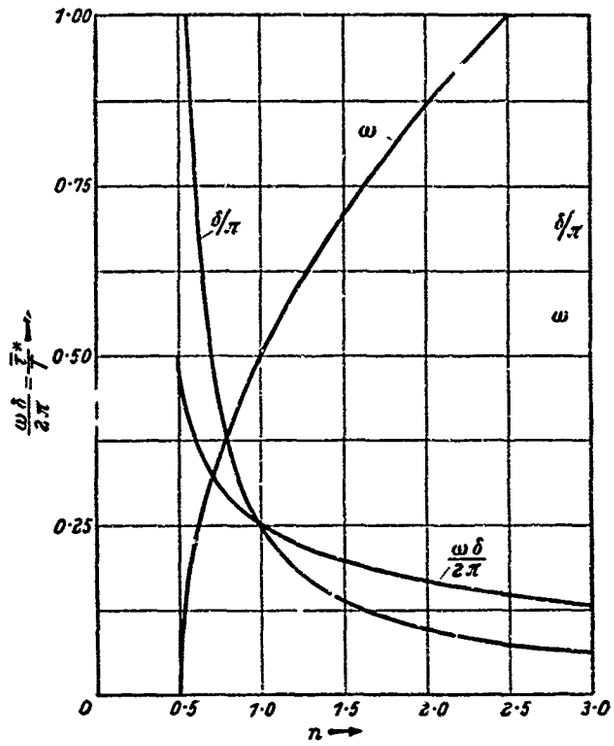

Figure 5. Critical values for intrinsic instability for different values of the interaction index n (courtesy of the American Rocket Society)

equations can be solved, giving the following critical values of $\bar{\tau}$ and Ω; i.e. δ and ω

$$\left.\begin{aligned} \omega &= (2n-1)^{\frac{1}{2}} \\ \cos\omega\delta &= -(1-n)/n \\ \delta &= \left[\pi - \cos^{-1}\frac{1-n}{n}\right](2n-1)^{-\frac{1}{2}} \end{aligned}\right\} \quad \ldots\ldots(2.03.10)$$

We see that neutral oscillations ($\Lambda = 0$) are not possible in our ideal system if $n < \frac{1}{2}$. This shows that if $n < \frac{1}{2}$, the system is always intrinsically stable no matter what the value of the time lag may be. For $n > \frac{1}{2}$ the values of the critical quantities for the fundamental mode are calculated from equations (2.03.10) and are plotted as shown in *Figure 6*. The stable and the unstable region for δ and ω can be easily determined from the ordinary

argument of smooth transition. It can also be seen analytically by determining the sign of $\frac{d\Lambda}{d\bar{\tau}}$ or $\frac{d\Lambda}{d\omega}$ evaluated from equations (2.03.06) at the critical point.

$$\left(\frac{d\Lambda}{d\bar{\tau}}\right)_{\Omega=\omega} = \frac{\omega^2}{1+\delta[(n-1)^2+1]} > 0$$

Thus for a system with a given value $n > \frac{1}{2}$, the system is intrinsically stable if $\bar{\tau} < \delta$ and intrinsically unstable if $\bar{\tau} > \delta$. The angular frequency of an unstable oscillation is less than ω while that of a stable oscillation is greater than ω.

From *Figure 6* it is clear that the critical time lag δ always decreases when n increases and its decrease is very fast when n is close to $\frac{1}{2}$. The unstable range of time lags, $\bar{\tau} > \delta$, δ widens with increasing n, which means that increasing n is destabilizing. The destabilizing effect of increasing the interaction index n is to be qualitatively expected on purely physical grounds.

The presence of the constant b which represents the phase lead of the nozzle transfer function increases the magnitude of the dimensional critical time lag $\bar{\tau}^* = \delta\theta_g(1+b)$ by the multiplier $(1+b)$, because δ is a constant for given n. Therefore the nozzle has a stabilizing effect in reducing the unstable range of time lags by increasing the critical value of $\bar{\tau}^*$, as compared with that of the limiting case of a very short nozzle in which the volume of its subsonic portion is negligibly small compared with the combustion chamber volume.

From *Figure 5* we see that the fundamental mode of the oscillating solutions does not exist when $f(n, \bar{\tau})$ is less than $1/e$. This situation arises either when $\bar{\tau}$ is sufficiently small for any given value of n or when $\bar{\tau}$ is sufficiently large and n is larger than unity. It can easily be seen that the latter case with $n > 1$ and large $\bar{\tau}$ corresponds to positive real roots for s and therefore to monotonically diverging solutions. Under this condition, the system is definitely unstable.

2.04. Systems with Constant Rate Feed

For a liquid rocket with a displacement pump or a cavitating Venturi that supplies propellant to the feeding line at a constant rate we have $D = \infty$ (*Figure 7*). Consider such a system without servo control, $F\left(\frac{d}{dz}\right) = 0$; divide equation (2.02.10) by D and let D go to infinity. Equation (2.02.10) is reduced to

$$PE\frac{d}{dz}p + \left[1 + E\frac{d}{dz} + (1-y)JE\frac{d^2}{dz^2}\right]\mu_i = 0 \qquad \ldots.(2.04.01)$$

It is clear that if the parameter J is computed from equation (2.02.09) using $l(1-y)$ as line length, the factor $(1-y)$ can be absorbed in J and cancelled from the equation. The physical meaning of this is that in this case the portion of the feed line between the pump and the equivalent line

capacitance operates at constant flow rate and therefore does not contribute to the dynamics of the system irrespective of its length. The only part of the line which has an influence on the dynamics is the one between the capacitance and the injector, of length $l(1-y)$.

Substituting μ_i from equation (2.04.01) into equation (2.03.01) with $\bar{\tau}_i = \bar{\tau}$ and with the new definition of J we have

$$\left(1-n+\frac{\mathrm{d}}{\mathrm{d}z}\right)\left(1+E\frac{\mathrm{d}}{\mathrm{d}z}+JE\frac{\mathrm{d}^2}{\mathrm{d}z^2}\right)\varphi(z)$$

$$+\left[n\left(1+E\frac{\mathrm{d}}{\mathrm{d}z}+JE\frac{\mathrm{d}^2}{\mathrm{d}z^2}\right)+PE\frac{\mathrm{d}}{\mathrm{d}z}\right]\varphi(z-\delta)=0 \qquad \ldots.(2.04.02)$$

By comparing equation (2.04.02) with equation (2.03.02) or postulating

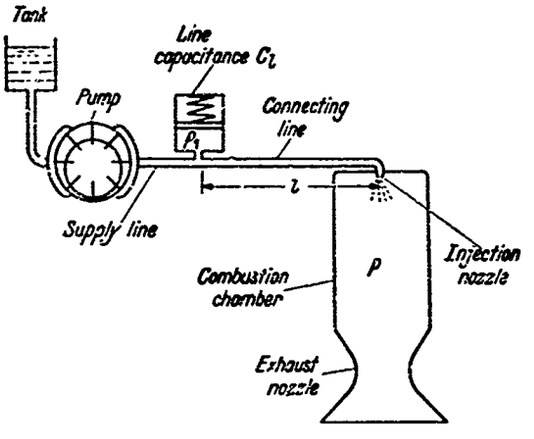

Figure 7. Schematic diagram of a constant rate feeding system (By courtesy of the American Rocket Society)

solutions of the exponential type $\exp(sz)$, the characteristic equation (2.03.03) takes the following form

$$(1+Es+JEs^2)\,[1+s-n+ne^{-\delta s}]+PEs\,e^{-\delta s}=0 \qquad \ldots.(2.04.03)$$

For the determination of the stability boundary, set $s=i\omega$, separate the real and imaginary parts of equation (2.04.03) and solve for $J\omega - 1/E\omega$ and δ. For convenience, let us define

$$\Psi = J\omega - 1/E\omega \qquad \ldots.(2.04.04)$$

which, in analogy to the terminology in the flow of alternating current in an electric circuit, may be tentatively called flow reactance of the feeding line for oscillations of frequency ω. We obtain:

$$\Psi^2 = \frac{(n+P)^2-n^2}{\omega^2-(2n-1)} - 1 \qquad \ldots.(2.04.05)$$

$$\delta = \frac{1}{\omega}\left[\pi - \tan^{-1}\frac{\omega}{1-n} - \tan^{-1}\frac{n+P}{n}\frac{1}{\Psi} + \tan^{-1}\frac{1}{\Psi}\right] \quad \ldots\ldots(2.04.06)$$

δ as obtained from equation (2.04.06) is multivalued. The smallest value of δ corresponds to the physical situation where the duration of the time lag is less than one oscillation period, and the neutral oscillation corresponding to this lowest value of δ can be given the name fundamental low frequency mode. Larger values of δ differ from the preceding one by multiples of π/ω, and these critical values of the time lag contain more than one complete oscillation period. The neutral oscillations corresponding to these larger values of δ are designated by integral number $h = 0, 1, 2, 3 \ldots$ indicating the number of oscillation periods that is contained in the time lag. The values of δ larger than the fundamental one, $h = 0$, may have an interesting physical meaning as will be discussed in the following.

Equations (2.04.05) and (2.04.06) define a relation between ω, n, P and δ. Thus δ depends only implicitly (through ω) on the other parameters E and J of the feeding system. This relation is represented in *Figures 8, 9* and *10* for

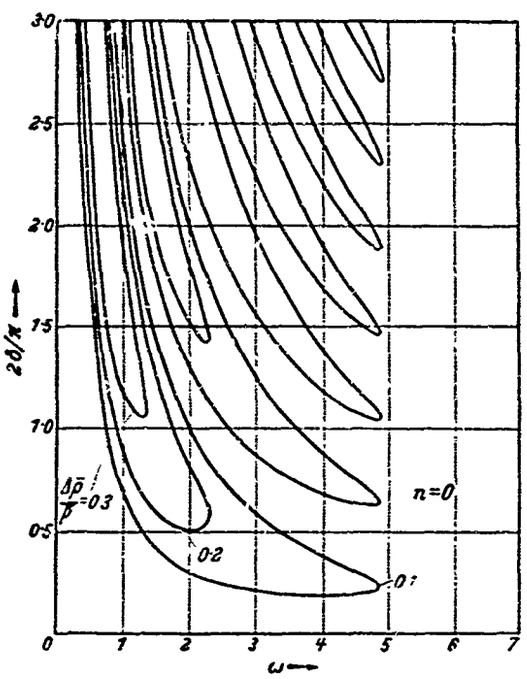

Figure 8. General relation between the critical values of the dimensionless sensitive time lag δ and the critical angular frequency of neutral oscillation ω, for different pressure drop parameters $\Delta\bar{p}/\bar{p}$ with $n = 0$

$n = 0$, $\frac{1}{2}$ and 1 respectively, and for a series of values of P. For given n and P equation (2.04.05) shows that a real Ψ, and hence a real δ, is obtained only if the following inequalities are satisfied:

$$2n - 1 \leqslant \omega^2 \leqslant (P+1)(P+2n-1) \quad \ldots\ldots(2.04.07)$$

The first inequality $\omega^2 \geqslant 2n - 1$ indicates that if $n < \frac{1}{2}$, the range of ω reaches 0; but if $n > \frac{1}{2}$, the range of possible critical frequencies starts with the positive value $(2n-1)^{\frac{1}{2}}$, which coincides with the critical frequency of intrinsic instability. In both cases the range of critical frequencies

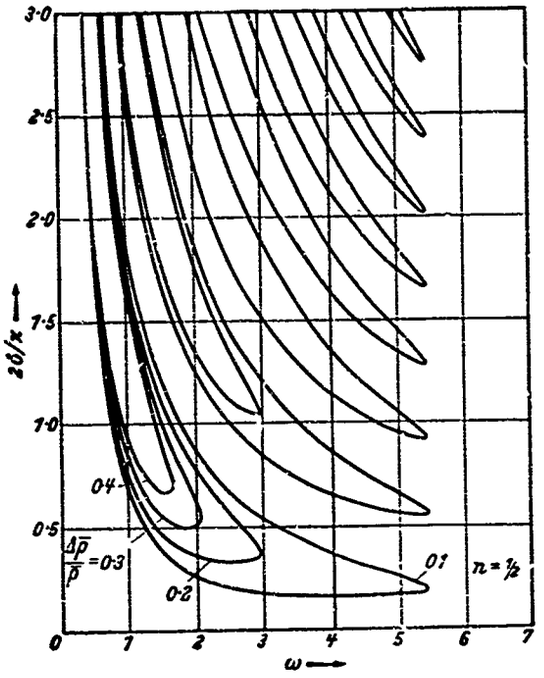

Figure 9. General relation between the critical values of the dimensionless sensitive time lag δ and the critical angular frequency of neutral oscillation ω, for different pressure drop parameters $\Delta\bar{p}/\bar{p}$ with $n = \frac{1}{2}$

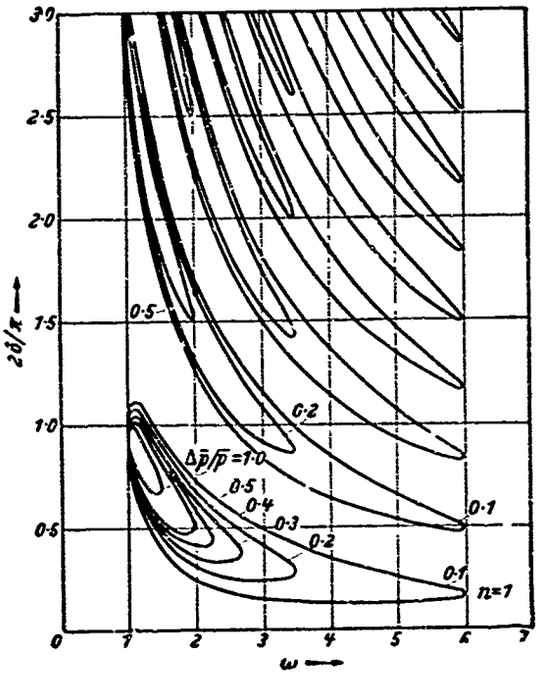

Figure 10. General relation between the critical values of the dimensionless sensitive time lag δ and the critical angular frequency of neutral oscillation ω, for different pressure drop parameters $\Delta\bar{p}/\bar{p}$ with $n = 1$

extends up to a maximum value defined by the second inequality (2.04.07) as is well illustrated in the figures.

For each value of ω within the possible range there are two fundamental values of δ, the smaller corresponding to the positive and the larger to the negative value of Ψ as given by equation (2.04.05). Both signs are physically possible, as is shown by equation (2.04.04). At the two limits of the inequality (2.04.07), that is when Ψ is infinite or zero, the two values of δ coincide. Therefore, if one takes into account the multiple values of δ, the curves of constant P appear as a multiplicity of half closed loops when $n < \frac{1}{2}$ or of completely closed loops when $n > \frac{1}{2}$. To understand the meaning of these loops we must introduce the conditions of the feeding system, as expressed by equation (2.04.04). Equating the values of Ψ given by this equation and by equation (2.04.05) we obtain

$$\frac{1}{E^2\omega^2} - 2\frac{J}{E} + J^2\omega^2 = \frac{(n+P)^2 - n^2}{\omega^2 - (2n-1)} - 1 \qquad \ldots.(2.04.08)$$

which can be developed as an equation of third degree in ω^2. The positive roots of this equation determine the critical frequencies as functions of n, P, E, and J. Without entering into a complicated analytical discussion of the roots, qualitative results can be obtained from the following considerations, as shown in detail in Appendix C.

(*1*) Increasing the interaction index n is strongly destabilizing in as much as the unstable ranges of $\bar{\tau}$ are widened.

(*2*) Increasing the pressure drop across the feeding system (essentially across the injector) generally has a stabilizing effect.

(*a*) When $n < \frac{1}{2}$, a sufficiently large pressure drop with $\Delta\bar{p}/\bar{p} < \frac{1}{2}.1/(1-2n)$ can guarantee stable combustion for arbitrary elasticity and inertia conditions of the feeding system and in particular for arbitrary values of the time lag. We call this unconditional stability. If the pressure drop is not large enough, the system is stable only when the value of the time lag $\bar{\tau}$ is ir a certain stable range or within ranges of values which depend on the elasticity and inertia of the feed system. We call this conditional stability. An increase in the pressure drop (decrease in P) tends to decrease the unstable ranges of the values of $\bar{\tau}$ and is therefore stabilizing.

(*b*) When $n > \frac{1}{2}$, no matter how large the pressure drop is, unconditional stability cannot be obtained. The system can be stable only when the time lag is less than a certain critical value depending on the magnitudes of P, E, and J. Increasing the pressure drop is in general stabilizing in increasing the critical values δ or the stable range of $\bar{\tau}$, except when E is very small so that the flow reactance $\Psi = J\omega - 1/E\omega$ is very large and negative.

(*3*) The elasticity parameter E and the inertia paramete. J have similar complicated effects.

(*a*) If the system is unconditionally stable when $n < \frac{1}{2}$, any increase in E or J makes the system less stable in the sense that the system is closer to the condition of marginal unconditional stability. Any decrease in E or J makes the system more stable.

(*b*) If a system is unstable when $n < \frac{1}{2}$ with given values of E, J, and P, the system can be made unconditionally stable by sufficiently decreasing

the parameters E and/or J. The system can also be made conditionally stable by sufficiently increasing the parameters E and/or J. However, a small change of E and/or J may make a stable system unstable and an unstable system stable depending upon the circumstances.

(*c*) For systems with $n > \frac{1}{2}$ and a given value of P, the system will always be unstable for any values of E and J if the time lag $\bar{\tau}$ of the system is larger than a certain value corresponding to the maximum value of δ of the lowest loop as shown in *Figure 10*. An unstable system of this kind can be

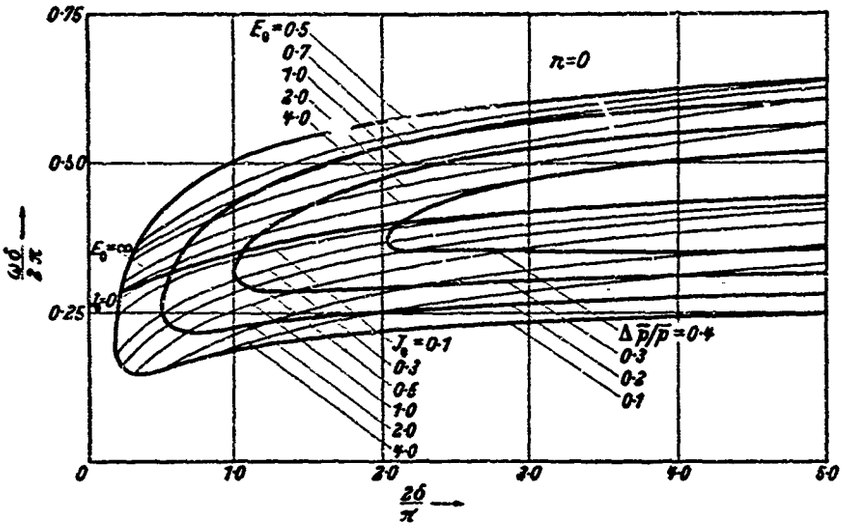

Figure 11. General relation between the critical time lag and the ratio of the critical time lag to the period of oscillations for different pressure drop parameters $\Delta\bar{p}/\bar{p}$ with $n = 0$
(By courtesy of the American Rocket Society)

made conditionally stable only by *decreasing* the pressure drop $\Delta\bar{p}$ across the feed system accompanied by a proper change of the parameters E and/or J.

(*d*) For an unstable system with $n > \frac{1}{2}$ and a given value of P, with the time lag $\bar{\tau}$ less than the maximum value of δ mentioned in (*c*), the system can be made conditionally stable either by a sufficiently large decrease of E and/or J (upper branch) or by a sufficiently large increase of E and/or J (lower branch). Again a small change of E and/or J may make a stable system unstable or make an unstable system stable depending upon the original configuration.

Before closing this section we observe that while it is impossible to present on a single graphical representation the quantitative results for general E and J, this is possible if either E or J is given a fixed value. The equation obtained from (2.04.08) after extracting the square root with the suitable sign furnishes the other parameter E as a function of n, P, and ω, if J is selected, so that the curves of constant P and given n (such as those of *Figures 8*, *9* and *10*) can be calculated using E as a parameter for the assigned value of J. This has been done for the particular value $J = 0$ in which case the curves of constant E are drawn; and for the value $E = \infty$, in

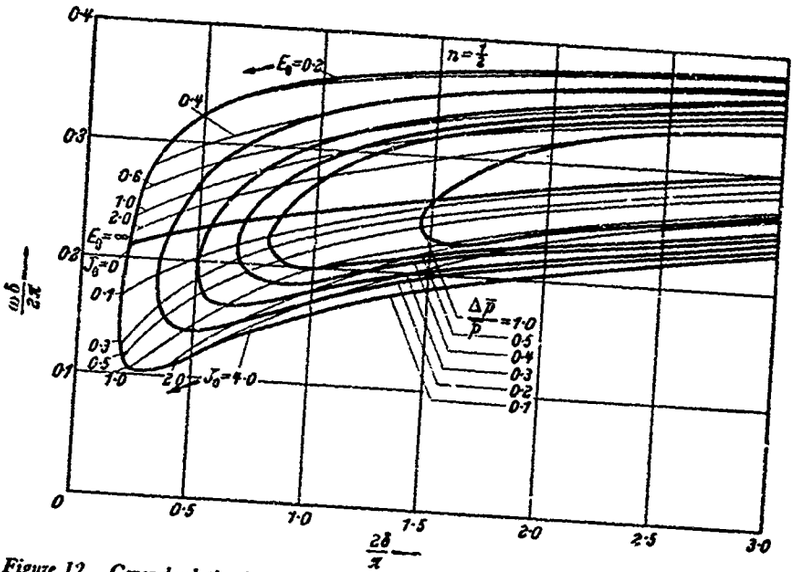

Figure 12. General relation between the critical time lag and the ratio of the critical time lag to the period of oscillations for different pressure drop parameters $\Delta\bar{p}/\bar{p}$ with $n = \frac{1}{2}$
(By courtesy of the American Rocket Society)

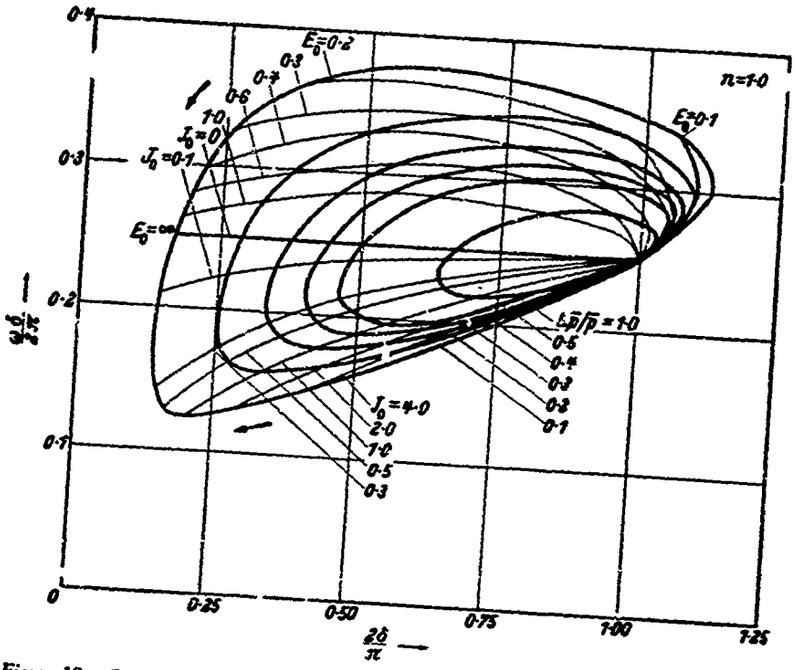

Figure 13. General relation between the critical time lag and the ratio of the critical time lag to the period of oscillations for different pressure drop parameters $\Delta\bar{p}/\bar{p}$ with $n = 1$
(By courtesy of the American Rocket Society)

which case lines of constant J are traced on the figures (this case corresponding, as already mentioned, to a particular system with constant feed pressure). The results are shown in *Figures 11, 12* and *13* where, however, for clarity the plane $(2\delta/\pi, \omega\delta/2\pi)$ has been used instead of the plane $(\omega, 2\delta/\pi)$. The ordinate $\omega\delta/2\pi$ has an interesting physical meaning, as shown by equation (2.03.07). The case $J = 0$ for $n = 0$ and $n = \frac{1}{2}$ exhibits the characteristic behaviour, already discussed, that a curve $E =$ constant may

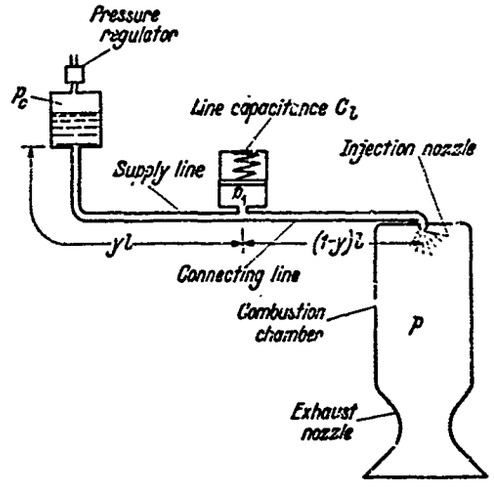

Figure 14. Schematic diagram of a constant pressure feeding system. (By courtesy of the American Rocket Society)

present two intersections with the lines $P =$ constant, thus determining finite unstable ranges of $\bar{\tau}$.

This behaviour is never present for $n = 1$; nor for $n = 0$ and $n = \frac{1}{2}$ when $E = \infty$. The line $J =$ constant shows only one intersection with each of the lines $P =$ constant. In this case the hyperbola of *Figure 64* degenerates into two straight lines through the origin, one being vertical. While the smaller root ω goes to zero and the corresponding δ to ∞, there is only one significant root ω left. The conditions in this case are similar to those of $n > \frac{1}{2}$ represented by *Figure 13.*

2.05. Systems with Constant Pressure Feed

In a liquid propellant rocket with constant pressure feed, as can be obtained through simple gas pressurization, the pump characteristics are represented by $D = 0$. A schematic diagram of such a system without servo control is shown in *Figure 14.* The feeding system equation is obtained from equation (2.02.10) by putting $D = 0$ and dropping the term $F(\mathrm{d}/\mathrm{d}z)$ related to the servo control, and can be written as

$$P\left[1 + JEy\frac{\mathrm{d}^2}{\mathrm{d}z^2}\right]\varphi + \left[1 + J\frac{\mathrm{d}}{\mathrm{d}z} + JEy\frac{\mathrm{d}^2}{\mathrm{d}z^2} + J^2Ey\,(1-y)\frac{d^3}{\mathrm{d}z^3}\right]\mu_i = 0 \quad \ldots.(2.05.01)$$

Substitute μ_i from equation (2.05.01) into equation (2.03.01) and take $\bar{\tau}_i = \bar{\tau}$ for the reasons discussed in the preceding section. For the particular

solution of exponential type exp (sz), equation (2.03.01) takes the form

$$[1 + Js + JEys^2 + J^2Ey(1-y)s^3](1 + s - n + ne^{-\tau s}) + Pe^{-\tau s}(1 + JEys^2) = 0 \quad \ldots (2.05.02)$$

Equating the moduli and the arguments of the two terms of equation (2.05.02) when $s = i\omega$ for neutral oscillations and $\tau = \delta$ we have

$$\left.\begin{aligned} &\{[1 - JEy^2\omega^2]^2 + J^2\omega^2[1 - JEy(1-y)\omega^2]^2\}[(1-n)^2 + \omega^2] \\ &\quad = [(1 - JEy^2\omega^2)n + (1 - JEy\omega^2)P]^2 \\ &\qquad\qquad + n^2J^2\omega^2[1 - JEy(1-y)\omega^2]^2 \\ &\tan^{-1}\frac{\omega}{1-n} + \tan^{-1}\frac{J\omega[1 - JEy(1-y)\omega^2]}{1 - JEy\omega^2} \\ &\quad = \pi + \tan^{-1}\frac{nJ\omega[1 - JEy(1-y)\omega^2]}{n[1 - JEy^2\omega^2] + P[1 - JEy\omega^2]} - \omega\delta \end{aligned}\right\} \quad \ldots (2.05.03)$$

A general discussion of equations (2.05.03) with arbitrary y is practically impossible. Therefore, leaving the general form of these equations for numerical computations with practical values of the parameters, we shall investigate here only those simple cases obtained with particular values of y. Suppose first that the capacitance is concentrated at the injector end of the line, that is $y = 1$. Then equations (2.05.03) are reduced to

$$[(1 - JE\omega^2)^2 + J^2\omega^2][(1-n)^2 + \omega^2] = (1 - JE\omega^2)^2(n + P)^2 + n^2J^2\omega^2$$

$$\tan^{-1}\frac{\omega}{1-n} + \tan^{-1}\frac{J\omega}{1 - JE\omega^2} = \pi + \tan^{-1}\frac{n}{P+n}\frac{J\omega}{1 - JE\omega^2} - \omega\delta$$

It is easily observed that the quantity $E\omega - 1/J\omega$ can represent all the feeding line parameters. We shall tentatively call this quantity Φ, the flow susceptance of the feed line when the oscillating flow has an equivalent frequency ω in analogy to the terminology in alternating current circuitry. Thus we have, solving for Φ^2 and δ:

$$\Phi = E\omega - 1/J\omega \quad \ldots (2.05.04)$$

$$\Phi^2 = \frac{\omega^2 + (1-n)^2 - n^2}{(n+P)^2 - \omega^2 - (1-n)^2} \quad \ldots (2.05.05)$$

$$\delta = \frac{1}{\omega}\left[\pi - \tan^{-1}\frac{\omega}{1-n} + \tan^{-1}\frac{n+P}{n}\Phi - \tan^{-1}\Phi\right] \quad \ldots (2.05.06)$$

Comparing equations (2.05.05) and (2.05.06) with equations (2.04.05) and (2.04.06) we see that the flow susceptance Φ, in a constant pressure system with $y = 1$, plays the same role as minus the reciprocal of the flow reactance, $-1/\Psi$, in a constant rate system. In fact, the relation between δ and n, P, ω as obtained from equations (2.05.05) and (2.05.06) is exactly the same as the one obtained from equations (2.04.05) and (2.04.06); a point corresponding to a given value of Φ is the same as the point corresponding to the identical value of $-1/\Psi$ in the two different problems.

Thus, the curves of *Figures 8, 9* and *10* apply also to the constant pressure system. The inequality (2.04.07) applies too, with $\Phi = \pm\infty$ at the upper limit of ω, and $\Phi = 0$ at the lower limit of ω (the latter being real only for $n \geqslant \frac{1}{2}$). The upper branches of the curves correspond to positive values of Φ and the lower ones to negative values. The discussion of the equation

$$E^2\omega^2 - 2\frac{E}{J} + \frac{1}{J^2\omega^2} = \frac{(n+P)^2 - n^2}{(n+P)^2 - (1-n)^2 - \omega^2} - 1 \quad \ldots.(2.05.07)$$

which is obtained from equations (2.05.04) and (2.05.05) can be conducted in a manner similar to the discussion of equation (2.04.08).

This has been done in Appendix D with qualitative conclusions similar to those of Section 2.04.

We have thus far discussed the constant pressure case with the particular value $y = 1$. For $y = 0$, equation (2.05.03) becomes exactly the same as if we put $E = 0$. Thus the general behaviour of the system would seem to be fundamentally unchanged by the location of the equivalent line capacitance, though the magnitude of the quantitative results may be significantly affected. An investigation on the effect of intermediate values of y has not yet been made.

Before closing this section let us observe that if we were interested in analysing the combustion stability with more complicated feeding systems, for example with some finite value of D, or the use of feedback servo control, the algebra involved in the analytical procedure illustrated in Sections 2.04 and 2.05 becomes increasingly heavy and makes it difficult to draw general conclusions.

2.06. Servo Stabilization

The importance of the characteristic constants, D, P, E and J of a feeding system has been illustrated by the previous special cases. It has been shown that a chugging liquid propellant rocket motor can be stabilized in certain circumstances by increasing sufficiently the pressure drop in the feeding system, by proper adjustment of the feeding line length, etc. Unfortunately, however, this is not always true, especially for large n, and even when it is true, it may result in impracticable length or size of lines or in excessive weights when large pressure drops are required. H. S. Tsien[9] analysed the possibility of stabilizing a chugging motor by introducing a feedback servo link as was suggested by W. Bollay[21]. The purpose of this servo system is to modify the overall characteristics of the feeding system in response to the chamber pressure oscillation without modifying the values of D, P, E and J which are favoured from other design points of view. In view of the heavy algebraic manipulations involved in analysing the feeding system, especially when an arbitrary control capacitance is introduced, Tsien preferred the use of the Satche diagram and the associated Nyquist diagram. The principles involved in this graphical analysis are explained in Appendix A. This graphical method can be used advantageously in determining whether a given system with known constants is stable or unstable. The procedure is to write the characteristic equation (2.03.03) as

$$G(s) = e^{-s} - g(s) = 0 \quad \ldots.(2.06.01)$$

with $$g(s) = L_1(s)/L_2(s)$$

where L_1 and L_2 are polynomials of s with known constant coefficients. Let s trace the contour C in the complex s plane in a clockwise direction. The contour C consists of the imaginary axis and a semicircle with infinitely large radius enclosing the entire right half of the complex plane. While s is tracing the contour C, $e^{-\bar{\tau}s}$ will follow the unit circle about the origin when s is on the imaginary axis, and will lie inside the unit circle when s is on the semicircle. The value of $g(s) = L_1(s)/L_2(s)$ is calculated from point to point and plotted in the complex s plane. Usually, it is only necessary to compute $g(s)$ while s is on the imaginary axis. The closing arc of $g(s)$ when s is on the semicircle can be obtained just by observation.

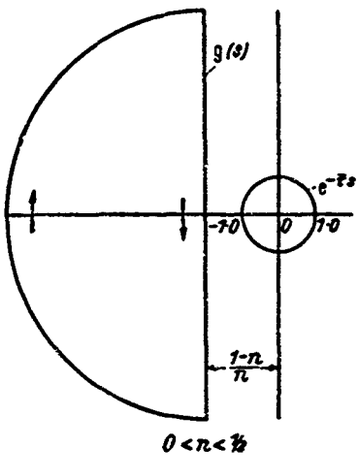

Figure 15. Schematic Satche diagram for a liquid rocket with $0 < n < \frac{1}{2}$. The system is intrinsically stable for arbitrary values of the time lag. (By courtesy of the American Rocket Society)

This plot in the complex s plane is called the Satche diagram. The vector with vertex on the plot of $e^{-\bar{\tau}s}$ and tail on the plot of $g(s)$ with the same value of s represents the complex quantity $G(s)$. A plot of $L_2(s)$ is also made while s traces the same contour C. This is the associated Nyquist diagram. If the vector $G(s)$ makes a_s complete counterclockwise revolutions and the vector $L_2(s)$ makes a_n complete clockwise revolutions while s traces the contour C, then the difference $a_s - a_n$ represents the number of zeros of $G(s)$ in the right half of the complex s plane. A system is stable if $a_s - a_n = 0$, which means that there is no root of the characteristic equation with positive real part. To illustrate the use of the Satche and associated Nyquist diagrams, we first consider a few simple examples.

For the case of intrinsic instability, we obtain from equation (2.03.02)

$$g(s) = L_1(s)/L_2(s) = -(1-n)/n - s/n \qquad \ldots.(2.06.02)$$

While s is travelling on the imaginary axis from $-i\infty$ to $+i\infty$, $g(s)$ traces a straight line parallel to the imaginary axis extending from $-(1-n)/n + i\infty$ to $-(1-n)/n - i\infty$. When s is at infinity on the real axis, $g(s)$ is also real but is negatively infinite. The closing arc of the trace of $g(s)$ is therefore a semicircle through the negative infinity. If $0 < n < \frac{1}{2}$, the trace of $g(s)$ is completely outside the unit circle and does not encircle the unit circle, *Figure 15*. An observation of this diagram shows that the vector $G(s) = e^{\bar{\tau}s} - g(s)$ will not make any counterclockwise revolutions, i.e. $a_s = 0$. Since $L_2(s)$ is a constant independent of s, we have $a_n = 0$. The system is therefore always stable regardless of the value of $\bar{\tau}$.

On the other hand, if $n > \frac{1}{2}$, the straight line portion of the plot of g (s) intersects the unit circle, *Figure 16.* In this case stability is possible only if the vector $e^{-i\delta}$ remains to the right side of the straight line $-(1-n)/n$ when the vector g (s) lies inside the unit circle. This condition is satisfied if

$$\cos [\bar{\tau}(2n-1)^{\frac{1}{2}}] > -(1-n)/n$$

The critical values ω and δ are thus found as:

$$\left.\begin{aligned} \omega &= (2n-1)^{\frac{1}{2}} \\ \delta &= [\pi - \cos^{-1}\{(1-n)/n\}]/(2n-1)^{\frac{1}{2}} \end{aligned}\right\} \quad \ldots . (2.06.03)$$

which agree with equations (2.03.10) as are given in Section 2.03.

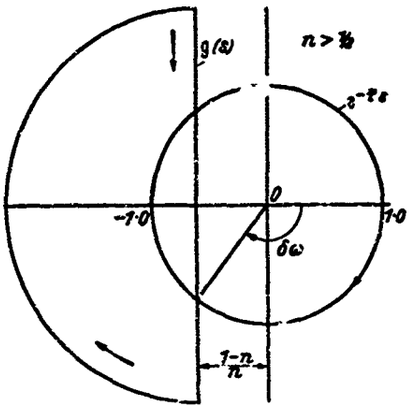

Figure 16. Schematic Satche diagram of a liquid rocket with $n > \frac{1}{2}$. The system is stable only for sufficiently small values of the time lag. (By courtesy of the American Rocket Society)

In the analysis of a more general system, the Satche diagram becomes a little more involved, and it is no longer possible to determine the frequency of neutral oscillation in a simple manner as in the case of intrinsic instability.

From equations (2.02.10), (2.03.01) and (2.06.01) we obtain the function for the plot of the Satche diagram as

$$g(s) = -\frac{s + (1-n)}{n + \frac{A}{B} + \frac{C}{B}F(s)} = -\frac{s + (1-n)}{n - N} \quad \ldots . (2.06.04)$$

where

$$\left.\begin{aligned} A &= P[1 + DE(P + \tfrac{1}{2})s + JEys^2] \\ B &= [1 + D(P + \tfrac{1}{2})] + [DE(P + \tfrac{1}{2}) + J]s \\ &\quad + [DJE(1-y)(P + \tfrac{1}{2}) + JEy]s^2 + J^2Ey(1-y)s^3 \\ C &= D(P + \tfrac{1}{2})s + Js^2 + DJE(1-y)(P + \tfrac{1}{2})s^3 \\ &\quad + J^2Ey(1-y)s^4 \end{aligned}\right\} \quad \ldots . (2.06.05)$$

The quantity $N(s)$ in equation (2.06.04) represents the ratio of the fractional variation of the injection rate and the fractional variation of

combustion chamber pressure, or the transfer function of the feeding system. With $s = i\Omega$, the function N is in general complex and can be written as

$$N(\Omega) = N_r(\Omega) + i\Omega N_i(\Omega) = -\left[\frac{A}{B} + \frac{C}{B}F(i\Omega)\right] \quad \ldots.(2.06.06)$$

where both N_r and N_i are real functions of Ω. The imaginary part must approach zero as Ω approaches zero. $N(0) = N_r(0)$ is a real constant for a given feed system. This constant represents the steady state value of the ratio of the fractional variation of injection rate and the fractional variation of chamber pressure. For systems that are not servo-controlled

$$N(0) = N_r(0) = -P/[1 + D(P + \tfrac{1}{2})] < 0 \quad \ldots.(2.06.07)$$

which is always less than zero. This last part has some important consequences as will be seen later [equation (2.06.13)].

To illustrate the application of the Satche diagram in determining the stability of a given system with known constants, let us consider the following examples as given by Tsien[9†].

Consider a system in which the dynamics of the feeding system is defined by the following constants [see equation (2.02.10)]

$$D = 1, \quad P = \tfrac{3}{2}, \quad J = 4, \quad E = \tfrac{1}{4}, \quad \text{and} \quad y = \tfrac{1}{2}$$

The index of interaction n is selected as $\frac{1}{2}$, which is the value of marginal intrinsic instability. The g (s) without servo control is

$$\mathrm{g}\,(s) = -\tfrac{1}{2}\,\frac{(2s+1)\,(2s^3 + 3s^2 + 9s + 6)}{s^3 + 3s^2 + 6s + 6} \quad \ldots.(2.06.08)$$

Owing to the symmetry of the diagram when s takes positive or negative values of Ω, it is only necessary to plot the diagram for positive values of Ω. The diagram for $\Omega = 0$–$5{\cdot}2$ is shown in *Figure 17*. The closing arc when $|s| \to \infty$ intersects the negative real axis at ∞. When s traces the imaginary axis, the curve of g (s) intersects the unit circle.

If a servo-controlled capacitance is introduced next to the injector and the transfer function of the servo link is

$$F(s) = -4{\cdot}875\,\frac{(s + 1{\cdot}0528)\,(s^2 + 0{\cdot}7164s + 2{\cdot}6304)}{s(s+2)\,(s+3)\,(s + 0{\cdot}5332)\,(s^2 + 0{\cdot}4668s + 3{\cdot}7511)} \quad \ldots.(2.06.09)$$

then the function g (s) becomes

$$\mathrm{g}\,(s) = -2\,\frac{(s+2)\,(s+3)}{s+6} \quad \ldots.(2.06.10)$$

† The data presented in the rest of this section as shown in *Figures 17* and *18* are reproduced from ref. 9, by courtesy of the American Rocket Society.

This function g (*s*) is also plotted in *Figure 17* and is seen to be completely outside the unit circle. The associated Nyquist diagrams for both cases do not encircle the origin. Thus we see that the system without servo control can become unstable if the time lag $\bar{\tau}$ is sufficiently large, but the same system equipped with the prescribed servo control is stable for all values of the time lag; that is, the servo-controlled system is unconditionally stable.

As a second example take

$n = \frac{1}{2}$, $P = \frac{3}{2}$, $J = 4$, $E = \frac{1}{4}$ and $D = 0$ (constant pressure feed)

Without using servo control, we have

$$g(s) = -\tfrac{1}{2}\frac{(2s+1)(2s^3+s^2+8s+2)}{s^3+2s^2+4s+4} \quad \ldots.(2.06.11)$$

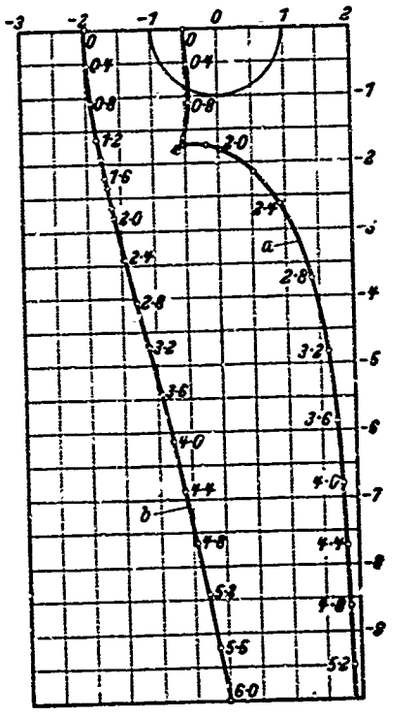

Figure 17. Satche diagrams of a monopropellant rocket with $n = \frac{1}{2}$ and the following feeding system constants: $E = \frac{1}{4}$, $J = 4$, $P = \frac{3}{2}$, $D = 1$, and $\gamma = \frac{1}{2}$.

(a) Satche diagram of the system without servo control; (b) Satche diagram of the system controlled by a capacitance servomechanism with its transfer function specified by equation (2.06.09).

Numerals on curves indicate values of Ω. (By courtesy of the American Rocket Society)

The Satche diagram for such a system is shown in *Figure 18*. The plot of g (*s*) intersects the unit circle. If a servo-controlled capacitance is introduced next to the injector with transfer function

$$F(s) = -4{\cdot}875\frac{(s+0{\cdot}8126)(s^2-0{\cdot}04337s+2{\cdot}6506)}{s^2(s+2)(s+3)(s^2+4)} \quad \ldots.(2.06.12)$$

the plot of g (*s*) is shifted completely out of the unit circle. Again, we see that a system which may possibly become unstable for certain values of time lags can be made stable for all time lags by the use of servo control.

In the first example the g (*s*) curve has a tendency to make a loop outside the unit circle of e^{-is}. In the second example the loop has grown up and is tangent to the unit circle at about $\Omega = 2{\cdot}0$. If the constants are further

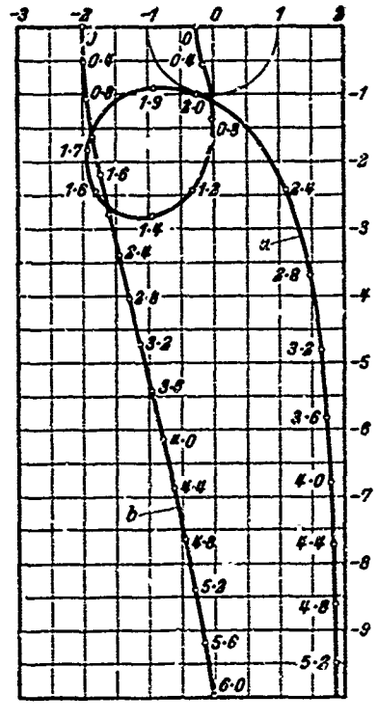

Figure 18. Satche diagrams of a monopropellant rocket with $n = \frac{1}{2}$ and the following feeding system constants: $E = \frac{1}{4}$, $J = 4$, $P = \frac{3}{2}$, $D = 0$, and $\gamma = \frac{1}{4}$.

(a) Satche diagram of the system without servo control; (b) Satche diagram of the system controlled by a capacitance servomechanism with its transfer function specified by equation (2.06.12).

Numerals on curves indicate values of Ω.

(By courtesy of the American Rocket Society)

adjusted, the loop may intersect the unit circle or even encircle the unit circle. Furthermore, more than one such loop may develop. Let us consider the Satche diagram with one loop intersecting the unit circle as shown

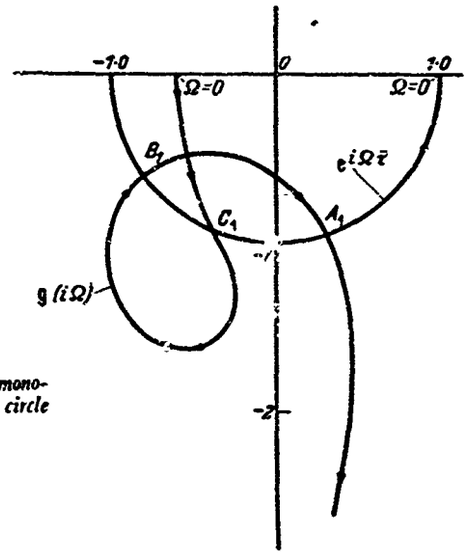

Figure 19. Schematic Satche diagram of a monopropellant rocket with a loop intersecting the unit circle

schematically in *Figure 19*. The three intersections are indicated by C_1, B_1 and A_1 in the order of increasing Ω. When $\Omega = 0$, the vector $G(0)$ lies on the abscissa with head at the point (1,0) and tail at the point [g(0), 0]. When Ω increases, g $(i\Omega)$ and $e^{-i\Omega\tau}$ move along their respective curves

toward A_1 as indicated by arrows in *Figure 19*. If $\bar{\tau}$ is sufficiently small, $e^{-i\Omega\tau}$ will not have passed A_1 before $g(i\Omega)$ reaches A_1. The system is therefore stable.

If $\bar{\tau}$ is slightly larger than a critical value corresponding to the situation where $g(i\Omega)$ and $e^{-i\Omega\tau}$ reach A_1 simultaneously (neutral oscillation or stability boundary), then it easily follows that the system will become unstable. If the magnitude of $\bar{\tau}$ is further increased, so that $e^{-i\Omega\tau}$ has passed the point B_1 before $g(i\Omega)$ reaches B_1, but $e^{-i\Omega\tau}$ has not reached C_1 before $g(i\Omega)$ leaves C_1, then an investigation shows that the vector $G(s)$ will not make complete revolutions, and the system will remain stable.

Finally if $\bar{\tau}$ is sufficiently large so that $e^{-i\Omega\tau}$ passes C_1 before $g(i\Omega)$ reaches C_1, instability is again obtained. Thus we see that there are two distinct ranges of values of $\bar{\tau}$ for unstable operation of the system, defined by the interval between points A_1, B_1 and the region beyond the point C_1. This characteristic phenomenon has been observed in Appendices C and D as shown schematically in *Figures 66*(a) and *69*(a). It should be noted that the intersection of the loop with the unit circle does not necessarily introduce discrete unstable ranges of the time lag. For example, if A_1 lies on the minor arc B_1C_1 of the unit circle, the intersection of the loop with unit circle B_1A_1 does not introduce any discrete unstable ranges of $\bar{\tau}$. The only critical value of $\bar{\tau}$ is defined by the intersection C_1. A simple observation of the Satche diagram cannot always reveal the stability of the system, and an investigation of the rotation of the vector $G(s)$ must be made, which is only possible when the value of the time lag $\bar{\tau}$ of the system is known. Thus if the time lag is known only up to its order of magnitude and if the Satche diagram is not simple as that shown in *Figure 17*, it is not straightforward to conclude from the Satche diagram whether the system is stable or not.

Since we do not know the value of the time lag of a given system with reasonable accuracy, we can consider a system as stable, from a practical design point of view, only when we are sure that the system is stable for a sufficiently wide range of the values of the time lag; or to be on the safe side, for arbitrary values of the time lag. The latter case is what we have called unconditional stability. This graphical method based on the Satche and Nyquist diagrams provides a simple geometrical criterion for unconditional stability, especially when the associated Nyquist diagram of $L_2(s)$ does not encircle the origin. Under this circumstance, the requirement for unconditional stability is simply that the Satche diagram of $g(s)$ must not intersect, nor encircle the unit circle. Thus if $g(0)$ with $\Omega = 0$ lies inside the unit circle, the system cannot be unconditionally stable because $g(i\Omega)$ becomes very large when Ω is large. From equation (2.06.04) we see that for unconditional stability it is necessary that

$$n < \tfrac{1}{2}[1 + N_r(0)] \qquad \ldots.(2.06.13)$$

For systems without servo control $N_r(0)$ is given by equation (2.06.07). Thus equation (2.06.13) becomes

$$n < \tfrac{1}{2}\{1 - P/[1 + D(P + \tfrac{1}{2})]\} \qquad \ldots.(2.06.14)$$

It should be noticed that equation (2.06.13) is not a sufficient requirement for unconditional stability, but only a necessary condition. It will be indicated in Section 2.07 that the inequality (2.06.13) is both sufficient and necessary for unconditional stability only for systems with small D or small E.

For a given feed system without servo control, the magnitude of $N(0)$ or $N_r(0)$ can be computed easily from known values of P and D by using equation (2.06.07) or experimentally determined by running a quasi-steady state test of the feeding system alone under simulated operating conditions. For liquid propellant rockets, if we increase the chamber pressure by a definite amount, the injection rate must eventually decrease. Hence the quantity $N_r(0)$ is always negative without servo control as is evident from equation (2.06.14) with both P and D positive. Therefore, if the value of n for the propellant is larger than the value of $[1 + N_r(0)]/2$ which is always less than $\frac{1}{2}$, and if we want to design such a system for unconditional stability, servo control will be necessary. The servo control must be powerful enough to contribute a positive real part of sufficient magnitude to the value of $N_r(0)$ so that the necessary condition of equation (2.06.13) can be satisfied. It is clear from equations (2.06.04) and (2.06.05) that, if the servo control is to be effective in the limit when $s = i\Omega$ approaches zero, the transfer function of the feedback circuit must have a simple pole at $s = 0$ when D is not equal to zero and have a double pole at $s = 0$ when D is zero. This is because the function $C(s)$ has a common factor of s or s^2 depending on $D \neq 0$ or $D = 0$. For systems without servo control, the function g $(i\Omega)$ behaves like some positive power of Ω at large values of Ω. That part of the curve of g $(i\Omega)$ will not intersect the unit circle. Therefore, the control of the feedback circuit can be cut off at large frequencies. In mathematical terms, if the transfer function $F(s)$ is written as the ratio of two polynomials of s, the denominator of $F(s)$ is of higher degree in s than the numerator. With this in mind, it is only necessary for us to investigate the required behaviour of the transfer function $F(i\Omega)$ at sufficiently small values of Ω where we can represent the transfer function as

$$\left.\begin{aligned} F(s) &= (\mathrm{f}/s)[1 + a_1 s + a_2 s^2 + a_3 s^3 + \ldots] \quad \text{when } D \neq 0 \\ F(s) &= (\mathrm{f}/s^2)\,[1 + b_1 s + b_2 s^2 + b_3 s^3 + \ldots] \quad \text{when } D = 0 \end{aligned}\right\} \quad \ldots . (2.06.15)$$

Substitute the series expansion of $F(s)$ and equation (2.06.05) into equation (2.06.04) and apply the conditions that the modulus of g (s) must be bigger than unity for arbitrary values of Ω. By comparing the coefficients of different powers of Ω, we can obtain a series of algebraic inequalities which form the necessary and sufficient conditions such that the feedback servomechanism will result in an unconditionally stable system. The condition which is obtained from terms independent of Ω corresponds to the condition of equation (2.06.07) for an uncontrolled system, that is

$$\left.\begin{aligned} -\mathrm{f} &\geqslant \frac{P + 2n - 1}{D(P + \frac{1}{2})} + 2n - 1 \qquad \text{for } D \neq 0 \\ -\mathrm{f} &\geqslant (P + 2n - 1)/J \qquad \text{for } D = 0 \end{aligned}\right\} \quad \ldots . (2.06.16)$$

It is easily verified that these conditions are satisfied by the transfer functions $F(s)$ given by equations (2.06.09) and (2.06.12) for the two examples respectively.

This condition (2.06.16) is particularly important because it sets a minimum output and therefore a minimum amplification required from the feedback circuit in actuating the variable capacitance of the servomechanism. It is obvious from equations (2.06.16) that a more powerful servo control is required if the interaction index n is larger. By increasing the parameter D, that is, by using pumps which are less sensitive to the delivery pressure variations, the requirement on the servo control is somewhat relieved, but in no case can $-f$ be less than $2n - 1$. For a constant pressure feed system ($D = 0$), this minimum power requirement is decreased for given values of n by increasing the inertia parameter J and by decreasing the pressure parameter P (increase in pressure drop across the feed system).

The inequalities that are obtained from the coefficients of terms of higher powers of Ω are the requirements to be satisfied by the a or b coefficients characterizing the nature of the feedback circuit. It is simple to show that the curve of g $(i\Omega)$ is normal to the real axis at $\Omega = 0$. For feed systems with small D or small E its curvature in the neighbourhood of $\Omega = 0$ is sufficiently small so that the curve will not penetrate into the unit circle. Therefore, instead of setting up the inequalities for the a or b coefficients, a sufficient condition may be that the introduction of the feedback circuit does not modify the curvature of g $(i\Omega)$ at $\Omega = 0$. This condition is satisfied if the transfer function $F(s)$ is such that the polynomial in the numerator of $CF(s)$ does not involve terms in s and s^2, that is, if a_1 and a_2 are selected as:

$$\left.\begin{cases} a_1 = -J/D(P + \tfrac{1}{2}) \\ a_2 = J^2/D^2(P + \tfrac{1}{2})^2 - JE(1 - y) \qquad \text{for } D \neq 0 \end{cases}\right\} \quad \ldots\ldots (2.06.17)$$

or b_1 and b_2 as:

$$\left.\begin{cases} b_1 = 0 \\ b_2 = -JEy(1 - y) \qquad \text{for } D = 0 \end{cases}\right\}$$

An example of a simple transfer function fulfilling these required conditions has been used by F. E. Marble for systems with $E = 0$ as

$$F(s) = \frac{f}{s} \frac{1 - a_1 s}{(1 - \tfrac{1}{2}a_2 s^2)^2} \qquad \ldots\ldots (2.06.18)$$

with a_1 and a_2 given by equations (2.06.17). This particular form of transfer function cuts out at large frequencies as Ω^{-4} and appears to be somewhat simpler than those given in equations (2.06.09) and (2.06.12), which are obtained by determining the $F(s)$ that will result in a selected stable g (s) curve. It should be noted, however, that such a simple transfer function can apply only to feed systems with small D or small E. The transfer functions applicable to arbitrary values of the feeding system parameters are given by Sin-I Cheng[32].

2.07. Bipropellant Rockets

In bipropellant systems, the dynamic behaviours of the fuel and the oxidizer lines are in general not identical. Thus the responses of the fuel flow and the oxidizer flow to the pressure oscillations in the combustion chamber are in general different, and the mixture ratio $r = \dot{m}_o/\dot{m}_f$ will vary with pressure oscillations. Since the adiabatic flame temperature of a given propellant combination depends to a certain extent on the strength of the mixture, the pressure oscillation in the combustion chamber will induce a variation of the stagnation temperature of the burnt gas. This variation is not present in a monopropellant system. Therefore for the analysis of bipropellant systems, the equation of mass balance in the combustion chamber must be corrected for this temperature variation. Except for this correction all the other assumptions that have been made for the analysis of monopropellant systems have been transferred to the bipropellant case.

The equation of mass balance in the combustion chamber is written in dimensionless form as

$$\frac{\mathrm{d}}{\mathrm{d}z}\left(\frac{M_g}{\bar{M}_g}\right) + \mu_e(z) = \mu_b(z) \qquad \ldots.(2.07.01)$$

The fractional variation of the burning rate $\mu_b(z)$ is given by equation (2.01.07), where, following what has been done in the monopropellant case, we assume the entire time lag to be sensitive, that is $\tau_t = \tau$,

$$\mu_b(z) = \mu_i(z - \bar{\tau}) + n[\varphi(z) - \varphi(z - \bar{\tau})] \qquad \ldots.(2.07.02)$$

The fractional variation of the injection rate μ_i is conveniently expressed[8] in terms of the fractional variations of the oxidizer flow rate $\mu_o = (\dot{m}_o - \bar{\dot{m}}_o)/\bar{\dot{m}}_o$ and the fuel flow rate $\mu_f = (\dot{m}_f - \bar{\dot{m}}_f)/\bar{\dot{m}}_f$,

$$\mu_i = (\tfrac{1}{2} + H)\mu_o + (\tfrac{1}{2} - H)\mu_f \qquad \ldots.(2.07.03)$$

where H is related to the steady state mixture ratio $\bar{r}$ by

$$H = \tfrac{1}{2}(\bar{r} - 1)/(\bar{r} + 1) \qquad \ldots.(2.07.04)$$

For ordinary bipropellant combinations, we have $\bar{r} > 1$ and as a result H is generally positive. The fractional variations of oxidizer and fuel flows, μ_o and μ_f, are related to the fractional pressure variation φ through the dynamics of the oxidizer and the fuel feed systems respectively as represented by equation (2.02.10).

The fractional variation of the mass injection rate μ_e is a function of the fractional variations of local pressure and local gas temperature entering the nozzle. Let us consider the case when the nozzle flow is quasi-steady. Then

$$\mu_e = \frac{\dot{m}_e}{\bar{\dot{m}}} - 1 = \frac{p}{\bar{p}}\left(\frac{T_g}{T_{g_e}}\right)^{\frac{1}{2}} - 1 \qquad \ldots.(2.07.05)$$

where T_{g_e} is the instantaneous temperature of the gas at combustion chamber exit, that is, the entrance to the nozzle. In the monopropellant case $T_{g_e} = T_g$, and $\mu_e = \varphi$ since we assumed the gas temperature to be independent of the pressure oscillations. In the bipropellant case the gas entering the nozzle

at the instant t was generated at the instant $t - \theta_g$, and the stagnation temperature of the gas is determined by the mixture ratio r of the propellant injected into the chamber at the instant $t - \bar{\tau}^* - \theta_g$. Therefore under the previous assumptions T_{g_s}/T_g is a function of $r(z - \bar{\tau} - 1)/\bar{r}$ alone. Since $|r - \bar{r}| \ll \bar{r}$, and $r = \dot{m}_o/\dot{m}_f = \bar{r}(1 + \mu_o - \mu_f)$, we can approximately evaluate T_{g_s}/T_g as

$$T_{g_s}/T_g(z) = 1 + \theta_e = 1 + 2K\left(\frac{r}{\bar{r}} - 1\right)$$

$$= 1 + 2K[\mu_o(z - \bar{\tau} - 1) - \mu_f(z - \bar{\tau} - 1)] \quad \ldots.(2.07.06)$$

where $2K = (\bar{r}/\bar{T}_g)(\mathrm{d}\bar{T}_g/\mathrm{d}\bar{r})$ is a property of the propellant combination and is a function of the steady state mixture ratio and the combustion chamber pressure. For conventional bipropellant combinations, K is usually a small positive quantity. Equations (2.07.05) and (2.07.06) give the fractional variation of ejection rate of the burnt gas under quasi-steady assumption as

$$\mu_e(z) = \varphi(z) - \tfrac{1}{2}\theta_e(z) = \varphi(z) - K[\mu_o(z - \bar{\tau} - 1) - \mu_f(z - \bar{\tau} - 1)]$$

$\ldots.(2.07.07)$

Observe that in equation (2.07.07) the effects of pressure and temperature oscillations are taken into account separately. Thus, the major effect of the entropy oscillation is included. The effect of the deviation of nozzle flow from quasi-steady condition is more complicated when entropy variations cannot be neglected[20, 24, 25]. It is, however, to be expected that the deviation will be small for sufficiently low frequencies. We shall therefore restrict the present discussion to quasi-steady nozzle conditions.

Consider now the mass accumulation term $\dfrac{\mathrm{d}}{\mathrm{d}z}(M_g/\bar{M}_g)$. With uniform pressure but non-uniform temperature in the combustion chamber, the density of the burnt gas varies from point to point. Thus,

$$\frac{M_g}{\bar{M}_g} = \frac{\rho}{\bar{\rho}}\frac{\bar{T}_g}{\bar{V}}\int_V \frac{\mathrm{d}V'}{T_g} = (1 + \varphi)\left[1 + \frac{1}{\bar{V}}\int_V \left(\frac{\bar{T}_g}{T_g} - 1\right)\mathrm{d}V'\right]$$

This integral can be evaluated by means of the complicated methods given in Chapter 3 for the case of arbitrarily distributed combustion. Neglecting higher order terms, we have

$$\frac{\mathrm{d}}{\mathrm{d}z}\left(\frac{M_g}{\bar{M}_g}\right) = \frac{\mathrm{d}\varphi}{\mathrm{d}z} + \frac{\mathrm{d}}{\mathrm{d}z}\left[\frac{1}{\bar{V}}\int_V \left(\frac{\bar{T}_g}{T_g} - 1\right)\mathrm{d}V'\right] \quad \ldots.(2.07.08)$$

In order to avoid complications and to obtain a rough estimate of the effects to be expected, Crocco[8] used the extreme assumption that all the propellant elements burn in the immediate neighbourhood of the injector end and that each propellant element preserves its temperature regardless of the pressure variation during the gas residence time θ_g which is taken to be the same for all propellant elements. With these simplifying assumptions, which result in constant flow velocity, the two variables V'/V and

$-z$ are proportional to each other and have the same limits 0 and 1 at the two ends of the combustion chamber volume. Thus the spacewise integration can be transformed into a timewise integration with $dV'/V = -dz'$. Therefore

$$\frac{d}{dz}\left(\frac{M_g}{\bar{M}_g}\right) = \frac{d\varphi}{dz} - \left(\frac{T_g}{T_{g_e}} - \frac{T_g}{T_{g_i}}\right)$$

where all the quantities are evaluated at the instant z and T_{g_i} is the temperature of the gas generated at the instant z. Thus, using equation (2.07.06) to obtain T_g/T_{g_e} and T_g/T_{g_i} we have

$$\frac{d}{dz}\left(\frac{M_g}{\bar{M}_g}\right) = \frac{d\varphi(z)}{dz} + 2K[\mu_o(z-\bar{\tau}-1) - \mu_f(z-\bar{\tau}-1)] - 2K[\mu_o(z-\bar{\tau}) - \mu_f(z-\bar{\tau})] \quad \ldots.(2.07.09)$$

Combining equations (2.07.01), (2.07.02), (2.07.03), (2.07.07) and (2.07.09), we obtain the equation of mass balance in the combustion chamber of a bipropellant rocket motor as

$$\frac{d\varphi}{dz} + (1-n)\varphi + n\varphi(z-\bar{\tau}) = -K[\mu_o(z-\bar{\tau}-1) - \mu_f(z-\bar{\tau}-1)] + (\tfrac{1}{2} + H + 2K)\mu_o(z-\bar{\tau}) + (\tfrac{1}{2} - H - 2K)\mu_f(z-\bar{\tau}) \ldots.(2.07.10)$$

There are three unknown quantities φ, μ_o and μ_f in equation (2.07.10). Two more equations relating μ_o and μ_f with φ are supplied by the equations of the dynamics of the feed systems, one for the oxidizer line and one for the fuel line. Each of the two equations is in the form of equation (2.02.10) with subscripts $_o$ and $_f$ added to indicate different quantities pertaining to the oxidizer and the fuel lines respectively.

If the fuel system and the oxidizer system are such that the dimensionless parameters D, P, E and J for both systems are identical, the response of the oxidizer and of the fuel flow will be expected to be identical in dimensionless form, and $\mu_o = \mu_f = \mu$. The bipropellant system then behaves in just the same manner as a monopropellant system with the equation of mass balance and the equation of the feeding system dynamics reduced to the form of the monopropellant case.

A study of the system formed by equation (2.07.10) and two equations of the form of equation (2.02.10) is not very practical if the constants involved in the equations are left arbitrary. The graphical method using the Satche and Nyquist diagrams can be advantageously used for the investigation of specific examples. The characteristic equation for the system with solutions for $\varphi(z)$ of the exponential type $\exp(sz)$ can be obtained by eliminating μ_o and μ_f from equation (2.07.10) and equations (2.02.10) for the oxidizer and the fuel systems respectively. The eliminant or the condition of nontrivial solutions for φ, μ_o and μ_f can be most conveniently obtained by equating the determinant formed by the coefficients of φ, μ_o and μ_f in the three equations to zero. This determinant can be easily expanded and rearranged to give the following form of the characteristic equation

$$L_1(s) = e^{-s\bar{\tau}}[L_2(s) + F_o(s)L_o(s) + F_f(s)L_f(s)] \quad \ldots.(2.07.11)$$

where

$$\left.\begin{aligned} L_1(s) &= [1 + s - n]B_oB_f \\ L_2(s) &= -nB_oB_f - [Ke^{-s} + (\tfrac{1}{2} - H - 2K)]A_fB_o \\ &\quad - [-Ke^{-s} + (\tfrac{1}{2} + H + 2K)]A_oB_f \\ L_o(s) &= [Ke^{-s} - (\tfrac{1}{2} + H + 2K)]B_fC_o \\ L_f(s) &= -[Ke^{-s} + (\tfrac{1}{2} - H - 2K)]B_oC_f \end{aligned}\right\} \quad \ldots.(2.07.12)$$

with A, B and C given by equations (2.06.05) in terms of the constants of the feeding systems with subscripts $_o$ and $_f$ denoting the quantities for the oxidizer and the fuel system respectively.

The function $G(s)$ for the plot of the Satche diagram is $G(s) = e^{-\bar{\tau}s} - g(s)$ where

$$g(s) = L_1(s)/[L_2(s) + F_o(s)L_o(s) + F_f(s)L_f(s)] \quad \ldots.(2.07.13)$$

The principle of the use of the Satche and Nyquist diagrams is explained in Appendix A, and the method of construction and several discussions of the diagrams have been described in Section 2.06. Examples for the bipropellant cases are given by Marble and Cox[10] as follows:

Example 1.

Feeding system constants $F_o(s) = F_f(s) = 0$

$$D_o = D_f = 1, \quad P_o = P_f = 1, \quad J_o = 2{\cdot}0, \quad J_f = 1{\cdot}5, \quad E_c = E_f = 0$$

Then,

$$L_1(i\Omega) = \left\{\frac{25}{4}(1-n) - \left[\frac{35}{4} + 3(1-n)\right]\Omega^2\right\} + i\Omega\left\{\left[\frac{25}{4} + \frac{35}{4}(1-n)\right] - 3\Omega^2\right\}$$

$$L_2(i\Omega) = -\left\{\frac{25}{4}n + \frac{5}{2} - 3n\Omega^2\right\} - i\Omega\left\{\frac{35}{4}n - \frac{1}{2}(H + 2K) + \frac{7}{4}\right\} - \frac{1}{2}K[i\Omega\cos\Omega + \Omega\sin\Omega] \quad \ldots.(2.07.14)$$

The Satche diagram and the associated Nyquist diagram when $n = 0{\cdot}2$, $\bar{\tau} = 2{\cdot}5$, $\bar{T}_g = 5010°\text{F}$, $\dfrac{d\bar{T}_g}{d\bar{\tau}} = 360$, $H = 0{\cdot}2125$ and $K = 0{\cdot}09$ are shown in *Figures 20*(a) and (b) respectively. The Satche diagram shows that $g(s)$ is completely outside the unit circle, and the Nyquist diagram of $L_2(s)$ does not encircle the origin. The system is, therefore, unconditionally stable.

When $n = 0{\cdot}6$, the Satche diagram is shown in *Figure 21*. It is found that the system can become unstable (when $\bar{\tau}$ is in certain ranges of values).

In these examples, the constants of the feed systems for the oxidizer and the fuel lines are not very different; therefore, the behaviour of such a bipropellant system is quite similar to that of a monopropellant system, and the variation of the mixture ratio r is expected to be small and not of great importance.

Example 2.

$$F_o(s) = F_f(s) = 0$$

$$D_o = D_f = 1, \quad P_o = 1, \quad P_f = 4, \quad J_o = 4, \quad J_f = 1, \quad E_o = E_f = 0$$

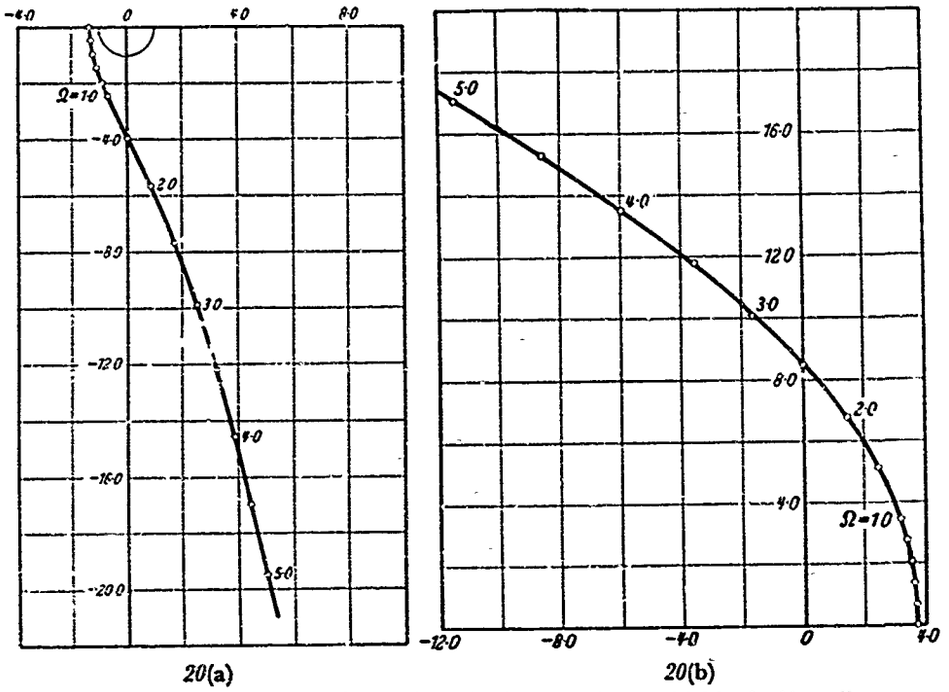

20(a) 20(b)

Figure 20. Satche diagram (left) and associated Nyquist diagram (right) of a bipropellant rocket with $n = 0{\cdot}2$, $\bar{r} = 2{\cdot}5$, $\bar{T}_g = 5010°\text{F}$, $d\bar{T}_g/d\bar{r} = 360$, $H = 0{\cdot}2125$, $K = 0{\cdot}09$ and the following feeding system constants: $E_o = 0$, $J_o = 2{\cdot}0$, $P_o = 1$, $D_o = 1$, $E_f = 0$, $J_f = 1{\cdot}5$, $P_f = 1$, $D_f = 1$. Numerals on the curves indicate values of Ω

Then

$$L_1(i\Omega) = \left\{\frac{55}{4}(1-n) - \left[\frac{49}{2} + 4(1-n)\right]\Omega^2\right\} + i\Omega\left\{\left[\frac{55}{4} + \frac{49}{2}(1-n)\right] - 4\Omega^2\right\}$$

$$L_2(i\Omega) = -\left\{\frac{55}{4}n + \frac{31}{4} - \frac{9}{2}(2K+H) - 4n\Omega^2\right\} - i\Omega\left\{\frac{49}{2}n + \frac{17}{2} - 15(2K+H)\right\} - K\left\{\frac{9}{2}(\cos\Omega - i\sin\Omega) + 15(i\Omega\cos\Omega + \Omega\sin\Omega)\right\} \quad \ldots.(2.07.15)$$

The Satche and Nyquist diagrams for $n = 0{\cdot}2$, $\bar{r} = 2{\cdot}0$, $\bar{T}_g = 4706°\text{F}$, $d\bar{T}_g/d\bar{r} = 850$, $H = 0{\cdot}167$ and $K = 0{\cdot}189$ are shown as *Figure 22* opposite. The system is unconditionally stable. These diagrams are distinguished from those in example 1 by having large loops. These loops originate

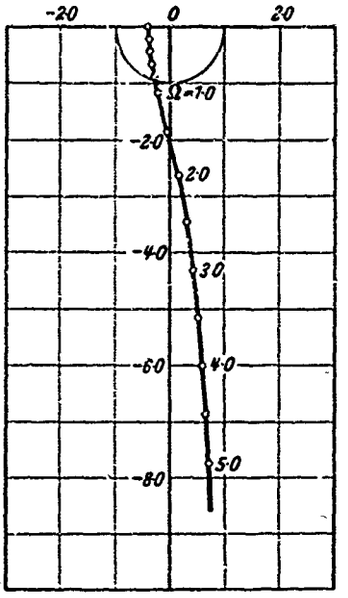

Figure 21. Satche diagram of a bipropellant rocket with $n = 0{\cdot}6$, $\bar{r} = 2{\cdot}5$, $\bar{T}_g = 5010°\text{F}$, $d\bar{T}_g/d\bar{\tau} = 360$, $H = 0{\cdot}2125$, $K = 0{\cdot}09$ *and the following feeding system constants:* $E_o = 0$, $J_o = 2{\cdot}0$, $P_o = 1$, $D_o = 1$, $E_f = 0$, $J_f = 1{\cdot}5$, $P_f = 1$, $D_f = 1$. *Numerals on the curve indicate values of* Ω

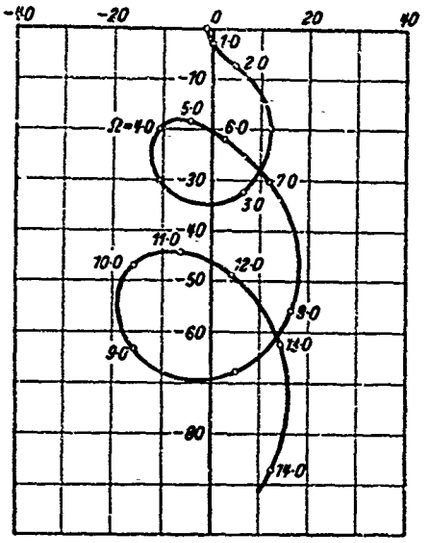

Figure 22(a).

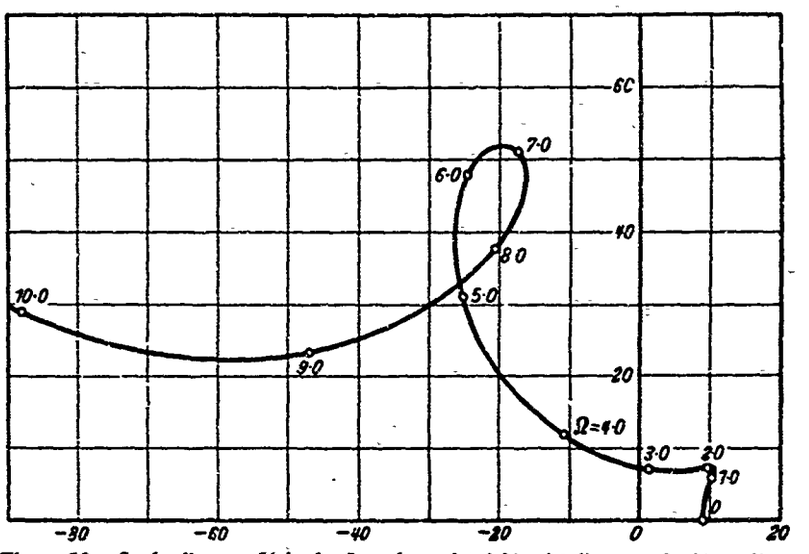

Figure 22. Satche diagram [(a) *above*] *and associated Nyquist diagram of a bipropellant rocket with* $n = 0{\cdot}2$, $\bar{r} = 2{\cdot}0$, $\bar{T}_g = 4706°\text{F}$, $d\bar{T}_g/d\bar{\tau} = 850$, $H = 0{\cdot}167$, $K = 0{\cdot}189$ *and the following feeding system constants:* $E_o = 0$, $J_o = 4$, $P_o = 1$, $D_o = 1$, $E_f = 0$, $J_f = 1$, $P_f = 4$, $D_f = 1$. *Numerals on the curves indicate values of* Ω

in the trigonometric terms of $L_2(i\Omega)$, which arise because the effect of the temperature variation on the rate of ejection is delayed by an amount θ_r with respect to the instant when the burnt gas is generated. Consequently the trigonometric terms in $L_2(i\Omega)$ are associated with a reduced

time lag of unity. The magnitude of these loops depends on K and on the quantity $B_f A_o - B_o A_f$ which increases with increasing difference of the parameters of the oxidizer and fuel lines. If the combustion temperature of the propellants becomes more sensitive to the mixture ratio variation, or if the constants of the fuel and oxidizer lines differ to a greater extent, these loops will grow in size and intersect the unit circle and eventually encircle the unit circle. Thus, even with the present simplifying assumptions about the quasi-steady flow in the nozzle, the temperature variations produced by the mixture ratio oscillation may affect considerably the stability conditions. Physically when the gas leaving the combustion chamber is at a temperature lower than the mean chamber temperature due to the unbalance of the mixture ratio of this particular element, the mass outflow rate is increased. This increase of mass outflow rate tends to decrease the chamber pressure. With proper timing, this decrease of chamber pressure may occur during a pressure defect period and help in exciting unstable oscillations. It can be observed from equation (2.07.15) that the loop will not develop until Ω is increased to the order of π. The intersections of the loop with the unit circle will correspond to neutral oscillations of frequencies of this order of magnitude, while the previous intersections are usually less than unity. As has been indicated in Section 1.10, these unstable oscillations will be classified in the intermediate frequency range. For such cases, a more careful analysis taking the frequency level into account should be developed.

The necessary condition for the unconditional stability of a bipropellant rocket corresponding to equation (2.06.13) for a monopropellant rocket is

$$n < \frac{1}{2}\left\{1 + \frac{N_{ro} + N_{rf}}{2} + (K + H)(N_{ro} - N_{rf})\right\}_{\Omega=0} \quad \ldots.(2.07.16)$$

which for systems without servo control reduces to

$$n < \frac{1}{2}\left\{1 - \frac{P_o(\frac{1}{2} + K + H)}{1 + D_o(P_o + \frac{1}{2})} - \frac{P_f(\frac{1}{2} - K - H)}{1 + D_f(P_f + \frac{1}{2})}\right\} \quad \ldots.(2.07.17)$$

For ordinary bipropellants, $K + H$ is positive but less than $\frac{1}{2}$. From equation (2.07.17), we can see that if n of the propellant combination is less than $\frac{1}{2}$, the system can be made unconditionally stable by increasing the pressure drop across the feed system and decreasing the pressure sensitivity of the feed pump. If $D_o = D_f$, it is clear that it is more effective, in ordinary bipropellant systems with $K + H > 0$, to decrease P_o than P_f. In other words, increasing the pressure drop across the oxidizer feed system has a greater stabilizing effect. If $P_o = P_f$, it is more effective to increase D_o than D_f. In general by comparing the two terms pertaining to the oxidizer and the fuel systems as given in equation (2.07.17) it can be determined easily whether it is more effective to change the oxidizer or the fuel system to obtain unconditional stability.

When n of the propellant is greater than $\frac{1}{2}$, it is necessary to control the feed system by a feedback servomechanism to obtain unconditional stability. Both the fuel and the oxidizer system can be controlled simultaneously by

the same or by different feedback circuits as shown in *Figure 23.* It would be theoretically sufficient, however, to control either the fuel or the oxidizer system. If the fuel system is not controlled, $F_f(s) = 0$, and the oxidizer system is controlled by a feedback servomechanism with transfer function $F_o(s)$ where

$$F_o(s) = (f_o/s)\,[1 + a_1 s + a_2 s^2 + a_3 s^3 + \ldots] \quad \text{when } D_o \neq 0,$$

$$F_o(s) = (f_o/s^2)\,[1 + b_1 s + b_2 s^2 + b_3 s^3 + \ldots] \quad \text{when } D_o = 0.$$

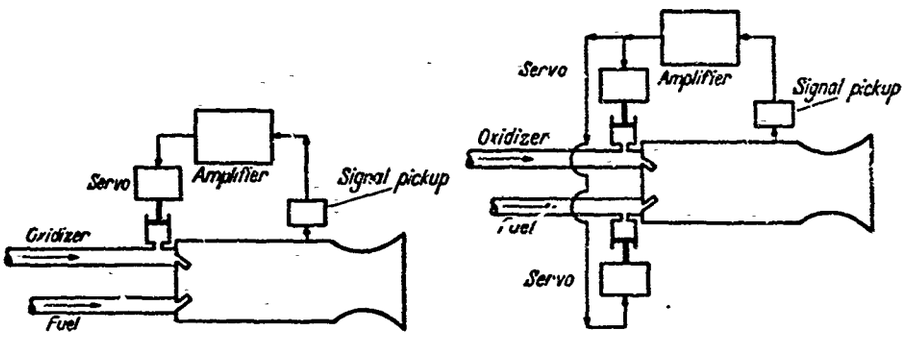

Figure 23. Schematic diagrams of the feeding systems of a bipropellant rocket with servo control

Then $-f_o$ must satisfy the following requirement corresponding to equation (2.06.16) for a monopropellant system,

$$-f_o \geqslant \left[(2n-1) + \frac{P_o(\frac{1}{2}+K+H)}{1+D_o(P_o+\frac{1}{2})} + \frac{P_f(\frac{1}{2}-K-H)}{1+D_f(P_f+\frac{1}{2})}\right] \frac{1+D_o(P_o+\frac{1}{2})}{D_o(P_o+\frac{1}{2})} \frac{1}{\frac{1}{2}+K+H}$$

when $D_o \neq 0$,

$$-f_o \geqslant \left[(2n-1) + P_o(\frac{1}{2}+K+H) + \frac{P_f(\frac{1}{2}-K-H)}{1+D_f(P_f+\frac{1}{2})}\right] \frac{1}{J_o(\frac{1}{2}+K+H)} \quad \ldots\ldots(2.07.18)$$

when $D_o = 0$.

Similar expressions for $-f_f$ can be obtained simply by interchanging the subscripts $_o$ and $_f$ and replacing K and H by $-K$ and $-H$. By comparing the requirements of $-f_o$ and $-f_f$, it can be easily determined whether it is more effective to control the oxidizer or the fuel system. If the fuel and the oxidizer feed systems have the same values of P and D (and J if $D = 0$), it is more effective to control the oxidizer system for ordinary bipropellant combinations with $K + H > 0$ because $\frac{1}{2} + K + H$ is in general bigger than $\frac{1}{2} - K - H$.

The coefficients a_1, a_2 or b_1, b_2 of the transfer function of the feedback circuit which does not change the curvature of the curve of $g(i\Omega)$ at $\Omega = 0$, are still given by equation (2.06.17) with the proper subscripts.

For the system with the Satche diagram shown in *Figure 21*, equation (2.07.18) gives $-f_o > 1{\cdot}247$ and equations (2.06.17) give $a_1 = 4/3$ and $a_2 = 16/9$. This system can be made unconditionally stable by controlling the oxidizer line with a feedback servomechanism having the transfer function

$$F_a(s) = -\frac{1{\cdot}40}{s}\frac{1 - 1{\cdot}33\,s}{(1 - 0{\cdot}89\,s^2)^2}$$

The resulting Satche diagram is shown in *Figure 24* where the curve of g (*s*)

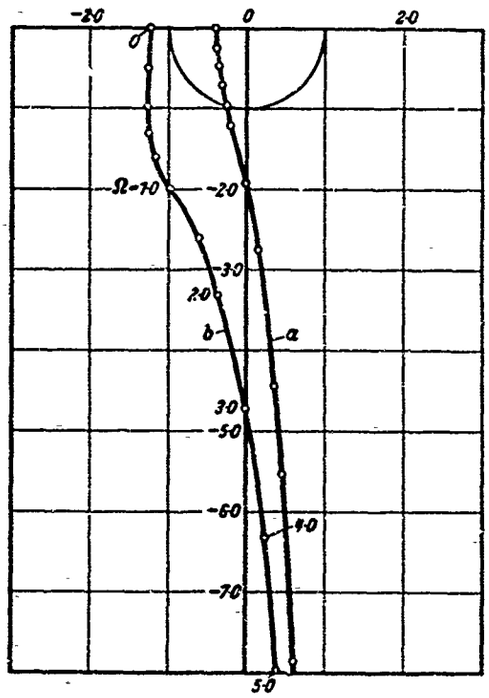

Figure 24. Satche diagram of the biprcpellant rocket of Figure 21 with $n = 0{\cdot}6$; (*a*) *not servo-controlled;* (*b*) *oxidizer line controlled by a capacitance servo-mechanism with transfer function*

$$F_a(s) = -\frac{1{\cdot}40}{s}\frac{1 - 1{\cdot}33\,s}{(1 - 0{\cdot}89s^2)^2}$$

Numerals on curve indicate values of Ω

is shifted completely out of the unit circle. Lee, Gore and Ross, cited by Randall[32], have also plotted a number of cases for the particular configurations with $n = 0$, $E = J = D = 0$, and stability boundaries are given for such systems.

The possibility of obtaining unconditional stability by the use of servo control is also illustrated. It is thus well demonstrated, theoretically, that a liquid rocket can be made stable in the low frequency range for all values of time lag. There are, however, important practical problems concerning the proper design not only of the feedback circuit, but also the capacitive servo control which finally converts the amplified electric signal into mechanical vibrations of sufficiently large amplitude in the frequency range under consideration.

Previous considerations of servo stabilization are made under the conditions that the different constants P, D, E, J and y are known for a given

feed system. In practical systems, however, it is hardly possible to estimate these constants with sufficient accuracy except the pressure drop parameter $P = \bar{p}/2\Delta\bar{p}$. The pump characteristic D, being taken previously as a quasi-steady value, may change in the frequency range under consideration. The application of equations (2.06.16), (2.06.17) and (2.07.18) in designing a feedback circuit will require an ingenious evaluation of the parameters involved.

From a practical point of view, the ratio of the fractional variation μ_i of injection rate to that of chamber pressure φ, that is, the transfer function $N(i\Omega) = \mu_i/\varphi$ can in principle be determined, for different oscillating frequencies Ω, for the isolated feed system under simulated operating conditions. This experimentally determined function $N(i\Omega) = N_r(\Omega) + i\Omega N_i(\Omega)$ replaces the lengthy equation (2.02.10). Then the equation of mass balance in the combustion chamber as given by equation (2.03.01) can be rewritten for neutral oscillations in a monopropellant system as

$$i\omega + (1 - n) + n\,e^{-i\omega\delta} = e^{-i\omega\delta}(R + iS)$$

where

$$\begin{aligned} R + iS &= e^{-i\omega\delta_i}N(i\omega) \\ &= e^{-i\omega\delta_i}[N_r(\omega) + i\omega N_i(\omega)] \end{aligned} \qquad \ldots.(2.07.19)$$

with δ_i indicating the insensitive time lag, when present. By separating the real and imaginary parts of equation (2.07.19) and eliminating δ, we obtain the critical values of n corresponding to neutral oscillations of frequency ω in the given system

$$n = \frac{1 + \omega^2 - [R^2(\omega) + S^2(\omega)]}{1 - R(\omega)} \qquad \ldots.(2.07.20)$$

When either $\delta_i = 0$ or when δ_i is known, both R and S are known functions of ω. A simple plot of n/ω can be made and a minimum value of n, let us call it $n_{\min}$, corresponding to certain $\omega = \omega_o$, can be found. If the value of n of the propellant is less than this $n_{\min}$, it is obvious that no neutral oscillations could exist in the system and the system is unconditionally stable. If n is slightly greater than $n_{\min}$, and if the value of τ is in the proper range of values, unstable oscillations with frequency in the neighbourhood of ω_o will occur. Equations (2.07.20) and (2.07.19) are applicable to the bipropellant case as well if $N(i\omega) = N_r(\omega) + i\omega N_i(\omega)$ is defined as

$$\left.\begin{aligned} N_r &= N_{ro}(\tfrac{1}{2} + 2K + H) + N_{rf}(\tfrac{1}{2} - 2K - H) \\ &\quad - (N_{ro} - N_{rf})K\cos\omega - (N_{io} - N_{if})K\omega\sin\omega \\ N_i &= N_{io}(\tfrac{1}{2} + 2K + H) + N_{if}(\tfrac{1}{2} - 2K - H) \\ &\quad + (N_{ro} - N_{rf})K\sin\omega/\omega - (N_{io} - N_{if})K\cos\omega \end{aligned}\right\} \ldots.(2.07.21)$$

with subscripts $_o$ and $_f$ indicating quantities pertaining to the oxidizer and the fuel systems respectively.

The expression for $N(i\omega)$ as given by equation (2.02.10) or as defined in equations (2.06.04) and (2.06.05) can be used to obtain the qualitative behaviour of the curve of n/ω. It is easy to see that $(dn/d\omega)_{\omega=0}$ vanishes at $\omega = 0$, and it is found that $n(0)$ is a minimum when $D = 0$ or $E = 0$,

but is a maximum when $D = \infty$. When $D = O(1)$, $n(0)$ can be either a maximum or a minimum depending upon the values of D, P, E, J and y. No simple relation can be obtained. The fact that $n(0)$ is a minimum when either D or E is small leads to the conclusion that, for such systems, $n_{min} = n(0)$ because both N_r and N_i approach zero when ω is large and $n(\omega)$ increases like ω^2. Thus $n(0) = \frac{1}{2}[1 + N_r(0)]$ becomes the criterion of unconditional stability as has been discussed in detail in connection with the Satche diagram. The present result indicates that the criterion of $n < n(0) = \frac{1}{2}[1 + N_r(0)]$ for unconditional stability can be both necessary and sufficient only for systems with small D or small E. For systems in which neither D nor E is small, n_{min} would be better determined from the plot of $n(\omega)/\omega$ for experimentally determined $N(i\omega)$. If servo stabilization were necessary, the transfer function of the feedback circuit should be selected so as to become most effective in the neighbourhood of the frequency ω_o where n_{min} occurs as shown in ref. 22.

2.08. Effects of the Non-uniformity of the Time Lag

It has been assumed in the previous analyses that all propellant elements have the same value of sensitive and of insensitive time lag, and for simplicity the insensitive time lag has been assumed to be zero. Now we would like to see the effect of the non-uniformity of the sensitive time lag τ.

We have already stressed the dependence of the time lag on the conditions encountered by the propellants on their path from the injection orifices to the point where they are entirely converted into burnt products. We have also noticed that the conditions encountered are different for different portions of propellants and therefore the corresponding values of the time lags are, in general, different. Knowing the largest and the smallest values of all the sensitive time lags, $\bar{\tau}_{max}$ and $\bar{\tau}_{min}$, we can always define an average reduced sensitive time lag $\bar{\tau}_m$ and the total extent of spread $\Delta\bar{\tau}$ thus:

$$\left.\begin{aligned} \bar{\tau}_m &= \tfrac{1}{2}(\bar{\tau}_{max} + \bar{\tau}_{min}) \\ \Delta\bar{\tau} &= \bar{\tau}_{max} - \bar{\tau}_{min} \end{aligned}\right\} \ldots\ldots (2.08.01)$$

Let $f(\tau)$ be the fractional amount of the propellant having a sensitive time lag lying between $\bar{\tau}_{min}$ and $\bar{\tau}$. Then the fractional amount of propellant having a sensitive time lag lying between $\bar{\tau}$ and $\bar{\tau} + d\bar{\tau}$ is given by $(df/d\bar{\tau})\, d\bar{\tau} = df$, and we have

$$f(\bar{\tau}_{max}) = 1, \qquad f(\bar{\tau}_{min}) = 0 \qquad \text{and} \qquad \int_{\bar{\tau}_{min}}^{\bar{\tau}_{max}} \frac{df}{d\bar{\tau}}\, d\bar{\tau} = 1 \quad \ldots\ldots (2.08.02)$$

Since $\bar{\tau}$ is a monotonically increasing function of $\bar{\tau}$ only, we can also consider $\bar{\tau}$ as a function of f only. From equation (1.11.15), we find that the rate at which the propellant elements, having steady state pressure sensitive time lag lying between $\bar{\tau}$ and $\bar{\tau} + d\bar{\tau}$, are burnt is

$$\partial \dot{m}_b = \dot{m}_i\,(z - \tau) \cdot \left(1 - \frac{d\tau}{dz}\right) \partial f$$

where $1 - d\tau/dz$ is evaluated from equation (1.11.13) or, in dimensionless form, from equation (2.01.06) with the value of $\bar{\tau}$ corresponding to this group of propellant elements.

Let us consider the simplest case of intrinsic instability, $\dot{m}_i = \text{const.}$ The algebraic complication of the feeding system can be dealt with, but is not considered to be essential for the present purpose. The fractional variation of the rate of burnt gas generation for all the propellant elements, covering the entire range of variation of the sensitive time lag, is thus

$$\frac{\dot{m}_b - \dot{m}_i}{\dot{m}_i} = \int_0^1 \left[\left(1 - \frac{d\tau}{dz} \right) - 1 \right] df$$

or from equations (2.01.06) and (2.08.02)

$$\mu_b = n \left[\varphi(z) - \int_0^1 \varphi(z - \bar{\tau})\, df \right]$$

The equation of mass balance in the combustion chamber corresponding to equation (2.03.01) with corrected reference time $(1 + b)\theta_g$ is

$$\left[\frac{d}{dz} + (1 - n) \right] \varphi = -n \int_0^1 \varphi(z - \bar{\tau})\, df \qquad \ldots.(2.08.03)$$

For solutions of the exponential type, $\varphi(z) \sim \exp(sz)$, we have the characteristic equation

$$s + (1 - n) + n \int_0^1 e^{-s\bar{\tau}(f)}\, df = 0 \qquad \ldots.(2.08.04)$$

which will be rewritten as

$$s + (1 - n) + Cne^{-s\bar{\tau}_e} = 0 \qquad \ldots.(2.08.05)$$

where C and $\bar{\tau}_e$ are defined by

$$C e^{-s\bar{\tau}_e} = \int_0^1 e^{-s\bar{\tau}(f)}\, df \qquad \ldots.(2.08.06)$$

By comparison of equation (2.08.05) with equation (2.03.05), we see that $\bar{\tau}_e$ stands for the effective mean time lag, that is, the time lag of an equivalent system in which the time lag for all the propellant elements would be the same. The modulus C of the complex integral defined by equation (2.08.06) represents a magnification or contraction factor of the overall effect, of the time lag spread, on the variation of the burning rate. In general, both C and $\bar{\tau}_e$ are functions of Λ and Ω. For neutral oscillations with $\Lambda = 0$ and $s = i\omega$, it is clear from equations (2.08.06) and (2.08.02) that

$$C = \left| \int_0^1 \exp\left[-i\omega \{ \bar{\tau}(f) - \bar{\tau}_m \} \right] df \right| \leqslant \int_0^1 df = 1 \qquad \ldots.(2.08.07)$$

C is equal to unity when the time lags for all the propellant elements are the same. When the time lags are different for different elements, C is less than unity.

The critical values of the effective time lag δ_e and the frequency of the neutral oscillation ω, are obtained from equation (2.08.05) with $s = i\omega$ and $\bar{\tau}_e = \delta_e$ given as:

$$\left.\begin{aligned} \omega &= [(2n-1) - (1-C^2)n^2]^{\frac{1}{2}} \\ \cos\omega\delta_e &= \cos(2\pi\delta_e/T) = -(1-n)/Cn \\ \delta_e &= [\pi - \cos^{-1}(1-n)/cn]/[(2n-1) - (1-C^2)n^2]^{\frac{1}{2}} \end{aligned}\right\} \quad \ldots\ldots (2.08.08)$$

Since the effect of the spread of time lag appears through the reduction of the magnitude of C from unity to some value less than unity, equations (2.08.08) show that the critical frequency ω of neutral oscillation is decreased and the critical time lag δ_e is increased. In addition, we see that for real ω and δ_e, n must be greater than $1/(1+C)$ which is greater than $\frac{1}{2}$. This means that intrinsic instability is not possible unless $n > 1/(1+C) > \frac{1}{2}$. Therefore, the effect of the spread of time lag is stabilizing and the stabilizing effect appears as an increase of the minimum value of the interaction index, $n_{\min}$, compatible with intrinsic instability, and also as a decrease of the unstable range of the time lag.

Equations (2.08.08) also indicate that the decrease of ω and the increase of δ_e are larger if the magnitude of C is smaller. In other words, the stabilizing effect of time lag spread is larger for smaller C. It should be noticed, however, that C depends not only on the distribution and the extent of time lag spread, but also on the frequency of the particular mode of oscillation under consideration. The stabilizing effect of a given time lag spread varies when the frequency of the oscillation varies.

In practical systems, the distribution of the amount of propellant elements having their time lags in a given range has never been determined. It probably depends to a great extent on the particular injection system, the propellant combination and on many other factors. It is not very likely that $df/d\bar{\tau}$ would be a constant, in which case there would be equal amounts of propellant in each elementary time lag range. It is more likely that there is a larger fraction of the propellant elements in the neighbourhood of some mean value than near the extremes of the entire range. The function $df/d\bar{\tau}$ is not necessarily symmetric about $\bar{\tau}_m$. But if it is symmetric, it is simple to show that for neutral oscillations of frequency ω

$$\left.\begin{aligned} \bar{\tau}_e &= \bar{\tau}_m \\ C &= 2\int_0^{1/2} \cos[\omega(\bar{\tau} - \bar{\tau}_m)]\, df \end{aligned}\right\} \quad \ldots\ldots (2.08.09)$$

that is, the effective time lag $\bar{\tau}_e$ is the same as the mean time lag $\bar{\tau}_m$. For other distributions $\bar{\tau}_e$ would be slightly different from $\bar{\tau}_m$, and the difference would also depend on the frequency of oscillation in addition to the time lag distribution. For illustrative purposes, the expressions for C for the following two simple cases are given as:

$$\left.\begin{aligned} &(i)\ \frac{df}{d\bar{\tau}} = \frac{1}{\Delta\bar{\tau}} = \text{constant};\ C_1 = \frac{\sin\omega\Delta\bar{\tau}/2}{\omega\Delta\bar{\tau}/2} \\ &(ii)\ \frac{df}{d\bar{\tau}} = \frac{\pi}{2\Delta\bar{\tau}}\cos\frac{\pi(\bar{\tau}-\bar{\tau}_m)}{\Delta\bar{\tau}};\ C_2 = \frac{\cos\omega\Delta\bar{\tau}/2}{1-(\omega\Delta\bar{\tau}/\pi)^2} \end{aligned}\right\} \quad \ldots\ldots (2.08.10)$$

Both C_1 and C_2 are equal to unity when $\omega\Delta\bar{\tau} = 0$ and oscillate when $\omega\Delta\bar{\tau}$ increases. The amplitude of the oscillation decreases with increasing $\omega\Delta\bar{\tau} = 2\pi\Delta\bar{\tau}/T$, linearly in the case of C_1 and quadratically in the case of C_2. Thus, when the actual extent of the time lag spread contains more than one period of oscillation. $\omega\Delta\bar{\tau} > 2\pi$, the stabilizing effect is considerably larger than that when $\omega\Delta\bar{\tau} < 2\pi$. In Section 2.03 it is shown

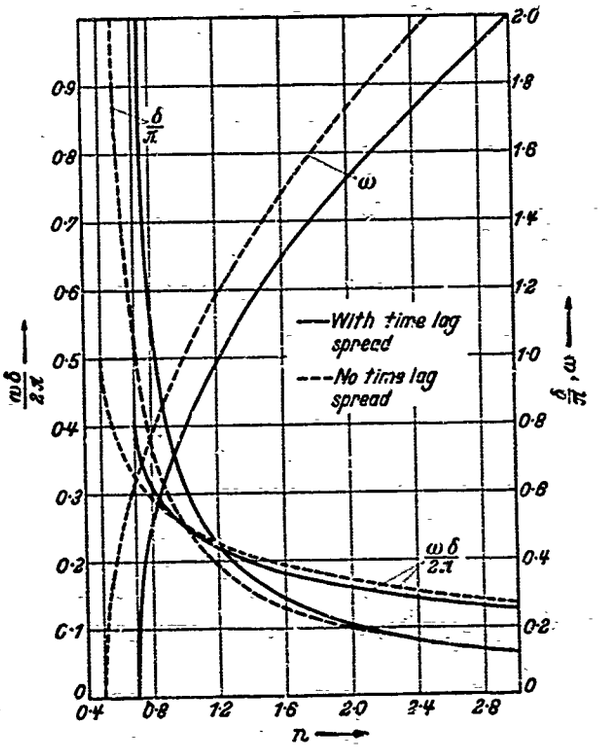

Figure 25. Effect of spreading the time lag on the critical values in systems with constant injection rate for different values of the interaction index n

that the only interesting critical time lag, in determining the intrinsic stability of a system, is the one corresponding to h = 0 or $\omega\delta < \pi$ in which case $\omega\Delta\bar{\tau} < 2\pi$ because $\Delta\bar{\tau}$ is always less than $2\bar{\tau}_m$. Accordingly it is sufficient to restrict our discussion of the effects of time lag spread on the intrinsic stability of a system to the lowest value of δ with h = 0.

Sample calculations, for the intrinsic stability boundary of the system, with time lag varying between 0 and $\bar{\tau}_{max} = 2\bar{\tau}_m$ and with distribution according to the second type of equation (2.08.10) are carried out based upon equations (2.08.08) and (2.08.10) with $C = C_2$ and $\Delta\bar{\tau}/2\bar{\tau}_m = 1$. The results are given in *Figure 25*. The dotted curves give the corresponding neutral curves for the case without time lag spread. The previous qualitative discussions on the decrease of critical frequency and the increase of critical time lag for neutral oscillations are verified.

In this section we have only discussed the effect of time lag spread on intrinsic instability. It is expected, however, that the qualitative effect of the time lag spread will be substantially the same for systems with variation of injection rate, both for the monopropellant and for the bipropellant case. The detailed picture is, of course, considerably more complicated.

2.09. Effect of Temperature Variation due to Pressure Oscillations

It has been assumed that the temperature of the burnt gas in the combustion chamber is not affected by the pressure oscillations, so that $T_g - \bar{T}_g$ vanishes for the monopropellant case and is a function only of the mixture ratio for the bipropellant case. In actual conditions, even if we assume that the adiabatic flame temperature or the stagnation temperature of the burnt gas is independent of the small variation of pressure under which the burnt gas is generated, after the generation, the static temperature of the burnt gas will change with local static pressure. If, in addition, the dissipative action of viscosity and conductivity is neglected, the instantaneous temperature of the gas can be determined by the instantaneous gas pressure through the equation of the isentropic change of state. Thus the fractional deviation of the gas temperature $T_g(z)$ from the adiabatic flame temperature $\bar{T}_g$ at the instant z is directly related to the fractional deviation of the gas pressure $p(z)$ from the pressure $p(z - z_0)$ under which the burnt gas element was generated at the instant $z - z_0$:

$$\frac{T_g(z) - \bar{T}_g}{\bar{T}_g} \simeq \frac{\gamma - 1}{\gamma} \cdot \frac{p(z) - p(z - z_0)}{p(z - z_0)} \simeq \frac{\gamma - 1}{\gamma} [\varphi(z) - \varphi(z - z_0)] \quad \ldots . (2.09.01)$$

The different burnt gas elements in the combustion chamber at a given instant z are generated at different previous instants. Gaseous elements near the chamber exit may have been in the chamber for a period almost equal to the residence time, that is, $z_0 \sim 1$, while elements near the injector end may have just been generated or may have spent a small fraction of the average residence time θ_g in the chamber, that is $z_0 \ll 1$. Therefore, when the pressure in the combustion chamber oscillates with relatively low frequency, and the gas pressure can be considered as practically uniform at any instant, the temperature of the burnt gas in the chamber is not uniform at any instant so that the density of the burnt gas is not uniform. In order to determine the mass of burnt gas stored in the combustion chamber and then the rate of mass accumulation in the chamber, we must know the temperature distribution at any instant. Equation (2.09.01) indicates that this is possible only if we have additional information concerning the distribution of combustion and the flow conditions in the combustion chamber.

The treatment of the general case will be given in Chapter 3. In this section we shall only illustrate the effect of this temperature variation by considering the following idealized configuration, in which all the propellant elements are transformed into burnt gas near the injector end and the residence time of all the elements is the same as the average gas residence time θ_g. In this case, the axial velocity of the burnt gas is constant throughout the chamber. The variable z_0 of a given gas element is thus equal to the fractional axial distance from the injector end, or to the fractional chamber volume upstream of the axial station of the corresponding element. Thus, in the evaluation of the mass stored in the chamber volume,

the integration over the chamber volume with the differential variable dV/V can be replaced by integration with the differential variable dz_0, with $0 \leqslant z_0 \leqslant 1$.

The rate of mass accumulation as given by equation (2.07.08) can be evaluated with the help of equation (2.09.01) and the fact that $dV/V = dz_0$. For the monopropellant case, we have

$$\frac{d}{dz}\left[\frac{M_g}{\bar{M}_g}\right] = \frac{d\varphi}{dz} - \frac{\gamma - 1}{\gamma}\left[\frac{d\varphi}{dz} + \varphi(z-1) - \varphi\right] \quad \ldots.(2.09.02)$$

The fractional variation of the mass ejection rate, as derived from equation (2.07.05) under the assumption of quasi-steady flow, is

$$\mu_e(z) = \varphi - \frac{\gamma - 1}{2\gamma}[\varphi(z) - \varphi(z-1)] \quad \ldots.(2.09.03)$$

The fractional variation of the rate of burnt gas generation μ_b is not affected by the temperature variation explicitly because the index n of interaction is supposed to include the effect of temperature variation. Thus the equation of mass balance in the combustion chamber for the analysis of intrinsic instability is

$$\frac{1}{\gamma}\frac{d\varphi}{dz} + \frac{\gamma - 1}{2\gamma}[\varphi - \varphi(z-1)] + \varphi = n[\varphi - \varphi(z-\tau)] \quad \ldots.(2.09.04)$$

The characteristic equation for the neutral solution of exponential type, $\varphi(z) \sim \exp(sz)$, is

$$\frac{i\omega}{\gamma} + \frac{\gamma - 1}{2\gamma}[1 - e^{i\omega}] + (1 - n) = -n\, e^{-i\omega\delta} \quad \ldots.(2.09.05$$

The following two real equations can be obtained by equating the moduli and the arguments of both sides of equation (2.09.05)

$$\left.\begin{aligned} n &= \frac{1}{2} + \frac{\gamma - 1}{4\gamma}(1 - \cos\omega) \\ &\quad + \left[\frac{\omega^2}{\gamma} + \frac{\gamma - 1}{2\gamma}\sin\omega\right]^2 \Big/ 2\left[1 + \frac{\gamma - 1}{2\gamma}(1 - \cos\omega)\right] \\ \omega\delta &= \pi - \tan^{-1}\left[\frac{\dfrac{\omega}{\gamma} + \dfrac{\gamma - 1}{2\gamma}\sin\omega}{1 - n + \dfrac{\gamma - 1}{2\gamma}(1 - \cos\omega)}\right] \end{aligned}\right\} \quad \ldots.(2.09.06)$$

In the first of equations (2.09.06) we see that when $\omega = 0$, n is equal to $\frac{1}{2}$ and that this is the minimum value of n compatible with any real solutions of ω and δ. This means that intrinsic instability is impossible if n is less than $\frac{1}{2}$ just as in the case investigated in Section 2.03 where the temperature oscillation of the burnt gas elements is neglected.

For small values of ω where $\cos\omega \simeq 1$ and $\sin\omega \simeq \omega$ the critical values of ω and δ can be easily solved from equations (2.09.06) for given values of n slightly greater than $\frac{1}{2}$.

$$\left.\begin{aligned}\omega &= \frac{2\gamma}{\gamma+1}(2n-1)^{\frac{1}{2}} \\ \delta &= \left[\pi - \cos^{-1}\left(\frac{1-n}{n}\right)\right](2n-1)^{-\frac{1}{2}}\frac{\gamma+1}{2\gamma}\end{aligned}\right\} \quad \ldots\ldots(2.09.07)$$

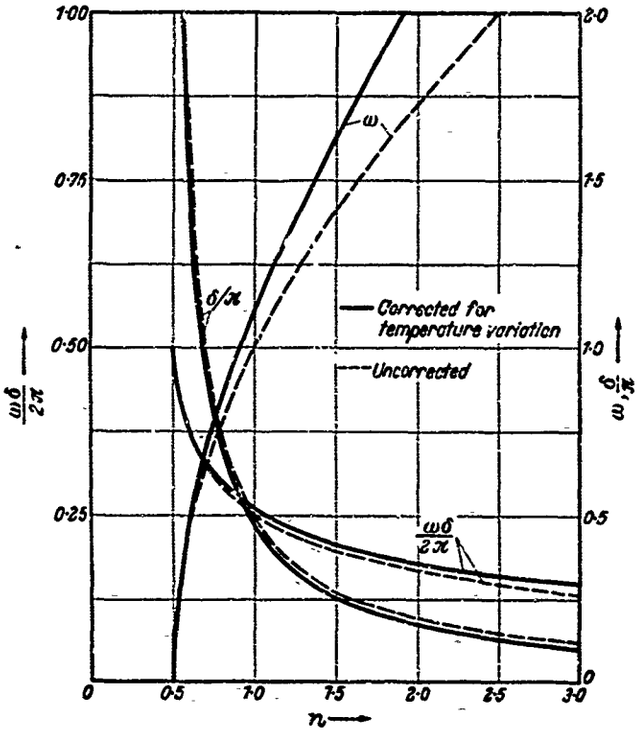

Figure 26. Effect of gas temperature oscillation on the critical values in systems with constant injection rate for different values of the interaction index n

Comparing equations (2.09.07) and equations (2.03.10) we see that for a given value of n which is only slightly greater than $\frac{1}{2}$, the critical value of ω is increased and that of δ decreased by the multiplying factor $2\gamma/(\gamma+1)$ and $(\gamma+1)/2\gamma$ respectively when the temperature variation of a given burnt gas element is taken into consideration. For most of the combustion gases at high temperature, the value of γ is only slightly larger than unity and the correction factor $2\gamma/(\gamma+1)$ is not very much different from unity. This correction is therefore not likely to be of great importance especially when we are interested primarily in the qualitative trend of the results.

When n is significantly larger than $\frac{1}{2}$, ω is not small and the critical values of ω and δ must be determined from equations (2.09.06). For illustrative purposes, the results when $\gamma = 1{\cdot}20$ are given in *Figure 26* as solid curves. The corresponding results when the temperature variation of the gas elements is neglected are also plotted as dotted curves for comparison.

It is clearly seen that the effect of the temperature variation of the gas elements is to decrease δ and increase ω for given n and that the minimum value of n compatible with any neutral or unstable oscillations is not affected. The qualitative trends are consistent with those as obtained from equations (2.09.07).

For more complicated monopropellant systems in which the injection rate responds to pressure oscillations in the chamber or for bipropellant systems, the qualitative trend of the effect of the temperature variation of a given burnt gas element is not expected to differ fundamentally.

3

ANALYSIS OF SCREAMING (LONGITUDINAL HIGH FREQUENCY INSTABILITY)

List of Symbols

Superscript *	indicates that the quantity is dimensional
Superscripts $^{(0)}$, $^{(1)}$	indicate the solutions obtained from the 0th or first iteration
Superscript $'$	indicates a small perturbation
Subscript $_o$	indicates the quantity evaluated at the stagnation region near the injector end
Subscript $_s$	indicates the isentropic stagnation value of the quantity
Subscript $_l$	indicates the quantity pertaining to unburnt (mostly in liquid phase) propellant element
Subscripts $_r$ and $_i$	indicate respectively the real part and the imaginary part of the quantity, if not otherwise stated
—	over a quantity indicates mean or steady state value
~	over a quantity indicates the quantity pertaining to the case with large ω
x^*	axial distance from injector end
L	axial length of the combustion chamber from injector end to entrance of de Laval nozzle
$x = x^*/L$	dimensionless distance from injector end
c_o^*	speed of sound in stagnant burnt gas at injector end
$\theta_w = L/c_o^*$	characteristic time required for sound wave to travel the chamber length L in stagnant burnt gas
u^*	mean axial velocity of burnt gas at each transverse section
$u = u^*/c_o^*$	dimensionless axial velocity of burnt gas
u_l^*	mean axial velocity of unburnt propellant elements at each transverse section
$u_l = u_l^*/c_o^*$	dimensionless axial velocity of unburnt propellant elements
$\bar{u}$	steady state value of u
M	Mach number of flow of burnt gas entering nozzle
t^*	time
$t = t^*/\theta_w$	dimensionless time
p^*	pressure of burnt gas
p_o^*	pressure of burnt gas in stagnation region near injector end

LIST OF SYMBOLS

$p = p^*/p_o^*$	dimensionless pressure of burnt gas
ρ^*	density of burnt gas
ρ_l^*	density of unburnt propellant element
ρ_o^*	density of burnt gas in stagnation region near injector end
$\rho = \rho^*/\rho_o^*$	dimensionless density of burnt gas
$\rho = \rho_l^*/\rho_o^*$	dimensionless density of unburnt propellant element
T^*	temperature of burnt gas
T_o^*	temperature of burnt gas in stagnation region near injector end
$T = T^*/T_o^*$	dimensionless temperature of burnt gas
h^*	enthalpy of burnt gas
h_p^*	enthalpy of unburnt propellant element
$h = (\overline{\gamma - 1}/c_o^{*2})h^*$	dimensionless enthalpy of burnt gas
h_p	dimensionless enthalpy of unburnt propellant element
w^*	instantaneous rate of burnt gas generation in the chamber volume from the injector end $x^* = 0$ to x^*
$w = w^*/\rho_o^* c_o^*$	dimensionless rate of burnt gas generation before x^*
$w_i = \rho_{lo} u_{lo}$	dimensionless injection rate
k^*	drag coefficient of the motion of the unburnt propellant element, = drag/velocity of unburnt element relative to surrounding gas
$k = k^* \theta_w$	dimensionless drag coefficient
p'	perturbation of burnt gas pressure
ρ'	perturbation of burnt gas density
h'	perturbation of burnt gas enthalpy
u'	perturbation of burnt gas velocity
u_l'	perturbation of velocity of unburnt propellant element
ρ_l'	perturbation of density of unburnt propellant element
w'	perturbation of rate of burnt gas generation before x
φ	time independent part of p'
σ	time independent part of ρ'
v	time independent part of u'
η	time independent part of u_l'
ζ	time independent part of ρ_l'
q	time independent part of w'
γ	adiabatic index of burnt gas = ratio of specific heats
Λ^*	dimensional amplification coefficient
Ω^*	dimensional angular frequency
$\Lambda = \Lambda^* \theta_w$	dimensionless amplification coefficient
$\Omega = \Omega^* \theta_w$	dimensionless angular frequency
ω	critical value or neutral angular frequency

$s = \Lambda + i\Omega$	a complex quantity which is the Laplace transformation variable and is the root of the characteristic equation for oscillations with exponential time dependence exp (st)
$\alpha = \alpha_r + i\alpha_i$	specific acoustic admittance ratio of de Laval nozzle
$\beta = \omega/\bar{u}_x$	reduced angular frequency
$B = (1 + \alpha\bar{u})/(1 - \alpha\bar{u})$	a parameter of boundary value at nozzle entrance $x = 1$
ψ	axial position of concentrated combustion front from injector end as a fraction of combustion chamber length
$\tau_t^* = \tau_i^* + \tau^*$	dimensional total time lag from instant of injection to instant of combustion of a given propellant element
τ_i^*	dimensional insensitive part of total time lag
τ^*	dimensional sensitive part of total time lag
$\tau_t = \tau_i + \tau = \tau_t^*/\theta_w$	dimensionless total time lag
$\tau_i = \tau_i^*/\theta_w$	dimensionless insensitive part of total time lag
$\tau = \tau^*/\theta_w$	dimensionless sensitive part of total time lag
δ	critical value of sensitive time lag τ corresponding to neutral oscillation
$\xi = \int_0^{\tau_i} u_t \, dt$	insensitive space lag, that is axial distance travelled by an unburnt propellant element during its insensitive time lag
l	integers indicating the number of half wavelengths contained approximately in the combustion chamber length with $l = 1, 2, 3\ldots$ corresponding to the fundamental, second, third, acoustic mode respectively
m	integers indicating the number of oscillating periods contained approximately in the sensitive time lag
$\chi_r + i\chi_i$	a complex function defined in equation (3.04.02)
X, Y, W, Z, E, F	functions of different perturbations and mean quantities defined in equations (3.07.08) and (3.07.09)
Q	time independent part of burning rate perturbation due to timewise condensation and rarefaction under variation of sensitive time lag [as defined in equation (3.08.17)]
S'	entropy perturbation of burnt gas
U, V	functions defined in equations (3.09.16)
$k = \int_0^x \cos \omega x' \frac{d\bar{u}}{dx'} \, dx'$	function defined in equation (3.11.03)
$\Xi = n\gamma(1 - e^{-i\omega\delta})$	function defined in equation (3.11.04)
A, B, C, D	functions defined in equations (3.11.06) and (3.11.07)
I, J	functions defined in equations (3.11.09)
A_1, B_1, C_1, D_1; $\bar{A}_1, \bar{B}_1, \bar{C}_1, \bar{D}_1$	functions defined in equations (3.11.18)
Γ, Δ	functions defined in equations (3.11.19)

C	magnification factor due to effect of spreading the sensitive time lag defined in equation (3.05.03)
$\bar{\tau}_e$	effective sensitive time lag defined in equation (3.05.03)
δ_e	critical value of $\bar{\tau}_e$ for neutral oscillation
O( )	order of magnitude of quantity in parentheses

3.01. Systems with Concentrated Combustion

As already explained in Chapter 1, when the frequency of gas oscillation in the combustion chamber is sufficiently high, the wavelength of standing oscillations may be comparable to the length of the combustion chamber and the gas pressure inside the combustion chamber is not uniform at any instant in unsteady state operation. In this case, not only the time interval but also the spatial range, in which each propellant element senses pressure oscillations, are important parameters in determining the contribution of this propellant element to the variation of the burning rate. Therefore, both the time lag and the space lag of each propellant element must be known for the analysis of high frequency oscillations. The spatial range, in which each propellant element senses pressure variations, is determined by the total space lag and the velocity of the unburnt propellant element during the sensitive time lag. Both the time lag and the space lag are in general different for different propellant elements. For the analysis of longitudinal oscillations in a combustion chamber of length L and of uniform cross sectional area, we shall consider the gas flow as one dimensional, and the only spatial coordinate which needs to be considered is the axial distance, x^*, from the injector end.

As a result, the only relevant characteristic time of such longitudinal oscillations is the wave propagation time, which is required for a sound wave to travel from the injector end, $x^* = 0$, to the combustion chamber exit, $x^* = L$, in steady state operation. Owing to the heterogeneous state in the rocket chamber even in steady state operation, the actual wave propagation time is not well defined. Therefore, we select the characteristic wave propagation time θ_{II} as the time required for a sound wave to travel a distance L (= length of combustion chamber) under conditions corresponding to the stagnant burnt gas near the injector face. In ordinary combustion chambers, where the velocity of mean mass motion is small compared to the speed of sound, $2\theta_{II}$ will be approximately equal to the time required for a sound wave to travel the length of the combustion chamber back and forth. Let us call c_0^* the speed of sound in the stagnant burnt gas, then $\theta_{II} = L/c_0^*$. We shall also express the velocity u^* of mass motion as a fraction of c_0^* and write $u = u^*/c_0^*$. Likewise, the pressure, density, and temperature of the burnt gas at stagnant condition will be taken as reference quantities. Thus, the dimensionless time, velocity, length, gas pressure, density, and temperature are defined as:

$$t = \frac{t^*}{\theta_{II}}, \quad u = \frac{u^*}{c_0^*}, \quad x = \frac{x^*}{L}, \quad p = \frac{p^*}{p_0^*}, \quad \rho = \frac{\rho^*}{\rho_0^*} \quad \text{and} \quad T = \frac{T^*}{T_0^*} \qquad \ldots.(3.01.01)$$

We shall first consider the simplest case in which all the propellant elements have the same sensitive time lag and the same total space lag;

accordingly they burn at the same axial position in steady state operation. In such an ideal system, all the propellant elements injected into the combustion chamber at a given instant move downstream through the burnt gas that was generated previously and was recirculated back to the injector end.

No gas is formed from these elements till they reach the position $x = \psi$, corresponding to the total space lag where all the propellant elements are transformed into burnt gases simultaneously and instantaneously. The burnt gases move downstream toward the exit of the combustion chamber, $x = 1$, without further chemical reactions. In steady state operation, the burnt gas upstream of the concentrated combustion front at $x = \psi$ has no mean axial velocity, though there is an active recirculating motion of the burnt gas in this region. At the combustion front $x = \psi$, the mean axial velocity of the burnt gas changes discontinuously to a finite value $\bar{u}$ because of the sources of burnt gases concentrated on this front. Both the burnt gases upstream and downstream of the combustion front are in active recirculating or turbulent motion. They differ only in the respect that the downstream burnt gas possesses a mean axial motion while the upstream burnt gas does not.

Since burnt gases in both regions are generated from the same propellant under similar conditions, the stagnation temperature, pressure, and density of the burnt gases in both regions are essentially the same. Thus, the concentrated combustion front in steady state is only a discontinuity of mean axial velocity while the temperature, pressure, and density are approximately the same across the combustion front. This is an important difference between the combustion front that we are considering here and the usual flame front, in which heat is added to an existing flow of cold gas with the consequence that the flame front is a discontinuity of the mean flow velocity, the gas density, and the temperature.

The burnt gas generated from the combustion front at a given instant mixes with the previously generated burnt gas and moves downstream in the cylindrical duct with a constant velocity $\bar{u}$, till it enters the nozzle where the gas is accelerated in the converging portion, goes through the sonic velocity at the throat, and leaves the nozzle at supersonic velocity through the diverging section. The geometry of the de Laval nozzle determines, in steady state operation, the Mach number M of the gas flow entering the nozzle. This Mach number M of the flow entering the nozzle is usually sufficiently small (see Section 3.06) so that $M^2 \ll 1$ and the dimensionless mean gas velocity $\bar{u}$ is approximately equal to M. Under this assumption, the dimensionless pressure, density, and temperature of the burnt gas in steady state operation are practically unity throughout the combustion chamber ($\bar{p} = 1$, $\bar{\rho} = 1$, $\bar{T} = 1$), and the flow of burnt gas in the region upstream of the concentrated combustion front can be considered as isentropic if fluid friction and heat transfer are neglected. The same assumption will be made without further discussion for the region downstream of the combustion front. A detailed discussion of these assumptions will be given in later sections in connection with systems with arbitrary combustion distribution. With these assumptions the unsteady flow of

the burnt gas in each of the two uniform flow regions is governed by the following equations:

$$\left.\begin{aligned} &\frac{\partial \rho^*}{\partial t^*} + \frac{\partial}{\partial x^*}(\rho^* u^*) = 0 \\ &\rho^* \frac{\partial u^*}{\partial t^*} + \rho^* u^* \frac{\partial u^*}{\partial x^*} = -\frac{\partial p^*}{\partial x^*} \\ &p^*/p_0^* = (\rho^*/\rho_0^*)^\gamma \end{aligned}\right\} \quad \ldots.(3.01.02)$$

Expressed in terms of the dimensionless quantities defined in equations (3.01.01), equations (3.01.02) can be written in the following form:

$$\left.\begin{aligned} &\rho_t + (\rho u)_x = 0 \\ &\rho u_t + \rho u u_x = -\frac{1}{\gamma} p_x \\ &p\rho^{-\gamma} = 1 \end{aligned}\right\} \quad \ldots.(3.01.03)$$

where subscripts denote partial differentiation with respect to the variable indicated.

For the analysis of the stability of small oscillations in the system, we shall consider the unsteady gas flow, as consisting of a small perturbation superposed on the steady state flow, with the perturbations assumed to be so small that the squares or the products of these perturbations can be neglected as compared to terms linear in these perturbations. Thus substituting

$$\rho = 1 + \rho', \qquad p = 1 + p' \qquad \text{and} \qquad u = \bar{u} + u'$$

into equations (3.01.03) under the approximation that $M^2 \simeq \bar{u}^2 \ll 1$, we obtain the following linearized equations for the perturbations of pressure, density and velocity:

$$\left.\begin{aligned} &\rho_t' + \bar{u}\rho_x' + u_x' = 0 \\ &u_t' + \bar{u}u_x' + \rho_x' = 0 \\ &p' = \gamma\rho' \end{aligned}\right\} \quad \ldots.(3.01.04)$$

Equations (3.01.04) are simply the wave equations governing the propagation of small disturbances in a one dimensional uniform flow field with constant flow velocity $\bar{u}$. The general solution of these wave equations is well known and is given as:

$$\left.\begin{aligned} &u' = u_r'(t - a_r x) + u_s'(t - a_s x) \\ &\rho' = \frac{1}{\gamma} p' = u_r'(t - a_r x) - u_s'(t - a_s x) \end{aligned}\right\} \quad \ldots.(3.01.05)$$

where u_r' and u_s' are arbitrary functions defining the downstream propagating and the upstream propagating velocity disturbances; $1/a_r = 1 + \bar{u}$ and $1/a_s = -(1 - \bar{u})$ are the speeds of propagation of the downstream and the upstream moving waves respectively relative to the wall of the

combustion chamber. This general solution, as given by equations (3.01.05), applies equally well in the flow region 1, bounded by $0 < x < \psi$ where $\bar{u} = 0$, and in the flow region 2, bounded by $\psi < x < 1$ where $\bar{u} \simeq M$. The solution in region 1 must satisfy the boundary condition at the injector end, $x = 0$, namely that both the mean flow velocity and the velocity disturbances must vanish at any instant. The solution in region 2 must satisfy the boundary condition at the combustion chamber exit, $x = 1$, that the ratio of the fractional velocity perturbation to the fractional density perturbation must be equal to the nozzle specific admittance ratio determined in Appendix B. Moreover, solutions in regions 1 and 2 must be properly related so that the boundary conditions at the concentrated combustion front can be satisfied. With all these boundary conditions, the functions u_r' and u_s' can be determined for a given initial disturbance. The solution of such an initial value problem is, however, not necessary since we are interested primarily in the stability of small arbitrary disturbances in the system. We shall therefore restrict our investigation to the stability of the solutions of exponential type:

$$\left.\begin{aligned} u_r' &= c_r \exp\left[s(t - a_r x)\right] \\ u_s' &= c_s \exp\left[s(t - a_s x)\right] \end{aligned}\right\} \quad \ldots.(3.01.06)$$

where $s = \Lambda + i\Omega$ is a complex constant. For simplicity, let us write the perturbations as:

$$\left.\begin{aligned} u' &= v(x) \exp(st) \\ \rho' &= \sigma(x) \exp(st) \\ p' &= \varphi(x) \exp(st) \end{aligned}\right\} \quad \ldots.(3.01.07)$$

then

$$\left.\begin{aligned} v(x) &= c_r \exp\left[-a_r s x\right] + c_s \exp\left[-a_s s x\right] \\ \frac{\varphi(x)}{\gamma} &= \sigma(x) = c_r \exp\left[-a_r s x\right] - c_s \exp\left[-a_s s x\right] \end{aligned}\right\} \quad \ldots.(3.01.08)$$

Let subscript $_1$ denote solutions in region 1 and subscript $_2$ denote solutions in region 2. Then the boundary condition at $x = 0$ gives

$$c_{r_1}/c_{s_1} = -1 \qquad \ldots.(3.01.09)$$

The boundary condition at $x = 1$ gives

$$\frac{c_{r_2}}{c_{s_2}} = -\frac{1 + \alpha\bar{u}}{1 - \alpha\bar{u}} \exp\left[s(a_r - a_s)\right] \qquad \ldots.(3.01.10)$$

where $\alpha = \alpha_r + i\alpha_i$ is the nozzle specific admittance ratio. For convenience let us define

$$B = (1 + \alpha\bar{u})/(1 - \alpha\bar{u}) \qquad \ldots.(3.01.11)$$

Thus the solutions in region 1 and region 2 are given as

$$v_1(x) = c_{s_1} \exp\left(-s_1 a_{s_1} x\right)\{1 - \exp\left[-s_1(a_{r_1} - a_{s_1})x\right]\} \qquad \ldots.(3.01.12a)$$

$$\frac{\varphi_1(x)}{\gamma} = \sigma_1(x)$$
$$= -c_{s_1} \exp(-s_1 a_{s_1} x)\{1 + \exp[-s_1(a_{r_1} - a_{s_1})x]\} \quad \ldots.(3.01.12b)$$

$$\left.\begin{aligned} v_2(x) &= c_{s_2} \exp(-s_2 a_{s_2} x)\{1 - B \exp[s_2(a_{r_2} - a_{s_2})(1-x)]\} \\ \frac{\varphi_2(x)}{\gamma} &= \sigma_2(x) \\ &= -c_{s_2} \exp(-s_2 a_{s_2} x)\{1 + B \exp[s_2(a_{r_2} - a_{s_2})(1-x)]\} \end{aligned}\right\} \quad \ldots.(3.01.13)$$

These two sets of solutions are to be matched at the concentrated combustion front $x = \psi$. As discussed previously, the concentrated combustion front is not a discontinuity of pressure, density, or temperature of the burnt gas, but is only a discontinuity of flow velocity. Hence the boundary condition at the concentrated combustion front consists of two parts:

(*1*) The steady state value, as well as the small perturbations of pressure and density are continuous at any instant across the concentrated combustion front*. That is

$$p_2' = p_1', \quad \text{and} \quad \rho_2' = \rho_1' \quad \text{at} \quad x = \psi$$

These are equivalent to the conditions:

$$\left.\begin{aligned} \varphi_2 &= \varphi_1 = \varphi \\ \sigma_2 &= \sigma_1 = \sigma \\ s_2 &= s_1 = s \end{aligned}\right\} \text{at } x = \psi \quad \ldots.(3.01.14)$$

(*2*) The fractional increase of the difference of mass flow rates across the concentrated combustion front is equal to the fractional increase of the burning rate at the concentrated combustion front.

The fractional increase of the difference of the mass flow rate is

$$\left[\frac{(\bar\rho_2 + \rho_2')(\bar u + u_2') - (\bar\rho_1 + \rho_1')u_1'}{\bar\rho \bar u}\right]_{x=\psi} = e^{st}\left[\sigma + \frac{v_2 - v_1}{\bar u}\right]_{x=\psi} \quad \ldots.(3.01.15)$$

To avoid the complications of the feeding system let us consider the case where the injection rate is kept constant regardless of the pressure oscillations in the combustion chamber. The instantaneous burning rate $\delta\dot m_b$ of each individual propellant element having steady state sensitive time lag lying between $\bar\tau$ and $\bar\tau + d\bar\tau$ is given by equations (1.11.13) and (1.11.18). In the present case where all elements have the same sensitive time lag, $\delta\dot m_b$ for each element can be replaced by the total variation of the burning rate $\dot m_b - \bar{\dot m}_b$ of all the elements. Thus the fractional increase of the total burning rate is

$$\mu_b = (\dot m_b - \bar{\dot m}_b)/\bar{\dot m}_b = -d\tau/dt = n[p'(\psi,t) - p'(\xi, t - \bar\tau)] \quad \ldots.(3.01.16)$$

* This is due to the fact that the combustion front in a rocket is a mass source where burnt gas is at essentially the same temperature as the previously burnt gas in both sides of the combustion front. This situation should be carefully distinguished from the flame front where heat is added to the flow of the cold gas upstream of the flame without substantial mass addition.

where ψ is the total space lag defining the position of the combustion front and ξ is the insensitive space lag corresponding to the position of the propellant element which burns at the instant t and became sensitive at the instant $t - \bar{\tau}$. Thus with u_l designating the axial velocity of the propellant element

$$\psi - \xi = \int_{t-\bar{\tau}}^{t} \bar{u}_l(t')\, dt'$$

Since $\bar{u}_l$ is of the order of M or less, $\psi - \xi = O(M) \cdot \bar{\tau}$. Therefore, if the sensitive time lag is of the order of unity in the dimensionless form, i.e. if $\bar{\tau}^* = O(\theta_w)$, then $\psi - \xi = O(M)$. Accordingly, $\xi \simeq \psi$ and equation (3.01.16) becomes

$$\mu_b = n\, e^{st}\, \varphi(\psi)[1 - e^{-s\bar{\tau}}] \qquad \ldots.(3.01.17)$$

Under this approximation $\xi \simeq \psi$, the position of the concentrated combustion front ψ will not oscillate because $\psi - \xi$ is the only variable part of the total space lag. Equating μ_b from equation (3.01.17) to the fractional increase of the difference of mass flow rate, from equation (3.01.15) we obtain the following boundary condition at $x = \psi$

$$\nu_2 - \nu_1 + \bar{u}(1 - \gamma n)\sigma + \bar{u}\gamma n\sigma \exp(-s\bar{\tau}) = 0 \qquad \ldots (3.01.18)$$

Substituting $\sigma_2(\psi)$ and $\sigma_1(\psi)$ from equations (3.01.12) and (3.01.13) into equation (3.01.14), we have

$$\frac{c_{s_2}}{c_{s_1}} = \frac{1 + \exp[-s(a_r - a_s)\psi]}{1 + B \exp[s(a_r - a_s)(1 - \psi)]} \qquad \ldots.(3.01.19)$$

Combining equations (3.01.12), (3.01.13), (3.01.14) and (3.01.19) with equation (3.01.18) we obtain the following characteristic equation for the determination of the complex quantity $s = \Lambda + i\Omega$

$$\frac{1 - B \exp[2s(1 - \psi)]}{1 + B \exp[2s(1 + \psi)]} - \frac{1 - \exp(-2s\psi)}{1 + \exp(-2s\psi)} = \bar{u}[(1 - \gamma n) + \gamma n \exp(-s\bar{\tau})] \qquad \ldots.(3.01.20)$$

where $a_r - a_s = 1/(1 + \bar{u}) + 1/(1 - \bar{u}) = 2/(1 - \bar{u}^2)$ has been taken equal to 2 under the approximation $M^2 \simeq \bar{u}^2 \ll 1$. By replacing s by $\Lambda + i\Omega$ and letting $\Lambda = 0$ in equation (3.01.20), we can obtain two real equations after separating the real and the imaginary parts of the resulting equation. The stability boundary for high frequency oscillations in such a system with concentrated combustion can then be obtained by eliminating Ω from the two real equations.

3.02. High Frequency Instability in Systems with Combustion Concentrated at the Injector End and Short Nozzle

Consider first the simplest case where the combustion chamber is very long, so that all the combustion is practically completed in the neighbourhood of the injector end, and the length of the subsonic portion of the nozzle is much smaller than the length of the combustion chamber. For this case $\psi \simeq 0$ and the nozzle flow can be reasonably expected to be quasi-steady with

$\alpha = (\gamma - 1)/2$. Thus let $\psi = 0$, $B = \{1 + \frac{1}{2}(\gamma - 1)M\}/\{1 - \frac{1}{2}(\gamma - 1)M\}$, $s = i\omega$ and $\bar{\tau} = \delta$ in equation (3.01.20), where ω and δ are the critical value of the dimensionless frequency of oscillation and the sensitive time lag corresponding to neutral oscillations. The following two real equations are obtained by separating the real and imaginary parts in equation (3.01.20) after neglecting M^2 as compared with unity.

$$\left.\begin{aligned} \gamma n \cos \omega\delta &= -(1 - \gamma n) - \frac{\gamma - 1}{2\cos^2 \omega} \\ \gamma n \sin \omega\delta &= \frac{\tan \omega}{\bar{u}} \end{aligned}\right\} \quad \ldots . (3.02.01)$$

When γn is of the order of unity, $\tan \omega$ must be of the order of M, and $\cos^2 \omega$ is approximately unity. Approximate solutions for ω and δ are thus:

$$\left.\begin{aligned} \omega &= l\pi + \gamma n\bar{u}\left[1 - \left(1 - \frac{\gamma + 1}{2\gamma n}\right)^2\right]^{\frac{1}{2}} \\ \delta &= \frac{1}{\omega}\left\{(2m + 1)\pi \mp \left[\frac{\pi}{2} - \sin^{-1}\left(\frac{\gamma + 1}{2\gamma n} - 1\right)\right]\right\} \end{aligned}\right\} \quad \ldots . (3.02.02)$$

where both m and l are positive integers, 0, 1, 2, etc. l indicates the number of half-wavelengths that are contained approximately in the combustion chamber length. In other words, the value of l designates the order of the successive higher modes of oscillation with frequencies corresponding to the lth acoustic mode in an organ pipe of length L, closed at both ends. m indicates the number of oscillation periods that are contained in the critical sensitive time lag and therefore designates the successive higher unstable ranges of values of the time lag $\bar{\tau}$. The lowest frequency of neutral oscillation is obtained when $l = 0$ where

$$\omega = \gamma n\bar{u}\left[1 - \left(1 - \frac{\gamma + 1}{2\gamma n}\right)^2\right]^{\frac{1}{2}} \quad \ldots . (3.02.03)$$

This frequency is based upon the characteristic time $\theta_w = Lc_0^*$. The gas residence time used as reference time for the low frequency analysis is $\theta_g = L/\bar{u}^* = \theta_w/\bar{u}$. This lowest frequency expressed in cycles per gas residence time θ_g is therefore

$$\gamma n\left[1 - \left(1 - \frac{\gamma + 1}{2\gamma n}\right)^2\right]^{\frac{1}{2}}$$

which coincides with the result given in equation (2.03.10) when $\gamma = 1$. This last restriction $\gamma = 1$ is due to the assumption made in the low frequency analysis that the gas temperature is constant regardless of the pressure oscillations, strictly correct only when $\gamma = 1$. The product $\omega\delta$ represents the phase shift of the oscillation during the time lag and is independent of the characteristic time. The second equation of (3.02.02) with $m = 0$ and the upper sign is easily seen to reduce to the second equation (2.03.10) when $\gamma = 1$. The solutions when $l = 0$ are therefore identified to be the low frequency result and will be discarded in the analysis for high frequency

oscillation. The fundamental mode of high frequency oscillation is thus taken to be the one with $l = 1$.

Either by determining the sign of Λ when $\omega = l\pi$ or by determining the sign of $d\Lambda/d\Omega$ on the stability boundary, the unstable ranges of frequencies are found as

$$l\pi - \gamma n\bar{u}\left[1 - \left(1 - \frac{\gamma+1}{2\gamma n}\right)^2\right]^{\frac{1}{2}} < \Omega < l\pi + \gamma n\bar{u}\left[1 - \left(1 - \frac{\gamma+1}{2\gamma n}\right)^2\right]^{\frac{1}{2}} \quad \ldots.(3.02.04)$$

and the unstable ranges of the time lag as

$$\frac{(2m+1)\pi - \left[\frac{\pi}{2} - \sin^{-1}\left(\frac{\gamma+1}{2\gamma n} - 1\right)\right]}{l\pi + \gamma n\bar{u}\left[1 - \left(1 - \frac{\gamma+1}{2\gamma n}\right)^2\right]^{\frac{1}{2}}} < \bar{\tau} < \frac{(2m+1)\pi + \left[\frac{\pi}{2} - \sin^{-1}\left(\frac{\gamma+1}{2\gamma n} - 1\right)\right]}{l\pi - \gamma n\bar{u}\left[1 - \left(1 - \frac{\gamma+1}{2\gamma n}\right)^2\right]^{\frac{1}{2}}} \quad \ldots.(3.02.05)$$

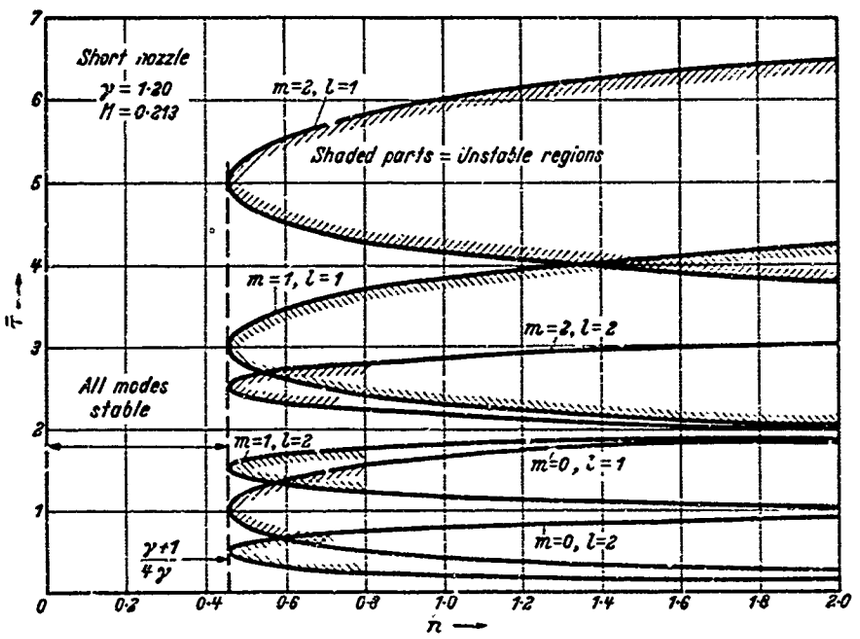

Figure 27. Unstable ranges of the sensitive time lag $\bar{\tau}$ for the fundamental ($l = 1$) and the second modes corresponding to different values of the interaction index n (short nozzle, entrance Mach number $M = 0{\cdot}213$). (By courtesy of the American Rocket Society)

where $l = 1, 2, 3, \ldots$ and $m = 0, 1, 2, 3, \ldots$. From equation (3.02.04) with $l = 1, 2 \ldots$ and when γn is of the order of unity, we see that the

frequencies of the unstable oscillations are always close to the natural (organ pipe) frequencies which under the present dimensionless scheme are $l\pi$. It is clear from equations (3.02.01)–(3.02.05) that in order to have real solutions of the stability boundary, the interaction index n must be sufficiently large so that

$$n \geqslant (\gamma + 1)/4\gamma \qquad \text{or} \qquad n_{\min} = (\gamma + 1)/4\gamma \qquad \ldots.(3.02.06)$$

Under the present approximations, the minimum value of n compatible with unstable oscillation is thus slightly less than one half because the value of γ of the combustion gases is always slightly larger than unity. From a more careful analysis in later sections, it will be shown that this minimum value of n is actually one half.

When n is equal to this minimum value $(\gamma + 1)/4\gamma$, we have

$$\omega = l\pi \quad \text{and} \quad \omega\delta = (2m + 1)\pi \qquad \ldots.(3.02.07)$$

with vanishing unstable ranges of Ω and $\bar{\tau}$. When n increases from this $n_{\min}$, both unstable ranges of Ω and $\bar{\tau}$ increase. When n becomes very large, almost any values of $\bar{\tau}$ fall in the unstable range. The unstable ranges of $\bar{\tau}$ for $m = 0$, 1 and 2 and $l = 1$ and 2 are plotted versus n in *Figure 27* when $\gamma = 1{\cdot}20$ and $M = 0{\cdot}213$.

3.03. Systems with Combustion Concentrated at an Arbitrary Axial Location and Short Nozzle

Consider next the more general case where the combustion chamber is much longer than the subsonic portion of the nozzle, so that the nozzle flow is approximately quasi-steady, but the insensitive time lag is sufficiently large so that the space lag is not negligibly small compared with the combustion chamber length. Then the two real equations obtained by separating the real and the imaginary parts of equation (3.01.20) become

$$\gamma n \cos \omega\delta = (1 - \gamma n) - \frac{\gamma - 1}{2 \cos^2 (1 - \psi)\omega}$$

$$\gamma n \sin \omega\delta = \frac{\sin \omega/\bar{u}}{\cos \psi\omega \cos (1 - \psi)\omega} \qquad \ldots.(3.03.01)$$

For real values of ω, $\cos^2 (1 - \psi)\omega$ is always less than, or at most equal to, unity; thus the following inequality must be satisfied in order to have real solutions for the frequency ω of neutral oscillation:

$$\bar{u}^2 \{\gamma[\gamma n + n - 1] - [(\gamma - 1)/2]^2\} \cos^2 \psi\omega \geqslant \sin^2 \omega \geqslant 0 \qquad \ldots.(3.03.02)$$

When n is equal to $n_{\min} = (\gamma + 1)/4\gamma$, the inequality (3.03.02) shows that the only possible values of ω are given by $\sin \omega = 0$ and the non-zero values of ω must be $l\pi$. Then equations (3.03.01) indicate that the only possible value of ψ is given by $\cos^2(1 - \psi)l\pi = 1$ or $\psi = 0$, $1/l$, $2/l$, etc., and the only possible values of the critical time lag δ are given by $\cos \omega\delta = -1$, with the consequence that there is no unstable range of the time lag $\bar{\tau}$. In other words, when $n = n_{\min} = (\gamma + 1)/4\gamma$, neutral oscillation of the lth mode

can occur only when both the combustion is concentrated at an antinodal position of the lth mode of pressure oscillation and the time lag has the optimum value in coordinating the pressure oscillation and the resulting burning rate oscillation. For any other combustion distribution, the lth mode of oscillations is stable with $n = n_{\min} = (\gamma + 1)/4\gamma$ and must be damped out eventually, even with optimum timing. This fact indicates that the combustion distribution which is most capable of exciting unstable oscillations of the lth mode is the one with combustion concentrated at the antinodal positions of the lth mode of pressure oscillation. This is physically reasonable because under the approximation of $\psi \simeq \xi$, the propellant elements, during the sensitive time lag, sense only the pressure variations at the combustion front. Thus when the combustion front is at the antinodal positions of the lth mode of pressure oscillation, all the propellant elements can sense the maximum amount of the variations of the pressure and other associated properties. Accordingly, the system is most liable to instability of the lth mode.

With combustion concentrated at the antinodal position of the lth mode, if the magnitude of the interaction index n increases from the minimum value $n_{\min}$, the magnitude of the variation of the burning rate is greater than that required to maintain neutral oscillations of the lth mode with optimum timing. Consequently, it can be expected that when n is greater than $(\gamma + 1)/4\gamma$, neutral and unstable oscillations can be obtained when both of the following conditions are fulfilled: the dimensionless sensitive time lag is contained in certain finite ranges about any of the optimum values given by $\cos l\pi\delta = -1$, and the combustion is concentrated in certain finite ranges in the neighbourhood of the antinodes of the lth mode of oscillation. Furthermore, when n is greater than $(\gamma + 1)/4\gamma$ but not much larger than unity, the inequalities (3.03.02) show that any neutral oscillation will have a frequency ω not significantly different from $l\pi$ as explained previously. Thus, there must be some position of the combustion front between 0 and 1 that will make $\cos \psi\omega = \cos \{\psi[l\pi + O(\bar{u}_{,})\} = 0$. For these values of ψ, which are somewhere in the neighbourhood of $1/2l$, $3/2l$, etc., the only possible real value of ω compatible with inequality (3.03.02) is $m\pi$. However, the simultaneous vanishing of $\cos \psi\omega$ and $\sin \omega$ makes $\cos (1 - \psi)\omega$ equal to zero which is incompatible with the first equation (3.03.01) because $|\gamma n \cos \omega\delta| \leqslant \gamma n$ is always finite. This fact indicates that when ψ takes some value in the neighbourhood of $1/2l$, $3/2l$, etc., no neutral oscillation can exist; in other words, the lth mode is always stable when combustion is concentrated in the neighbourhood of the node of pressure oscillation. This again can be expected on purely physical grounds because around a pressure node, the propellant elements cannot sense any pressure variations. Therefore for a given value of $n > (\gamma + 1)/4\gamma$, unstable and neutral oscillations of a given mode are possible when combustion is concentrated at some axial position in the neighbourhood of a pressure antinode; and oscillations of a given mode are always stable when combustion is concentrated around a pressure node. The stable region about a node is separated from the regions of possible instability about the neighbouring antinodes by critical values of ψ which we call ψ_c. These positions ψ_c of the combustion front are characterized by the fact that both the two critical values of the frequencies

ω and the two critical values of the time lag δ coincide so that there cannot be any unstable oscillations of the given mode, and only neutral or stable oscillation is possible at the given value of n. Thus, the values of ψ_c corresponding to a given value of n can be determined by putting $\sin \omega = 0$ in equations (3.03.01) as

$$1 \geqslant \psi_{c,} = 1 - \frac{1}{2l\pi} \cos^{-1} \left[\frac{\gamma - 1}{2\gamma n - 1} - 1 \right] \geqslant 0 \quad \ldots . (3.03.03)$$

For the fundamental mode there is only one node at $\psi = \frac{1}{2}$ and there are two values of ψ_c symmetric with respect to $\frac{1}{2}$. For the lth mode, there are $2l$ values of ψ_c defining l stable regions about l nodes. Calculated results are plotted as shown in *Figure 28* for $l = 1$, 2 and 3, and $\gamma = 1{\cdot}20$. For a

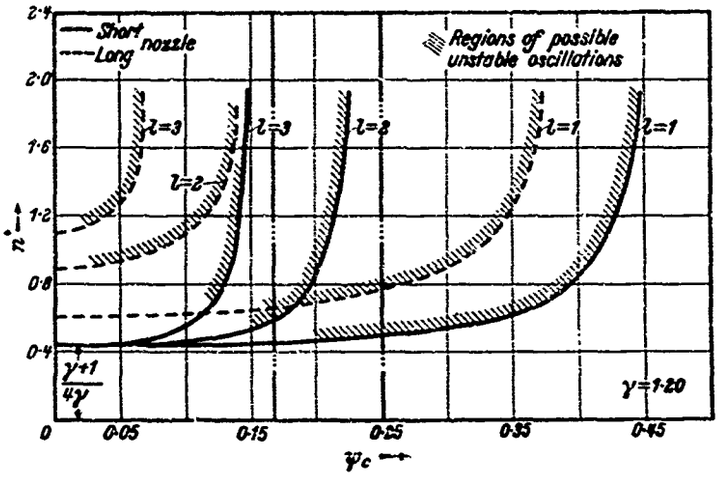

Figure 28. Critical values ψ_c, dividing the unstable range and the stable range of the fractional axial position ψ of the concentrated combustion front corresponding to different values of the interaction index n (ψ is measured from the injector face as a fraction of the chamber length).
(By courtesy of the American Rocket Society)

given value of n, this plot gives the value ψ_c which separates the region in which a concentrated combustion front is always stable for any values of $\bar{\tau}$, from the region in which a concentrated combustion front can possibly become unstable when $\bar{\tau}$ is in the proper range of values. From another point of view, this curve gives the minimum value of n, i.e. $n_{\min}$, compatible with unstable oscillations of the given mode when combustion is concentrated at the position $\psi = \psi_c$. *Figure 28* shows that when the combustion is concentrated at the node of the lth mode of pressure oscillation, that is $\psi = 1/2l$, $3/2l$, etc., $n_{\min}$ is infinitely large; therefore the lth mode of oscillation is always stable for any large but finite values of the interaction index. If the combustion is concentrated at the antinodal positions $\psi = 0$, $1/l$, $2/l$, etc., the magnitude of n required to excite unstable oscillation is the smallest compared to other positions; and therefore, such positions are the most undesirable positions for the combustion front if a stable system is

desired. Since the injector end is an antinode of all modes of pressure oscillations, the configuration with combustion concentrated at the injector end is the most undesirable one from the stability considerations alone. This qualitative conclusion, however, does not help us very much in selecting the most desirable position for the concentrated combustion front, because

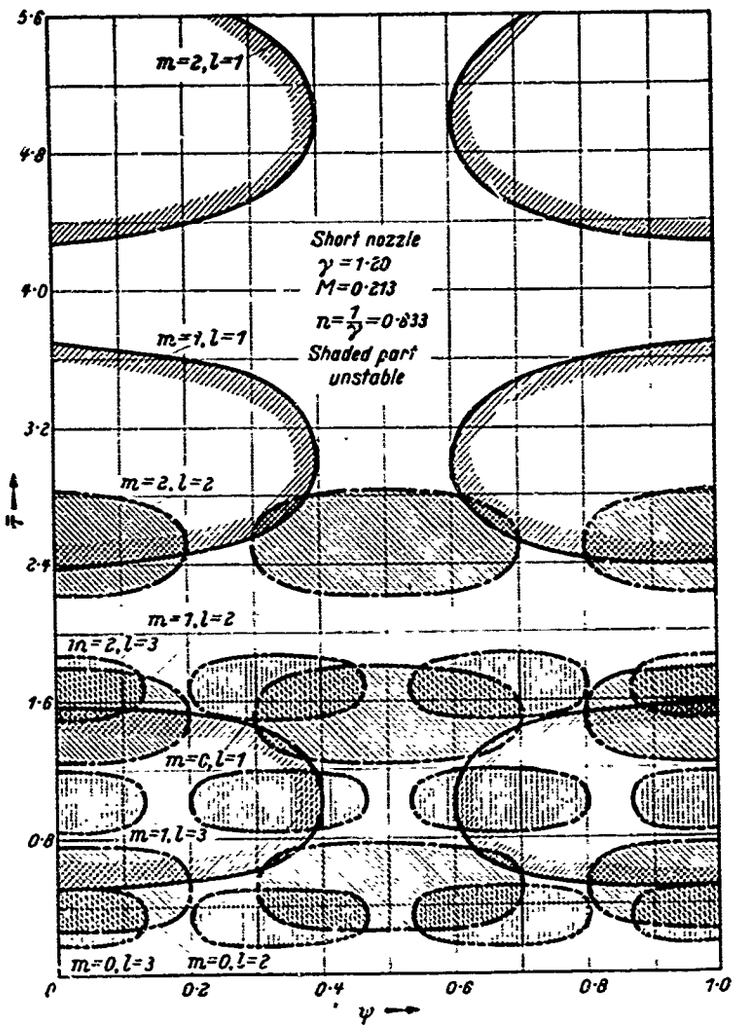

Figure 29. Unstable ranges of the sensitive time lag $\bar{\tau}$ for the first three modes when the combustion is concentrated at different fractional axial positions ψ for $n = 0{\cdot}833$ (short nozzle).
(By courtesy of the American Rocket Society)

the nodal position of a given mode will be the antinodal positions for other modes. For example, the node of the fundamental mode, $\psi = \frac{1}{2}$, is the antinode of the second mode. Thus, while the configuration with combustion concentrated at the middle of the chamber will guarantee the stability of the fundamental mode, it is most liable to cause an unstable oscillation of the second mode. An important modification of these results

will be shown in the next section, due to the presence of a nozzle which has its subsonic part not negligibly short as compared to combustion chamber length, in which case the quasi-steady state condition of the nozzle flow cannot be applied.

The critical values ω and δ can be obtained from equation (3.03.01) with a numerical iteration procedure which converges very rapidly. The unstable ranges of the time lag $\bar{\tau}$ for oscillation of the first few high frequency modes are plotted against the position ψ of the concentrated combustion front as shown in *Figure 29* with $\gamma = 1{\cdot}20$, $M = 0{\cdot}213$ and $n = 1/\gamma = 0{\cdot}833$. We observe that the regions of instability of the various modes have a tendency to cover all the available area. That is, a system with any values of $\bar{\tau}$ and ψ would encounter some unstable mode of oscillation. If such were the actual case, it would be hardly possible to design a rocket with concentrated combustion and $n > n_{\min}$, stable for all high frequency modes. It will be shown in the next section how the possibility for the higher modes to become unstable is significantly reduced by the presence of a nozzle.

3.04. Systems with Concentrated Combustion and Long Nozzle

In practical cases, the subsonic portion of the nozzle is not too short, usually $\frac{1}{3}$ or $\frac{1}{4}$ of the combustion chamber length. For such a nozzle, and for the

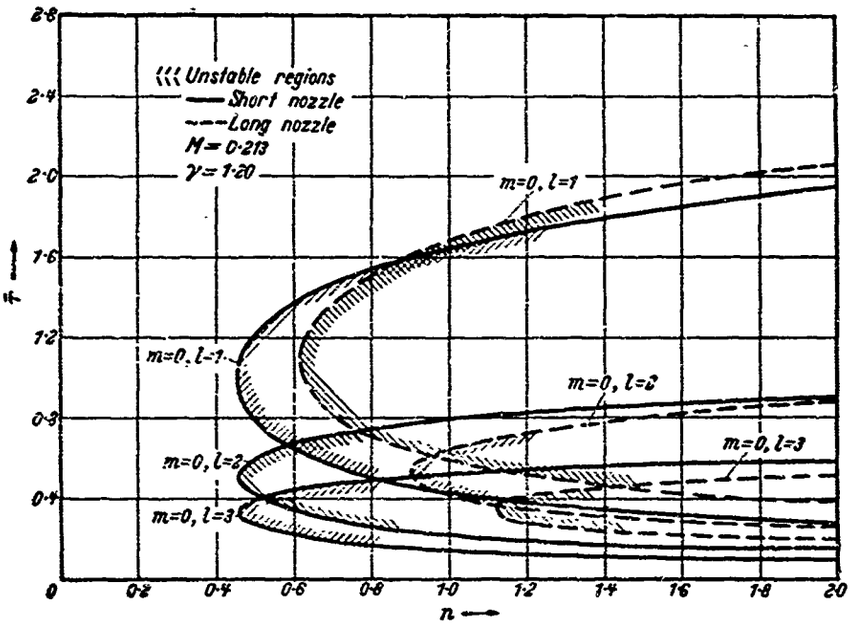

Figure 30. Lowest unstable ranges of the sensitive time lag $\bar{\tau}$ for the first three modes corresponding to different values of the interaction index n.
(By courtesy of the American Rocket Society)

frequency range under consideration, the nozzle flow is significantly different from the quasi-steady conditions. The nozzle specific admittance ratio $\alpha = (v/\bar{u})/(\delta/\bar{p})$ is in general found to be a complex function of the frequency of oscillation and of the geometry of the nozzle as shown in Appendix B.

For a special shape of nozzle with linear steady state velocity distribution in the subsonic portion, the real and imaginary parts of the specific admittance ratio $\alpha = \alpha_r(\beta) + i\alpha_i(\beta)$ are given in *Figures 59* and *60* as a function of the reduced frequency β, and the Mach number of the gas entering the nozzle M. The parameter β is the ratio of the angular frequency of the oscillation to the dimensionless velocity gradient $\bar{u}_x$ in the subsonic portion of the nozzle in steady state operation. Thus $\beta = \omega/\bar{u}_x = \omega l_{sub}/[\{2/(\gamma+1)\}^{\frac{1}{2}} - \bar{u}]$ with l_{sub} indicating the length of the subsonic portion of the nozzle as a fraction of the combustion chamber length. The complex quantity $B = (1 + \alpha\bar{u})/(1 - \alpha\bar{u})$ as defined in equation (3.01.11) can be calculated for given frequencies ω, and given entering Mach number M when the steady state velocity gradient $\bar{u}_x$ in the subsonic portion of the nozzle is known. The following calculation is performed with $\bar{u}_x = \pi$. This value corresponds to an l_{sub} in the neighbourhood of 1/3. With this value of $\bar{u}_x$, we have $\omega = \beta\pi$ so that integral values of β correspond to the pure acoustic modes in an organ pipe with closed ends.

For determination of the stability boundary rewrite equation (3.01.20) as

$$\gamma n \exp[-i\omega\delta] = \chi_r + i\chi_i + (\gamma n - 1) \qquad \ldots.(3.04.01)$$

where

$$\chi_r + i\chi_i = \frac{1}{M}\left[\frac{1 - B\exp[2i\omega(1-\psi)]}{1 + B\exp[2i\omega(1-\psi)]} - \tanh i\omega\psi\right]$$

$$= \frac{-\alpha_r}{[\cos^2(1-\psi)\omega + (\alpha_r^2 + \alpha_i^2)M^2\sin^2(1-\psi)\omega - \alpha_i M\sin 2(1-\psi)\omega]}$$

$$- i\frac{(1/\pi)\sin\omega\cos(1-\psi)\omega - (\alpha_r^2 + \alpha_i^2)M\cos\omega\sin(1-\psi)\omega + \alpha_i\cos(2-\psi)\omega}{\cos\psi\omega[\cos^2(1-\psi)\omega + (\alpha_r^2 + \alpha_i^2)M^2\sin^2(1-\psi)\omega - \alpha_i M\sin 2(1-\psi)\omega]}$$

$$\ldots.(3.04.02)$$

For given values of $\bar{u}$ and ψ with $\gamma = 1{\cdot}20$, $\chi_r + i\chi_i$ can be calculated for each value of ω. Equating the moduli of the two sides of equation (3.04.01) and solving for n we find

$$n = (1 - \chi_r)/2\gamma + \chi_i^2/\{2\gamma(1 - \chi_i)\} \qquad \ldots.(3.04.03)$$

The corresponding critical values of the time lag are found by equating the imaginary parts of equation (3.04.01) as

$$\delta = (1/\omega)\sin^{-1}[\chi_i/\gamma n] = (1/\omega)\cos^{-1}[1 - \chi_r/\gamma n] \qquad \ldots.(3.04.04)$$

where the value of the inverse circular function is taken in the quadrant consistent with both of the two equalities in equation (3.04.04).

The unstable ranges of $\bar{\tau}$, when $M = 0{\cdot}213$ and when the combustion is concentrated at the injector end, have been determined for different values of n. The results are plotted as shown in *Figure 30* along with the results

obtained in the previous section for a very short nozzle. It is seen that the minimum value of n compatible with unstable oscillations of a given mode is significantly increased from the value $(\gamma + 1)/4\gamma$ pertaining to all modes in the case of a very short nozzle. Even more significant is the fact that when the finite length of the nozzle is considered, $n_{\min}$ increases for higher modes of oscillation. The minimum values of n compatible with unstable

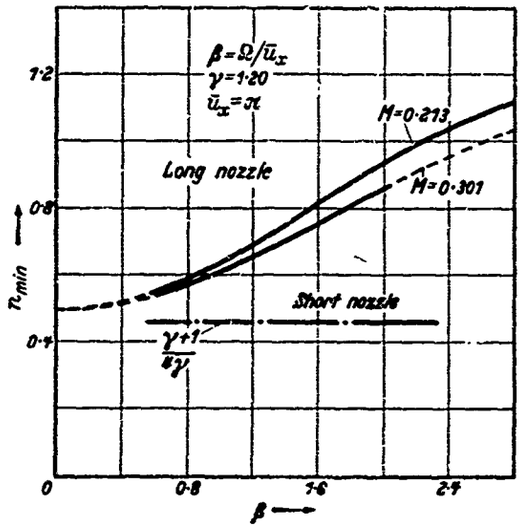

Figure 31. Minimum values of the interaction index, $n_{\min}$, compatible with unstable oscillations as a function of the reduced angular frequency β (By courtesy of the American Rocket Society)

oscillations of the first few modes, when combustion is concentrated at the position ψ, have been plotted for comparison in *Figure 28*. The values used in the computations are $\gamma = 1{\cdot}20$ and $M = 0{\cdot}213$. The absolute minimum value $n_{\min}$ for arbitrary location of the concentrated combustion front is plotted in *Figure 31* against the reduced frequency parameter β for $\gamma = 1{\cdot}20$ and two values of the Mach number $M = 0{\cdot}213$ and $0{\cdot}301$. The stabilizing effect of the length of the nozzle is clearly seen to be increasing for higher modes of oscillations, and the damping effect of a long nozzle is much larger than that obtained from a very short nozzle.

The critical values $\bar{\tau} = \delta$ and ψ are plotted in *Figure 32* for the case $\gamma = 1{\cdot}20$, $n = 1/\gamma = 0{\cdot}833$ and $M = 0{\cdot}213$. The unstable ranges of time lag $\bar{\tau}$ are shown as shaded regions. For comparison, the dotted curves indicating the stability boundary of *Figure 29* are also included. From *Figure 32* it is clear that while the result, with a very short nozzle, shows definite unstable regions for all higher modes of oscillation, the result with a conventional nozzle shows that only the fundamental mode can possibly become unstable when the combustion is concentrated near the two ends of the combustion chamber. More specifically a system using a propellant combination with $n = 0{\cdot}833$ is intrinsically unconditionally stable if the combustion front is located in the region from 28–78 per cent of the combustion chamber length. Either from *Figure 28* or based upon physical

grounds, the unconditionally stable range of positions of the concentrated combustion front is expected to increase if the value of n of the propellant combination is less than 0·833. Thus, unconditional stability can be obtained when the combustion front is situated in a region from 28–78 per cent of the chamber length if the n of the propellant combination is less

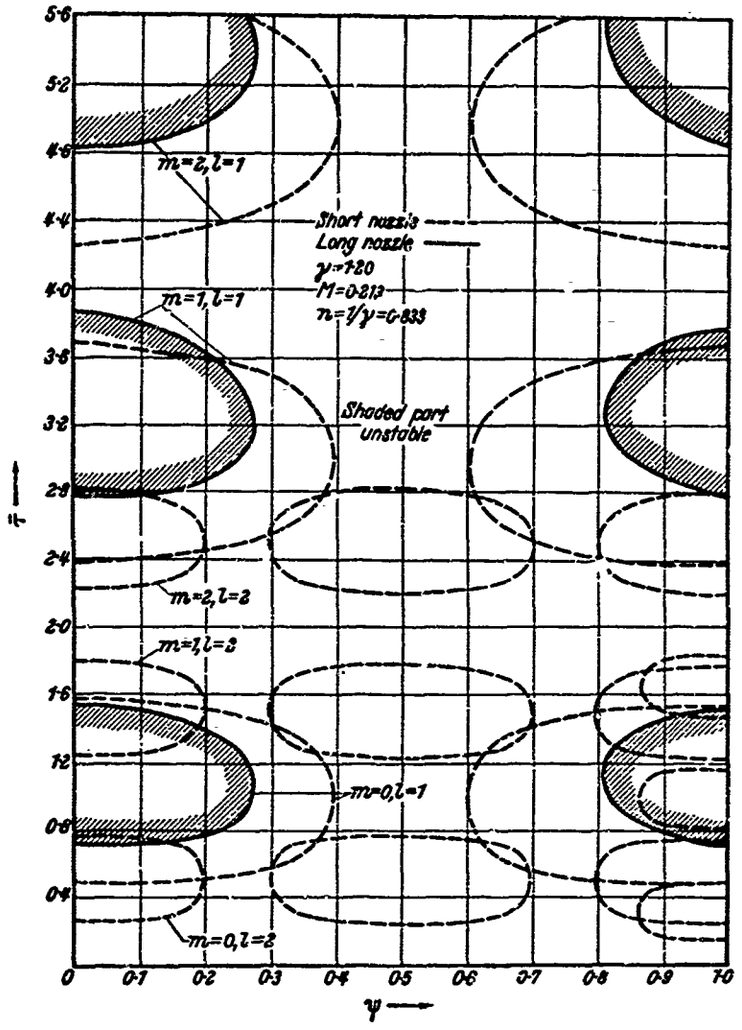

Figure 32. Effect of the nozzle geometry on the unstable ranges of the sensitive time lag $\bar{\tau}$, when the combustion is concentrated at different fractional axial positions ψ for $n = 0{\cdot}833$. (Stability boundaries for modes higher than the second for short nozzle are not reproduced in this figure.) (By courtesy of the American Rocket Society)

than 0·833. On the other hand, if the n of the propellant combination is larger than 0·833, the stable region will decrease; and with sufficiently large n, unstable regions for the second mode, and eventually the successive higher modes, may appear. In *Figure 33* the stability boundary δ/ψ and the unstable regions of $\bar{\tau}/\psi$ are shown with $n = 1{\cdot}00$. For this value of n,

small unstable regions for the second mode are obtained near each of the three values $\psi \gtrsim 0$, $\psi \simeq \frac{1}{2}$ and $\psi \lesssim 1$ respectively. Thus either the fundamental mode or the second mode can become unstable when both the combustion is concentrated in a certain region and the time lag is in the

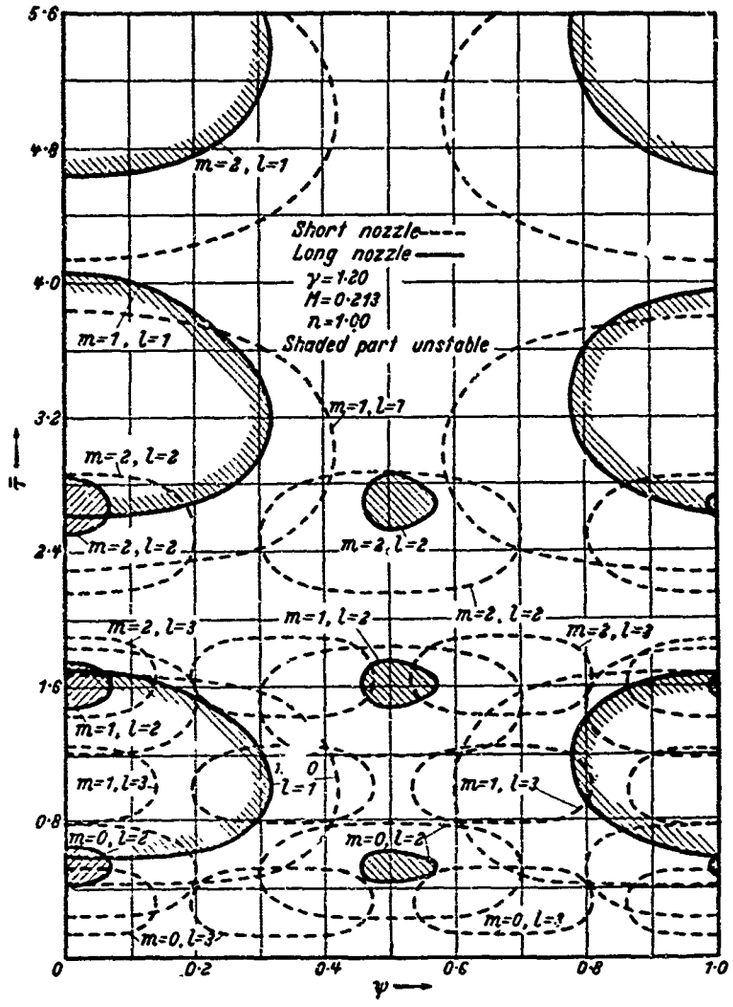

Figure 33. Effect of the nozzle geometry on the unstable ranges of the sensitive time lag $\bar{\tau}$, when the combustion is concentrated at different fractional axial positions ψ for $n = 1{\cdot}00$. (Stability boundaries for modes higher than the third for short nozzle are not reproduced in this figure.) (By courtesy of the American Rocket Society)

proper range. Both modes can become unstable simultaneously (for example, with $\psi \simeq 0$ and $\bar{\tau} \simeq 0{\cdot}6$). The dotted curves again outline the unstable regions of *Figure 29* for the purpose of comparison. The strong stabilizing effect of the nozzle toward higher modes of oscillation is demonstrated to be of great importance.

The following qualitative conclusions concerning the stability behaviour

of liquid rockets with all propellant elements having the same total space lag and the same sensitive time lag are therefore obtained.

(*1*) The minimum value of n_{min} compatible with unstable oscillation of a given frequency increases when the concentrated combustion front is shifted away from the nearest antinode of the pressure oscillation of that mode, and becomes very big when the neighbouring node of pressure oscillation of that mode is approached. This means that the oscillation of a given frequency is most unstable when combustion is concentrated at an antinode and becomes completely stable when combustion is concentrated at a node. Since the injector end is an antinode of all modes of oscillation, any mode of oscillation is most likely to become unstable when the combustion is concentrated at the injector end. Under this configuration the minimum value of n compatible with unstable oscillations of the fundamental mode is smaller than the values of n_{min} of any other higher mode.

(*2*) For a system with a fixed value of n of the given propellant combination, a given mode of oscillation is always stable when combustion is concentrated in any of the discrete stable regions about the nodes of that mode of pressure oscillations. The extent of such stable regions increases for higher modes of oscillations, and these stable regions cover the whole length of the combustion chamber axis when the value of n_{min} of that mode becomes greater than the value of n of the given propellant combination.

(*3*) Rockets with a longer subsonic portion of the nozzle as compared with the combustion chamber length are more stable than rockets with a shorter subsonic part. A nozzle with a negligibly short subsonic part, as compared with the combustion chamber length, is the nozzle configuration that is most likely to exhibit unstable combustion.

(*4*) If combustion is mostly concentrated in a region the width of which is only a small fraction of the combustion chamber length, the stability behaviour of the fundamental and the next few higher modes of oscillations can be satisfactorily analysed by using the simplified model of a concentrated combustion front. If the combustion is distributed so that the combustion zone covers a considerable portion of both the stable and unstable regions of ψ of a given mode of oscillation, there is no obvious position that can be attributed to the concentrated combustion front in order to analyse approximately the stability behaviour of this mode with the simplified model. Since the number of pressure nodes increases for higher modes of oscillation, the extent of each stable or each unstable region of ψ decreases. The simplified model is therefore not quite satisfactory for the analysis of the stability of the higher modes of oscillations even if the combustion zone is narrow. Fortunately, the stabilizing effect of the nozzle increases with the higher modes of oscillation and we can expect these higher modes to be stable under ordinary circumstances. Therefore, we are interested only in the fundamental mode and the next few higher modes of oscillation and the simplified model of concentrated combustion gives a very convenient idea of the high frequency stability behaviour of systems with combustion distributed over a sufficiently narrow region. On the other hand, if the combustion is distributed over a considerable portion of the combustion chamber axis, the simplified model of a concentrated combustion front is not suitable and a more careful formulation is necessary.

3.05. Effect of Time Lag Spread on Systems with Concentrated Combustion

It has been assumed in the previous sections that all the propellant elements have the same sensitive time lag in addition to the same total space lag. Both assumptions, of course, represent only ideal limiting cases. In the following sections, we shall discuss the effect of lifting these assumptions, one at a time, in order to obtain a more realistic result. Let us first consider the case where the space lags of all propellant elements are the same but the sensitive time lags of different propellant elements are different. Since the unburnt propellant elements are assumed to occupy negligible volume, the steady state flow of the burnt gas on either side of the concentrated combustion front is not affected by the spread of the sensitive time lag. The solutions for small perturbations as given by equations (3.01.12) and (3.01.13) are still valid in each of the two regions. The effect of the spread of time lag appears only in the boundary condition at $x = \psi$ where the two solutions in regions (1) and (2) are to be matched.

The first part of the boundary condition at the concentrated combustion front is still given by the continuity of the pressure and the density of burnt gas at any instant across the combustion front as shown in equation (3.01.14). The second part of the boundary condition at $x = \psi$ relates the instantaneous velocity discontinuity to the local burning rate. The spread of the time lag changes the burning rate and therefore the velocity discontinuity. Let us denote the fractional amount of the propellant elements having dimensionless sensitive time lag less than or equal to $\bar{\tau}$ by $f(\bar{\tau})$ with $f(\bar{\tau}_{min}) = 0$ and $f(\bar{\tau}_{max}) = 1$. As shown in Section 2.08, we can define

$$\bar{\tau}_m = (\bar{\tau}_{max} + \bar{\tau}_{min})/2$$

and

$$\Delta\bar{\tau} = \bar{\tau}_{max} - \bar{\tau}_{min}$$

The fractional burning rate perturbation is

$$\mu_b = n\, e^{st} \int_0^1 \{\varphi(\psi) - \varphi[\xi(t - \bar{\tau})]\, e^{-s\bar{\tau}}\}\, df \qquad \ldots.(3.05.01)$$

where both t and $\bar{\tau}$ are now non-dimensionalized by the use of the wave propagation time θ_w, and $\xi(t - \bar{\tau})$ means that ξ must be evaluated at the instant $t - \bar{\tau}$. Since by definition $\int_0^1 df = 1$, we can rewrite equation (3.05.01) for isentropic small oscillations with $\varphi(\psi) = \gamma\delta(\psi) \neq 0$ as

$$\mu_b = \gamma_n\, e^{-st}\, \sigma(\psi)\, [1 - C\, e^{-s\bar{\tau}_e}] \qquad \ldots.(3.05.02)$$

with

$$C\, e^{-s\bar{\tau}_e} = \int_0^1 \frac{\sigma[\xi(t - \bar{\tau})]}{\sigma(\psi)}\, e^{-s\bar{\tau}}\, df \qquad \ldots.(3.05.03)$$

The constants C and $\bar{\tau}_e$ have the physical meaning explained in Section 2.08.

With equation (3.05.02) the second part of the boundary condition at the concentrated combustion front becomes

$$\nu_2 - \nu_1 + \bar{u}(1 - \gamma n)\sigma + \bar{u}\gamma n\sigma C \exp(-s\bar{\tau}_e) = 0 \qquad \ldots.(3.05.04)$$

The characteristic equation for the determination of the complex quantity $s = \Lambda + i\Omega$ becomes

$$\left.\begin{aligned}(1 - \gamma n) + \gamma n C \exp(-s\bar{\tau}_e) \\ = \frac{1}{\bar{u}}\left\{\frac{1 - B\exp[2s(1-\psi)]}{1 + B\exp[2s(1-\psi)]} - \tanh s\psi\right\} \\ = \chi_r + i\chi_i\end{aligned}\right\} \ldots.(3.05.05)$$

which is the same as equation (3.01.15) except that the factor $C \exp(-s\bar{\tau}_e)$ replaces $\exp(-s\bar{\tau})$.

With the simplifying assumption $\xi \simeq \psi$ already used in previous sections, equation (3.05.03) becomes identical with equation (2.08.06) and thus, for neutral oscillations where $s = i\omega$,

$$C = \left| \int_0^1 e^{-i\omega(\bar{\tau} - \bar{\tau}_m)} df \right| \leqslant 1$$

If in addition $df/d\bar{\tau}$ is symmetric with respect to $\bar{\tau}_m$, we have

$$\left.\begin{aligned}\bar{\tau}_c = \bar{\tau}_m \\ C = 2\int_0^{\frac{1}{2}} \cos[\omega(\bar{\tau} - \bar{\tau}_m)]\, df\end{aligned}\right\} \qquad \ldots.(3.05.06)$$

The critical values n and δ_e can be determined from equations (3.05.05) and (3.05.06) with known types of distribution of time lag. To illustrate the effect of the spread of time lag, let us consider first the case where the extent of time lag spread $-\Delta\bar{\tau}$ is sufficiently small, so that C will be substantially constant for a given mode of oscillation regardless of the small variations of ω, and the magnitude of C will be slightly less than unity. For these cases, the determination of the stability boundary is especially simple.

By separating the real and imaginary parts of equation (3.05.05) we have for neutral oscillations

$$\left.\begin{aligned}\gamma n C \cos\omega\delta_e = \gamma n - (1 - \chi_r) \\ \gamma n C \sin\omega\delta\chi = -\chi_i\end{aligned}\right\} \ldots.(3.05.07)$$

Both χ_r and χ_i are given explicitly in equation (3.04.02) as known functions of ω for a given rocket. The critical values of n and δ_e corresponding to neutral oscillation of frequency ω can then be calculated from

$$\left.\begin{aligned}n = \frac{(1 - \chi_r) - [(1 - \chi_r)^2 C^2 - (1 - C^2)\chi_i^2]^{\frac{1}{2}}}{2\gamma(1 - C^2)} \\ \delta_e = (1/\omega)\sin^{-1}[\chi_i/(\gamma n C)]\end{aligned}\right\} \ldots.(3.05.08)$$

The results with $C = 0{\cdot}9$ for different positions ψ of the concentrated combustion front are given in *Figures 34*(a) and (b), and *35*(a) and (b).

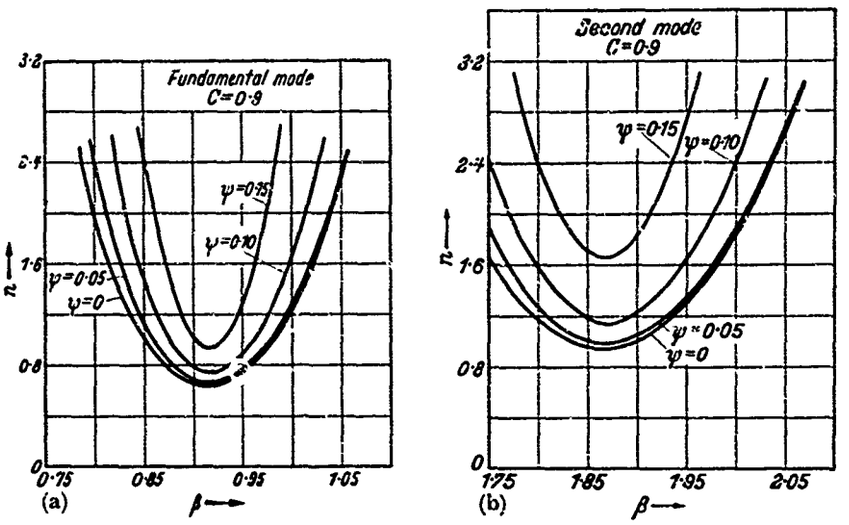

Figure 34. Critical values of the interaction index n required to maintain neutral oscillations of reduced frequency β (long nozzle) when the combustion is spatially concentrated at different fractional axial positions ψ and the sensitive time lag is spread in a small range corresponding to magnification factor C = 0·9: (a) fundamental mode (natural frequency of the chamber with closed ends, β = 1); (b) second mode (natural frequency of the chamber with closed ends, β = 2)

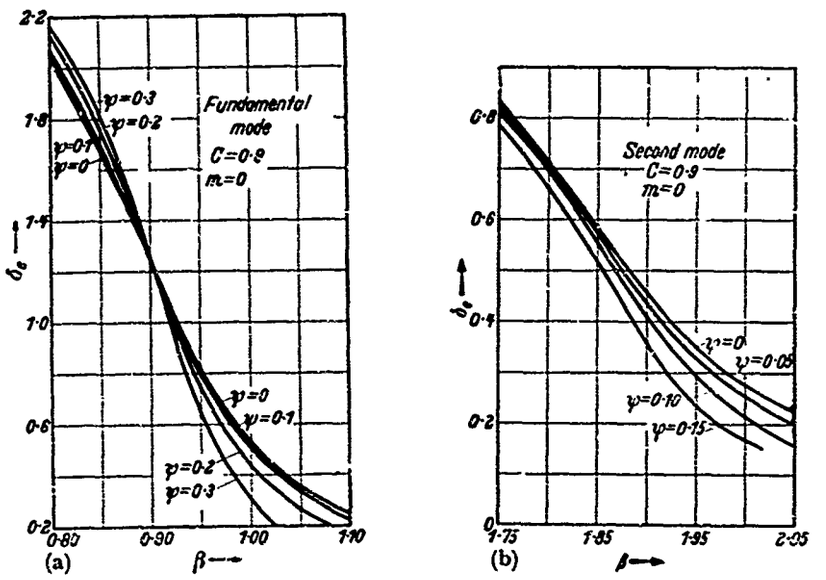

Figure 35. Critical values δ_c of the effective sensitive time lag, corresponding to neutral oscillations of reduced frequency β (long nozzle) when the combustion is spatially concentrated at different fractional axial positions ψ and the sensitive time lag is spread in a small range corresponding to magnification factor C = 0·9: (a) fundamental mode (natural frequency of the chamber with closed ends, β = 1); (b) second mode (natural frequency of the chamber with closed ends, β = 2)

The unstable ranges of the effective time lag $\bar{\tau}_e$ for systems with $n = 1$ and different positions of the concentrated combustion front are shown in *Figure 36*. The result without time lag spread, $C = 1$, is also shown by the dotted line for comparison. It is observed that the unstable ranges are reduced when $C = 0{\cdot}9$ as compared to those when $C = 1$. The spreading

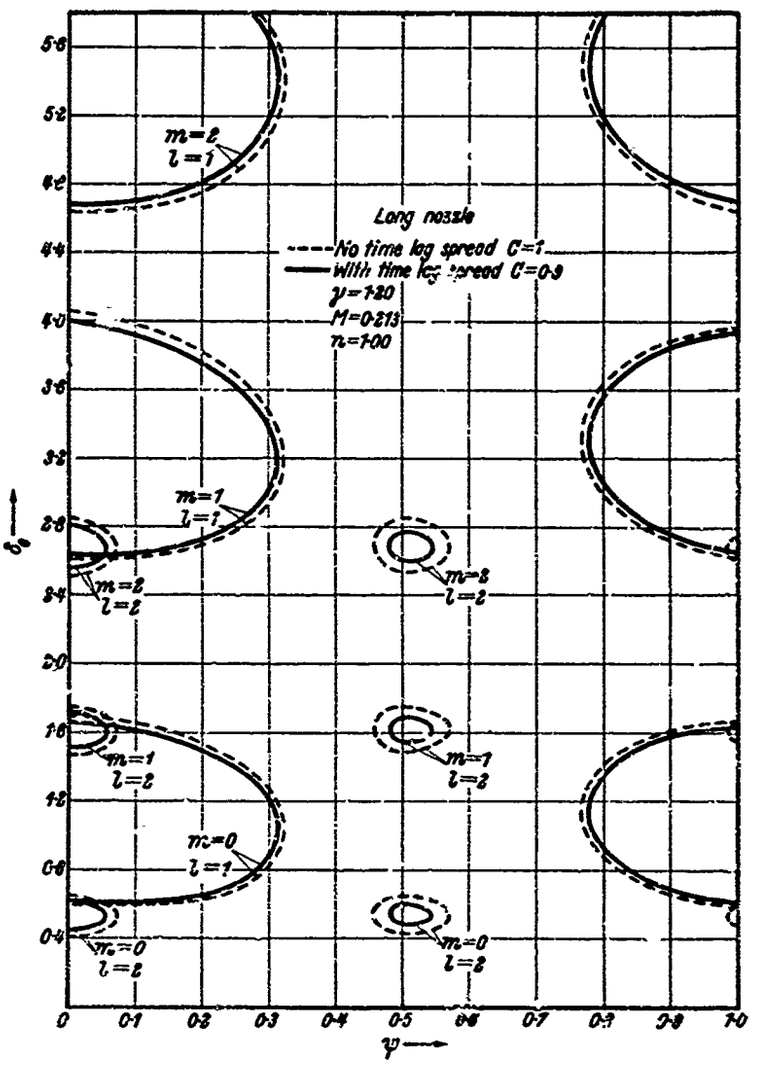

Figure 36. Effect of the small timewise spread of the sensitive time lag on the critical values $\bar{\tau}_e$ corresponding to neutral oscillations when the combustion is concentrated spatially at the fractional axial positions ψ for $n = 1$ (long nozzle)

of the time lag is therefore stabilizing. In *Figure 37* the minimum value of n compatible with unstable oscillations in systems with combustion concentrated at an arbitrary axial location is plotted against C and is seen to be

increasing monotonically when C decreases from unity. When the magnitude of C is too much smaller than unity, the curve is shown dotted because the approximation of constant C is no longer valid even for small variations of ω. Qualitatively the stabilizing effect of spreading the time lag increases with decreasing C.

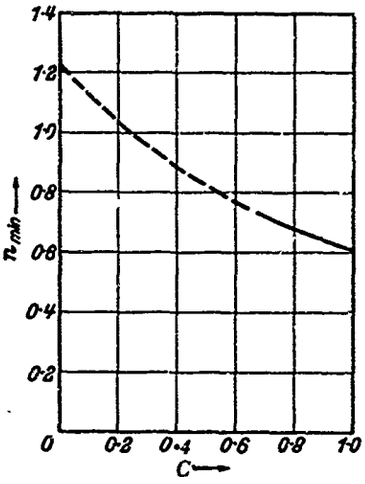

Figure 37. Effect of the timewise spread of the sensitive time lag on the minimum value of the interaction index, n_{min}, compatible with unstable oscillations with combustion concentrated at an arbitrary axial position. A smaller value of C indicates a larger spread of the sensitive time lag; $C = 1$ indicates no spread

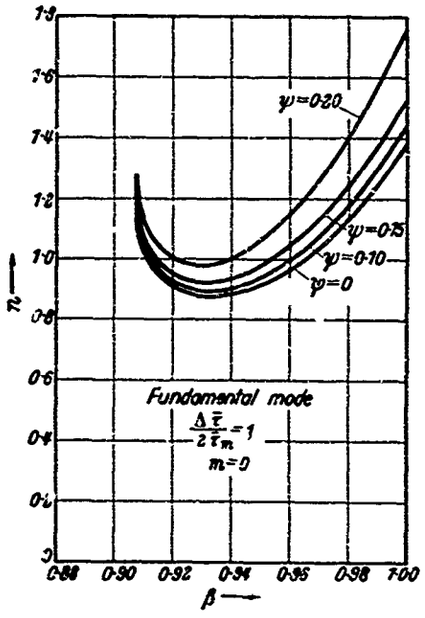

Figure 38

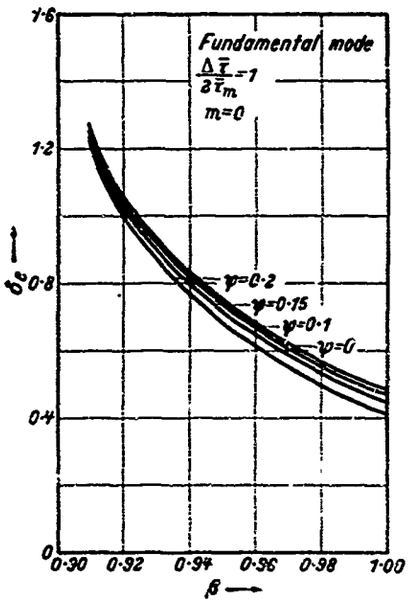

Figure 39

Figure 38. Critical values of the interaction index n required to maintain neutral oscillation of reduced frequency β of the fundamental mode with combustion spatially concentrated at the fractional axial position ψ and for the maximum amount of sensitive time lag spread

Figure 39. Critical values of the effective sensitive time lag δe corresponding to neutral oscillations of reduced frequency β of the fundamental mode with combustion spatially concentrated at the fractional axial position ψ and for the maximum amount of sensitive time lag spread

Next consider the case when the extent of time lag spread is no longer small so that the variation of C with ω must be taken into account. Consider the following example where the distribution function is specified as

$$\frac{df}{d\bar{\tau}} = \frac{\pi}{2\Delta\bar{\tau}} \cos\left(\pi \frac{\bar{\tau} - \bar{\tau}_m}{\Delta\bar{\tau}}\right) \qquad \ldots.(3.05.09)$$

which is symmetric with respect to $\bar{\tau}_m$ and is maximum at $\bar{\tau}_m$. Equation (3.05.06) gives

$$C = \frac{\cos \omega\Delta\bar{\tau}/2}{1 - (\omega\Delta\bar{\tau}/\pi)^2} \qquad \ldots.(3.05.10)$$

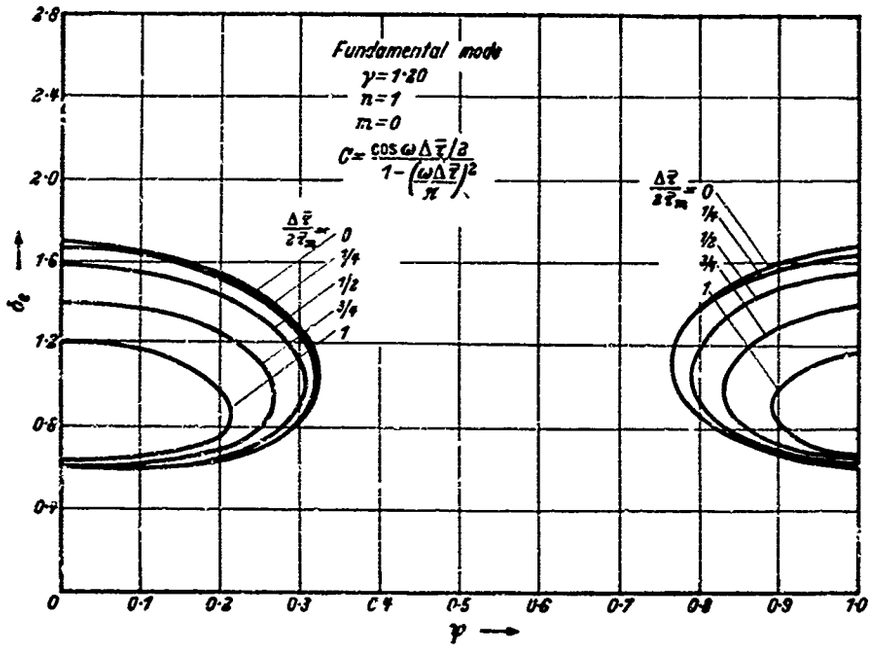

Figure 40. Effect of the large timewise spread of sensitive time lag on the critical values δ_e for the lowest unstable ranges of the fundamental mode as a function of the fractional axial position ψ of the concentrated combustion, $n = 1{\cdot}00$

Thus C is a function of the angular displacement of the oscillation during the extent of the time lag spread. The critical values n and δ_e corresponding to frequency ω of neutral oscillations have to be determined from equations (3.05.07) and (3.05.10) simultaneously. The critical values n and δ_e for the largest possible extent of spread, $\Delta\bar{\tau} = 2\bar{\tau}_m$ with $\bar{\tau}_{min} = 0$, and $\bar{\tau}_{max} = 2\bar{\tau}_m$, are shown in *Figures 38* and *39* and the unstable ranges of $\bar{\tau}_e$ for $\Delta\tau/2\bar{\tau}_m = 1$, $\frac{3}{4}$, $\frac{1}{2}$, and $\frac{1}{4}$ are shown in *Figure 40* for $n = 1$. The effect of spreading the time lag is again shown to be stabilizing and the stabilizing effect increases with increasing fractional extent of spread. It should be noticed, however, that the stabilizing effect is rather small if $\Delta\tau/2\bar{\tau}_m < \frac{1}{4}$ which will probably include a large number of practical situations.

The previous results are obtained only under the assumption that the sensitive space lag is negligibly small compared to the total space lag, so that $\xi \simeq \psi$ and the oscillations of the position of the concentrated combustion front are neglected. If ξ is not taken to be equal to ψ, then

$C \exp(-s\bar{\tau}_c)$ is defined by equation (3.05.03) not by equation (3.05.06). It is obviously seen that the previous formulation is not adequate for a certain mode of oscillation when the combustion front is in the neighbourhood of a pressure node of this mode. The modification of the results is, however, shown[23] to be non-essential. The effect of the fact that $\xi < \psi$ is that the stable region about each node is shifted slightly downstream. The effect of spreading the time lag is still stabilizing.

3.06. Formulation for Systems with Distributed Combustion

The analysis for systems with concentrated combustion shows that the position of the concentrated combustion front is quite important in determining the stability of the system. It is therefore necessary to analyse the stability behaviour of systems with combustion distributed arbitrarily along the combustion chamber axis. The analysis of systems with concentrated combustion is mathematically simple because the gas flow on both sides of the concentrated combustion front is uniform and the propagation of pressure disturbances in such a uniform flow field can be easily determined from the simple wave equation as the ordinary acoustical solution when both the Mach number of the gas flow is small and the entropy perturbations are neglected. In the case of distributed combustion the flow field is no longer uniform and there are mass, momentum, and energy sources throughout the combustion chamber. It is evident that the equations governing the motion will be different from those of a simple wave at all points where such sources are present.

A particular treatment of this problem has been previously published by the authors with the restrictive assumption that the combustion is uniformly distributed in the axial direction and with a few other simplifying assumptions. In the rest of this chapter the problem has been treated for the most general distribution of combustion and without making use of the aforesaid simplifying assumptions. As a result the equations are considerably more involved and a different method of solution, which proves to be quite general and powerful, has to be used. The equation can be formulated without difficulty for the model discussed at Section 1.03. For this model the whole flow is divided into two phases: a flow of burnt gases, with a rate $\rho^* u^*$ per unit area; and a flow of liquid propellants (in droplets), with a rate $\rho_l^* u_l^*$. Here ρ^* and u^* are the actual density and velocity of the gaseous phase, u_l^* is the velocity of the liquid phase supposed uniform for a given section, and ρ_l^* the mass of droplets per unit volume of gas. The volume of the droplets is neglected. The equation of mass conversion can be expressed by writing that the rate of mass accumulation between sections x^* and $x^* + dx^*$ plus the outgoing flow of mass is zero, that is,

$$\frac{\partial}{\partial t^*}(\rho^* + \rho_l^*) + \frac{\partial}{\partial x^*}(\rho^* u^* + \rho_l^* u_l^*) = 0$$

This can also be written as

$$\frac{\partial \rho^*}{\partial t^*} + \frac{\partial}{\partial x^*}(\rho^* u^*) = -\frac{\partial \rho_l^*}{\partial t^*} - \frac{\partial}{\partial x^*}(\rho_l^* u_l^*) = \frac{\partial w^*}{\partial x^*} \qquad \ldots.(3.06.01)$$

where t^* and x^* are the physical time and space variables and the quantity

w^* represents the instantaneous rate with which burnt gases are produced in the whole volume between $x^* = 0$ (injector face) and x^*.

Similarly the conservation of momentum states that for the element between x^* and $x^* + \mathrm{d}x^*$ the rate of accumulation of momentum plus the outgoing flow of momentum must be equal to the total force acting on the boundaries of the element. Neglecting friction on the walls we can write

$$\frac{\partial}{\partial t^*}(\rho^* u^* + \rho_l^* u_l^*) + \frac{\partial}{\partial x^*}(\rho^* u^{*2} + \rho_l^* u_l^{*2}) = -\frac{\partial p^*}{\partial x^*} \qquad \ldots.(3.06.02)$$

The conservation of energy can be expressed by writing that the rate of increase of the total stagnation energy content of the element under consideration, plus the outgoing flow of total stagnation enthalpy, must balance the energy introduced into the element through the boundaries. Neglecting heat exchanges through the walls the last-mentioned energy is zero. Therefore we can write

$$\frac{\partial}{\partial t^*}[\rho^* e_s^* + \rho_l^*(h_p^* + \tfrac{1}{2}u_l^{*2})] + \frac{\partial}{\partial x^*}[\rho^* u^* h_s^* + \rho_l^* u_l^*(h_p^* + \tfrac{1}{2}u_l^{*2})] = 0$$

$\ldots.(3.06.03)$

Here $e_s^* = e^* + (\frac{1}{2}u^{*2})$ and $h_s^* = h^* + \frac{1}{2}u^{*2}$ represent the stagnation interval energy and the stagnation enthalpy for the gaseous phase. For the liquid phase, the internal energy and the enthalpy are very nearly the same; the corresponding common value h_p^* is intended to include the chemical energy of the propellants. In writing the preceding equations, it has been assumed that the velocity and heat content of the droplets are the same for all droplets at any given station and that, in accordance with the one-dimensional treatment, the droplets are uniformly distributed over the section.

The four equations (3.06.01), (3.06.02) and (3.06.03) contain eight unknowns ρ^*, u^*, p^*, T^* (of which e^* and h^* are functions), w^*, ρ_l^*, u_l^*, and h_p^*. The four additional equations needed are easily located.

First, we have the equation of state for the gas phase

$$p^* = \rho^* R T^* \qquad \ldots.(3.06.04)$$

The second equation expresses the functional relationship between the burning rate w^* and the other variables. Such a relationship will be obtained later, based on the assumptions of Section 1.11.

A third equation is obtained from the dynamic behaviour of the droplets. Assuming that the force exerted by the gases on the droplets is inversely proportional to the Reynolds number one can write

$$\frac{\mathrm{d}u_l^*}{\mathrm{d}t} = \frac{\partial u_l^*}{\partial t} + u_l^* \frac{\partial u_l^*}{\partial x^*} = k^*(u^* - u_l^*) \qquad \ldots.(3.06.05)$$

where the acceleration of the droplet has been obtained following the droplet path. The coefficient k^* depends on various parameters, including the diameter of the droplets, and therefore should be variable when the droplets are losing weight by evaporation and combustion. Here, however, we shall overlook this variation and assume for k^* a convenient constant value.

The fourth equation could be obtained from the heat balance of the droplets. This would give us an equation for h_p^*, or for the temperature of the droplets. The droplets are actually picking up heat and increasing their h_p^* in the initial part of their journey; they release it again when they burn. The extent of increase of h_p^* is, however, seriously limited by the presence of evaporation. In order to avoid additional complications in our problem, and to take into account the fact that while h_p^* is increasing, the kinetic energy of the droplets is decreasing, we shall replace the heat balance equation by the simpler relation

$$h_p^* + \tfrac{1}{2}u_l^{*2} = \text{const.} = h_{p0}^* = \tfrac{1}{2}u_{l0}^{*2} \qquad \ldots.(3.06.06)$$

It can be shown that reasonable deviations from this constancy would only introduce higher order effects in the following developments.

We can now proceed to the non-dimensionalization of the preceding equation. This can be done by using the reference values p_0^*, ρ_0^*, T_0^* and $c_0 = (\gamma R T_0^*)^{\frac{1}{2}}$ as in Section 3.01, which are the pressure, density, and temperature of the gas and the sound velocity in the gas at the injector face ($x^* = 0$), and by choosing as representative length the length of the combustion chamber L. We take therefore

$$\left.\begin{aligned} &x = \frac{x^*}{L};\ t = \frac{c_0^* t^*}{L};\ p = \frac{p^*}{p_0^*};\ \rho = \frac{\rho^*}{\rho_0^*};\ T = \frac{T^*}{T_0^*};\ \rho_l = \frac{\rho_l^*}{\rho_0^*} \\ &u = \frac{u^*}{c_0^*};\ u_l = \frac{u_l^*}{c_0^*};\ w = \frac{w^*}{\rho_0^* c_0^*};\ h = \frac{\gamma - 1}{\gamma R T_0^*} h^*;\ h_p = \frac{\gamma - 1}{\gamma R T_0^*} h_p^* \end{aligned}\right\} \ldots.(3.06.07)$$

where γ is the adiabatic index for the gases, assumed to be constant together with the specific heats within the range of variation of T^*. This assumption allows us to write in this range

$$\mathrm{d}h = \mathrm{d}T \quad \text{and} \quad \Delta h = \Delta T \qquad \ldots.(3.06.08)$$

independently of the behaviour of the specific heats out of this range.

The non-dimensional equations can be written as

$$\frac{\partial \rho}{\partial t} + \frac{\partial(\rho u)}{\partial x} = \frac{\partial w}{\partial x} = -\frac{\partial \rho_l}{\partial t} - \frac{\partial(\rho_l u_l)}{\partial x} \qquad \ldots.(3.06.01a)$$

$$\frac{\partial(\rho u)}{\partial t} + \frac{\partial(\rho u^2)}{\partial x} = -\frac{1}{\gamma}\frac{\partial p}{\partial x} - \frac{\partial(\rho_l u_l)}{\partial t} - \frac{\partial(\rho_l u_l^2)}{\partial x} \qquad \ldots.(3.06.02a)$$

$$\rho\left(\frac{\partial h_s}{\partial t} + u\frac{\partial h_s}{\partial x}\right) = \frac{\gamma - 1}{\gamma}\frac{\partial p}{\partial t} - (h_s - h_{p_\infty})\frac{\partial w}{\partial x} \qquad \ldots.(3.06.03a)$$

$$p = \rho T \qquad \ldots.(3.06.04a)$$

$$\frac{\partial u_l}{\partial t} + u_l\frac{\partial u_l}{\partial x} = k(u - u_l) \qquad \ldots.(3.06.05a)$$

$$h_p + \tfrac{1}{2}(\gamma - 1)u_l^2 = h_{p_\infty} \qquad \ldots.(3.06.06a)$$

where we have introduced the two quantities $k = (L/c_0^*)k^*$ and $h_{p_{s0}} = \{(\gamma - 1)/(\gamma R T_0^*)\}\,(h_{p_0}^* + \tfrac{1}{2}u_{l_0}^{*2})$. In the derivation of equation (3.06.03a) from (3.06.03), use has been made of the relation $\rho^* e_s^* = \rho^* h_s^* - p^*$, the two equations (3.06.01) and of equation (3.06.06). If the flow is steady the corresponding relations are immediately obtained from the preceding equations by suppressing the time derivations, and integrating with the following boundary conditions: at $x = 0$, $u = 0$, $\rho = 1$, $p = 1$, $T = 1$, $u_l = u_{l_0}$, $\rho_{l_0} u_{l_0} = w_i$, $h_p = h_{p_0}$. Here w_i represents the known injection rate per unit area of chamber divided by $\rho_0^* c_0^*$. Indicating the steady state quantities with a superposed bar we find:

$$\bar{\rho}\bar{u} = \bar{w}; \quad \bar{\rho}_l \bar{u}_l = w_i - \bar{w} \qquad \ldots.(3.06.09)$$

$$\bar{p} = 1 - \gamma(\bar{\rho}\bar{u}^2 + \bar{\rho}_l \bar{u}_l^2 - \rho_{l_0} u_{l_0}^2) = 1 - \gamma[\bar{w}(\bar{u} - \bar{u}_l) + w_i(\bar{u}_l - \bar{u}_{l_0})] \qquad \ldots.(3.06.10)$$

$$h_s = h + \tfrac{1}{2}(\gamma - 1)\bar{u}^2 = h_{p_{s0}} = h_0, \qquad \bar{p} = \bar{\rho}\bar{T} \qquad \ldots.(3.06.11)$$

$$\bar{u}_l \, \mathrm{d}\bar{u}_l/\mathrm{d}x = k(\bar{u} - \bar{u}_l) \qquad \ldots.(3.06.12)$$

The first equation (3.06.11) can be rewritten, using equation (3.06.08), as

$$\bar{T} = 1 - \tfrac{1}{2}(\gamma - 1)\bar{u}^2 \qquad \ldots.(3.06.11a)$$

This system can be easily solved if instead of prescribing the burning rate, i.e. starting from a known $\bar{w}(x)$, we assume a known $\bar{u}(x)$. In this case the integration of equation (3.06.12) provides $\bar{u}_l(x)$; $\bar{T}(x)$ is provided by equation (3.06.11a) and $\bar{p}$, $\bar{\rho}$ and $\bar{w}$ are found from the preceding equation as

$$\bar{\rho} = \frac{\bar{p}}{1 - \tfrac{1}{2}(\gamma - 1)\bar{u}^2} = \frac{\bar{w}}{\bar{u}} = \frac{1 - \gamma w_i(\bar{u}_l - u_{l_0})}{1 + \tfrac{1}{2}(\gamma + 1)\bar{u}^2 - \gamma \bar{u}\bar{u}_l} \qquad \ldots.(3.06.13)$$

If the combustion must be complete at the end of the chamber ($x = 1$), where the velocity takes the prescribed value $\bar{u}_1$, from the last of equations (3.06.13) we obtain

$$\bar{w}_1 = w_i = \frac{\bar{u}_1}{1 + \tfrac{1}{2}(\gamma + 1)\bar{u}_1^2 - \gamma \bar{u}_1 u_{l_0}}$$

This relation can be inserted in equations (3.06.13) to obtain $\bar{\rho}$, $\bar{p}$ and $\bar{w}$ in terms of $\bar{u}(x)$ and $\bar{u}_l(x)$ only.

Let us discuss now the order of magnitude of the fundamental quantities involved. The velocity $\bar{u}_1$ in the final section of the chamber is connected with the Mach number M and depends on the area ratio of the nozzle. For a throatless motor, $M = 1$. For ordinary motors, however, M is generally around 0·1. Therefore, excluding the case of a tubular motor we shall consider M as a small quantity and we shall compare the magnitude of the other quantities with M. For such small values of M we have very closely $\bar{u}_1 = M$. The sound velocity in the burnt gases of a rocket is generally around 3000 f/s. Thus the velocity $\bar{u}_1^*$ is around 300 f/s. The injection velocity $u_{l_0}^*$ is generally below this value even for high injection pressures. Immediately after injection $\bar{u} - \bar{u}_l$ is negative so that equation (3.06.12) shows that $\bar{u}_l$ decreases. In the same time $\bar{u}$ increases, until at a certain

station $\bar{u}$ becomes equal to $\bar{u}_l$. After this station $\bar{u}$ stays larger than $\bar{u}_l$ and $\bar{u}_l$ increases again, though lagging behind $\bar{u}$†. We conclude that $\bar{u}_l$ is always smaller than, or equal to, the larger of the two quantities $\bar{u}_{l_0}$ and $\bar{u}_1$, and therefore in general is of the same order as M; in mathematical form both $\bar{u}$ and $\bar{u}_l$ are $O(M)$. Consider now the quantity k. In the simplest case where $\bar{u} = 0$ the integration of equation (3.06.12) gives $\bar{u}_l = \bar{u}_{l_0} - kx$. The velocity of the droplets is therefore reduced to zero at a finite distance $x_0 = \bar{u}_{l_0}/k$, which might be called 'penetration'. For the usual densities of the burnt gases in a rocket chamber the penetration is of the order of a few inches. On the safe side, let us assume that the penetration is equal to half the length of the chamber, i.e. $x_0 = \frac{1}{2}$ and $k = 2\bar{u}_{l_0}$. Thus k is probably larger than $\bar{u}_{l_0}$ but of the same order, that is k is of $O(M)$. As a result of the order of magnitude of $\bar{u}$ and $\bar{u}_l$ we see from equations (3.06.11a) and (3.06.13) that the deviations of $\bar{T}$, $\bar{\rho}$ and $\bar{p}$ from unity and of $\bar{w}$ from $\bar{u}$ are $O(M^2)$. Up to terms of this order we can therefore write

$$\bar{p} = \bar{\rho} = \bar{T} = 1; \qquad \bar{w} = \bar{u} \qquad \ldots.(3.06.14)$$

The practical equality of $\bar{w}$ and $\bar{u}$ has the consequence that the description of a combustion process in steady state can be obtained equally well by prescribing the rate of burning or the velocity distribution.

Within the approximation (3.06.14), the second equation (3.06.09) can be written

$$\bar{\rho}_l \bar{u}_l = \bar{u}_1 - \bar{u} \qquad \ldots.(3.06.15)$$

3.07. Perturbation Equations with Arbitrarily Distributed Combustion

We can now proceed to obtain the perturbation equations corresponding to equations (3.06.01a)–(3.06.06a). We consider each of the dependent variables as the sum of the steady state value plus a perturbation, so small that the terms higher than those linear in these perturbations can be neglected. We indicate with a prime these perturbations and as before we investigate the stability of solutions of the exponential type:

$$\frac{\rho'}{\sigma(x)} = \frac{p'}{\varphi(x)} = \frac{u'}{v(x)} = \frac{\rho_l'}{\zeta(x)} = \frac{u_l'}{\eta(x)} = \frac{w'}{q(x)} = e^{st} \qquad \ldots.(3.07.01)$$

where the denominators are independent of time. The exponent $s = \Lambda + i\Omega$ is generally complex. Our purpose, as in the preceding sections, is to determine the conditions under which the solution is stable, neutral or unstable, that is $\Lambda \lesseqgtr 0$, or simply to determine the stability boundary, where $\Lambda = 0$, and the unstable side of the boundary. At neutral conditions, the denominators of (3.07.01) represent the complex amplitudes of oscillation of the corresponding quantities. The perturbations are therefore given as complex quantities of which only the real part has a physical meaning. The alternate interpretation of these complex perturbations as rotating vectors in the complex plane allows us to consider their complex amplitudes as fixed vectors; it is clear that the angle between any two

† If the diameter of the droplets is decreasing from evaporation, k increases steadily and becomes infinite at the end. In this case $\bar{u}_l$ finally catches up with $\bar{u}$.

vectors represents the phase angle between the corresponding oscillating quantities. Letting $\rho = \bar{\rho} + \rho'$, $u = \bar{u} + u'$, etc. in equations (3.06.01a), (3.06.02a) and (3.06.03), subtracting the corresponding steady state equations and neglecting terms other than those linear in the perturbations we obtain, after introduction of equations (3.07.01) and suppression of the factor exp (st),

$$s\sigma + \frac{\mathrm{d}}{\mathrm{d}x}(\bar{\rho}v + \bar{u}\sigma) = \frac{\mathrm{d}q}{\mathrm{d}x} = -s\zeta - \frac{\mathrm{d}}{\mathrm{d}x}(\bar{\rho}_l\eta + \bar{u}_l\zeta) \quad \ldots.(3.07.02)$$

$$s(\bar{\rho}v + \bar{u}\sigma) + \frac{\mathrm{d}}{\mathrm{d}x}(2\bar{\rho}\bar{u}v + \bar{u}^2\sigma)$$

$$= \frac{31}{\gamma}\frac{\mathrm{d}\varphi}{\mathrm{d}x} - s(\bar{\rho}_l\eta + \bar{u}_l\zeta) - \frac{\mathrm{d}}{\mathrm{d}x}(2\bar{\rho}_l\bar{u}_l\eta + \bar{u}_l^2\zeta) \quad \ldots.(3.07.03)$$

From the energy equation (3.06.03a) replacing $h_s = \bar{h}_s + h_s' = h_{p_{s0}} + h_s'$ [because of equation (3.06.10)], we obtain

$$\bar{\rho}\left(\frac{\partial h_s'}{\partial t} + \bar{u}\frac{\partial h_s'}{\partial x}\right) = \frac{\gamma - 1}{\gamma}\frac{\partial p'}{\partial t} - h_s'\frac{\partial \bar{w}}{\partial x}$$

or

$$\frac{\partial}{\partial t}\left(\bar{\rho}h_s' - \frac{\gamma - 1}{\gamma}p'\right) = -\frac{\partial}{\partial x}(\bar{\rho}\bar{u}h_s')$$

We can introduce in this equation $h_s' = h' + (\gamma - 1)\bar{u}u'$, that is, since by equation (3.06.08) $h' = T'$ and by equation (3.06.04a) $\bar{\rho}T' = p' - \bar{T}\rho'$, we can substitute

$$\bar{\rho}h_s' = p' - \bar{T}\rho' + (\gamma - 1)\bar{\rho}\bar{u}u'$$

The result is

$$\frac{\partial}{\partial t}\left(\frac{p'}{\gamma} - \bar{T}\rho'\right) = -(\gamma - 1)\bar{\rho}\bar{u}\frac{\partial u'}{\partial t} - \frac{\partial}{\partial x}[\bar{u}\{p' - \bar{T}\rho' + (\gamma - 1)\bar{\rho}\bar{u}u'\}]$$

Replacing from equation (3.07.01) we obtain the energy equation in the following form

$$s\left(\frac{\varphi}{\gamma} - \bar{T}\sigma + (\gamma - 1)\bar{\rho}\bar{u}v\right) = -\frac{\mathrm{d}}{\mathrm{d}x}[\bar{u}\{\varphi - \bar{T}\sigma + (\gamma - 1)\bar{\rho}\bar{u}v\}]$$

$\ldots.(3.07.04)$

The equation of state (3.06.04a) has already been used to eliminate T' and is not needed any more. Similarly, equation (3.06.06a) need not be used further. The equation (3.06.05a) representing the motion of the droplets gives

$$\bar{u}_l\frac{\mathrm{d}\eta}{\mathrm{d}x} + \left(s + \frac{\mathrm{d}\bar{u}_l}{\mathrm{d}x} + k\right)\eta = kv$$

This first order equation for η can easily be integrated. However, a simple approximate solution, valid under the present circumstances, can be given by observing that k is $O(M)$, and therefore from equation (3.06.12) $\frac{\mathrm{d}\bar{u}_l}{\mathrm{d}x}$ also is $O(M)$ while on the other hand the modulus of s is around a

multiple of π for nearly neutral oscillations in the high frequency range as will be shown later. Therefore, the predominant term of the left member of the equation is $s\eta$ and one can write approximately

$$\eta = k/s \cdot \nu \qquad \ldots.(3.07.05)$$

This approximate solution satisfies the boundary condition (3.07.06) given in the next paragraph. We see that the fluctuations of droplet velocity are, for small k, considerably damped with respect to those of the gas velocity, and for neutral oscillations, $s = i\omega$, η follows ν with a 90° phase shift. Equations (3.07.02)–(3.07.05), together with the equation, still to be derived, for the burning rate, are in principle sufficient to solve our problem under appropriate boundary conditions. It is interesting to observe that the only traces left of the equations (3.06.05) or (3.06.05a) governing the motion of the droplets are in the relation $\bar{u}_l(x)$ and in the equation (3.07.05), that is in a form much less restrictive than the original equation of motion (3.06.05), particularly if k is considered, in general, as an empirical factor correlating the two velocity fluctuations, and capable of taking complex values.

Let us now write the conditions at the injector end, $x = 0$. Here $u(x, t) = 0$ at each instant, so that $u'(0, t) = 0$. If the injection velocity and the injection rate are supposed to be unaffected by changes in the chamber conditions (a logical assumption for sufficiently high frequencies) we have $u_l'(0, t) = 0$ and $\mu_l'(0, t) = 0$. Similarly $w(0, t) = \bar{w}(0) = 0$ and therefore $w'(0, t) = 0$. Hence from equations (3.07.01) we have

$$\nu_0 = \zeta_0 = \eta_0 = q_0 = 0 \qquad \ldots.(3.07.06)$$

At the nozzle end we assume complete combustion, which means that for $x = 1$, $\bar{\rho}_l$ and ρ_l' are 0 at every instant. The terms deriving from the motion of the droplets in equations (3.07.02) and (3.07.03) disappear; dq/dx vanishes and the two remaining equations become those of the adiabatic motion of a gas. Evidently, equation (3.07.05) becomes meaningless. At $x = 1$ it is therefore necessary only to prescribe the behaviour of the de Laval nozzle in the presence of oscillations, as in previous sections; this is done by equating the ratio of the fractional variations of velocity and density to the specific nozzle admittance ratio (Appendix B).

Equations (3.07.02)–(3.07.04) are quite involved. We shall now put them in a different form which allows a simple iterative approach to the solution. It is immediately checked by direct substitution and with the help of equation (3.07.04) that equations (3.07.02) and (3.07.03) are exactly equivalent to the following two equations:

$$\left.\begin{aligned} \frac{d}{dx}\left(\frac{\nu}{\varphi_0}\right) + s\frac{\varphi}{\gamma\varphi_0} &= -sX + \frac{dY}{dx} \\ \frac{1}{\gamma}\frac{d}{dx}\left(\frac{\varphi}{\varphi_0}\right) + s\frac{\nu}{\varphi_0} &= -sZ - \frac{dW}{dx} \end{aligned}\right\} \qquad \ldots.(3.07.07)$$

where:

$$\left.\begin{aligned} X &= (\gamma-1)\bar{\rho}\bar{u}\,\frac{v}{\varphi_0} + (1-\bar{T})\,\frac{\sigma}{\varphi_0} \\ Y &= \frac{q}{\varphi_0} - \bar{u}\,\frac{\varphi}{\varphi_0} + (1-\bar{\rho})\,\frac{v}{\varphi_0} - \bar{u}(1-\bar{T})\,\frac{\sigma}{\varphi_0} - (\gamma-1)\bar{\rho}\bar{u}^2\,\frac{v}{\varphi_0} \\ Z &= \bar{u}\,\frac{\sigma}{\varphi_0} - (1-\bar{\rho})\,\frac{v}{\varphi_0} + \bar{\rho}_l\,\frac{\eta}{\varphi_0} + \bar{u}_l\,\frac{\zeta}{\varphi_0} \\ W &= 2\bar{\rho}\bar{u}\,\frac{v}{\varphi_0} + 2\bar{\rho}_l\bar{u}_l\,\frac{\eta}{\varphi_0} + \bar{u}^2\,\frac{\sigma}{\varphi_0} + \bar{u}_l^2\,\frac{\zeta}{\varphi_0} \end{aligned}\right\} \quad \ldots\ldots (3.07.08)$$

Equations (3.07.07) can be rewritten as:

$$\left.\begin{aligned} \frac{d}{dx}\left(\frac{v}{\varphi_0} - Y\right) + s\left(\frac{\varphi}{\gamma\varphi_0} + W\right) &= s(W-X) = sE \\ \frac{d}{dx}\left(\frac{\varphi}{\gamma\varphi_0} + W\right) + s\left(\frac{v}{\varphi_0} - Y\right) &= -s(Y+Z) = -sF \end{aligned}\right\} \quad \ldots\ldots (3.07.09)$$

It is directly checked that these equations are equivalent to the two following integral equations, obtainable by solving the non-homogeneous linear system (3.07.09) as if X, E and F were known functions of x:

$$\left.\begin{aligned} \frac{\varphi}{\gamma\varphi_0} + W &= C_1 \sinh sx + C_2 \cosh sx \\ &\quad - s\int_0^x [F(x')\cosh s(x-x') + E(x')\sinh s(x-x')]\,dx' \\ \frac{v}{\varphi_0} - Y &= -C_1 \cosh sx - C_2 \sinh sx \\ &\quad + s\int_0^x [F(x')\sinh s(x-x') + E(x')\cosh s(x-x')]\,dx' \end{aligned}\right\} \quad \ldots\ldots (3.07.10)$$

On the left-hand side, the different quantities are evaluated at station x; but we can now introduce the boundary conditions (3.07.06) at $x = 0$, after observing that from these conditions and from $\bar{u}(0) = 0$ we derive $W(0) = 0$ and $Y(0) = 0$.

The arbitrary constants C_1 and C_2 can be completely eliminated if we prescribe the value of $\varphi(0) = \varphi_0$. Equations (3.07.10) become:

$$\left.\begin{aligned} \frac{\varphi}{\varphi_0} &= \cosh sx - \gamma W \\ &\quad - s\int_0^x [\gamma F(x')\cosh s(x-x') + \gamma E(x')\sinh s(x-x')]\,dx' \\ \frac{\gamma v}{\varphi_0} &= -\sinh sx + \gamma Y \\ &\quad + s\int_0^x [\gamma F(x')\sinh s(x-x') + \gamma E(x')\cosh s(x-x')]\,dx' \end{aligned}\right\} \quad \ldots\ldots (3.07.11)$$

These two integral equations together with equations (3.07.04) and (3.07.05), plus the equation for the burning rate to be derived in Section 3.08, will be used for the solution of our problem.

3.08. The Burning Rate

In Section 1.11 we have formulated certain relations concerning the time lag and its variations. These relations were written in terms of dimensional quantities. However, it is immediately verified that the introduction of the non-dimensional quantities defined by (3.06.07) leaves the equations in exactly the same form. It is also apparent that the rate function, f, can be multiplied, by any arbitrary factor if E_a is also multiplied by the same factor, so that we do not have to give explicitly the factors of non-dimensionalization of f and E_a, provided they are equal. Therefore, we can utilize directly the relations of Section 1.11 as if they had been written originally in terms of non-dimensional variables. Particularly simple relations were derived for uniform steady state conditions in the chamber. If, in accordance with the discussion of Section 3.06, quantities of $O(M^2)$ can be neglected with respect to unity, the state of the gas can be considered uniform, the dimensionless steady state values of pressure, density and temperature being equal to unity [equations (3.06.14)]. However, we can observe that all of the following developments of this section and of those following can in principle be repeated for non-uniform conditions.

Consider the fraction of the injected propellants burning in steady state between stations x and $x + dx$. We assume for the moment that the time lag $\bar{\tau}(x)$ is the same for all the elements of the fraction considered, though it can be different for fractions burning at different stations x. The burning rate of the fraction considered is, by definition,

$$\delta\bar{m}_b = \frac{d\bar{w}(\bar{x})}{d\bar{\tau}}\,\delta\bar{x}$$

In non-steady operation the same fraction burns between stations x and $x + dx$ and, again, by definition, its burning rate is

$$\delta\dot{m}_b = \frac{\partial w(x, t)}{\partial x}\,\delta x$$

If the rate of injection is constant we can apply equation (3.11.18) and obtain

$$\frac{\partial w(x, t)}{\partial x}\,dx = \frac{d\bar{w}(\bar{x})}{d\bar{x}}\,d\bar{x}\left(1 - \frac{d\tau}{dt}\right) \qquad \ldots.(3.08.01)$$

Integrating over all fractions burning in steady state between 0 and $\bar{x}$, and in non-steady state between 0 and $x(\bar{x}, t)$, and noticing that $\bar{w}(0) = w(0, t) = 0$ we obtain

$$w(x, t) = \bar{w}(\bar{x}) - \int_0^{\bar{x}} \frac{d\tau}{dt}\,\frac{d\bar{w}(x')}{dx'}\,dx' \qquad \ldots.(3.08.02)$$

Under the integral, $d\tau/dt$ is given by equation (1.11.13) computed at time t and station x', that is by

$$d\tau/dt = -n\{p'(x', t) - p'[\bar{\xi}(x'), t - \bar{\tau}(x')]\} \qquad \ldots.(3.08.03)$$

$\bar{\xi}(x)$ being the station where, in steady state, an element burning at station x enters the sensitive phase. Of course, $\bar{\xi}$ and $\bar{\tau}$ are related by

$$\int_{\bar{\xi}(x)}^{x} \frac{dx'}{\bar{u}_l(x')} = \bar{\tau}(x) \qquad \ldots.(3.08.04)$$

so that when $\bar{u}_l(x)$ is known, it is equivalent to assigning $\bar{\tau}(x)$ or $\bar{\xi}(x)$. From equation (3.08.02) we can find the perturbation of the burning rate

$$w'(x,t) = w(x,t) - \bar{w}(x) = \bar{w}(\bar{x}) - \bar{w}(x) - \int_0^t \frac{d\tau}{dt}\frac{d\bar{w}}{dx'}\,dx' \qquad \ldots.(3.08.05)$$

It is now necessary to evaluate $x(\bar{x}, t)$. At every instant, the relation between the station $\xi(\bar{x}, t)$ where an element enters the sensitive phase and the insensitive time lag τ_i is given by

$$\int_0^{\xi} \frac{dx'}{u_l(x')} = \tau_i \qquad \ldots.(3.08.06)$$

where the velocity u_l has to be evaluated at the station x' and at the time $t'(x')$ when the element considered was at station x':

$$u_l(x') = u_l[x', t'(x')] = \bar{u}_l(x') + u_l'[x', t'(x')] \qquad \ldots.(3.08.07)$$

Hence in terms of the spatial variable equation (1.11.05) can be written as:

$$\int_0^{\bar{x}} \frac{dx'}{u_l(x')} = \int_0^{\bar{\xi}} \frac{dx'}{\bar{u}_l(x')} = \int_0^{\xi} \frac{dx'}{\bar{u}_l(x')} + \int_{\xi}^{\bar{\xi}} \frac{dx'}{\bar{u}_l(x')} \qquad \ldots.(3.08.08)$$

Neglecting terms of higher order in the perturbations we can write

$$\int_{\bar{\xi}}^{\xi} \frac{dx'}{\bar{u}_l(x')} = \frac{\xi - \bar{\xi}}{\bar{u}_l(\xi)}$$

Thus after introduction of equation (3.08.07), equation (3.08.08) becomes

$$\xi - \bar{\xi} = \bar{u}_l(\xi) \int_0^{\xi} \frac{u_l'(x')}{\bar{u}_l^2(x')}\,dx' \qquad \ldots.(3.08.09)$$

when the dependence of u_l' on x' has to be considered as indicated in equation (3.08.07). Similarly in terms of the spatial variable, equation (1.11.09) becomes for uniform conditions [$\bar{f}(x') = \text{const.}, \bar{p}(x') = 1$]:

$$\int_{\xi}^{x} \frac{dx'}{u_l(x')} f(x') = E_a = \int_{\bar{\xi}}^{x} \frac{dx'}{\bar{u}_l(x')} \bar{f}(x') = \bar{f} \int_{\bar{\xi}}^{x} \frac{dx'}{\bar{u}_l(x')} \qquad \ldots.(3.08.10)$$

From equation (1.11.02), we have

$$f(x') = f[x', t'(x')] = \bar{f}[1 + np'\{x', t'(x')\}] \qquad \ldots.(3.08.11)$$

The integration on the right-hand side of equation (3.08.10) can be split into the integrations from $\bar{\xi}$ to ξ, from ξ to x and from x to $\bar{x}$. Neglecting higher order terms we have:

$$\int_{\bar{\xi}}^{\xi} \frac{dx'}{\bar{u}_l(x')} = \frac{\xi - \bar{\xi}}{\bar{u}_l(\xi)} \quad ; \quad \int_{x}^{\bar{x}} \frac{dx'}{\bar{u}_l(x')} = \frac{\bar{x} - x}{\bar{u}_l(x)} \qquad \ldots.(3.08.12)$$

and finally, making use of equations (3.08.12), (3.08.11), (3.08.09) and (3.08.07), equation (3.08.10) gives

$$x - \bar{x} = \bar{u}_l(x) \left[\int_0^x \frac{u_l'(x')}{\bar{u}_l^2(x')} \, dx' - n \int_\xi^x \frac{p'(x')}{\bar{u}_l(x')} \, dx' \right] \quad \ldots . (3.08.13)$$

In this expression one can clearly distinguish between the effect of time lag changes, represented by the second integral, and the effect of the velocity changes, represented by the first integral, which constitutes a purely kinematic phenomenon.

It is clear that since we are limited to terms of first order in the perturbations, the right-hand side of equation (3.08.13) can be written with $\bar{x}$ and $\bar{\xi}$ instead of x and ξ. We can now complete the evaluation of equation (3.08.05); since, by neglecting higher order quantities, we can write

$$\bar{w}(x) - \bar{w}(\bar{x}) = (x - \bar{x}) \frac{d\bar{w}(\bar{x})}{d\bar{x}}$$

Taking $x - \bar{x}$ from equation (3.08.13), this relation can be inserted into equation (3.08.05) together with equation (3.08.03) and we obtain finally

$$w'(x, t) = n \int_0^x \left[p'(x', t) - p'[\bar{\xi}(x'), t - \bar{\tau}(x')] \right] \frac{d\bar{u}(x')}{dx'} \, dx'$$

$$+ \bar{u}_l(x) \frac{d\bar{u}(x)}{dx} \left\{ n \int_{\bar{\xi}(x)}^x \frac{p'[x', t'(x')]}{\bar{u}_l(x')} \, dx' - \int_0^x \frac{u_l'[x', t'(x')]}{\bar{u}_l^2(x')} \, dx' \right\} \quad \ldots . (3.08.14)$$

Here we have everywhere replaced $\bar{x}$ by x, and $\xi(x)$ or $\bar{\xi}(\bar{x})$ by $\bar{\xi}(x)$, the resulting changes being negligible because they are of higher order in the perturbations. Also, according to equation (3.06.13), $\bar{w}$ has been replaced by $\bar{u}$.

The time $t'(x')$ is related to x' by the relation

$$t'(x') = t - \int_{x'}^x \frac{dx''}{u_l[x'', t''(x'')]}$$

and since it is only used in the computation of the perturbations it can be replaced by the corresponding steady state expression

$$t'(x') = t - \int_{x'}^x \frac{dx''}{\bar{u}_l(x'')} \quad \ldots . (3.08.15)$$

The expression (3.08.14) for w' just obtained consists of a first term, which is originated directly by the time variations of the local burning rate, and will therefore be called the timewise contribution to the variation of the total burning rate up to station x, and of two additional terms which are due to the displacement of the location where a given element burns and will be called the spacewise contribution.

It will be seen in Section 3.09 that the timewise contribution is of an order of magnitude larger than the spacewise contribution and therefore represents the more important contribution of the two. This result justifies

the previous developments of this chapter for systems with concentrated combustion. Observe also that the same timewise contribution is the only one present in the low frequency case.

For a solution of the exponential type, replacing from equations (3.07.01), making use of equations (3.07.05) and (3.08.15) and cancelling the common factor exp (st), we obtain from equation (3.08.14)

$$\frac{\varphi_1(x)}{\varphi_0} = n\,Q(x) + \bar{u}_1(x)\frac{\mathrm{d}\bar{u}(x)}{\mathrm{d}x}\left\{n\int_{\bar{\xi}(x)}^{x}\frac{\varphi(x')}{\varphi_0}\,\frac{\mathrm{e}^{s\int_x^{x'}\frac{\mathrm{d}x''}{\bar{u}_1(x'')}}}{\bar{u}_1(x')}\,\mathrm{d}x' - \frac{k}{s}\int_0^x \frac{\nu(x')}{\varphi_0}\,\frac{\mathrm{e}^{s\int_x^{x'}\frac{\mathrm{d}x''}{\bar{u}_1(x'')}}}{\bar{u}_1^2(x')}\,\mathrm{d}x'\right\} \quad \ldots.(3.08.16)$$

where the first term represents the timewise contribution, and the second two terms the spacewise contribution to the burning rate variation. The quantity

$$Q(x) = \int_0^x \left[\frac{\varphi(x')}{\varphi_0} - \frac{\varphi[\bar{\xi}(x')]}{\varphi_0}\,\mathrm{e}^{-s\bar{\tau}(x')}\right]\frac{\mathrm{d}\bar{u}(x')}{\mathrm{d}x'}\,\mathrm{d}x' \quad \ldots.(3.08.17)$$

plays an important role in the following developments.

For practical purposes we are interested primarily in the determination of the stability boundary, that is $s = i\omega$†. For brevity in writing, we shall, however, still use s in the following development with the understanding that s is equal to $i\omega$. By analysing the order of magnitude of the terms, we shall first show that equations (3.08.16) and (3.08.17) can be simplified when the maximum local values of $\mathrm{d}\bar{u}/\mathrm{d}x$ are of order unity, and when $\bar{\tau}(x)$ is of order unity (that is $\bar{\tau}^*$ is of the same order as the wave propagation time θ_w).

Let us assume that

$$\frac{\varphi}{\varphi_0},\ \frac{\sigma}{\varphi_0},\ \frac{\nu}{\nu_0},\ \frac{1}{\varphi_0}\frac{\mathrm{d}\varphi}{\mathrm{d}x},\ \frac{1}{\varphi_0}\frac{\mathrm{d}\nu}{\mathrm{d}x} \quad \text{are} \quad \mathrm{O}(1) \qquad \ldots.(3.08.18)$$

an assumption that will be checked later to be true when ω is not too large‡. If $\bar{\tau}(x)$ is O(1), equation (3.08.04) shows easily that

$$x - \bar{\xi}(x) = \bar{u}_1(x)\bar{\tau}(x) + \mathrm{O}(M^2)$$

so that $x - \bar{\xi}$ is $\mathrm{O}(M)$. Thus, because of (3.08.18), $\varphi(\bar{\xi})/\varphi_0$ differs from $\varphi(x)/\varphi_0$ by a quantity of $\mathrm{O}(M)$§. Hence equation (3.08.17) can be written as

$$Q(x) = \int_0^x \frac{\varphi(x')}{\varphi_0}\left[1 - \mathrm{e}^{-s\bar{\tau}(x')}\right]\frac{\mathrm{d}\bar{u}(x')}{\mathrm{d}x'}\,\mathrm{d}x' \qquad \ldots.(3.08.19)$$

Since $\exp[-s\tau(x)] = -\exp[-i\omega\tau(x)]$ is always O(1) the whole integral is of the same order as $\bar{u}(x)$, that is $\mathrm{O}(M)$, no matter how large $\mathrm{d}\bar{u}(x)/\mathrm{d}x$ may be locally.

The second term of equation (3.08.16) can be obtained by observing that since $x - x' \leqslant x - \bar{\xi}$ is $\mathrm{O}(M)$, $\varphi(x')/\varphi_0$ differs from $\varphi(x)/\varphi_0$ by a quantity

† ω will indicate the value of the reduced frequency Ω for neutral condition, that is at the stability boundary.

‡ The case of large ω and the corresponding modifications is also discussed in the following section.

§ For large ω this formula has to be modified, as shown at Section 3.13.

of $O(M)$, so that the value of the integral is of $O(1)$ and can be expanded in the form

$$\frac{1}{s}\frac{\varphi(x)}{\varphi_0}\left[1-e^{-s\int_0^x \frac{dx'}{\bar{u}_1(x')}}\right]+O(M)=\frac{1}{s}\frac{\varphi(x)}{\varphi_0}\left[1-e^{-s\bar{\kappa}(x)}\right]+O(M) \quad \ldots.(3.08.20)$$

Integration by parts of the integral in the third term with $\nu(0)=0$ leads to

$$\frac{1}{s\bar{u}_1(x)}\frac{\nu(x)}{\varphi_0}-\frac{1}{s^2}\left[\overline{\bar{u}_1\frac{d}{dx}\left(\frac{\nu}{\bar{u}_1\varphi_0}\right)}\right]\left(1-e^{-s\int_0^x \frac{dx'}{\bar{u}_1(x')}}\right)+O(M) \quad \ldots.(3.08.21)$$

The barred quantity in square brackets represents a proper mean value of the corresponding expression. Since

$$\bar{u}_1\frac{d}{dx}\left(\frac{\nu}{\bar{u}_1\varphi_0}\right)=\frac{1}{\varphi_0}\frac{d\nu}{dx}-\frac{1}{\bar{u}_1}\frac{d\bar{u}_1}{dx}\frac{\nu}{\varphi_0} \qquad \text{is } O(1)$$

because of the relations (3.08.18) and because, from equation (3.06.11), $d\bar{u}_1/dx$ is $O(M)$; and since for $s=i\omega$ also the exponential in parentheses in equation (3.08.21) is $O(1)$, we conclude that the value of the third integral is $O(1/M)$ and can be expressed as

$$\frac{1}{s\bar{u}_1(x)}\frac{\nu(x)}{\varphi_0}+O(1) \quad \ldots.(3.08.22)$$

Replacing into equation (3.08.16) the expressions (3.08.20) and (3.08.22) for the two integrals, and recalling that k is $O(M)$ and that $d\bar{u}(x)/dx$ is at most $O(1)$ we obtain

$$\frac{q(x)}{\varphi_0}=nQ(x)+\frac{n}{s}\bar{u}_1(x)\frac{d\bar{u}(x)}{dx}\frac{\varphi(x)}{\varphi_0}\left[1-e^{-s\bar{\kappa}(x)}\right]-\frac{k}{s^2}\frac{d\bar{u}(x)}{dx}\frac{\nu(x)}{\varphi_0} \quad \ldots.(3.08.23)$$

with $Q(x)$ given by equation (3.08.19). The only terms retained are at most $O(M)$ if n is $O(1)$. We can conclude that under the present assumptions $q(x)/\varphi_0$ is $O(M)$, though dQ/dx, and therefore $dq/\varphi_0\,dx$, is locally of the same order as $d\bar{u}/dx$ and therefore can be $O(1)$.

3.09. Solution by Iteration for Moderate ω

We are now going to examine the order of magnitude of the terms of equations (3.07.11) for the case of neutral oscillations $s=i\omega$. Let us first consider the integral terms. They can be reduced to the following integrals:

$$\int_0^x \gamma sF(x')\,e^{\pm s(x-x')}\,dx';\quad \int_0^x \gamma sE(x')\,e^{\pm s(x-x')}\,dx' \quad \ldots.(3.09.01)$$

From equations (3.07.08) and (3.07.09) we have:

$$\gamma sF=\gamma s\frac{q}{\varphi_0}-\gamma s\bar{u}\frac{\varphi-\sigma}{\varphi_0}+\gamma s\bar{\rho}_1\frac{\eta}{\varphi_0}+\gamma s\bar{u}_1\frac{\zeta}{\varphi_0}+O(M^2) \quad \ldots.(3.09.02)$$

$$\gamma sE=(3-\gamma)s\bar{u}\frac{\gamma\nu}{\varphi_0}+2\gamma s\bar{\rho}_1\bar{u}_1\frac{\eta}{\varphi_0}+\gamma s\bar{u}_1^2\frac{\zeta}{\varphi_0}+O(M^2) \quad \ldots.(3.09.03)$$

where all the terms not written explicitly are definitely of $O(M^2)$ because of the assumptions (3.08.18) and because of the results of Section 3.06 about the order of magnitude of the steady state quantities. Let us first consider the contribution to the integrals (3.09.01) due to $\gamma sq/\varphi_0$. This contribution can be split into three terms by the use of equation (3.08.23), the integrands being all of $O(M)$. The second of these three terms can be written as

$$n\gamma \int_0^x \bar{u}_l \frac{\varphi}{\varphi_0} [1 - e^{-s\tau}]\, e^{\pm s(x-x')}\, d[\bar{u}(x')]$$

The modulus of this integrand is at most equal to the product of the maximum modulus of

$$\bar{u}_l \frac{\varphi}{\varphi_0} (1 - e^{-s\tau})\, e^{\pm s(x-x')}$$

which for $s = i\omega$ is of the same order as $\bar{u}_l$, that is $O(M)$, times the variation of $\bar{u}$, which is also $O(M)$. Thus this second term is $O(M^2)$. The same result is derived for the third term, which can be written as

$$\frac{k}{s} \int_0^x \frac{\gamma\nu}{\varphi_0} e^{\pm s(x-x')}\, d[\bar{u}(x')] = O(M^2)$$

because both the integral and k are $O(M)$ (see Section 3.06). Hence all contributions to the integrals (3.09.01) from (3.08.23) are $O(M^2)$ except the one due to the first term, so that the spacewise contribution to the burning rate can be completely neglected in the following development, and only the timewise contribution retained. For $\omega = O(1)$ it is clear that the integral in equation (3.09.04) is $O(M)$; when ω is large, that is, when $|s|$ is large, one can integrate by parts so that this first term can be written

$$\begin{aligned}\int_0^x \gamma s \frac{q}{\varphi_0} e^{\pm s(x-x')}\, dx' &= n\gamma s \int_0^x Q(x')\, e^{\pm s(x-x')}\, dx' \\ &= \mp n\gamma \left[Q(x) - \int_0^x \frac{dQ}{dx'} e^{\pm s(x-x')}\, dx' \right] \\ &= \mp n\gamma \left\{ Q(x) - \int_0^x \frac{\varphi}{\varphi_0} (1 - e^{-s\tau})\, e^{\pm s(x-x')}\, d[\bar{u}(x')] \right\}\end{aligned} \quad \ldots\ldots (3.09.04)$$

which is $O(M)$ no matter how large $d\bar{u}/dx$ is locally, and how large ω is. Thus we conclude, in general, that for n of $O(1)$, the expression (3.09.04) is $O(M)$.

Consider next in the integrals (3.09.01) the contribution due to the term in $(\varphi - \sigma)/\varphi_0$ of equation (3.09.02). Rewrite equation (3.07.04) in the form

$$\begin{aligned}&\frac{d}{dx}\left[\bar{u}\left(\frac{\varphi}{\varphi_0} - T\frac{\sigma}{\varphi_0} + (\gamma - 1)\bar{\rho}\bar{u}\frac{\nu}{\varphi_0}\right)\right] \\ &\qquad + s\left[\frac{\varphi}{\varphi_0} - T\frac{\sigma}{\varphi_0} + (\gamma - 1)\bar{\rho}\bar{u}\frac{\nu}{\varphi_0}\right] = s\frac{\gamma - 1}{\gamma}\frac{\varphi}{\varphi_0} \qquad \ldots\ldots (3.09.05)\end{aligned}$$

and integrate this linear equation to obtain

$$\frac{\varphi}{\varphi_0} - \bar{T}\frac{\sigma}{\varphi_0} + (\gamma-1)\bar{\rho}\bar{u}\frac{v}{\varphi_0} = \frac{\gamma-1}{\gamma}\frac{1}{\bar{u}}\int_0^x \bar{u}(x')\frac{\varphi(x')}{\varphi_0}\,\mathrm{d}\left(\mathrm{e}^{s\int_{x'}^{x}\frac{\mathrm{d}x''}{\bar{u}}}\right) \quad \ldots.(3.09.06)$$

An alternate form of this expression is

$$\frac{1}{\gamma}\frac{\varphi}{\varphi_0} - \bar{T}\frac{\sigma}{\varphi_0} = -\frac{\gamma-1}{\gamma}\left\{\bar{\rho}\bar{u}\frac{\gamma v}{\varphi_0} + \frac{1}{\bar{u}}\int_0^x \mathrm{e}^{s\int_{x'}^{x}\frac{\mathrm{d}x''}{\bar{u}}}\,\mathrm{d}\left[\bar{u}(x')\frac{\varphi(x')}{\varphi_0}\right]\right\} \quad \ldots.(3.09.07)$$

The expression (3.09.06) represents the time independent factor of the stagnation enthalpy perturbation, $\bar{\rho}h_s'\,\mathrm{e}^{-st}/\varphi_0$ (as is immediately checked from Section 3.07), and the expression (3.09.07), the time independent factor of the entropy perturbation, $\bar{\rho}S'\,\mathrm{e}^{-st}/c_p\varphi_0$. For neutral oscillations, $s = i\omega$; both quantities, and therefore h_s'/φ_0 and S'/φ_0 can be O(1) as can be checked from equations (3.09.06) and (3.09.07). Therefore the quantity $(\varphi - \bar{T}\sigma)/\varphi_0 \simeq (\varphi - \sigma)/\varphi_0$, representing the temperature perturbation, is also of O(1), a result consistent with the assumptions (3.08.13). Neglecting terms of $O(M^2)$, equation (3.09.05) becomes

$$\frac{\varphi-\sigma}{\varphi_0} = \frac{\gamma-1}{\gamma}\left(\frac{\varphi}{\varphi_0} - \bar{u}\frac{\gamma v}{\varphi_0}\right) - \frac{1}{s}\frac{\mathrm{d}}{\mathrm{d}x}\left[u\left(\frac{\varphi-\sigma}{\varphi_0} + \frac{\gamma-1}{\gamma}\bar{u}\frac{\gamma v}{\varphi_0}\right)\right]$$

From this expression we find that

$$\gamma s\int_0^x \bar{u}\frac{\varphi-\sigma}{\varphi_0}\,\mathrm{e}^{\pm s(x-x')}\,\mathrm{d}x' = (\gamma-1)s\int_0^x \bar{u}\frac{\varphi}{\varphi_0}\,\mathrm{e}^{\pm s(x-x')}\,\mathrm{d}x' + \mathrm{O}(M^2) \quad \ldots.(3.09.08)$$

since the value of

$$\gamma\int \bar{u}\,\mathrm{e}^{\pm s(x-x')}\,\mathrm{d}\left[\bar{u}\left(\frac{\varphi-\sigma}{\varphi_0} + \frac{\gamma-1}{\gamma}\bar{u}\frac{\gamma v}{\varphi_0}\right)\right]$$

is evidently of $O(M^2)$. We see also that the value of the integral (3.09.08) is of $O(M)$. An interesting observation is that, as equation (3.09.08) shows, within terms of $O(M)$, the value of the integral can be determined using the isentropic relation $\sigma = \varphi/\gamma$, despite the fact that the entropy variation itself can be of O(1). This shows that some sort of compensating effect depresses the order of the integral

$$\int_0^x \bar{u}\left(\frac{\varphi}{\gamma\varphi_0} - \frac{\sigma}{\varphi_0}\right)\mathrm{e}^{\pm s(x-x')}\,\mathrm{d}x'$$

from $O(M)$ to $O(M^2)$.

The contribution to the integrals (3.09.01) of the third term of the expression (3.09.02) can be written, using equation (3.07.05), as

$$\gamma s \int_0^x \bar{\rho}_l \frac{\eta}{\varphi_0} e^{\pm s(x-x')}\, dx' = k \int_0^x \bar{\rho}_l \frac{\gamma v}{\varphi_0} e^{\pm s(x-x')}\, dx' + O(M^3) \quad \ldots.(3.09.09)$$

and is of $O(M)$. The contribution of the fourth term of equation (3.09.02) can be evaluated as follows. Let us first determine the order of magnitude of ζ/φ_0. Equation (3.07.02) can be rewritten as

$$\frac{d}{dx}\left(\bar{u}_l \frac{\zeta}{\varphi_0}\right) + \frac{s}{\bar{u}_l} \bar{u}_l \frac{\zeta}{\varphi_0} = -\frac{1}{\varphi_0}\frac{dq}{dx} + O(M) \quad \ldots.(3.09.10)$$

because of equation (3.07.05) and assumptions (3.08.18). The solution of this equation satisfying the boundary condition (3.07.06) can be put in the form

$$s\bar{u}_l \frac{\zeta}{\varphi_0} = -\int_0^x \bar{u}_l \left[\frac{1}{\varphi_0}\frac{dq}{dx} + O(M)\right] \frac{d}{dx}\left(e^{s\int_x^{x'} \frac{dx''}{\bar{u}_l}}\right) dx'$$

which shows that $\bar{u}_l(\zeta/\varphi_0)$ is at most $O(M)$, because $(1/\varphi_0)\ (dq/dx)$ is at most $O(1)$. Thus neglecting the contribution of the term $O(M)$ in equation (3.09.10) we can write

$$\gamma \int_0^x s\bar{u}_l \frac{\zeta}{\varphi_0} e^{\pm s(x-x')}\, dx' = -\gamma \int_0^x \bar{u}_l\, e^{\pm s(x-x')}\, d\left[\frac{q(x')}{\varphi_0}\right]$$

$$-\gamma \int_0^x s\bar{u}_l \frac{\zeta}{\varphi_0} e^{\pm s(x-x')}\, d\left[\bar{u}_l(x') \frac{\zeta(x')}{\varphi_0}\right] = O(M^2) \quad \ldots.(3.09.11)$$

since it is immediately recognized that both integrals are at most $O(M^2)$. Finally it is immediately checked that of the contributions from the various terms of the expression (3.09.03) only the first one is $O(M)$:

$$(3-\gamma)s \int_0^x \bar{u} \frac{\gamma v}{\varphi_0} e^{\pm s(x-x')}\, dx'$$

$$= \mp(3-\gamma) \int_0^x \bar{u} \frac{\gamma v}{\rho_0}\, d\left[e^{\pm s(x-x')}\right] = O(M) \quad \ldots.(3.09.12)$$

and the others are all $O(M^2)$:

$$\gamma s \int_0^x \left(3\bar{\rho}_l \bar{u}_l \frac{\eta}{\varphi_0} + \bar{u}_l^2 \frac{\zeta}{\varphi_0}\right) e^{s(x-x')}\, dx' = O(M^2) \quad \ldots.(3.09.13)$$

The results represented by the equations (3.09.04), (3.09.08), (3.09.09), (3.09.11), (3.09.12) and (3.09.13) can be summarized by saying that for the purpose of evaluating the integrals (3.09.01), and therefore those of equations (3.07.11) within terms of $O(M)$, the expressions (3.09.02) and (3.09.03) can be replaced by the following:

$$\gamma sF = s(n\gamma Q - U); \qquad \gamma sE = -isV \quad \ldots.(3.09.14)$$

with:

$$Q(x) = \int_0^x \frac{\varphi}{\varphi_0}\,(1 - e^{-s\bar{r}})\,\frac{d\bar{u}}{dx'}\,dx'; \qquad \ldots.(3.09.15)$$

$$\left.\begin{aligned} U(x) &= (\gamma - 1)\,\bar{u}\,\frac{\varphi}{\varphi_0} - \frac{k}{s}\,\bar{\rho}_1\,\frac{\gamma v}{\varphi_0}; \\ V(x) &= i(3 - \gamma)\,\bar{u}\,\frac{\gamma v}{\varphi_0} \end{aligned}\right\} \ldots.(3.09.16)$$

These quantities, and the corresponding terms of the integrals (3.09.01) are all of $O(M)$.

In the preceding analysis we did not take into account the effects of the magnitude of $s = i\omega$ except for equation (3.09.04) which was shown to retain the same order of magnitude no matter how large ω is. In the same manner one can show that the orders of magnitude of equations (3.09.09), (3.09.11) and (3.09.13) are unchanged no matter how large ω is. However, the same is not true for equations (3.09.08) and (3.09.12). In both cases it can be seen that the integral on the left-hand side stays of $O(M)$ no matter how large ω is, and therefore the whole expression is $O(\omega M)$. Its order of magnitude depends on the value of ω; if ω is $O(1/M)$, for instance, it becomes $O(1)$, and keeps increasing for increasing ω. It will be seen later that if n is $O(1)$, ω must be close to $l\pi$, l being an integer. We conclude that if $M = 0{\cdot}1$ and $l = 1$, ωM is around $0{\cdot}3$ and can still be considered of $O(M)$; but for $l \geqslant 2$ it is more proper to consider the quantities (3.09.08) and (3.09.12) to be of $O(1)$†. Thus the previous results about U and V being of $O(M)$ apply only if ω has moderate values. It will be seen in Section 3.10 how this restriction upon the validity of the iteration procedure that follows can be easily eliminated.

Following the same lines as those already used one finds that equation (3.07.08) gives:

$$\left.\begin{aligned} \gamma Y &= \gamma\,\frac{q}{\varphi_0} - \gamma\bar{u}\,\frac{\varphi}{\varphi_0} + O(M^2) \\ \gamma W &= 2\bar{u}\,\frac{\gamma v}{\varphi_0} + O(M^2) \end{aligned}\right\} \ldots.(3.09.17)$$

and that these two quantities are also of $O(M)$. Hence, introducing $s = i\omega$, with ω of $O(1)$ at most, equations (3.07.11) can be written as:

$$\left.\begin{aligned} \varphi/\varphi_0 &= \cos\omega x + O(M) \\ \gamma v/\varphi_0 &= -i\sin\omega x + O(M) \end{aligned}\right\} \ldots.(3.09.18)$$

This form of the equations suggests the following iteration procedure valid for moderate values of ω. Neglect first the terms of $O(M)$ with respect to the terms of $O(1)$; the resulting solution of zero order:

$$\varphi^{(0)}/\varphi_0 = \cos\omega x; \qquad \gamma v^{(0)}/\varphi_0 = -i\sin\omega x \qquad \ldots.(3.09.19)$$

† The magnitude of the expression (3.09.08) is reduced by the presence of the factor $(\gamma - 1)$, which for rockets can be considered of $O(M)$. No reduction of magnitude exists for the expression (3.09.12).

coincides with the acoustic solution satisfying the condition $v = 0$ at $x = 0$. This is an exact solution of the problem when $M = 0$. If M is exactly zero, there is no combustion and we can replace the nozzle at $x = 1$ with a closed end; so that at $x = 1$, v must again be zero. The phenomenon is now reduced to the one dimensional oscillation in a pipe closed at both ends. The corresponding eigenvalues ω satisfy the equation $\sin \omega = 0$, so that they take the values $\omega = l\pi$ $(l = 0, 1, 2 \ldots)$ characteristic of the organ pipe oscillations. The oscillations are always neutral at these well defined frequencies.

If there is combustion and M is small but different from zero, two things happen. Terms of $O(M)$ are added in equations (3.09.18); and the boundary condition at $x = 1$, instead of $v = 0$, will be given by

$$\gamma v_1/\varphi_1 = \bar{u}_1 \alpha \qquad \ldots.(3.09.20)$$

even if we neglect the terms of $O(M)$ in (3.09.18), in which case the form of the solutions is still given by (3.09.19).

The specific admittance ratio of the nozzle, α, has been determined for isentropic oscillations in Appendix B, and has already been used at Section 3.04 for the case of concentrated combustion. The change of the boundary conditions affects the values of ω for neutral oscillations. Hence leaving ω for the moment as the unknown eigenvalue to be determined later, we can compute the additional terms of equation (3.09.18) by using the expressions of $\varphi^{(0)}/\varphi_0$ and $\gamma v^{(0)}/\varphi_0$ from equations (3.09.19) of the 0th iteration. If the quantities:

$$Q^{(0)}(x) = \int_0^x \cos \omega x' [1 - e^{-i\omega \bar{\tau}(x')}] \frac{d\bar{u}}{dx'} dx' \qquad \ldots.(3.09.21)$$

$$\left.\begin{aligned} U^{(0)}(x) &= (\gamma - 1)\bar{u} \cos \omega x + \frac{k}{\omega} \bar{\rho}_l \sin \omega x \\ V^{(0)}(x) &= (3 - \gamma)\bar{u} \sin \omega x \end{aligned}\right\} \ldots.(3.09.22)$$

are introduced in equations (3.09.14), and then in equations (3.07.10), together with the 0th approximations for the quantities given in (3.09.17), one obtains:

$$\left.\begin{aligned} \frac{\varphi^{(1)}}{\varphi_0} &= \cos \omega x + i \Big\{ 2\bar{u} \sin \omega x \\ &\quad - \omega \int_0^x [\{n\gamma Q^{(0)}(x') - U^{(0)}(x')\} \cos \omega(x - x') \\ &\quad + V^{(0)}(x') \sin \omega(x - x')] \, dx' \Big\} \\ \frac{\gamma v^{(1)}}{\varphi_0} &= -i \sin \omega x + \gamma \frac{q^{(0)}}{\varphi_0} - \gamma \bar{u} \cos \omega x \\ &\quad - \omega \int_0^x [\{n\gamma Q^{(0)}(x') - U^{(0)}(x')\} \sin \omega(x - x') \\ &\quad - V^{(0)}(x') \cos \omega(x - x')] \, dx' \end{aligned}\right\} \ldots.(3.09.23)$$

The expression for $q^{(0)}$ is obtained from equation (3.08.23) after introducing the relations (3.09.19). The result of this first iteration is correct up to terms of $O(M)$ provided ω is not too large. In principle it would be possible to proceed further with additional iterations; however, all the terms of $O(M^2)$ that have been neglected in the developments of this section should be introduced, and the result would become very involved. The corresponding refinement does not appear to be justified in view of the roughness of certain of our assumptions, and is certainly not required if M is sufficiently small, in the neighbourhood of 0·1, say.

3.10. Solution by Iteration for Large ω

The procedure outlined in the previous section cannot be applied if ω is $O(1/M)$ or larger. It is possible, however, to locate the terms that are responsible for the inconvenience and introduce the necessary alterations so that the procedure may converge at higher ω. The trouble comes from the expressions (3.09.06) and (3.09.12), that is from the second term in the right-hand member of equation (3.09.02) and the first term in the right-hand member of equation (3.09.03). If we rewrite them in the following way:

$$\gamma s\bar{u}\frac{\varphi-\sigma}{\varphi_0} = (\gamma-1)s\bar{u}\frac{\varphi}{\varphi_0} + s\bar{u}\frac{\varphi-\gamma\sigma}{\varphi_0}$$

$$= s\bar{u}\frac{\varphi}{\varphi_0} - (2-\gamma)s\bar{u}\frac{\varphi}{\varphi_0} + s\bar{u}\frac{\varphi-\gamma\sigma}{\varphi_0}$$

$$(3-\gamma)s\bar{u}\frac{\gamma\nu}{\varphi_0} = s\bar{u}\frac{\gamma\nu}{\varphi_0} + (2-\gamma)s\bar{u}\frac{\gamma\nu}{\varphi_0}$$

it is possible to show that the contribution of the first terms of these two expressions to equations (3.09.23) is of $O(sM)$; the contribution of the terms in $2-\gamma$ is always $O(M)$ no matter how large ω is; and finally the contribution of the third term of the first expression, representing the deviation from isentropic conditions, is $O(sM^2)$. This suggests that in order to eliminate terms of $O(sM)$ from the equations (3.09.24) we start from equation (3.07.09) modified as follows:

$$\left.\begin{aligned}&\frac{\mathrm{d}}{\mathrm{d}x}\left(\frac{\nu}{\varphi_0}-Y\right)+s\left(\frac{\varphi}{\gamma\varphi_0}+W\right)-s\bar{u}\left(\frac{\nu}{\varphi_0}-Y\right)\\&\qquad=s\left(W-X-\bar{u}\frac{\nu}{\varphi_0}+\bar{u}Y\right)=s\bar{E}\end{aligned}\right\}\quad\ldots.(3.10.01)$$

$$\left.\begin{aligned}&\frac{\mathrm{d}}{\mathrm{d}x}\left(\frac{\varphi}{\gamma\varphi_0}+W\right)+s\left(\frac{\nu}{\varphi_0}-Y\right)-s\bar{u}\left(\frac{\varphi}{\gamma\varphi_0}+W\right)\\&\qquad=-s\left(Y+Z+\bar{u}\frac{\varphi}{\gamma\varphi_0}+\bar{u}W\right)=-s\bar{F}\end{aligned}\right\}$$

The homogeneous equations obtained from relations (3.10.01) by putting $\bar{E}=\bar{F}=Y=W=0$ have the solution

$$\frac{\tilde{\varphi}^{(0)}}{\varphi_0} = \mathrm{e}^{s\int_0^x \bar{u}\,\mathrm{d}x'}\cosh sx; \qquad \frac{\gamma\tilde{\nu}^{(0)}}{\varphi_0} = -\mathrm{e}^{s\int_0^x \bar{u}\,\mathrm{d}x'}\sinh sx \quad\ldots.(3.10.02)$$

satisfying at $x=0$ the conditions $\tilde{\varphi}^{(0)}=\varphi_0$, $\tilde{\nu}^{(0)}=0$. With the same

boundary conditions the non-homogeneous system (3.10.01) has, for known $\tilde{E}$ and $\tilde{F}$, the solution:

$$\left.\begin{aligned}
\frac{\varphi}{\varphi_0} &= \frac{\tilde{\varphi}^{(0)}}{\varphi_0} - \gamma W \\
&\quad - s e^{s\int_0^x \tilde{u}\,dx'} \int_0^x e^{-s\int_0^{x'} \tilde{u}\,dx''} [\gamma \tilde{F}(x') \cosh s(x-x') \\
&\quad + \gamma \tilde{E}(x') \sinh s(x-x')]\,dx' \\
\frac{\gamma v}{\varphi_0} &= \frac{\gamma \tilde{v}^{(0)}}{\varphi_0} + \gamma Y \\
&\quad + s e^{s\int_0^x \tilde{u}\,dx'} \int_0^x e^{-s\int_0^{x'} \tilde{u}\,dx''} [\gamma \tilde{F}(x') \sinh s(x-x') \\
&\quad + \gamma \tilde{E}(x') \cosh s(x-x')]\,dx'
\end{aligned}\right\} \quad \ldots\ldots (3.10.03)$$

analogous to the system (3.07.10). Again since $\tilde{E}$ and $\tilde{F}$ are not known but contain the unknowns, equations (3.10.03) can be considered as a system of integral equations. Using the same techniques used in Section 3.09 we can check that for $s = i\omega$ the integrals appearing in (3.10.03) contain either terms of an order of magnitude which does not change with ω and is at most $O(M)$, or terms with order of magnitude increasing with ω, but at most $O(\omega M^2)$. Thus we can say that with ω up to $O(1/M)$ equations (3.10.03) can be written as:

$$\frac{\varphi}{\varphi_0} = \frac{\tilde{\varphi}^{(0)}}{\varphi_0} + O(M); \qquad \frac{\gamma v}{\varphi_0} = \frac{\gamma \tilde{v}^{(0)}}{\varphi_0}$$

and we can apply the iteration technique previously discussed. The zero order iteration is now given by equations (3.10.02) with $s = i\omega$, instead of equations (3.09.19). We can see that the only difference between the two is a phase change, the amplitude remaining unchanged; and that the difference in phase is equal to $\omega \int_0^x \tilde{u}\,dx'$ and is of the order of 1 radian if ω is $O(1/M)$†. The first iteration is obtained by introducing into equations (3.10.03) the values of $\tilde{Y}^{(0)}$, $\tilde{W}^{(0)}$, $\tilde{E}^{(0)}$, $\tilde{F}^{(0)}$ computed from the solutions (3.10.02) of the 0th iteration:

$$\left.\begin{aligned}
\frac{\varphi^{(1)}}{\varphi_0} &= e^{i\omega\int_0^x \tilde{u}\,dx'} \{\cos \omega x + i2\tilde{u} \sin \omega x \\
&\quad - i\omega \int_0^x e^{-i\omega\int_0^{x'} \tilde{u}\,dx''} [(n\gamma \tilde{Q}^{(0)} - \tilde{U}^{(0)}) \cos \omega(x-x') \\
&\quad + \tilde{V}^{(0)} \sin \omega(x-x')]\,dx'\} \\
\frac{\gamma v^{(1)}}{\varphi_0} &= \gamma \frac{\tilde{q}^{(0)}}{\varphi_0} + e^{i\omega\int_0^x \tilde{u}\,dx'} \{-i \sin \omega x - \gamma \tilde{u} \cos \omega x \\
&\quad - \omega \int_0^x e^{-i\omega\int_0^{x'} \tilde{u}\,dx''} [(n\gamma \tilde{Q}^{(0)} - \tilde{U}^{(0)}) \sin \omega(x-x') \\
&\quad - \tilde{V}^{(0)} \cos \omega(x-x')]\,dx'\}
\end{aligned}\right\} \quad \ldots\ldots (3.10.04)$$

†This phase shift is substantially an effect of the mean motion of the gases on the absolute velocity of wave propagation.

where $\tilde{Y}^{(0)}$, $\tilde{W}^{(0)}$ have been obtained again from equations (3.09.17) with $\tilde{\varphi}^{(0)}/\varphi_0$, etc. In the quantities†:

$$\left.\begin{aligned}
\tilde{Q}^{(0)}(x) &= \int_0^x \frac{\tilde{\varphi}^{(0)}(x')}{\varphi_0}[1 - e^{-i\omega t(x')}]\frac{d\bar{u}}{dx'}\,dx' \\
\tilde{U}^{(0)}(x) &= -(2-\gamma)\bar{u}\frac{\tilde{\varphi}^{(0)}}{\varphi_0} - \frac{k}{i\omega}\bar{\rho}_l\frac{\gamma\tilde{r}^{(0)}}{\varphi_0} \\
&\quad + \bar{u}\frac{\tilde{\varphi}^{(0)} - \gamma\tilde{\sigma}^{(0)} + (\gamma-1)\bar{u}\gamma\tilde{r}^{(0)}}{\varphi_0} - 2\bar{u}^2\frac{\gamma\tilde{r}^{(0)}}{\varphi_0} \\
\tilde{V}^{(0)}(x) &= i\left[(2-\gamma)\bar{u}\frac{\gamma\tilde{r}^{(0)}}{\varphi_0} - \frac{3(\gamma-1)}{2}\bar{u}^2\frac{\tilde{\varphi}^{(0)}}{\varphi_0}\right]
\end{aligned}\right\} \quad \ldots\ldots (3.10.05)$$

only those terms have been retained which, after the integrations of equations (3.10.04), produce terms of $O(M)$ or $O(\omega M^2)$. The first two terms of $\tilde{U}^{(0)}$ and the first of $\tilde{V}^{(0)}$ correspond to those of equations (3.09.22) except for the fact that $\gamma - 1$ and $3 - \gamma$ are replaced by $2 - \gamma$. Observe that the phase shift of the new 0th iteration is cancelled by the exponential factor under the integral sign of equations (3.10.04) so that these terms result in the same expressions (except for the change in the numerical factor) for both iteration procedures. However, the additional factors of equations (3.10.05) are new. From equation (3.09.07) we obtain the value of the term

$$\bar{u}\frac{\tilde{\varphi}^{(0)} - \gamma\tilde{\sigma}^{(0)} + (\gamma-1)\bar{u}\gamma\tilde{r}^{(0)}}{\varphi_0} = -\gamma\int_0^x e^{i\omega\int_x^{x'}\frac{dx''}{\bar{u}}}\frac{d}{dx'}\left(\bar{u}\frac{\tilde{\varphi}^{(0)}}{\varphi_0}\right)dx'$$

All new terms are of $O(\omega M^2)$ and become important only when ω is $O(1/M)$.

3.11. Solution of the Eigenvalue Problem for $\bar{\tau} =$ Constant

The stability problem can be stated as follows. In a chamber with a given nozzle, for which we know the specific admittance ratio α as a function of the frequency, we prescribe a given combustion law, represented by a known distribution of space and time lags and by a value of the interaction index n. As has been observed while discussing equations (3.06.13), the steady state combustion distribution is represented by the distribution $\bar{u}(x)$. Similarly the unsteady effects on combustion are represented by the distribution of sensitive time lags $\bar{\tau}(x)$ and by the interaction index n.

Now the question is: for given α, $\bar{u}(x)$, $\bar{\tau}(x)$ and n, will an arbitrary perturbation of the steady state conditions be amplified or damped? Mathematically the answer to this question is given, as in previous sections, by analysing the sign of the real part A of $s = A + i\Omega$. In practice, as has been stated several times, we need only determine the neutral condition under which A changes its sign. If α and $\bar{u}(x)$ are fixed, these neutral conditions will be possible only when a certain relation involving $\bar{\tau}(x)$ and n is satisfied; and they will take place with a well determined critical frequency ω.

† This formula is not quite exact under the assumption of this section. The changes to be made are indicated in Section 3.13. They have not been introduced to avoid the additional complication of the following developments.

Equation (3.09.20) represents such a functional relationship between the three quantities, and since it is a complex relationship, it corresponds to two real ones. If for simplicity we assume (as we will in the rest of this section) that the sensitive time lag is the same for all elements, equation (3.09.20) represents two equations between the three quantities δ, n and ω, where δ is the critical value of the constant time lag $\bar{\tau}$. This means that for a given value of n, equation (3.09.20) will determine the values of δ and ω for which neutral oscillations can be obtained; in other words they represent the characteristic equations for the set of eigenvalues δ and ω. However, the direct solution of these equations would require laborious numerical calculations because ω appears in a very involved form, and it would be hard to find the qualitative trends. We can obtain results in a much faster and easier way by reversing the procedure, that is prescribing the value of ω and looking for the eigenvalues δ and n compatible with neutral oscillations for that value of ω.

An idea of the ranges of ω that will be particularly interesting can be obtained from equation (3.09.20) after neglecting in the left-hand side quantities of $O(M)$; that is from the equation

$$\sinh s/\cosh s = \bar{u}_1(\alpha_r + i\alpha_i)^\dagger \qquad \ldots.(3.11.01)$$

which can be obtained from system (3.09.19) or from (3.10.02). It is clear that if $\alpha_r \neq 0$ this equation cannot be satisfied for $\Lambda = 0$. Let us therefore take $s = \Lambda + i\Omega$, and split equation (3.11.01) into the corresponding two real equations:

$$\frac{\sinh \Lambda \cosh \Lambda}{\sinh^2 \Lambda + \cos^2 \Omega} = -\alpha_r \bar{u}_1; \qquad \frac{\sin \Omega \cos \Omega}{\sinh^2 \Lambda + \cos^2 \Omega} = -\alpha_i \bar{u}_1$$

If $\alpha_r \bar{u}_1$ and $\alpha_i \bar{u}_1$ are $O(M)$ these equations are satisfied, within our order of approximation, by:

$$\sinh \Lambda = -\alpha_r \bar{u}_1 \qquad \tan \Omega = -\alpha_i \bar{u}_1$$
$$\cosh \Lambda \simeq 1 \qquad \cos^2 \Omega \simeq 1$$

We see that since α_r is positive the oscillation must always be damped, and that the damping is related only to the value of $\alpha_r \bar{u}_1$, while $\alpha_i \bar{u}_1$ affects only the frequency, which is given by

$$\Omega = l\pi - \tan^{-1}(\alpha_i \bar{u}_1) \qquad \ldots.(3.11.02)$$

One can show that if $\alpha_i \bar{u}_1$ is $O(1)$ but $\alpha_r \bar{u}_1$ is still $O(M)$, the frequency is given by the same relation (3.11.02) and the damping by

$$\sinh \Lambda = -\alpha_r \bar{u}_1/(1 + \alpha_i^2 \bar{u}_1^2)$$

so that now the damping is affected also by the value of $\alpha_i \bar{u}_1$, but still $\alpha_r \bar{u}_1$ is the most important element in determining its order of magnitude. If finally both $\alpha_r \bar{u}_1$ and $\alpha_i \bar{u}_1$ are $O(1)$, both $\tan \Omega$ and $\tanh \Lambda$ become $O(1)$, depending in a mixed way upon $\alpha_r \bar{u}_1$ and $\alpha_i \bar{u}_1$. We conclude that though equation (3.11.01), obtained from equation (3.09.20) neglecting the effects of combustion and the other terms of $O(M)$, does not provide any eigenvalue

† Note $\bar{u}_1 = \bar{u}_r$, where $\bar{u}_r$ is to be found in the graphs of Appendix B.

for neutral oscillations, it provides, however, a well determined value (3.11.02) of the frequency when the damping Λ is of $O(M)$. If the combustion terms generate enough energy to balance the damping and produce neutral oscillations, it can be expected that the frequency will still be around the value given by equation (3.11.02). Another important result is that the real and imaginary parts of α have separate and well defined functions at least so long as they stay of $O(1)$. The real part is substantially responsible for damping, and the imaginary part for the change in frequency with respect to the closed-end organ-pipe condition.

Coming back to the determination of the eigenvalues n and δ for given ω, let us discuss first the case of moderate ω. For constant δ the value of $n\gamma Q^{(0)}$ which appears in equations (3.09.23) can be written as

$$n\gamma Q^{(0)} = \Xi \int_0^x \cos \omega x' \frac{d\bar{u}}{dx'} dx' = \Xi K(x, \omega) \qquad \ldots.(3.11.03)$$

where the quantity

$$\Xi = n\gamma(1 - e^{-i\omega\delta}) \qquad \ldots.(3.11.04)$$

is now the only quantity appearing in the equation (3.09.20) containing the parameters n and δ of non-steady combustion.

As already stated in Section 3.07 we suppose that the combustion is completed at $x = 1$. From this assumption, consistent with the calculations of Appendix B where no combustion has been supposed to take place in the nozzle, it follows that at $x = 1$, $d\bar{u}/dx = 0$, so that the last two terms of equation (3.08.23) vanish. Thus applying equations (3.09.23) at $x = 1$ we obtain:

$$\left.\begin{aligned} \frac{\varphi_1^{(1)}}{\varphi_0} &= \cos\omega + i[2\bar{u}_1 \sin\omega - \Xi C(\omega) + A(\omega)] \\ \frac{\gamma v_1^{(1)}}{\varphi_0} &= -i\sin\omega - \gamma\bar{u}_1\cos\omega + \Xi D(\omega) + B(\omega) \end{aligned}\right\} \ldots.(3.11.05)$$

where the functions A, B are given by:

$$A(\omega) = \omega \int_0^1 [U^{(0)}(x') \cos\omega(1 - x') - V^{(0)}(x') \sin\omega(1 - x')]\, dx'$$

$$B(\omega) = \omega \int_0^1 [U^{(0)}(x') \sin\omega(1 - x') + V^{(0)}(x') \cos\omega(1 - x')]\, dx'$$

that is, after using relation (3.09.22), by:

$$\left.\begin{aligned} A(\omega) &= \omega\cos\omega \int_0^1 \bar{u}\, dx' - (2 - \gamma)\omega \int_0^1 \bar{u}\cos\omega(1 - 2x')\, dx' \\ &\quad + \frac{k}{2}\int_0^1 \bar{\rho}_i[\sin\omega - \sin\omega(1 - 2x')]\, dx' \\ B(\omega) &= \omega\sin\omega \int_0^1 \bar{u}\, dx' - (2 - \gamma)\omega \int_0^1 \bar{u}\sin\omega(1 - 2x')\, dx' \\ &\quad - \frac{k}{2}\int_0^1 \bar{\rho}_i[\cos\omega - \cos\omega(1 - 2x')]\, dx' \end{aligned}\right\} \ldots.(3.11.06)$$

and the quantities C and D are given by the following equivalent expressions:

$$\left.\begin{aligned} C(\omega) &= \omega\int_0^1 K(x',\omega)\cos\omega(1-x')\,dx' \\ &= \int_0^1 \frac{dK}{dx'}\sin\omega(1-x')\,dx' \\ &= \tfrac{1}{2}\int_0^1 \frac{d\bar{u}}{dx'}\left[\sin\omega+\sin\omega(1-2x')\right]dx' \\ &= \omega\int_0^1 \bar{u}\cos\omega(1-2x')\,dx' \\ D(\omega) &= K(1,\omega)-\omega\int_0^1 K(x',\omega)\sin\omega(1-x')\,dx' \\ &= \int_0^1 \frac{dK}{dx'}\cos\omega(1-x')\,dx' \\ &= \tfrac{1}{2}\int_0^1 \frac{d\bar{u}}{dx'}\left[\cos\omega+\cos\omega(1-2x')\right]dx' \\ &= \bar{u}_1\cos\omega-\omega\int_0^1 \bar{u}\sin\omega(1-2x')\,dx' \end{aligned}\right\} \quad \ldots.(3.11.07)$$

In the first term of each of the equations (3.11.07) we recognize the term which becomes of O(1) where ω is O(1/M), while the remaining terms are at most of O(M). The order of magnitude of A, B, C and D is O(M) if ω is of O(1); but if ω is O(M) the order of magnitude decreases to O(M^2) for A and C and to O(M^3) for B, the order of magnitude of D being unchanged.

Replace equations (3.11.05) in (3.09.20) with $\alpha = \alpha_r + i\alpha_i$ and solve the ensuing equation for Ξ. The result is

$$\Xi = (I_r + iI_i)/(J_r + iJ_i) \qquad \ldots.(3.11.08)$$

with:

$$\left.\begin{aligned} I_r(\omega) &= (\gamma+\alpha_r)\bar{u}_1\cos\omega - 2\alpha_i\bar{u}_1^2\sin\omega - B(\omega) - \alpha_i\bar{u}_1A(\omega) \\ I_i(\omega) &= \sin\omega + \alpha_i\bar{u}_1\cos\omega + 2\alpha_r\bar{u}_1^2\sin\omega + \alpha_r\bar{u}_1A(\omega) \\ J_r(\omega) &= D(\omega) - \alpha_i\bar{u}_1C(\omega) \\ J_i(\omega) &= \alpha_r\bar{u}_1C(\omega) \end{aligned}\right\} \quad \ldots.(3.11.09)$$

From equations (3.11.08) and (3.11.04) one obtains the eigenvalues n and δ as:

$$n(\omega) = \frac{1}{2\gamma}\,\frac{I_r^2 + I_i^2}{I_rJ_r + I_iJ_i} \qquad \ldots.(3.11.10)$$

$$\delta(\omega) = \frac{1}{\omega}\left[(2m+1)\pi - 2\tan^{-1}\frac{I_i}{I_r} + 2\tan^{-1}\frac{J_i}{J_r}\right] \qquad \ldots.(3.11.11)$$

Before we discuss these results, let us observe that if α_r and α_i were of O(1) some terms, being of O(M^2), should be suppressed from the system (3.11.09).

However, for small M, both α_r and α_i can become large for sufficiently high frequency. This is shown clearly in *Figures 62* and *63* of Appendix B where the values of $\alpha_r\bar{u}_1$ and $\alpha_i\bar{u}_1$, computed for linear velocity distribution in the nozzle, are plotted against the reduced frequency β defined in the appendix. We see that though both $\alpha_r\bar{u}_1$ and $\alpha_i\bar{u}_1$ decrease when M decreases, they decrease quite slowly with the result that for high β and low M they must be considered as of O(1) rather than of O(M).

The relation between the reduced frequencies β and ω is obtained from the definitions of both as

$$\beta = \omega l_{sub}/(\bar{c}_t - \bar{u}_1) \qquad \ldots.(3.11.12a)$$

where l_{sub} represents the length of the convergent part of the nozzle divided by the chamber length, and $\bar{c}_t = [2/(\gamma + 1)]^{\frac{1}{2}}$ is the non-dimensional value of the critical velocity, reached at the throat of the nozzle. If, for example, $(\bar{c}_t' - \bar{u}_1)/l_{sub} = \pi$, which means that the length of the convergent part of the nozzle is roughly a third of the chamber length, and if ω is not far from one of the organ-pipe eigenvalues $l\pi$, the corresponding β is around l, that is, around unity for the fundamental mode, around two for the second, and so on. This is, however, only a particular case and a change in l_{sub} affects proportionately the values of β. The examination of the *Figures 62* and *63* shows that if we confine ourselves to values of M around 0·1 and if β goes from 0 to O(M), then $\alpha_r\bar{u}_1$ is O(M^2) and $\alpha_i\bar{u}_1$ goes from 0 to O(M^2). If β is around unity both $\alpha_r\bar{u}_1$ and $\alpha_i\bar{u}_1$ are around O(M); however, $\alpha_r\bar{u}_1$ stays considerably smaller than M (say, around $M/2$) and $\alpha_i\bar{u}_1$ stays considerably larger than M (around $2M$). With increasing β, $\alpha_r\bar{u}_1$ tends to stay O(M) up to β around three, and becomes O(1) for larger β while already at $\beta = 2$, $\alpha_i\bar{u}_1$ changes to O(1) and tends to decrease again only for much larger β.

With these orders of magnitude in mind, let us examine equations (3.11.10) and (3.11.11). Suppose first that ω is O(M), then we obtain immediately:

$$I_r = \gamma\bar{u}_1 + \mathrm{O}(M^2);\ I_i = \omega + \mathrm{O}(M^2);\ J_r = \bar{u}_1 + \mathrm{O}(M^3);\ J_i = \mathrm{O}(M^4)$$

and from equations (3.11.10) and (3.11.11), neglecting higher order terms, we have:

$$\left.\begin{aligned} \omega &= \gamma\bar{u}_1(2n-1)^{\frac{1}{2}} \\ \omega\delta &= (2m+1)\pi - 2\tan^{-1}(2n-1)^{\frac{1}{2}} \end{aligned}\right\} \ldots.(3.11.12b)$$

These results can be compared with those of the low frequency intrinsic instability, equation (2.03.10). For the comparison, the reduced frequency just derived has to be multiplied by the ratio of the two different characteristic times used, θ_g/θ_w, which is found to be equal to $1/\bar{u}$; no change, however, is to be applied to $\omega\delta$. It is easily checked that the results coincide, except for the non-essential numerical factor γ in the expression of the critical frequency. This factor arises because, in the low frequency part, the oscillations were assumed isothermal, while in the present calculations no predetermined oscillation behaviour was assumed. The present result

shows that actually the situation is better described by an isentropic oscillation, and equations (3.11.12b) are to be considered more accurate than the previous ones. Except for the slight numerical difference, we now have an indirect check of our basic assumption of Chapter 2 that the wave mechanism can be neglected at low frequencies and the gas can be assumed to oscillate as a whole. Actual calculations for increasing values of ω would show the limits of validity of this assumption.

Suppose next that ω is O(1), but that the value of β is below three, so that $\alpha_r\bar{u}_1$ is O(M). Equations (3.11.09) show that in this case I_r is O(M), J_r is O(M) and J_i is O(M) and I_i is, in general, of O(1). Thus from equation (3.11.10) n is O($1/M^2$). If, however, $\tan\omega = -\alpha_i\bar{u}_1 + O(M)$, I_i becomes of O(M). In the denominator of (3.11.10) I_iJ_i can be neglected as compared to I_rJ_r, and we obtain

$$n = \frac{1}{2\gamma}\left(\frac{I_r}{J_r} + \frac{I_i^2}{J_r I_r}\right)$$

both terms of which are of O(1). If we now take

$$\tan\omega = -\alpha_i\bar{u}_1 + O(M^2) \qquad \ldots.(3.11.13)$$

I_i turns out to be of O(M^2), while I_r and J_r will have changed their values only by an amount of O(M^2) but are still of O(M). Thus in the ranges of ω specified by equation (3.11.13), n takes a minimum value

$$n_{\min} = (1/2\gamma)\ (I_r/J_r) \qquad \ldots.(3.11.14)$$

It is to be observed that only the smallest positive value of ω satisfying equation (3.11.13), that is, neglecting terms of O(M^2), only

$$\omega = \pi - \tan^{-1}(\alpha_i\bar{u}_1) \qquad \ldots.(3.11.15)$$

can be considered of O(1). This coincides with the first value (3.11.02). As already shown, if l_{sub} is about one third of L, the corresponding value of β is around unity, in which case both $\alpha_r\bar{u}_1$ and $\alpha_i\bar{u}_1$ are O(M). If, however, the length of the nozzle is increased both $\alpha_r\bar{u}_1$ and $\alpha_i\bar{u}_1$ increase. Correspondingly, the value (3.11.15) of ω decreases, but the decrease is limited to a maximum amount of the order of 25° because the maximum value of $\alpha_i\bar{u}_1$ never goes much above 0·4, as appears clearly from *Figure 63*. Thus starting from a value close to 180°, ω would first decrease rapidly, reach a minimum around 155° and then increase again slowly. The value of β would therefore increase at first slower than l_{sub}, and later faster, but altogether it is bound to increase. When β reaches values around and above three, $\alpha_r\bar{u}_1$ which has been steadily increasing, must be considered to be no longer of O(M) but rather of O(1). As a consequence I_r is O(1) instead of O(M), while J_r and J_i are both O(M); I_i is O(1) in general but reduces to O(M) if ω is around the value (3.11.15). It is immediately deduced that n is now always of O($1/M$), even around the value (3.11.15) of ω where, however, it still takes its minimum value. Thus with increasing l_{sub}, due to the increase of $\alpha_r\bar{u}_1$, $n_{\min}$ increases steadily; and the variation of n from $n_{\min}$ when ω shifts from the value (3.11.15) becomes less sharp; in other words the minimum of n becomes less marked.

Finally let us examine the situation for higher ω, up to O($1/M$). One

can treat equations (3.10.04) applied at $x = 1$ exactly like equations (3.11.05), and again solve for Ξ obtaining

$$\Xi = \frac{I_r + iI_i}{J_r + iJ_i} \qquad \ldots.(3.11.16)$$

with:

$$\left.\begin{aligned} I_r(\omega) &= (\gamma + \alpha_r)\bar{u}_1 \cos\omega - 2\alpha_i\bar{u}_1^2 \sin\omega \\ &\quad - \bar{B} - \alpha_i\bar{u}_1\bar{A} - \alpha_r\bar{u}_1\bar{A}_1 \\ I_i(\omega) &= \sin\omega + \alpha_i\bar{u}_1 \cos\omega + 2\alpha_r\bar{u}_1^2 \sin\omega \\ &\quad - \bar{B}_1 + \alpha_r\bar{u}_1\bar{A} - \alpha_i\bar{u}_1\bar{A}_1 \\ J_r(\omega) &= \bar{D} - \alpha_i\bar{u}_1\bar{C} - \alpha_r\bar{u}_1\bar{C}_1 \\ J_i(\omega) &= \bar{D}_1 + \alpha_r\bar{u}_1\bar{C} - \alpha_i\bar{u}_1\bar{C}_1 \end{aligned}\right\} \ldots.(3.11.17)$$

The different functions appearing in these expressions are given by:

$$\left.\begin{aligned} \bar{A}(\omega) &= -(2-\gamma)\omega \int_0^1 \bar{u} \cos\omega(1-2x')\,dx' \\ &\quad + \frac{k}{2}\int_0^1 \bar{\rho}_i[\sin\omega - \sin\omega(1-2x')]\,dx' \\ &\quad - \gamma\omega \int_0^1 \cos\omega(1-x')\,dx' \int_0^{x'} \Delta(\omega, x'') \\ &\quad \times \cos[\omega\Gamma(x', x'')]\,dx'' \\ \bar{A}_1(\omega) &= \omega \int_0^1 \bar{u}^2[\tfrac{1}{4}(1+3\gamma)\sin\omega \\ &\quad - \tfrac{1}{4}(7-3\gamma)\sin\omega(1-2x')]\,dx' \\ &\quad - \gamma\omega \int_0^1 \cos\omega\,(1-x')\,dx' \int_0^{x'} \Delta(\omega, x'') \\ &\quad \times \sin[\omega\Gamma(x', x'')]\,dx'' \\ \bar{B}(\omega) &= -(2-\gamma)\omega \int_0^1 \bar{u} \sin\omega(1-2x')\,dx' \\ &\quad - \frac{k}{2}\int_0^1 \bar{\rho}_i[\cos\omega - \cos\omega(1-2x')]\,dx' \\ &\quad - \gamma\omega \int_0^1 \sin\omega(1-x')\,dx' \int_0^{x'} \Delta(\omega, x'') \\ &\quad \times \cos[\omega\Gamma(x', x'')]\,dx'' \\ \bar{B}_1(\omega) &= -\omega \int_0^1 \bar{u}^2[\tfrac{1}{4}(1+3\gamma)\cos\omega \\ &\quad - \tfrac{1}{4}(7-3\gamma)\cos\omega(1-2x')]\,dx' \\ &\quad - \gamma\omega \int_0^1 \sin\omega(1-x')\,dx' \int_0^{x'} \Delta(\omega, x'') \\ &\quad \times \sin[\omega\Gamma(x', x'')]\,dx'' \end{aligned}\right\} \ldots.(3.11.18)$$

$$
\left.
\begin{aligned}
\bar{C}(\omega) &= \omega \int_0^1 \cos\omega(1-x')\,dx' \int_0^{x'} \cos\omega x'' \\
&\quad \times \cos\left(\omega \int_{x'}^{x''} \bar{u}\,dx'''\right) \frac{d\bar{u}}{dx''}\,dx'' \\
\bar{C}_1(\omega) &= \omega \int_0^1 \cos\omega(1-x')\,dx' \int_0^{x'} \cos\omega x'' \\
&\quad \times \sin\left(\omega \int_{x'}^{x''} \bar{u}\,dx'''\right) \frac{d\bar{u}}{dx''}\,dx'' \\
\bar{D}(\omega) &= \int_0^1 \cos\omega x' \cos\left(\omega \int_1^{x'} \bar{u}\,dx''\right) \frac{d\bar{u}}{dx'}\,dx' \\
&\quad - \omega \int_0^1 \sin\omega(1-x')\,dx' \int_0^{x'} \cos\omega x'' \\
&\quad \times \cos\left(\omega \int_{x'}^{x''} \bar{u}\,dx'''\right) \frac{d\bar{u}}{dx''}\,dx'' \\
\bar{D}_1(\omega) &= \int_0^1 \cos\omega x' \sin\left(\omega \int_1^{x'} \bar{u}\,dx''\right) \frac{d\bar{u}}{dx'}\,dx' \\
&\quad - \omega \int_0^1 \sin\omega(1-x')\,dx' \int_0^{x'} \cos\omega x'' \\
&\quad \times \sin\left(\omega \int_{x'}^{x''} \bar{u}\,dx'''\right) \frac{d\bar{u}}{dx''}\,dx''
\end{aligned}
\right\} \quad \ldots.(3.11.18)\ \textit{cont.}
$$

Here the expressions for $\Gamma(x', x'')$ and $\Delta(\omega, x'')$ are:

$$
\left.
\begin{aligned}
\Gamma(x', x'') &= \int_{x'}^{x''} \left(\frac{1}{\bar{u}} + \bar{u}\right) dx''' \\
\Delta(\omega, x'') &= e^{-i\omega\int_0^{x''} \bar{u}\,dx'''} \frac{d}{dx''} \left[\bar{u}(x'') \cos\omega x'' \, e^{i\omega\int_0^{x''} \bar{u}\,dx'''}\right] \\
&= \cos\omega x'' \left(\frac{d\bar{u}}{dx''} + i\omega\bar{u}^2\right) - \omega\bar{u} \sin\omega x'' \\
&\simeq \cos\omega x'' \frac{d\bar{u}}{dx''} - \omega\bar{u} \sin\omega x''
\end{aligned}
\right\} \quad \ldots.(3.11.19)
$$

The term $\omega\bar{u}^2$, in the second expression for Δ, can be neglected because its contribution in the quantities defined in equations (3.11.18) is $O(M^3)$. With this simplification, Δ and Γ are real functions, and so are all the quantities given in equations (3.11.18) and (3.11.17). The terms containing Δ and Γ are due to the entropy variation. Observe that if $\omega \int_{x'}^{x''} \bar{u}\,dx'''$ is $O(M)$, that is, if ω is $O(1)$, the quantities $\bar{A}_1, \bar{B}_1, \bar{C}_1, \bar{D}_1$ are $O(M^2)$ and can therefore be neglected in equations (3.11.17). Also, $\cos\left(\omega \int_{x'}^{x''} \bar{u}\,dx'''\right)$ can be replaced by 1 and the quantities $\bar{A}, \bar{B}, \bar{C}, \bar{D}$ can be transformed to

the A, B, C and D of (3.11.06) and (3.11.07), the only difference being that the first term of the two equations (3.11.06), which represented the cause of trouble for ω of $O(1/M)$, are now absent.

All the quantities given in equations (3.11.18) are at most of $O(M)$ even when ω is $O(1/M)$, as are those given in equations (3.11.17). $J_r(\omega)$ and $J_i(\omega)$ are always $O(M)$; $I_r(\omega)$ is $O(M)$ if $\alpha_r\bar{u}_1$ is $O(M)$, $(\beta < 3)$, and it is $O(1)$ if $\alpha_r\bar{u}_1$ is $O(1)$, $(\beta \geqslant 3)$; and $I_i(\omega)$ is $O(1)$ in general, but it is $O(M)$ when ω is in a range of $O(M)$ around the values

$$\omega = l\pi - \tan^{-1}(\alpha_i\bar{u}_1) \qquad \ldots\ldots(3.11.20)$$

Therefore, proceeding as before, we find that if $\beta < 3$, n is $O(1/M)$ for general ω, but takes a minimum value of $O(1)$ when ω is around the values (3.11.20); if on the contrary $\beta \geqslant 3$, n always stays of $O(1/M)$. These conclusions coincide with those of the previous discussion for ω of $O(1)$, with the exception that n never becomes $O(1/M^2)$ even for these larger values of ω.

3.12. Discussion of the Results

The qualitative results of the previous section are represented schematically in *Figure 41*, where n is represented as a function of ω in the range $0 < \omega < 3\pi$. It is supposed that in all this range β stays below three so that $\alpha_r\bar{u}_1$ never becomes of $O(1)$, though increasing with ω. Near $\omega = 0$ we have the portion of the curve corresponding to equation (3.11.12a). With increasing ω, n becomes of $O(1/M^2)$ reaches a maximum and decreases again to a minimum of $O(1)$ for $l = 1$, given by relation (3.11.15). Then it increases again, reaches a new maximum, which is likely to be lower than the first one, and decreases to a new minimum (higher than the first) for $l = 2$; there are other minima of increasing height for $l = 3$, 4 and so on; and other maxima of decreasing height in between. Thus the curve tends to become flatter, with less sharp minima and maxima, as ω increases.

The values of δ, equation (3.11.11), can be qualitatively discussed by observing that around the minimum of n both I_i/I_r and J_i/J_r are $O(M)$ if ω is $O(1)$ and if $\alpha_i\bar{u}_1$, $\alpha_r\bar{u}_1$ are of $O(M)$. Thus in the corresponding ranges the value of δ will be close to the value obtained by neglecting the last two terms of equation (3.11.11), that is close to the rectangular hyperbolae $\omega\delta = (2m + 1)\pi$. When ω is of $O(1/M)$ both I_i/I_r and J_i/J_r become of $O(1)$, and therefore we find a divergence of $O(1)$ of $\omega\delta$ from $(2m + 1)\pi$, which is not a very substantial divergence. If $\alpha_r\bar{u}_1$ is $O(1)$ the divergence takes its maximum value around $\frac{1}{2}\pi$. Altogether the values of δ in the ranges around $n_{\min}$ will not differ too much from those of the hyperbolae, which have been drawn schematically in *Figure 41*. With the help of this figure it is easy to discuss the stability characteristics of our system. Suppose we know the interaction index n proper of the system, we can draw on the figure the corresponding horizontal line. This has been done in the figure with the particular value $n = 1$. There are 5 intersections with the curve $n(\omega)$, one, ω_1, near $\omega = 0$; two, ω_2, ω_3 close to the value (3.11.15) of $\omega(l = 1)$; two, ω_4, ω_5 close to the value (3.11.20) with $l = 2$. For higher values of l no intersection is found. For each intersection we can draw a vertical line which will intersect all δ hyperbolae. The intersections at

$\omega = \omega_1$ on the hyperbolae are out of the range of the figure. They correspond to equation (3.11.12b). From the discussions of Chapter 2 we know that the lowest of these low frequency intersections is the only important one, because as a general trend the system with larger $\bar{\tau}$ is always unstable, and no low frequency instability can be present in a system with smaller $\bar{\tau}$.

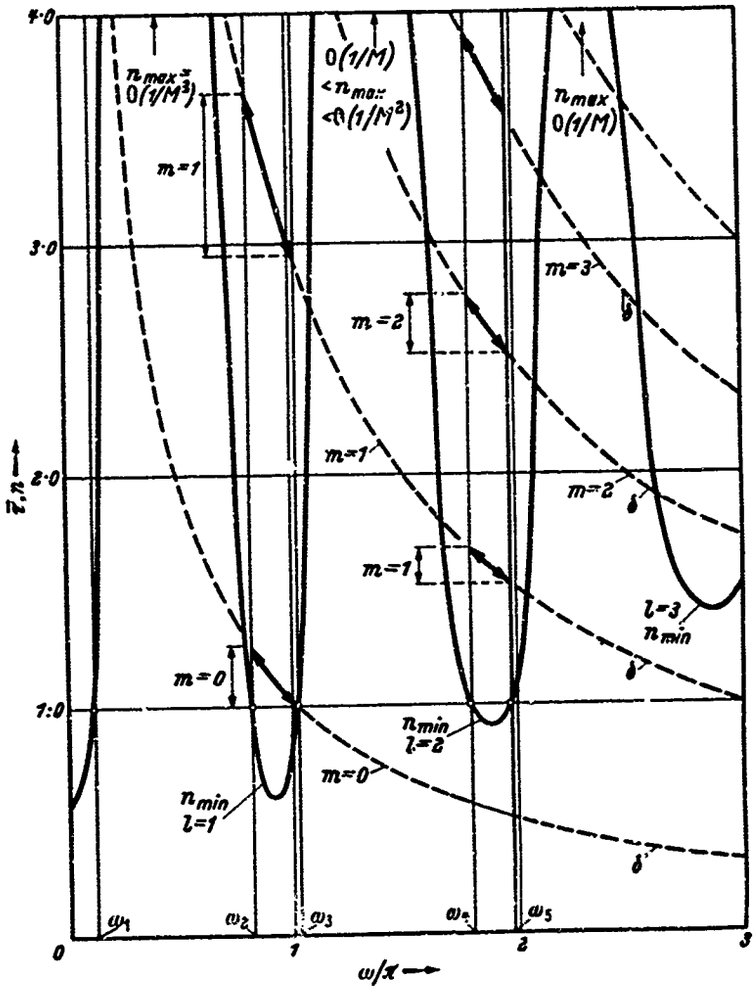

Figure 41. Composite schematic diagram of the stability characteristics of a liquid propellant rocket. Solid curves: critical values of the interaction index n corresponding to neutral oscillations of different modes ($l = 1, 2, 3 \ldots$). Dotted curves: critical values δ_c of the sensitive time lag $\bar{\tau}$ for different numbers of oscillation periods contained in $\bar{\tau}$ ($m = 0, 1, 2 \ldots$)

If, however, we extend our considerations to the high frequency range several new ranges of $\bar{\tau}$ appear where instability is present. Each range is bounded by the two intersections corresponding to a given value of l with a given δ hyperbola (a given m); for instance we have a range between ω_2 and ω_3 and one between ω_4 and ω_5 on each hyperbola. We have a value of δ (for given m) and of ω at each intersection. These values constitute, for

the prescribed n, two eigenvalues of our system, that is, the values compatible with neutral oscillations. If $\bar{\tau}$ has a value between the two eigenvalues δ corresponding to a given value of l, the system is unstable, only self-amplifying oscillations are possible, with a frequency contained between the two corresponding eigenvalues of ω.

We see that the spectrum of the unstable ranges of $\bar{\tau}$ can be quite complicated, and its complexity increases with the number of intersections of the $n(\omega)$ curve with the prescribed value of n. The spectrum of the unstable frequency ranges is, however, much simpler and it shows that high frequency instability is always connected with frequencies close to the organ-pipe frequencies of the system, but generally lower than the corresponding organ-pipe frequency by an amount determined by the value of $\alpha_i\bar{u}_1$ of the nozzle.

As has been mentioned the larger the number of ranges of instability in the ω spectrum, the larger is the complexity of the $\bar{\tau}$ spectrum, and the more difficult it is to obtain stable conditions. Fortunately due to the increase of $\alpha_r\bar{u}_1$ the values of $n_{\min}$ steadily increase with ω, so that for l sufficiently large it goes out of the range in which n can be expected to be, and no intersections can exist. There is therefore always a trend toward increased stability for higher modes of organ-pipe oscillation, as has already been found in the case of concentrated combustion. If one wants to improve the stability characteristics of a given system the best way is to reduce the number of intersections. This can be obtained either by decreasing the value of n, characteristic of the system, or increasing the level of the minima of the curve $n(\omega)$. The first result can probably be reached through modifications in the injection system and through changes in the reactivity of the propellants. The nature of the required modification and its effectiveness is still to be investigated. But it is very clear how the second result can be attained acting only on the geometry of the nozzle. In fact if one increases l_{sub}, as has already been seen, $\alpha_i\bar{u}_1$ increases at most up to a limited maximum, so that ω decreases by an amount which is around 25° at most. At the same time $\alpha_r\bar{u}_1$ increases steadily with l_{sub}, and asymptotically reaches a maximum value close to 1 for infinite length. Hence no matter what is the value of ω (or l) corresponding to a minimum of n, one can always obtain, through a sufficient increase of l_{sub}, that the $\alpha_r\bar{u}_1$ grows enough to raise the value of $n_{\min}$ above the practical range of the interaction index n. The effect on *Figure 41* of a steady increase of l_{sub} would be an increase of all $n_{\min}$; the one corresponding to $l = 3$ would be the first to increase fast and disappear from the range of the figure, followed by the one at $l = 2$; and finally by the one at $l = 1$ when the length of the convergent portion of the nozzle becomes comparable with the length of the chamber. Observe that in practice this condition would be overabundant, and an l_{sub} sufficient to bring $n_{\min}$ for $l = 1$ above the known value of n of the system would be perfectly adequate.

On the subject of the strong effects of the length of the nozzle on longitudinal stability we should add some remarks. The stabilizing effect is not merely due to the additional length, but it is closely connected with the shape of the convergent portion of the nozzle. This can be shown easily with the following argument. Our discussion has been based so far on the

results of Appendix B concerning a nozzle with linear velocity distribution, such as those represented schematically in *Figures 42*(a), (b) and (c). Here for a given length of combustion chamber, represented in our reduced units by unity, we have increased l_{sub} from the value l'_{sub} of *Figure 42*(a) to

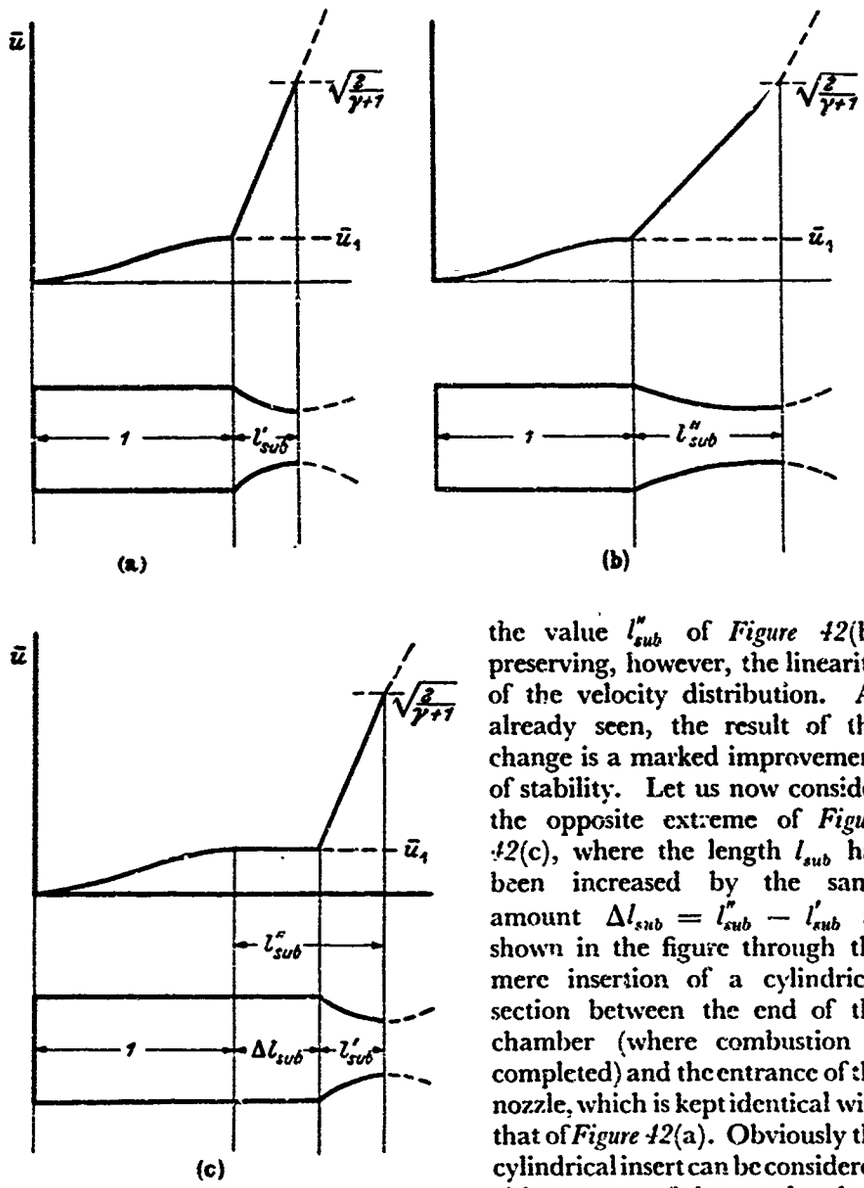

Figure 42. Schematic diagrams indicating changes in geometry of nozzle

the value l''_{sub} of *Figure 42*(b) preserving, however, the linearity of the velocity distribution. As already seen, the result of the change is a marked improvement of stability. Let us now consider the opposite extreme of *Figure 42*(c), where the length l_{sub} has been increased by the same amount $\Delta l_{sub} = l''_{sub} - l'_{sub}$ as shown in the figure through the mere insertion of a cylindrical section between the end of the chamber (where combustion is completed) and the entrance of the nozzle, which is kept identical with that of *Figure 42*(a). Obviously the cylindrical insert can be considered either a part of the nozzle where the velocity remains constant, or a portion of the combustion chamber where no combustion takes place. If we consider it in the last way, then substantially we are reduced to the same case as *Figure 42*(a) with a chamber of different length and of different velocity distribution. Disregarding the effects of the velocity distribution,

which cannot be expressed in a simple way, and concentrating on the effects of the nozzle we see immediately that for the new chamber length the eigenvalues ω will be found around the values

$$\omega = l\pi/(1 + \Delta l_{sub}) - \tan^{-1} \alpha_i \bar{u}_1$$

The corresponding value of β, given by equation (3.11.12a) with l'_{sub} in place of l_{sub}, will also be decreased from that of *Figure 42*(a), approximately in the proportion $1/(1 + \Delta l_{sub})$ (not exactly, because $\alpha_i \bar{u}_1$ also changes slowly with β). Therefore $\alpha_i \bar{u}_1$ must decrease, by an amount which can be substantial, when the length of the combustion chamber is increased without changing that of the convergent part of the nozzle. We conclude that the increase of length works in opposite directions for the two cases of *Figure 42*(b) and of *Figure 42*(c), being stabilizing for the first, destabilizing for the second.

Physically this result can be interpreted in the following way. The stabilizing effect of the convergent part of the nozzle is due to the manner in which the incoming waves are reflected back to the chamber. The reflection of waves at each point is determined substantially by the corresponding velocity gradient. The longer the region over which the velocity gradient is spread and the larger the frequency, the more the reflection pattern will be dispersed, and the smaller the chance of resonance and instability. Of course the cylindrical insert of *Figure 42*(c) does not spread the reflection pattern but only decreases the resonant frequencies, thus reducing the spreading effects of the nozzle and the stability characteristics. It is possible that the nozzle with linear velocity distribution in the subsonic region, originally introduced by H. S. TSIEN[24], probably with the sole intent of simplifying the mathematics, has also the remarkable property of the largest stabilizing effect for a given l_{sub}. This has not been rigorously proved, but could follow from the fact that for this type of nozzle the velocity gradient has the most uniform distribution. It can be observed that if $\bar{u}_1$ is not too small, the generatrix of an axisymmetrical nozzle with linear velocity distribution has approximately a circular shape. It must also be observed that all the previous results are based on the assumption of one dimensional flow in the nozzle, an assumption which is approximately true only if l_{sub} is not too small. Let us finally stress the fact that the supersonic portion of the nozzle has nothing to do with the behaviour of the combustion chamber and can be selected arbitrarily, provided it does not interfere with the conditions at the sonic throat.

So far we have in this section discussed the general shape of the results and the effects of the nozzle geometry. Let us now examine the effects of the velocity distribution in the combustion chamber, and in particular let us concentrate our attention on its effects on the values of n_{min}. These values can be obtained from numerical calculations based on the formulae given in Section 3.11 for any of the cases discussed. But for a general idea we can limit our discussion to the case when ω can be considered of O(1) and $\alpha_r \bar{u}_1$, $\alpha_i \bar{u}_1$, are both of O(M). In this case n_{min} can be derived from equation (3.11.14), with I_r and J_r given by equation (3.11.09) simplified in the following way:

$$I_r = (\gamma + \alpha_r)\bar{u}_1 \cos \omega - B(\omega); \qquad J_r = D(\omega)$$

$B(\omega)$ and $D(\omega)$ can be obtained from equations (3.11.06) and (3.11.07) in simplified form using the fact that ω is within $O(M)$ from $l\pi$ so that $\cos\omega \simeq \pm 1$ and $\sin\omega$ is $O(M)$. Then, neglecting quantities of $O(M^2)$,

$$B(\omega) = \cos\omega[(2-\gamma)\omega\int_0^1 \bar{u}\sin 2\omega x'\,dx' - k\int_0^1 \bar{\rho}_l \sin^2\omega x'\,dx']$$

$$D(\omega) = \cos\omega[\bar{u}_1 + \omega\int_0^1 \bar{u}\sin 2\omega x'\,dx']$$

Finally from equation (3.11.14) there results

$$n_{\min} = \frac{(\gamma+\alpha_r)\bar{u}_1 - (2-\gamma)\omega\int_0^1 \bar{u}\sin 2\omega x'\,dx' + k\int_0^1 \bar{\rho}_l \sin^2\omega x'\,dx'}{2\gamma\left[\bar{u}_1 + \omega\int_0^1 \bar{u}\sin 2\omega x'\,dx'\right]} \quad \ldots.(3.12.01)$$

where $\bar{\rho}_l$ can be obtained from equation (3.06.15) once $\bar{u}_l$ is known.

This formula which has the great advantage of simplicity has been used to calculate the effects on $n_{\min}$ of changing the velocity distribution. In general the last term in the numerator has been set equal to zero; it has only been taken into account in a few cases. But it is clear from the fact that this term as well as the denominator of equation (3.12.01) is always positive that it results in an increase of $n_{\min}$, that is, an improvement of stability. This is a logical result indeed, since this term substantially represents the dissipative effects of the droplets drag in the unsteady part of their relative motion with respect to the gases. In practice, however, as some calculations show, the contribution of this dissipative term is relatively insignificant.

The examples that we are going to discuss are carried out for the first mode $\omega \simeq \pi$ as well as for the second mode $\omega \simeq 2\pi$. For this second mode at least one of the assumptions on which equation (3.12.01) is based fails to be satisfied. In fact it is true that for a sufficiently small l_{sub}, for instance 1/6, it is possible to keep β well below 2 at $\omega = 2\pi$, and therefore keep both $\alpha_r\bar{u}_1$ and $\alpha_i\bar{u}_1$ of $O(M)$; but on the other hand ω cannot be considered of $O(1)$ and the more complicated expressions derived for ω of $O(1/M)$ should be used. This has not been done because it would lead to the following inconsistency. In equations (3.11.18) terms containing the quantities Δ and Γ appear, which, as already mentioned, are due to the entropy variation. These terms should be considered in the calculations. On the other hand the nozzle admittance ratio used in the calculation only applies to isentropic oscillations. It is believed that the entropy oscillations have more substantial effects on the behaviour of the nozzle than on the behaviour of the combustion chamber, and it is therefore inconsistent to use a more accurate formula taking these effects into account in the combustion chamber while they are neglected in the nozzle.

Let us observe, moreover, that the effects of the entropy oscillation on the behaviour of the nozzle can be important even at lower frequencies, where they have negligible effects on the combustion chamber. All the results of the discussion and of the calculations of this section must therefore

be accepted with reserve, until the availability of data on the non-isentropic behaviour of the nozzle will allow more reliable calculations. For this reason we have used equation (3.12.01) even for the second mode, for which the results are not to be considered accurate but only indicative.

For simplicity, we shall first neglect the damping contribution of the droplet. Thus let $k = 0$ and let us consider the systems with combustion uniformly distributed from the injector end $x = 0$ to $x = \xi_c$ and with no combustion from $x = \xi_c$ to the combustion chamber exit $x = 1$. Thus the mean velocity in steady state is

$$\bar{u}(x) = \bar{u}_1 \cdot \frac{x}{\xi_c} \qquad \text{when } 0 \leqslant x \leqslant \xi_c$$

$$\bar{u}(x) = \bar{u}_1 \qquad \text{when } \xi_c \leqslant x \leqslant 1$$

As was done in the examples of previous sections, let us assume that the steady state velocity is linear in the convergent portion of the nozzle and consider

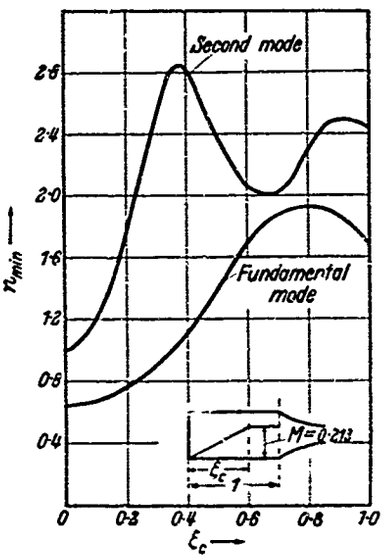

Figure 43. Effect of the spanwise spread of combustion on the minimum value of the interaction index, n_{min}, compatible with unstable oscillations of the fundamental and the second mode. Combustion spread linearly starting from the injector face as shown in the figure

only the case that the steady state velocity gradient is equal to π in the present dimensionless scheme. The length of the subsonic portion of such a nozzle is approximately 1/3 of the combustion chamber length. With $\bar{u}_x$ nozzle $= \pi$, we see that the reduced frequency parameter $\beta = \omega/\bar{u}_x$ for the nozzle takes integral values 1, 2, 3 etc. when the frequency of the oscillation is equal to the frequency of the first, second and third organ-pipe modes with closed ends. The Mach number of the flow entering the nozzle is taken to be $M = 0{\cdot}213$ ($\bar{u}_1 \simeq 0{\cdot}213$) for the following calculations. The value of n_{min} computed from equation (3.12.01) for the cases just mentioned is given in *Figure 43* for both the fundamental and the second modes. When ξ_c increases from zero, that is when combustion is spread farther and farther away from the injector end, we see that for either the fundamental or the second mode, the value of n_{min} increases gradually and reaches a maximum when the combustion terminates somewhere downstream of the neighbouring

node of the given mode of pressure oscillation. Then n_{min} decreases toward the next antinode and as demonstrated in *Figure 43* the next minimum of n_{min} for the second mode occurs in between the second antinode and the second node, and the value of that minimum is considerably higher than the magnitude of n_{min} when $\xi_e = 0$. This trend is expected to persist for all higher modes.

It is important to observe from *Figure 43* that the second mode is always more stable than the fundamental because the corresponding values of n are always higher. This is in line with the results of the general discussion developed previously. However, observe that the two curves of n_{min} come rather close together for values of ξ_e in the neighbourhood of the node of the fundamental mode; and that, owing to the inaccuracy involved in using equation (3.12.01) for the calculations of n_{min} for the second node, the n_{min} of the second mode in this range of ξ_e may actually be the smaller (as will be shown later, the n_{min} of the second mode will be the smaller in the present calculation if combustion is not uniformly distributed from $x = 0$ to $x = \xi_e$. However, for this range of values of ξ_e, the n_{min} for the second mode is still in the range of 1·5–2·0 as is that of the fundamental mode in a wider range of ξ_e. The smaller value of n_{min} for both the fundamental and the second mode is essentially given by the n_{min} of the fundamental mode. For a system with given combustion distribution, it is the smallest value of n_{min} of all the high frequency modes that determines the unconditional stability of the system. Therefore for the comparison of unconditional stability of different systems, the second mode is rather unimportant, at least for the cases with uniformly distributed combustion considered in this example. It can probably be inferred even without any numerical results for higher modes that the presence of all the other higher modes is not of significant importance so far as the smallest value of n_{min} of all high frequency modes is concerned. As already observed in the general discussion, this is essentially a consequence of the increase of α_r with frequency as can be visualized quite simply from the following considerations. First, the curve of n_{min} for a given mode plotted against ξ_e behaves like a damped oscillating function starting with a minimum at $\xi_e = 0$. The mean value about which n_{min} of a given mode oscillates can be approximately given as $3/2 + (\alpha_r - 1)/\gamma$ which increases for higher modes of oscillation due to the increase of $\alpha_r(\omega)$ for higher modes. Secondly, the initial value of n_{min} at $\xi_e = 0$ can also be given approximately as $(\alpha_r + \gamma)/2\gamma$ which is also larger for higher modes. Consequently the value of n_{min} given in *Figure 43* for the fundamental mode can be considered as the n_{min} which characterizes the relative unconditional stability of different systems when all high frequency modes are considered, except possibly in the neighbourhood of $\xi_e = 0{\cdot}75$, where n_{min} for the fundamental mode attains its maximum.

From *Figure 43* we see that the configurations with combustion uniformly distributed from injector end to a position somewhere in the downstream half of the chamber possess a value of n_{min} ranging from 1·5–2·0 when all high frequency modes are considered. Thus such systems will be unconditionally stable if the interaction index n of the propellant combination is less than 1·5. It is very likely that this condition is fulfilled by

conventional liquid propellant combinations even though no value of n has been determined experimentally. Thus the result of *Figure 43* indicates that under the combined effects of the nozzle and of the spatial distribution of combustion, the configuration with combustion uniformly distributed over a major portion, say eight or nine tenths of the chamber length, is one of the most effective in obtaining longitudinal stability in a liquid propellant rocket.

If the combustion is uniformly distributed over a region less than one third of the chamber length from the injector end, *Figure 43* indicates $n_{\min} \lesssim 0{\cdot}8$. Thus if the interaction index n of a propellant combination is, say, 1·0 or slightly less than 1, a rocket which is stable with combustion distributed uniformly over the major portion of the chamber axis can very likely be made to scream by sufficiently increasing the length of the combustion chamber without modifying the geometry of other parts of the rocket motor. As an extreme case, if a sufficiently long cylindrical section is added to the motor so that the width of the combustion zone becomes small as compared to the total length of the chamber, the system is reduced essentially to the one with a concentrated combustion front near the injector end. Unstable oscillations can occur when the value of ξ_c is sufficiently reduced by lengthening the chamber so as to give $n_{\min}$ less than the value of n of the propellant combination. As observed in the general discussion, by increasing the length of the chamber the relative length of the convergent portion of the nozzle l_{sub} is decreased, with the result that α_r decreases too. This further decreases the value of $n_{\min}$ from that proper of the system before the increase in chamber length. Thus the destabilizing effect of increasing the chamber length consists of two parts, one from the direct modification of the combustion distribution relative to the acoustic wave form and the other from the modified reaction of the nozzle.

It has just been pointed out that when $\xi_c = 0$ the system is of the configuration considered in Section 3.04. Comparing the values of $n_{\min}$ obtained from *Figure 43* for $\xi_c = 0$ with the corresponding $n_{\min}$ determined in Section 3.04 and plotted in *Figure 28*, one finds that the present result is slightly higher than the corresponding previous result. For this particular case with $\xi_c = 0$. it can be shown easily that the expression for $n_{\min}$ deduced from equations (3.04.02) and (3.04.03) differs from the simplified form of equation (3.12.01) with $\xi_c = 0$ only in that the constant γ in the numerator of equation (3.12.01) is replaced by unity [k in equation (3.12.01) is assumed to be zero]. This is due to the fact that in the previous analysis of concentrated combustion, the flow field in the combustion chamber is assumed isentropic while in the general analysis of Section 3.11 which led to equation (3.12.01) the major effect of the entropy variation of different burnt gas elements generated under different pressure conditions is taken into account. While the entropy variation is of the same order as the pressure perturbation as explained previously its net effect on the qualitative behaviour of $n_{\min}$ is not important with the possible exception of its influence on the behaviour of the nozzle, neglected here. With this entropy correction taken into consideration, the value of $n_{\min}$ for $\xi_c = 0$ and very short nozzle becomes $\frac{1}{2} + (\gamma - 1)/4\gamma$ instead of $\frac{1}{2} - (\gamma - 1)/4\gamma$ as obtained in Section 3.04. It is interesting to note also that $\frac{1}{2}$ is the value of $n_{\min}$ for low frequency

instability of the intrinsic type [equation (2.03.10)] which was obtained under the assumption of isothermal chamber conditions.

Let us consider next the systems with combustion uniformly distributed in an intermediate region ξ_c around the mean position ψ with $\frac{1}{2}\xi_c \leqslant \psi$. If $\frac{1}{2}\xi_c$ is very much smaller than ψ, the system approaches the configuration with combustion concentrated at the axial position ψ. The present result will therefore indicate how well the approximate scheme of concentrated combustion can represent the actual conditions. For such systems we have:

$$\bar{u} = 0 \qquad 0 \leqslant x \leqslant \psi - \tfrac{1}{2}\xi_c$$

$$\bar{u} = \bar{v}_1 \quad \{x - (\psi - \xi_c/2)\}/\xi_c \qquad \psi - \tfrac{1}{2}\xi_c \leqslant x \leqslant \psi + \tfrac{1}{2}\xi_c$$

$$\bar{u} = \bar{u}_1 \qquad \psi + \tfrac{1}{2}\xi_c \leqslant x \leqslant 1$$

The values of $n_{\min}$ as calculated from equation (3.12.01) for different values of ψ are plotted versus ξ_c for the fundamental mode of oscillation in *Figure 44*. The values of $n_{\min}$ for different ψ with $\xi_c = 0$ correspond to

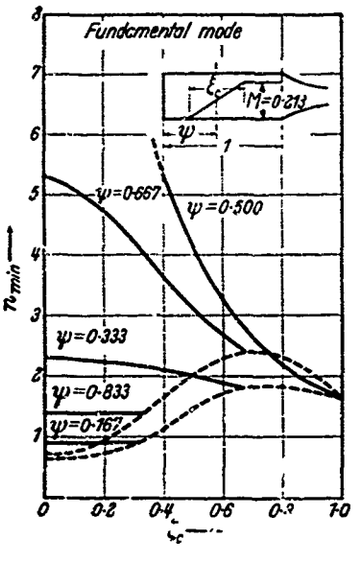

Figure 44. Effect of the spacewise spread of combustion on the minimum value of the interaction index, $n_{\min}$, compatible with unstable oscillations of the fundamental mode. Combustion spread linearly in an intermediate region as shown in the figure

the values of $n_{\min}$ given in *Figure 28* but for the reason mentioned in the previous example the present values are slightly larger. It is clearly seen that so far as the magnitude of $n_{\min}$ is concerned, the spatial spread of combustion about the mean position $\psi = 1/6$ and $\psi = 5/6$ has practically no effect (being slightly stabilizing) for the total extent of spread as large as 1/3 of the chamber length i.e. 1/6 of the wavelength of the fundamental mode. When the mean position is shifted toward the antinodal position ($\psi = \frac{1}{2}$) of the fundamental mode, the effect of spatial spread of combustion becomes destabilizing and the destabilizing effect, that is the decrease of $n_{\min}$ from the value of $n_{\min}$ corresponding to concentrated combustion at the mean position ψ, increases significantly when ψ approaches $\frac{1}{2}$. This phenomenon can be physically expected on the ground that the spatial slope of the amplitude of the pressure oscillation φ_x is exactly zero at an antinode and is small in its vicinity, while that near a node is large. Thus the maximum

possible amount of excitation of unstable oscillation is not substantially changed by the small spread of combustion near an antinode. Since the damping action of the nozzle is little affected by the spatial spread of combustion, the unconditional stability of a given mode in the system as indicated by n_{min} is not substantially changed. It should further be noted that a node of the fundamental mode is the antinode of the second mode. Therefore the destabilizing action of the spatial spread of combustion in the nodal region of a given mode is not important because the n_{min} of this mode will still be considerably higher than the n_{min} of some other mode having an antinode near the combustion zone. With this in mind and with the help of the computed results it can be inferred that so far as the unconditional stability of a system is concerned, the effect of the spatial spread of combustion in a region less than, say, 1/8 of the chamber length is insignificant; and the much simplified model of concentrated combustion is adequate for the analysis and comparison of the overall relative unconditional stability of such systems.

In *Figure 44* there is a dotted line connecting the ends of the n_{min} versus ξ_c curves for different ψ. The lower branch of this dotted curve corresponds to the configurations with combustion uniformly distributed from injector end to $x = \xi_c = 2\psi$. The upper branch curve corresponds to the configurations with combustion uniformly distributed from $x = 1 - \xi_c = 2\psi - 1$ to the combustion chamber exit $x = 1$. Thus when $\xi_c = 0$, the lower branch corresponds to concentrated combustion at the injector end and the upper branch corresponds to concentrated combustion at the chamber exit. The fact that the upper branch always gives a larger value of n_{min} for the same extent of spatial spread of combustion means that the configuration with more combustion distributed in the downstream end of the chamber is likely to be more stable. This is primarily because the frequency of oscillations for minimum n is slightly below the corresponding organ pipe value.

So far we have only considered the cases in which the combustion is uniformly distributed in a certain region. The next object is to investigate the relative importance of the manner in which the combustion is distributed in this region. Consider systems with $\bar{u}$ given by:

$$\bar{u} = \bar{u}_1 \left(\frac{x}{\xi_c}\right)^j \qquad \text{for } 0 \leqslant x \leqslant \xi_c$$

$$\bar{u} = \bar{u}_1 \qquad \text{for } \xi_c \leqslant x \leqslant 1$$

with the positive exponential index j indicating the manner of combustion distribution. When $j = 1$, this becomes the case of uniformly distributed combustion as has been discussed in the previous example. When $j > 1$, more of the combustion is shifted towards the tail end of the combustion zone as compared with the uniformly distributed case. Likewise when $j < 1$ more of the combustion is shifted towards the head end of the combustion zone. In *Figure 45*, the computed values of n_{min} for the fundamental mode are given for $j = 0, \frac{1}{2}, 1, 2, 3, \infty$ and plotted against the total extent of spread ξ_c. The case $j = 0$ corresponds to the configuration with combustion concentrated at the injector end with n_{min} independent of ξ_c. When j gradually increases, more and more combustion is shifted towards the

other end $x = \xi_c$, and when j becomes very large, $j = \infty$, all combustion is concentrated at $x = \xi_c$ and the n_{min} calculated for $j = \infty$ corresponds to that determined in connection with the simplified model of concentrated combustion. The curves of n_{min} versus ξ_c for different values of j are of similar shape and the transition of the curves from that of $j = 0$ to $j = \infty$ is quite clear. The increase of n_{min} when ξ_c reaches the node of the pressure oscillation becomes more significant for the cases with larger j. As has been indicated previously, this is physically clear because more combustion is carried to nodal regions where the amplitude of the pressure oscillation is smaller, that is, where the capability of each propellant element in exciting unstable oscillation is smaller.

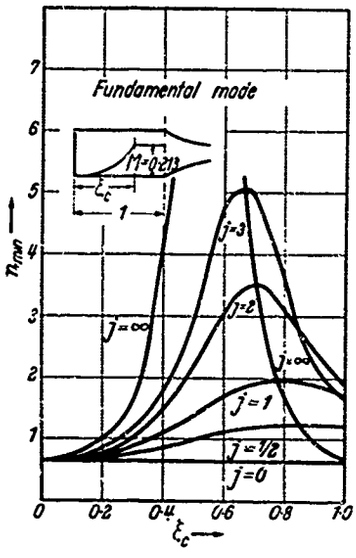

Figure 45. Effect of the spacewise spread of combustion on the minimum value of the interaction index, n_{min}, compatible with unstable oscillations of the fundamental mode. Combustion distributed according to the power law

$$\bar{u} = M(x/\xi_c)^j$$

from the injector face to the fractional axial position $x = \xi_c$ as shown in the figure.

If the n_{min} of the second mode is determined from equation (3.12.01) and superposed on *Figure 45*, we find again that when $j \leqslant 2{\cdot}5$ the n_{min} for the second mode is always larger than the n_{min} for the fundamental mode at the same value of ξ_c. Even for $j = 3$ the n_{min} for the second mode becomes slightly lower than the n_{min} for the fundamental mode only in the small range of ξ_c around $\xi_c = 0{\cdot}7$, and the smallest n_{min} of all high frequency modes is still given essentially by the n_{min} of the fundamental mode. It should be noticed that $(x/\xi_c)^3$ profile is already quite flat when x/ξ is less than, say, $\frac{1}{2}$ and almost 50 per cent of the combustion is completed in the narrow zone of $0{\cdot}8 < x/\xi_c < 1{\cdot}0$. The combustion is thus quite concentrated toward ξ_c. It is only when j is considerably larger than 3 that the n_{min} of the second mode plays its role in determining the smallest n_{min} when ξ_c is in the nodal region of the fundamental mode. Even in this case, so far as the overall unconditional stability of all high frequency modes is concerned, all the other higher modes will still be unimportant.

In most of the practical cases, with combustion fairly uniformly distributed over certain regions, only the fundamental mode is the important one in determining the unconditional stability of the system.

Now the integral term involving k in the numerator of equation (3.12.01) will be considered. As has been observed previously $k/\bar{u}_1$ is of the order of unity and the integral divided by $\bar{u}_1$ i.e. $\int_0^1 \frac{\bar{u}_1 - \bar{u}}{\bar{u}_l} \sin^2 \omega x' \, dx'$ is of the order of unity, and both factors of the integrand are positive. Thus this term essentially constitutes an increase of the value of n_{min}. This term represents the damping due to the unsteady motion of the droplets. For illustrative purposes a few points have been calculated with the following simplified form of $\bar{u}_l$

$$\bar{u}_l = \bar{u}_{l_0} (1 - 4x)$$

for $0 \leqslant x \leqslant x_0$, where $\bar{u}_l(x_0) = \bar{u}(x_0)$ in the rest of the chamber, $x_0 \leqslant x \leqslant 1$, $\bar{u}_l$ is assumed to be the same as $\bar{u}$ of the gas, i.e. $\bar{u}_l(x) = \bar{u}(x)$. The constant k is taken to be 1/20 in the present dimensionless scheme which corresponds roughly to a penetration distance in still air of one quarter of the chamber length. The mean gas velocity is taken for example:

$$\bar{u}(x) = \bar{u}_1 \cdot x/\xi_c \qquad \text{for } 0 \leqslant x \leqslant \xi_c$$

$$\bar{u}(x) = \bar{u}_1 \qquad \text{for } \xi_c \leqslant x \leqslant 1$$

The n_{min} for the fundamental mode obtained for the configurations with $\xi_c = 0{\cdot}2$ and $\xi_c = 0{\cdot}5$ shows a very small increase as compared to those neglecting this damping term. The accuracy of the present calculation does not justify this correction which cannot be differentiated in the scale of *Figure 43* for the particular values of k and u_{l_0} selected. For extreme conditions, the damping term due to the oscillation of the droplets may have some effect.

3.13. Non-uniformity of $\bar{\tau}$

The developments of the last three sections apply to the simplest case when $\bar{\tau}$ is uniform for the whole combustion chamber and of O(1). However, the derivations of Section 3.08 were obtained under the more general assumption that $\bar{\tau}$ is a function of x without limiting its magnitude. The only restriction in Section 3.08 was the uniformity of $\bar{\tau}$ among all propellant elements burning at a given station. It is not difficult to remove all these restrictions, including the last one. However, the developments become much more complicated, and explicit solutions for the eigenvalues are in general impossible. In this section we will briefly indicate how the formulae are modified, and will confine our discussion to a few points only.

As in Section 3.08, we can subdivide all propellant elements that burn at a given station x into fractions, each fraction possessing a well defined value of $\bar{\tau}$. Thus if df represents the fraction considered, all elements burning at x can be ordered in such a way that $\bar{\tau}$ increases steadily from its minimum value, $\bar{\tau}_{min}$, corresponding to $f = 0$, to its maximum value $\bar{\tau}_{max}$, corresponding to $f = 1$. At a given station x, the sensitive time lags of different propellant elements, $\bar{\tau}(x, f)$ will be a monotonically increasing function of f. A fraction df contributes to the total burning rate q a portion dq. It is clear that the expression of dq/df divided by φ_0 is given by equations (3.08.16) and (3.08.17) derived previously, and is a function of x and f, because both $\bar{\tau}(x, f)$ and $\xi(x, f)$ are functions of x and f. The last

is connected to $\bar{\tau}$ by the relation corresponding to (3.08.04)

$$\int_{\bar{\xi}(x,\mathrm{f})}^{x} \frac{\mathrm{d}x'}{\bar{u}_l(x',\mathrm{f})} = \bar{\tau}(x,\mathrm{f})$$

which can be also written as

$$x - \bar{\xi}(x,\mathrm{f}) = \bar{u}_{l_m}(x,\mathrm{f})\bar{\tau}(x,\mathrm{f}) \qquad \ldots.(3.13.01)$$

where $\bar{u}_{l_m}$ represents each element burning at station x for the proper average of $\bar{u}_l$ during its sensitive time lag. In general, $\bar{u}_l$ can be different for different propellant elements, even if they have the same sensitive time lag $\bar{\tau}(x,\mathrm{f})$ and burn at x. In this last case the value of $\bar{u}_l$ used in the derivations of Section 3.06 should be considered as a proper average value between these different propellant elements.

The value of dq/df will thus consist of three terms, of which only the first one, representing the timewise contribution to the burning rate, need be retained, because the other two have only higher order effects on the final results. This can be easily shown following the same procedure as is given in Section 3.09. Integrating with respect to f from 0 to 1 we can write

$$\frac{\mathrm{q}}{\varphi_0} = n\,Q(x)$$

where $Q(x)$ is given by the generalized equation corresponding to (3.08.17):

$$\begin{aligned} Q(x) &= \int_0^1 \mathrm{df} \int_0^x \left[\frac{\varphi(x')}{\varphi_0} - \frac{\varphi[\bar{\xi}(x',\mathrm{f})]}{\varphi_0}\,\mathrm{e}^{-s\bar{\tau}(x',\mathrm{f})}\right]\frac{\mathrm{d}\bar{u}}{\mathrm{d}x'}\,\mathrm{d}x' \\ &= \int_0^x \left[\frac{\varphi(x')}{\varphi_0} - \int_0^1 \frac{\varphi[\bar{\xi}(x',\mathrm{f})]}{\varphi_0}\,\mathrm{e}^{-s\bar{\tau}(x',\mathrm{f})}\,\mathrm{df}\right]\frac{\mathrm{d}\bar{u}}{\mathrm{d}x'}\,\mathrm{d}x' \end{aligned} \qquad \ldots.(3.13.02)$$

In order to obtain the value of $Q^{(0)}$ to be inserted in equation (3.09.24) or (3.10.04) one uses again the 0th iteration solution (3.09.19) or (3.10.02). In both cases the expression for $\varphi(\bar{\xi})$ contains the quantity $\cos\omega\bar{\xi}$ which, due to equation (3.13.01), can be written as

$$\cos\omega\bar{\xi} = \cos\left(\omega x - \omega\bar{u}_{l_m}\bar{\tau}\right) \qquad \ldots.(3.13.03)$$

Similarly the exponential factor of (3.10.02) for neutral oscillations can be written as

$$\mathrm{e}^{s\int_0^{\bar{\xi}}\frac{\mathrm{d}x'}{\bar{u}}} = \mathrm{e}^{i\omega\int_0^x\frac{\mathrm{d}x'}{\bar{u}}}\cdot\mathrm{e}^{-i\omega\bar{u}_m\bar{u}_{l_m}\bar{\tau}} \qquad \ldots.(3.13.04)$$

where $\bar{u}_m$ stands for a proper mean value in the interval from $\bar{\xi}$ to x. We see that if $\bar{\tau}$ is O(1) and ω is O(1) we can neglect the term $\omega\bar{u}_{l_m}\tau$, of O(M), with respect to ωx in equation (3.13.03), and our previous relation, $\varphi(\bar{\xi}) = \varphi(x)$, leading to equation (3.08.19) is perfectly justified. If $\bar{\tau}$ is O(1) but ω is O($1/M$) the exponent of the second factor of equation (3.13.04) is O(M), so that within the proper order of approximation one can write $\exp\left(i\omega\int_0^{\bar{\xi}}\frac{\mathrm{d}x'}{\bar{u}}\right) = \exp\left(i\omega\int_0^x\frac{\mathrm{d}x'}{\bar{u}}\right)$ and the corresponding factor can

be extracted out of the second integral of equation (3.13.02) and used as a common factor for the whole integrand. However, in this case $\omega\bar{u}_{i_m}\bar{\tau}$ becomes O(1) and cannot be neglected in equation (3.13.03). To be consistent, this term should and can be included in the development of Section 3.10, without introducing any difficulty. However, this has not been done in order to avoid the additional formal complication. Finally, if $\bar{\tau}$ is $O(1/M)$ the complete expressions (3.13.03) and (3.13.04) must be used. When equation (3.13.02) is introduced into equation (3.09.24) or (3.10.04) and the condition (3.09.21) is written explicitly, the problem of determining the eigenvalues explicitly is found in general impossible, because $\bar{\tau}$ is now contained in a complicated fashion and cannot be extracted as a simple factor $\Xi = n(1 - e^{s\bar{\tau}})$ as was done in Sections 3.11 and 3.12. However, one can still solve for n

$$n = (N_r + iN_i)/(D_r + iD_i)$$

of which both numerator and denominator are complex and depend in a complicated way on ω and $\bar{\tau}(x, f)$. Obviously if n must be real this splits into two real equations

$$n = N_r/D_r = N_i/D_i$$

The (numerical) solution of the equation $N_rD_i = N_iD_r$ with respect to ω for given $\bar{\tau}(x, f)$, and the following evaluation of n from the preceding formula provide the two eigenvalues of n and ω for the given $\bar{\tau}(x, f)$. We see that while in principle the problem is solved, the procedure is too long and tedious to permit a general discussion of the results even qualitatively.

Let us consider the simple case when $\bar{\tau}$ is independent of x but is not uniform for the various fractions, i.e. $\bar{\tau} = \bar{\tau}(f)$ only. In addition if we assume that both ω and $\bar{\tau}$ are O(1). equation (3.13.02) becomes

$$Q(x) = (1 - Ce^{-s\bar{\tau}_e}) \cdot \int_0^x \frac{\varphi(x')}{\varphi_0} \frac{d\bar{u}}{dx'} dx'$$

with

$$Ce^{-s\bar{\tau}_e} = \int_0^1 e^{-s\bar{\tau}(f)} df$$

where both C and $\bar{\tau}_e$ are real functions of Λ, Ω and of the parameters characterizing the distribution of the sensitive time lags. For neutral oscillations where $\Lambda = 0$, $\Omega = \omega$ and $\bar{\tau}_e = \delta_e$ and for any arbitrary but general type of time lag distribution, both C and δ_e are functions of the frequencies of neutral oscillations and therefore can be considerably different for different modes of oscillation. While the method of determining the eigenvalues of n and δ_e for different frequencies of neutral oscillations has been found to be very convenient when $C = 1$ (corresponding to uniform time lag for all propellant elements) and δ_e = constant, it becomes rather complex when both C and δ_e depend on ω.

The two quantities C and δ_e are the same as those defined in Sections 2.08 and 3.05. It has been noted there that if the function $\bar{\tau}(f) - \bar{\tau}_m$ is antisymmetric with respect to the mass average $\bar{\tau}_m = \bar{\tau}(0{\cdot}5) = (\bar{\tau}_{max} + \bar{\tau}_{min})/2$ the effective average $\bar{\tau}_e$ and mass average $\bar{\tau}_m$ coincide and are constant

for a given system and therefore independent of the frequency of neutral oscillation. As a result, the solution of the eigenvalue problem becomes slightly simpler for systems with such antisymmetric distribution than for those without. It is only slightly simpler because the magnification factor C being in general a function of $\omega\Delta\bar{\tau} = \omega(\bar{\tau}_{max} - \bar{\tau}_{min})$ still depends upon ω for a given type and extent of time lag distribution. Therefore we shall for illustrative purposes consider first those systems in which the total extent of time lag spread is so small that C is essentially constant when ω varies slightly in the neighbourhood of π and that the distribution of $\bar{\tau} - \bar{\tau}_m$ is antisymmetric about $\bar{\tau}_m$. Thus C can be taken as the constant evaluated with $\omega = \pi$. As has been shown in Section 3.05, the magnification factor C for neutral oscillations in systems with $\bar{\tau} = O(1)$ is always less than unity and for systems with small time lag spread where C can be taken as constant for a given mode, the magnitude of C is always close to but less than unity.

Thus, following the identical procedure as in Section 3.11, one finds the following equation with both C and δ_e constant

$$n\gamma(1 - Ce^{-i\omega\delta_e}) = (I_r + iI_i)/(J_r + iJ_i) \qquad \ldots.(3.13.05)$$

which is similar to equation (3.11.08) except for the constant factor C on the left-hand side. If $C = 1$ (uniform time lag for all elements), equation (3.13.05) reduces exactly to equation (3.11.08). The quantities I and J are still given by equation (3.11.09). Eliminating δ_e from the two real equations corresponding to equation (3.13.05) we obtain

$$\frac{n}{n_1} = 1 + \left(\frac{n}{n_1}\right)^2 \frac{(1 - C^2)}{4} \cdot \frac{(I_r^2 + I_i^2)\,(J_r^2 + J_i^2)}{(I_rJ_r + I_iJ_i)^2} \qquad \ldots.(3.13.06)$$

where

$$n_1 = \frac{1}{2\gamma} \frac{I_r^2 + I_i^2}{I_rJ_r + I_iJ_i}$$

is the critical value of the interaction index when there is no time lag spread ($C = 1$). Since $C < 1$ for $\bar{\tau} = O(1)$, it is apparent that $n > n_1$ when there is time lag spread. In other words, more excitation is required to maintain neutral oscillation of any frequency in a given system with time lag spread than without. Naturally, $n_{min} > n_{1min}$; in other words the system with time lag spread is unconditionally more stable for any spatial distribution of combustion.

Equation (3.13.06) also indicates that the ratio of n/n_1 increases with decreasing C, as does n_{min}/n_{1min}. This means a larger stabilizing effect for a larger spread of time lag. All these results agree with the results of Section 3.05 for the simple case of spatially concentrated combustion. As a matter of fact equation (3.13.06) reduces after some manipulation to equation (3.05.08) when I and J are evaluated for the concentrated combustion.

For the cases in which $\Delta\bar{\tau} = \bar{\tau}_{max} - \bar{\tau}_{min}$ is not sufficiently small, C must be considered as a function of ω even for small variations of ω around π or its integral multiples. The eigenvalues δ and ω can be determined

for a given value of n and a given distribution of time lag following the procedure analogous to the one used in reference 23. The calculation has not been carried out but it can be expected to give essentially the same qualitative results as to the effect of the spread of the sensitive time lag.

4

DISCUSSION AND COMPARISON WITH EXPERIMENT

4.01. General Notions

In this chapter we shall look into the possibility of comparing the theoretical results presented in the previous chapters with published experimental findings. It has been brought out in Chapter 1 that, because of our meagre knowledge concerning the physicochemical processes of combustion in a liquid rocket chamber, any analytical approach to the problem must start with some hypothetical simple model. No matter how rational the simple model may seem to be, the ultimate justification of the postulated simple model lies in the qualitative, and possibly quantitative, agreement between the theoretically predicted trends and the experimental findings. The present theoretical treatments are concerned only with the problem of incipient instability, not with the properties of the fully developed unstable oscillations of large amplitude. On the other hand, the known available experiments on unstable operation belong essentially to the domain of fully developed instability, characterized by the fact that the amplitudes, instead of undergoing steady amplification, stay in-average around a certain level determined by non-linear effects.

Thus, even if the onset of instability is of a linear nature, as assumed in the theoretical treatment, the observed facts contain a strong non-linear influence and one must not expect a close quantitative agreement between theoretical predictions and experimental results. A better situation would result if one tried to determine experimentally the stability boundary by changing some well determined parameters of the system. However, this determination has not yet been attempted, and would probably meet many difficulties. One difficulty is that it is not easy to change one parameter at a time in a rocket motor. For instance, the easiest way of varying the mixture ratio in a bipropellant motor is by changing the injection pressure of one of the two propellants. However, this change is accompanied by a change in injection velocity of one of the propellants and therefore a change in the flow situation in the combustion chamber. The whole process of combustion may be affected so that it would be impossible to isolate the effects of the mixture ratio change alone. From this point of view, it would be preferable to keep the injection pressures unaltered and change only the area of the injection ports. But this solution would substantially increase the complexity of the tests because it would require mechanical modifications to the injectors for every small change of mixture ratio. The same can be said for changes in the chamber pressure which should not be obtained through a simple change of injection pressure with fixed geometry, but should rather be obtained through changes in geometry with fixed pressures, or with pressure drops following an independently determined law.

Another difficulty, common to many other processes involving combustion, probably resides in the fact that this kind of test is not exactly reproducible.

As in other processes in which combustion plays an essential role, small uncontrollable changes in local conditions or in the characteristics of the system may produce considerable dispersion of the observed results. For instance, a system which ordinarily is stable may occasionally exhibit instability without any plausible or controllable reason; and a system usually unstable may have some stable runs. The conditions, of course, can become more confused in an intermediate condition where it would be nearly impossible to determine the stability situation from a few runs. This difficulty can in principle be solved, as in similar cases, only through a statistical approach; but with rockets this statistical approach means a considerable increase of the time and of the economic loads.

The statistical determination of the stability boundaries would be the most effective way of checking the theoretical results, and also of showing the possible existence of independent non-linear instabilities. Non-linear phenomena may result in two kinds of effects. They may simply shift the stability boundaries with respect to those pertaining to very small disturbances and linear theory, with the result that the stable ranges may shrink or expand when the amplitude of the initial disturbance increases. On the other hand, they may introduce new regions of instability when the amplitudes exceed certain levels. The first category of effects is relatively uninteresting, since the corresponding conditions for stability can be obtained continuously from the linear ones, and are likely to be affected by the different parameters of the system in the way the linear theory predicts. If only this category of effects were present, it would be sufficient to design a motor with such parameters that it would operate in stable conditions and sufficiently far away from the stability limits determined by linear theory; this would be enough to assure against instability even when disturbances of sufficient amplitude to introduce non-linear effects are applied to the system. The possible presence of new instability ranges for large disturbances is a more serious effect, and its possibility could be checked through the experimental determination of the stability boundaries, possibly with the introduction of controlled disturbances in an otherwise smooth system.

We emphasize again that the fact that actual instabilities generally operate in the non-linear range does not mean that the reason for instability cannot be explained by a linear theory. Actually, observation has often shown large amplitude oscillations produced during a previously stable run through the gradual amplification of small disturbances. Observations of this kind exist both for low frequency oscillations[2,34] and for high frequency oscillations[26]. One observes, not infrequently, a cyclic (though not periodic) appearance and decay of these unstable conditions during a run. A behaviour of this type would be expected if the conditions of stability were marginal and small changes in some parameters were determining the transition from stability to instability and back†. In these cases it seems logical to infer that the instability is of a linear type. In the other cases, in which the run is oscillatory from the start, no definite conclusion can be

† Analogous effects have been found in solid propellant rockets where, however, the continuous change in the geometry of the propellant grain during operation might be responsible for the peculiar behaviour[33].

reached, but nothing can be inferred against the linear explanation, because the existence of the ignition transients may produce strong disturbances at the beginning of the operation that never decay completely if the system is unstable.

The only possible test which would definitely indicate the presence of non-linear instability is the one already mentioned where a system is triggered to instability by a strong disturbance (such as the transients of a hard ignition), but remains stable if the disturbance level is low.

As already explained, the best test of the theoretical treatment, constituted by the determination of the stability boundary, has not yet been made. The only experiments available to date belong to the realm of fully developed instability, to which the linear theory does not apply even when it contains the essential explanation for the appearance of instability. Nevertheless, in the absence of better tests, some of the data obtained from these experiments may be compared with the theoretical results and some of the theoretical stability trends may be checked.

One of the quantities that seems likely to be less influenced by non-linear effects is the frequency of the oscillations. For instance if a shock wave of plausible strength, instead of a wave of small amplitude, is travelling back and forth in a combustion chamber, the propagation speed and the wave propagation time change only by a few per cent, and the result is a change in frequency of the same order[2]. This is true despite the considerable change in the shape and the amplitude of the corresponding pressure and velocity waves. Fortunately, the frequency is also the quantity easiest to measure from pressure records or optical observations. For this reason most of the comparisons between theory and experiments are based on the values of the frequency.

In accordance with our theoretical treatment, we shall consider separately the range of low frequencies and high frequencies. No fundamental disagreement seems to exist in the world of rocket research about the definition of the high frequency range, which is definitely connected, in agreement with our theory, to the natural modes of oscillation of an acoustic chamber obtained from the actual rocket chamber by replacing the nozzle with a closed end. To the knowledge of the authors, there is also fundamental agreement about the most probable cause for high frequency instability, which is definitely attributed, in agreement with the idea first advanced by the senior author[3], to the interaction of pressure waves and burning rates. It is true that this interaction is often visualized as being related to shock waves, rather than continuous waves, but as already explained previously the fact that shock waves can be generated progressively after a period of amplification of continuous waves shows that the essence of the phenomenon is independent of its non-linearity and only the quantitative results may be more or less affected.

Some discrepancy is present, however, in the definition of the low frequency range. For practical values of the parameters, the frequencies predicted by the theories of chugging are below 100 c/s. This is the range that we attribute to low frequency oscillations in rockets of usual dimensions. Only in extremely small rockets will the low frequency range extend to a frequency as high as 200–300 c/s. Instabilities in this range have often been observed

with results that substantiate the theoretical predictions (Section 4.02). However, in their recent survey of the problem of rocket combustion instability[2], C. C. Ross and P. P. Datner broadened the definition of low frequency instability by including observed frequencies of the order of 300 c/s, and were forced to conclude that the existing theories of low frequency instability cannot explain the observed phenomena. They also attempted a different explanation for the observed frequency, an explanation which can be definitely shown (Section 4.04) to be without correct physical basis. The truth is, clearly, that instabilities with frequencies as high as 300 c/s can be included neither in the low frequency type of instability, nor in the high frequency type, and that we have here a clear example of an instability of the intermediate frequency type, such as those mentioned in Section 1.10, for which no detailed theoretical treatment is as yet available. The conclusion of Ross and Datner's discussion that the predictions of the present theories of chugging do not correspond to experimental observation, with the possible exception of a seldom observed type of instability which they called 'divergent', is based on experiments that are not pertinent to the problem, as is proved by the fact that other sets of experiments[34] give, on the contrary, a satisfactory justification of the fundamental correctness of these theories.

4.02. Comparison between Experiments and Theory—Chugging

The experimental information about chugging is too incomplete and scattered to provide material for accurate comparisons with theory. The most important sources of information are the recent work of M. Barrere and A. Moutet[34], the paper by A. O. Tischler and D. R. Bellman[35] and that by C. C. Ross and P. P. Datner[2]. It should be pointed out that with the exception of reference [34], the experimental results are reported without details of the test conditions so that it is impossible to determine how many variables have been changed between different tests.

Figure 46. Development of low frequency unstable oscillations. (By courtesy of Office National d'Etudes et de Recherches Aéronautiques)

The following qualitative experimental observations are either reported by Barrere and Moutet or can be inferred from their reported data:

1. Low frequency instability is developed from the progressive amplification of small oscillations during a transition period, without any substantial change in frequency (*Figure 46*).

2. Oscillations of flow rate and pressure in the feed lines are of the same

frequency as, but with a smaller fractional amplitude than, oscillations of chamber pressure.

3. The frequency of unstable oscillation increases when the characteristic length of the motor, L^*, is decreased (*Figure 47*).

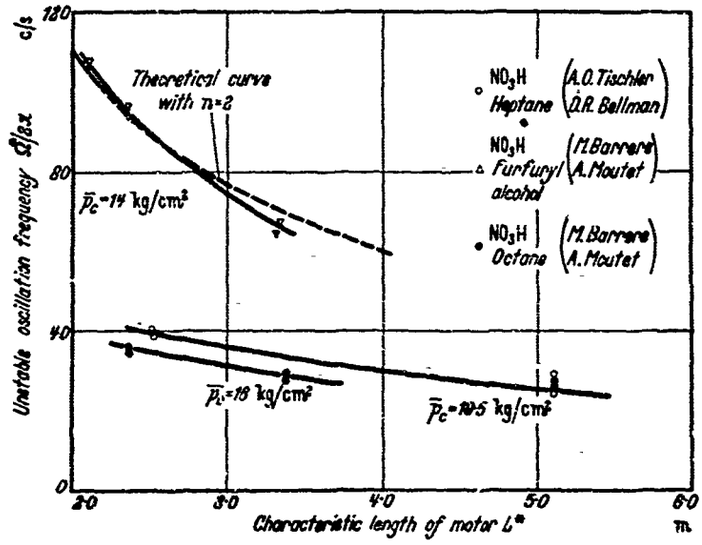

Figure 47. Frequency of unstable oscillations versus characteristic chamber length L^*. (By courtesy of Office National d'Etudes et de Recherches Aéronautiques)

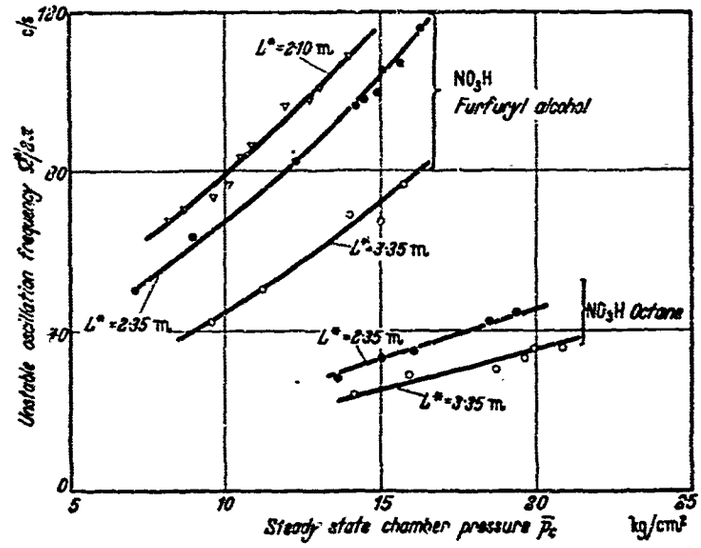

Figure 48. Frequency of unstable oscillations versus chamber pressure. (By courtesy of Office National d'Etudes et de Recherches Aéronautiques)

4. The frequency of unstable oscillation increases as the steady state chamber pressure is increased (*Figure 48*).

5. The frequency of unstable oscillation is rather insensitive to the variation of the steady state mixture ratio. From the measured frequencies

one can derive a value for the interaction index n of a given propellant combination by means of an approximate theoretical formula. The resulting value of n is independent of the shape of the chamber, the value of L^* and the value of the inertia parameter J of the feeding system.

7. The calculated value of the interaction index n of a given propellant combination shows a strong dependence on the chamber pressure; n increases as p_c increases.

8. When the chamber pressure is increased, the stability of the motor is improved.

9. The low frequency type of instability is found to be the predominating type in liquid propellant rockets operating under low chamber pressures and low injection pressures. Under relatively high chamber pressures, high frequency modes of the acoustic type develop concurrently, and may become preponderant in some cases.

Let us discuss these items in turn:

Item *1.* This observation is of fundamental importance because it demonstrates that low frequency oscillations of large amplitude can develop progressively from small amplitudes, thus proving the existence of the linear type of instability analysed in this monograph. The so-called 'divergent' type of instability reported by Ross and Datner[2] might possibly be an example of the same phenomenon.

Item *2.* This observation has been made by many and was also specifically mentioned by Ross and Datner[2]. This indicates the importance of the feeding system characteristics to the low frequency stability of the rocket, and the necessity of considering the complicated dynamics of the feeding system.

Items *3*, *4* and *5.* These behaviours have also been reported by Tischler and Bellman[35]. The effect of L^* on the frequency is clearly indicated by the theory through the corresponding change of residence time θ_g. The effect of chamber pressure p_c can also be derived from the theory through the decrease of the time lag when the chamber pressure is increased.

Item *6.* These observations tend to substantiate the assumption that the interaction index n is a characteristic property of the propellant combination for a given injection pattern. However, not too much weight should be attributed to this result, due to the reasons mentioned in connection with Item *7.*

Item *7.* This result might indicate that the interaction between the combustion process and the chamber oscillations is more intense and complicated than that indicated by the law assumed in the monograph. However, this result should not be considered too seriously. The value of n has in fact been derived by Barrere and Moutet, from the observed values of the frequency and the known characteristics of the feeding system, with the help of an equation which substantially coincides with equation (2.07.20) with $D = E = K = 0$. Without discussing the validity of the approximations involved in neglecting the possible effects of the imperfect rigidity of the feeding system ($E \neq 0$) and of the variation of temperature ($K \neq 0$), we have to recall that equation (2.07.20) is valid only under the condition of incipient instability. The fundamental difference between the conditions of incipient instability and those of fully developed unstable oscillations,

where non-linear effects are certainly present, has been emphasized in Section 4.01. Hence, the values of n as evaluated by Barrere and Moutet include errors from a number of possible sources due to the difference between these two conditions, and cannot be taken as a satisfactory determination of n except in a very qualitative way. More direct and precise determination of n, and of the other parameters characterizing the time lag, are discussed in Section 4.05.

Items *8* and *9*. As explained in Section 1.11, the time lag should consistently decrease for increasing pressures. The effects observed here could be interpreted as a simple consequence of this decrease. However, other complicated effects of the chamber pressure, injection pressure, and changes in recirculation pattern might be present.

4.03. Comparison between Experiments and Theory—Screaming

Very useful information can be drawn from the experiments of K. Berman and S. H. Cheney, Jr[16a, 26], corroborated by those of H. Ellis and his group[27]. Both are based on the use of a slit window cylindrical chamber and on simultaneous pressure measurements. Both are concerned with the longitudinal type of high frequency instability.

The main results of the works of Berman and Cheney can be summarized as follows:

1. High frequency instability is characterized by the presence of pressure waves travelling back and forth in the combustion chamber.

2. Under appropriate conditions self-sustained pressure oscillations can be observed in the combustion chamber. In certain cases, these oscillations consist of continuous pressure waves; in other cases, they may be complicated by the presence of shock waves. In the latter, the amplitudes are usually larger.

3. Self-sustained oscillations containing shock waves are preceded by a transition stage during which only continuous waves are observed. During this transition stage the amplitude of these waves increases until shock waves are eventually established (*Figure 49*).

Figure 49. Development of high frequency unstable oscillations. (By courtesy of American Rocket Society and the General Electric Company of America)

4. With or without shock waves, the observed frequencies of self-sustained oscillations in the high frequency range are closely associated with the fundamental acoustic mode in the combustion chamber with both ends closed (*Figure 50*). The effect of shock waves is a slight increase in frequency.

5. For self-sustained high frequency oscillations of relatively large amplitude, a dark region is observed to commence from the region next to the

injector end whenever a pressure pulse† reaches there from downstream. This dark region once produced moves downstream with the gases. The dark region indicates the presence of gases of lower temperature‡. The periodic occurrence of this dark region at a given position indicates a local temperature oscillation, and therefore a local entropy oscillation which in fact must propagate at the speed of the mass motion.

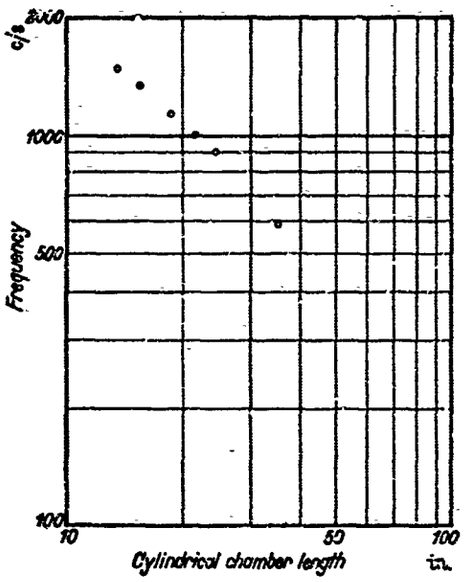

Figure 50. Frequency of the unstable oscillations in the high frequency range as a function of chamber length. (By courtesy of American Rocket Society and the General Electric Company of America)

6. By decreasing the convergent conical angle of the subsonic portion of the nozzle, a relatively weak self-sustained oscillation in an unstable motor can be made to disappear and a self-sustained strong oscillation can be made weaker.

7. High frequency instability in a given motor assembly can be induced by sufficiently increasing the length of the combustion chamber. This change does not substantially affect the combustion zone. The instability becomes more severe when the chamber length is increased farther. At a chamber length below 10 inches (with chamber of 3 inches diameter) it was very difficult to obtain high frequency instability.

8. High frequency instability can be induced in a given motor by lowering the pressure in the propellant tank which results in a simultaneous decrease

† The pressure pulses need not be shock waves as was put forth by Berman and Cheney. The upstream moving continuous pressure waves also result in periodic variations of the luminosity near the injector end. The change in luminosity produced by a shock wave, which is of considerably larger amplitude than a continuous wave, is of course more easily observed.

‡ Berman and Cheney conjectured that 'the non-luminous region represents a cool mixture, consisting of an off-ratio fuel–oxidizer composition'. However, this is not necessarily so. In view of the fact that the radiation intensity of a given gas increases very fast with its absolute temperature, a slight decrease in gas temperature can reduce its luminosity significantly.

of the chamber pressure, the pressure drop across the injector, and the flow rate.

Items *1–3* above confirm the basic postulates of the theory developed in Chapter 3. Items *4*, *6* and *7* verify the predictions (Sections 3.04 and 3.11). Item *5* is in agreement with the theoretical prediction (Section 3.09) that an entropy wave is produced whenever pressure oscillations are present (even for the case of continuous waves), and that the entropy wave should be well discernible whenever pressure waves are of sufficient magnitude. The importance of such an entropy wave on the stability behaviour in the high frequency range has, however, not yet been investigated either theoretically or experimentally. About item *8* we observe that, as discussed in Section 4.01, a variation of pressure drop is accompanied by changes in many other essential parameters such as chamber pressure, injection velocity, time lags, etc. According to the theory, the variation of any of these parameters could justify the observed trend. Therefore, no precise conclusion about causes and effects can be formulated.

With so much discussion about Berman and Cheney's work, we shall now turn our attention to the work of Ellis and his associates[27]. The following observations can be obtained from their report:

1. The measured instantaneous chamber pressure distribution along the chamber length shows that, in the case of high frequency instability, pressure waves propagating both in the upstream and in the downstream directions are significant, but in the case of low frequency instability the non-uniformity of chamber pressure produced by pressure waves is relatively insignificant.

2. The frequency of unstable oscillations in the high frequency range varies inversely with the chamber length.

3. Simultaneous optical determinations of velocity in the chamber and pressure measurements at corresponding stations give consistent results in both phase and frequency.

4. Simultaneous pressure measurements in the chamber, and optical measurements of the exhaust shock pattern for low frequency pressure oscillations, give consistent results. The observations of Ellis and his group substantiate Berman and Cheney's results which are mostly based on optical measurements of velocity.

Finally, it has been mentioned in Section 1.08 that modes of oscillation other than purely longitudinal may be expected to exhibit instability. This is confirmed by experiments reported by Ross and Datner[2]. The frequencies of the observed unstable pressure oscillations in these tests, when the length to diameter ratio of the combustion chamber is less than three, are in good agreement with the frequencies of the 'sloshing' mode in the combustion chamber as calculated from acoustic theory.

4.04. Intermediate Frequencies

We have pointed out in Section 4.01 that the explanation advanced by Ross and Datner to explain the frequencies in the intermediate range encountered during certain tests, cannot stand the rigour of scientific criticism. These authors have actually suggested the identification of the observed frequency of pressure oscillation in the operating rocket with the resonant frequency

of the same rocket in no-flow conditions, when it oscillates as a Helmholtz cavity resonator.

The classical Helmholtz resonator is substantially constituted of a chamber of comparable dimensions in all directions with an opening of relatively small diameter and length. The accumulations of mass, and the time required for the wave propagation in the opening can be neglected. Since the diameter of the opening is also small, the rates of variation of pressure in the chamber are small and the wave propagation effects can be neglected. These are the basis for the Helmholtz calculations. We see immediately that these calculations can apply to a rocket chamber without flow only when the nozzle is small in comparison with the chamber. When, however, the size of the nozzle is comparable with that of the chamber, or even the nozzle length is considerably larger than the chamber length, it is quite possible that the wave propagation time in such a long system cannot be ignored (even if it could be considered negligible for the chamber alone). Furthermore, if the throat diameter is comparable with that of the chamber, the pressure variation can be quite fast and both of the original assumptions about Helmholtz resonators are no longer valid. Since the geometry of the chamber–nozzle combination of conventional rockets is of this type, the Helmholtz calculation is not valid. I. ELIAS and R. GORDON[28], on the suggestion of Dr von Kármán, devised a method to overcome this difficulty. Their analysis is still for the no-flow condition, corresponding to rockets under non-operating conditions. This method of Elias and Gordon was used by Ross and Datner to determine analytically the acoustic frequencies of cavity resonators for purposes of comparison with experimentally determined frequencies of unstable oscillations in operating rockets of the same geometry.

It is important to observe, as Elias and Gordon themselves have noticed, that the computed frequencies under no-flow conditions are quite close to those of the organ-pipe oscillations in a constant area duct of the same total length as the chamber–nozzle combination with one closed end and one open end. The total length, consisting of the chamber length plus the length of the convergent and divergent portions of the nozzle, therefore, corresponds to approximately one quarter wavelength. This result of Elias and Gordon's work simply means that any change of cross section at any intermediate longitudinal station is not very important, and the natural frequency is essentially determined by the total length of the gas column. Elias and Gordon have stressed the fact that their calculations are for non-operating rockets only, and that certain factors, including supersonic outflow, should be considered in extending their calculations to operating conditions. The following simple consideration will immediately reveal to what extent Elias and Gordon's estimate of the acoustic frequency must be corrected, when the flow in the nozzle is increased from zero to the value corresponding to supercritical flow (when supersonic velocities are established in the divergent part of the nozzle).

An important characteristic of supersonic flow fields is that a small disturbance introduced at a given point can influence the flow field only in the downstream nappe of the Mach cone of this point. The flow field upstream of this Mach cone will not 'know' whether a disturbance is introduced or

not. This is because of the fact that a small disturbance is propagated in all directions with the local speed of sound relative to the mass motion. When the speed of mass motion is greater than the speed of sound, any upstream directed signal will be washed downstream of the point of initial disturbance. In the case of no-flow, the boundary condition at the exit of the nozzle (which can be approximately expressed by the constancy of the local pressure) will influence the acoustic oscillations inside the cavity. But in the supercritical case with supersonic outflow, the conditions at the exit cannot influence the acoustic oscillations in the cavity in any way. Moreover, the entire divergent portion of the de Laval nozzle where the flow is supersonic has nothing to do with the acoustic oscillations in the cavity so long as there remains a sonic region somewhere in the vicinity of the throat during the oscillation. Accordingly, when the rocket is operating, the length of the gas column of the divergent portion of the nozzle must be discounted in the calculation of the natural frequency of the acoustic oscillations.

This is still not the whole story. Because of the absence of any reflected waves from the supersonic region, two important things happen. The first is that the boundary condition at the sonic throat is not the same as at the open end of a classical organ pipe. There is no reflected wave from downstream to compensate the incoming pressure wave and maintain a constant local pressure (or density, in the case of isentropic oscillation). The local specific acoustic admittance ratio $(v/\delta)_*$ at the sonic throat is not infinite (as it is for the open end of an organ pipe) but is definite function (Appendix B) of the ratio β of the frequency of oscillation to the local velocity gradient, i.e. $\beta = \Omega/(d\bar{u}/dx)_*$

$$\left(\frac{v}{\delta}\right)_* = \frac{2(\gamma - 1) + \beta^2}{4 + \beta^2} + i\beta\frac{3 - \gamma}{4 + \beta^2}$$

The modulus of this ratio is always less than unity. Thus the condition at the sonic throat is not very different from that at a closed end (corresponding to $v/\delta = 0$). Only the reflection from the sonic throat is weaker and is displaced in phase. The second factor is that the convergence of the walls in the convergent portion produces reflections analogous to those at a closed end even before the waves reach the sonic throat. Thus the entire convergent duct with sonic outflow behaves more like a closed end than like an open end. The specific admittance ratio (v/δ) at the entrance of the nozzle can be determined for specific shapes of the convergent nozzle as described in Appendix B.

As a result of this situation, a good approximation in estimating the frequencies of the characteristic oscillations with the rocket in operating conditions can be obtained by considering an organ pipe with both ends closed and somewhat longer than the chamber length. This is shown better by the analysis of Chapter 3 where the frequencies of the unstable oscillations are found in general slightly lower than the organ pipe modes in the chamber with closed ends. The difference depends on the magnitude of $\alpha_i \bar{u}_e$ which is not only a function of the geometry of the nozzle but also of the frequency of the oscillation under consideration.

The equivalent length of an organ pipe with closed ends is schematically shown in *Figure 51* for rockets both in non-operating conditions (a) and in operating conditions (b). We recognize from the figure that the equivalent length for case (b) is around one fourth of the equivalent length for case (a). It is thus apparent that with chambers similar to those considered by Elias and Gordon, and by Ross and Datner, a frequency of 300 c/s in non-operating

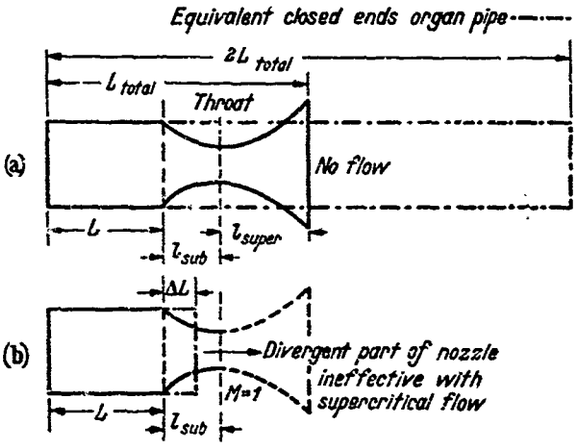

Figure 51. Equivalent organ pipe length for rockets under operating and non-operating conditions

conditions corresponds to a frequency of the order of 1200 c/s in operating conditions and coincides with the fundamental organ-pipe mode. The shift from the one to the other frequency would take place continuously if the flow was gradually brought from zero to its critical value. The agreement between the calculated resonant cavity frequency with no flow and the frequency of oscillation in the operating rocket mentioned by Ross and Datner cannot be considered as anything except mere coincidence. It can be said with assurance that if other tests on the same rocket had been conducted with the divergent cone of the nozzle mostly cut off, unstable oscillations of the same intermediate frequency would still be observed there, but the method of Elias and Gordon would predict a considerably different frequency. Therefore, the justification for the observed intermediate range of unstable frequencies cannot be found in the theory of resonant cavities, but in some more fundamental mechanism. Such a fundamental mechanism has already been mentioned briefly in Section 1.10, and is substantiated by the experiments of Berman and Cheney[16a]. *Figure 52* shows schematically the principle involved. The space lag of all propellant elements is assumed to be the same; therefore the combustion takes place at a definite station (combustion front). At a certain instant, an upstream moving pressure pulse reaches the injector face, is reflected and attenuated by its own course. The effect of the pressure pulse on the injection rates of the two propellants is in general different due to the different response times of the two injection systems. An off-ratio mixture is thus produced, travels downstream and, after the total time lag τ_t has elapsed, burns as it reaches the combustion front. An entropy pulse (defect or excess) is thus created by the combustion

of the off-ratio mixture. After it has been carried downstream by the motion of the gas, the entropy pulse penetrates the convergent portion of the nozzle and generates a new pressure pulse which propagates upstream toward the injector face. If this pressure pulse is sufficiently strong, the conditions for self-amplification and instability are created. It is easily seen that the period of the cycle is approximately equal to the sum of (*1*) the combustion

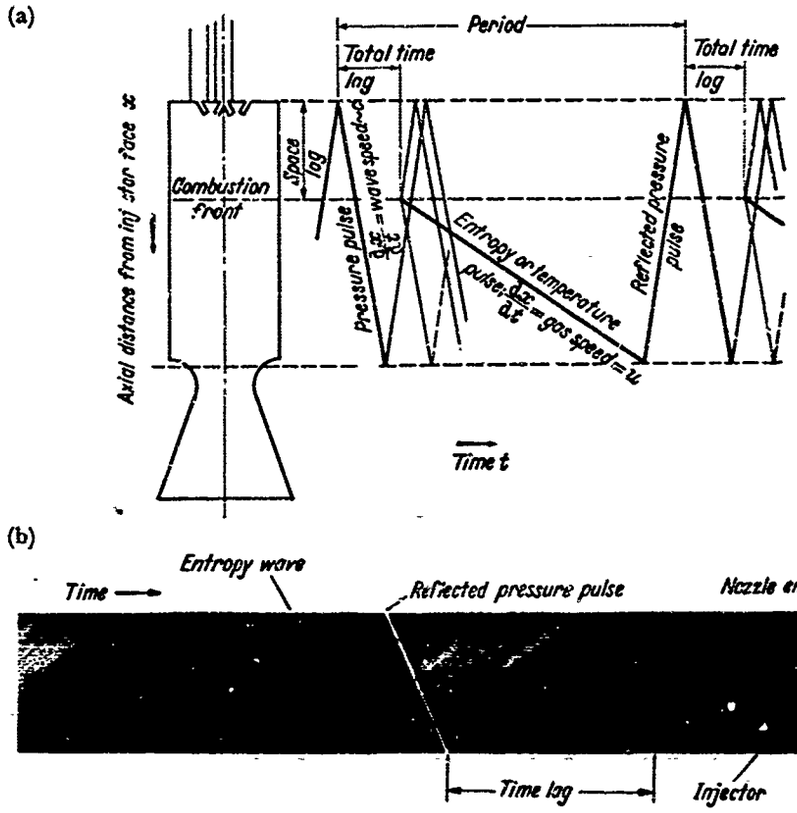

Figure 52. (a) *Schematic diagram for the successive processes during a period of unstable oscillation in the unsteady frequency range;* (b) *radiation streak photograph showing low frequency type instability obtained with an assembly consisting of a conventional impinging head, a* 10-inch *long motor body and a* 41° *convergent angle nozzle. Frequency of oscillation was about* 240 c/s. (*By courtesy of the General Electric Company of America*)

time lag, (*2*) the time for propagation of the entropy wave from the combustion front to the nozzle, and (*3*) the time for propagation of the pressure pulse from the nozzle to the injector face. Berman and Cheney[16a] made a rough estimate of the frequency, as has just been explained, and found that the predicted and the measured values of the frequency are in agreement. A photograph is quoted from reference [16a] and corresponding processes are marked on the photograph and the schematic diagram, *Figure 52.* A careful analysis of the stability conditions for oscillations in this intermediate frequency range is still to be developed.

4.05. Measurements of the Time Lag

The time lag between the injection and the production of burnt gases, and its sensitivity to the chamber conditions are the fundamental causes of the

kinds of instability discussed by the theories of the present monograph. Instead of justifying these theories by comparison with experimental results on unstable rockets, one can pursue the more fundamental approach of checking the properties of the time lag through a direct measure of its duration and of its dependence on the chamber conditions, that is, with the symbols used in this monograph, of the values of $\bar{\tau}$ and n.

The difficulties of measuring these quantities lie not only in the requirement of accurate and reliable instrumentation, but also in the fact that the proper value of the time lag to be measured is the average of the time lags of different propellant elements. This has been made clear by the developments of Sections 2.08 and 3.13. Thus the technique of the 'pulse' which has been suggested and applied does not appear satisfactory, except for very rough evaluations. If a pulse is introduced in the injection rate, a pressure pulse will appear in the chamber pressure at a later time. Assuming that the beginning of the two pulses is sharply defined, the corresponding time interval represents the minimum value of the time lag. However, there is no way of measuring the maximum value of the time lag, because the pressure pulse does not end at the instant the burning rate has dropped again to normal, but extends beyond this instant through a kind of relaxation process (*Figure 53*).

In *Figure 53*(a), the chamber pressure p_c response, to a step increase in feed line pressure p_l, would enable us to determine $\bar{\tau}_{\min}$, if the response of p_c is sharply defined initially. In *Figure 53*(b), the square pulse in feed line pressure could, in the ideal case, yield both $\bar{\tau}_{\min}$ and $\bar{\tau}_{\max}$ if the turning points of p_c response were sharply defined. *Figure 53*(c) represents a typical pulse we can put in a feed line and the typical response of chamber pressure which is smeared out over a considerable range; and here it is difficult to obtain $\bar{\tau}_{\min}$ and impossible to get $\bar{\tau}_{\max}$. In other words, even if the minimum and maximum time lag coincide, and the injection rate pulse is of negligible duration, the pressure pulse has a tail which makes it impossible to measure the actual value of the maximum time lag. Therefore, it is impossible to obtain accurately, from the pulse method, the proper average value of the time lag, even when the chamber pressure pulses are sharply defined. The situation is made worse by the absence of sharp definition of the pulses due to the unavoidable roughness of combustion.

A more rational method[17] consists of the production of sustained sinusoidal modulation of the injection rate, which produces a corresponding sustained oscillation of the chamber pressure. The amplitude and phase relations between the two oscillations (or, synthetically, the transfer function of the particular system under consideration) is a complicated function of the geometry, chamber, nozzle, frequency, residence time, time lag, interaction index and so on. The functional relationship relating the transfer function to these quantities is provided by the theoretical formulations of previous chapters. In principle it is possible, by performing the tests in a sufficient range of frequencies, to derive the values of $\bar{\tau}_l$, $\bar{\tau}$, n, and the residence time θ_r.

Preliminary measurements on a monopropellant motor have already been made with encouraging results. The accuracy of the instrumentation was not yet sufficient for the determination of the four mentioned unknowns;

but the total time lag and the residence time have been obtained. *Figure 54* shows the results for the total time lag at different pressure levels. The scatter of the results is too large in these experiments to obtain an exact

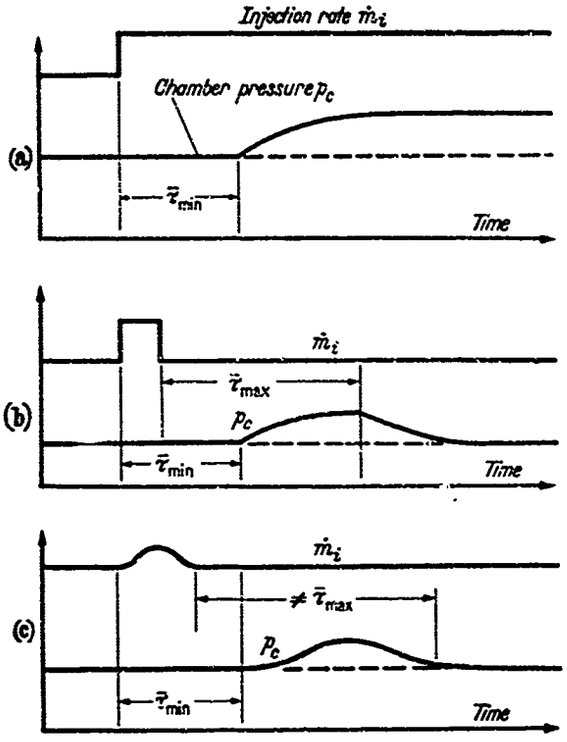

Figure 53. Schematic diagram of the response of chamber pressure to a feed line pressure perturbation

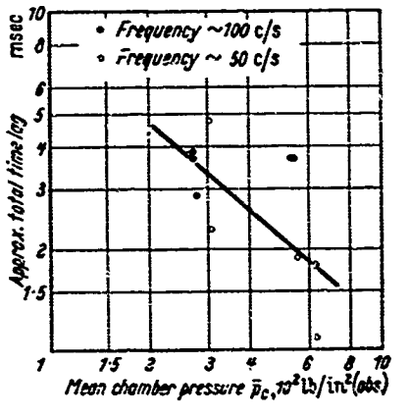

Figure 54. Preliminary data on the steady state total time lag as a function of mean chamber pressure

definition of the dependence of the steady state time lag on pressure, but the general trend shows an evident decrease, in agreement with the discussions of Chapter 1. It is hoped that more detailed experimental information on the time lag and the related quantities will soon be available.

APPENDIX A

ANALYTICAL NATURE AND METHODS OF SOLUTIONS OF EQUATION (2.03.02)

THE equation of mass balance in the combustion chamber and the equation of the dynamics of the feeding system can be reduced by elimination to a single ordinary linear differential equation (2.03.02) involving a retarded variable of the form

$$L_1[\varphi(z)] = L_2[\varphi(z - \delta)] \qquad \ldots.(A.01)$$

where L_1 and L_2 are polynomials of the ordinary differential operator d/dz with coefficients independent of z. The degrees of the polynomials are determined by the nature of the feeding system dynamics. Particular forms of equation (A.01) have been discussed by many authors[29–31]. Equation (A.01) differs from an ordinary differential equation in the fact that the operator L_2 operates on the dependent variable φ as a function of the retarded independent variable $z - \delta$ instead of the independent variable z. If δ is constant and if $\varphi(z - \delta)$ can be expanded into a Taylor series about z, equation (A.01) will stand as an ordinary differential equation of infinite order with constant coefficients. This transcendental equation will therefore admit an infinite number of solutions of exponential type e^{sz} where s is a root of the characteristic equation of the ordinary differential equation and is in general a complex quantity. The characteristic equation is given as

$$f(s) = L_1(s) - e^{-s\delta} L_2(s) = 0 \qquad \ldots.(A.02)$$

Since the coefficients in the operators L_1 and L_2 are real, the infinite number of roots s of the characteristic equation must exist as complex conjugate pairs. Each complex conjugate pair of s leads to two exponential solutions which combine to form an oscillatory solution with varying amplitude. The general solution of equation (A.01) will be a linear combination of an infinite number of oscillatory solutions having amplitudes which will either grow or die out exponentially; only in rare circumstances will the amplitude remain constant. The imaginary part of the complex quantity s then represents the angular frequency, and the real part, the amplification coefficient of the particular oscillatory mode. The stability of a feedback system governed by equation (A.01) requires simply that no root s of the characteristic equation (A.02) shall have a positive real part. In other words, the function $f(s)$ has no 0's in the right half of the complex plane with positive real part. It should be noted, however, that this stability criterion is a sufficient condition (for the system to be stable) if and only if the arbitrary disturbance introduced into the system can be resolved into a sum of the oscillatory components as are determined by the infinite number of roots of the characteristic equation (A.02). The present elementary approach does indicate that, in determining the constants in the general solution, we need an infinite number of initial values corresponding, for instance, to the specification of the initial disturbance $\varphi(z)$ during the

interval $-\delta \leqslant z \leqslant 0$. But there is no indication that the infinite number of exponential solutions will form a complete set, the linear combination of which can represent arbitrary initial disturbance functions. Furthermore the assumption that $\varphi(z-\delta)$ can be expanded into a Taylor series about z is rather restrictive as to the applicability of the foregoing elementary considerations.

A somewhat more elegant mathematical approach using Laplace transforms is directly suggested by the presence of the retarded variable, which is the only source of difficulty in equation (A.01), because the retarded variable is removed by the Laplace transform. Let us define the Laplace transform of the dependent variable $\varphi(z)$

$$\Phi(s) = \int_0^\infty e^{-sz}\,\varphi(z)\,dz \qquad \ldots.(A.03)$$

where s is an arbitrary complex quantity being used as an independent variable of the transform. It is rather difficult to trace the physical meaning of the transform Φ and the variable s from the mathematical definition of the transform when $\varphi(z)$ is defined by equations much more complicated than equation (A.01). In the present case if we multiply equation (A.01) by $e^{-sz}\,dz$, integrate from 0 to ∞ and introduce the initial conditions, we have after manipulation,

$$\Phi(s)\,.\,[L_1(s) - e^{-s\delta}\,L_2(s)] = F_1(s) - e^{-s\delta}\,L_2(s)\int_{-\delta}^{0} e^{-sz'}\varphi(z')\,dz' \qquad \ldots.(A.04)$$

where $F_1(s)$ is a new polynomial of s, the coefficients of which depend on $\varphi(0)$, $\varphi(-\delta)$ and the coefficients of $L_1(s)$ and $L_2(s)$. The transform will exist if $\varphi(z)$ is sectionally continuous and satisfies certain conditions at $z = 0$ and $z = \infty$. These conditions will in general be satisfied by $\varphi(z)$ in physical problems which may not possess a Taylor series expansion.

From equation (A.04) the Laplace transform $\Phi(s)$ of $\varphi(z)$ is easily found. The function $\varphi(z)$ can then be obtained using Mellin's inverse transform theorem by evaluating the following integral

$$\varphi(z) = \int_\Gamma \frac{F_1(s) - e^{-s\delta}\,L_2(s)\displaystyle\int_{-\delta}^{0} e^{-sz'}\,\varphi(z')\,dz'}{L_1(s) - e^{-s\delta}\,L_2(s)}\,e^{sz}\,ds \qquad \ldots.(A.05)$$

over the contour Γ enclosing all the poles of the integrand. This contour integral can be evaluated by the use of the theorem of residues. It is interesting to note that the integral has no poles other than those introduced by the 0's of the denominator. Let s_n be one of the 0's, then there is a term in $\varphi(z)$ of the type $c_n e^{s_n z}$, where c_n is a constant depending on the initial disturbance, the operators L_1 and L_2 and the value of s_n. The function $\varphi(z)$ is thus given as

$$\varphi(z) = \sum_{n=0}^{\infty} c_n e^{s_n z} \qquad \ldots.(A.06)$$

where s_n satisfies equation (A.02). This result, equation (A.06), is identical with, but more general than, the one obtained previously based on elementary considerations. The physical meaning of the transformation

variable s can thus be inferred. The imaginary part represents the angular frequency while the real part represents the amplification coefficient.

The stability of a feedback system represented by equation (A.01) can be determined in general by investigating the 0's of the function f (s) as given by equation (A.02). A sufficient stability criterion is that no 0's of f (s) exist in the right half of the complex s plane.

We are interested in two types of practical problems. The first is to determine whether a given system with known numerical constants is stable or unstable. The other problem is to investigate the qualitative trends of the stability behaviour of a certain type of system when various parameters are changed. The first problem is concerned with the determination of the stability of a given system before it is built. The second problem is intended to supply information to the designer on how to design a stable system and how to modify a given unstable system to make it stable. In the first problem, that is, when we are analysing a given system, the function $f(s) = L_1(s) - e^{-s\delta}L_2(s)$ involves only numerical coefficients. Thus we can use Cauchy's theorem with advantage. The theorem states:

'If f (s) is analytic inside a given domain D bounded by a contour C except for a finite number of poles in the domain, then when s traces the contour C in a clockwise direction, the vector representing f (s) in a complex plane will rotate about the origin, and the number of complete clockwise revolutions that f (s) makes is equal to the difference between the number of 0's and the number of poles of f (s) in the domain D'.

For a stability investigation, the domain D is the right half of the complex s plane and the contour C is conveniently chosen as consisting of the imaginary axis and an infinitely large semicircle in the right half plane connecting $\pm i\infty$ as shown in *Figure 55*. The plot of f (s) in the complex plane is known as the Nyquist diagram. The sum of the number of complete clockwise turns of the Nyquist diagram about the origin and the number of poles of f (s) in the domain is equal to the number of 0's of f (s) in D. If the system is to be stable, the Nyquist diagram must make as many complete counterclockwise turns about the origin as there are poles of f (s) in D. If in addition f (s) is analytic everywhere inside D, as for the function f (s) defined by equation (A.02), the stability criterion is that the Nyquist diagram of f (s) should not encircle the origin.

The Nyquist diagram of f (s) is considerably complicated by the presence of the factor $e^{-s\delta}$ introduced by the retarded variable. For example, when s is purely imaginary, the real and imaginary parts of $e^{-s\delta}$ are periodic and 90° out of phase. Thus $e^{-s\delta}$ introduces a number of loops in the Nyquist diagram and makes it necessary, in the numerical evaluation of f (s), to take small steps of Ω in order to have a reasonably accurate plot. M. SATCHE[31] proposed an ingenious method to avoid these loops in problems involving a retarded variable. Divide equation (A.02) by $L_2(s)$ and define

$$G(s) = e^{-s\delta} - g(s) = 0 \qquad \ldots.(A.07)$$

with $g(s) = L_1(s)/L_2(s)$, where we have introduced artificially a finite number of poles in the function $G(s)$ corresponding to the 0's of $L_2(s)$. The stability criterion is still the same as it was before, that is, no 0's of $G(s)$ may exist in the domain D. Instead of making a vector plot of $G(s)$,

we interpret the vector $G(s)$ as the difference of the vector $e^{-s\delta}$ and the vector g (s), that is, $G(s)$ is a vector with vertex lying inside or on the unit circle of $e^{-s\delta}$, with its tail on the corresponding point of the vector diagram of g (s) (*Figure 56*). A system is stable if the vector $G(s)$ makes as many complete counterclockwise revolutions when s traces the contour C as there are 0's of $L_2(s)$ in the domain D. The number of 0's of $L_2(s)$ in D can be determined by making a Nyquist diagram for $L_2(s)$ separately. The determination of the stability of a given system therefore consists of tracing two Nyquist diagrams for the two functions g $(s) = L_1(s)/L_2(s)$ and $L_2(s)$. We shall call the combination of the Nyquist diagram for the function g $(s) = L_1(s)/L_2(s)$ and of the unit circle for $e^{-s\delta}$ the Satche diagram.

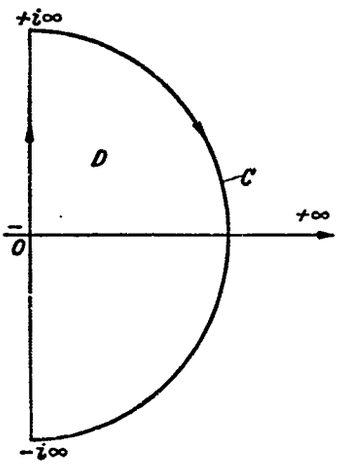

Figure 55. Schematic diagram of integration contour

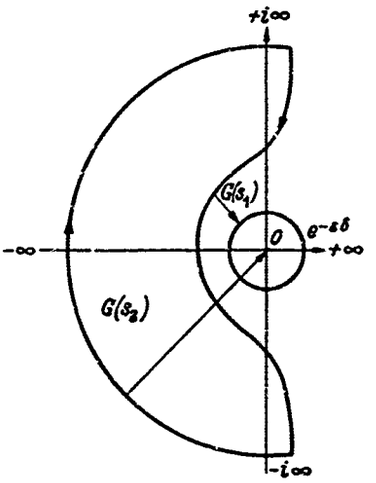

Figure 56. Schematic Satche diagram

An examination of the Satche diagram and of the associated Nyquist diagram for $L_2(s)$ will reveal whether the system is stable.

In the second problem mentioned, that is, when we are interested in determining the qualitative trends of the stability behaviour as a function of the constants of combustion n, $\bar{\tau}$ and of the parameters of a certain type of system, the graphical method using the Satche and Nyquist diagrams becomes undesirable. The analytical treatment of equation (A.02) is more advantageous. We are primarily interested in determining the stability boundary (or neutral boundary) of a certain type of system. The stability boundary for a given oscillatory mode is expressed by a relation between the combustion constants n, $\bar{\tau}$ and the parameters of the system such that the oscillatory mode in question is neither stable nor unstable, in other words, the real part of s vanishes for that mode. The stability boundary divides the space formed by the combustion constants and the parameters of the given type of system into different domains in which the system is stable on one side of the boundary and unstable on the other side. If, by varying a certain parameter of the system, the stability boundary of a given mode is shifted in such a way that the unstable domain is diminished, this variation of the particular constant or parameter is stabilizing in so far as that oscillatory mode is concerned.

The stability boundary is defined by equation (A.02) when $s = i\omega$ where ω is the frequency of the neutral oscillation. By separating the real and imaginary parts, we obtain two real equations from which we can eliminate ω; the eliminant is the equation of the stability boundary. From another point of view, the two real equations represent the stability boundary in parametric form. This point of view is important because the elimination of ω cannot be carried out explicitly with ease except when $L_1(s)$ and $L_2(s)$ are in greatly simplified form. It should be noted that the parameters of the feeding system dynamics are responsible for most of the complications of the operators L_1 and L_2. It is likely that the effect of certain important parameters characterizing the combustion chamber and the processes of combustion on the qualitative stability behaviour should not be fundamentally changed by the complication of the feeding system. The analytical study of certain simple feeding system configurations can be expected to give a number of important results.

APPENDIX B

SUPERCRITICAL GASEOUS DISCHARGE WITH HIGH FREQUENCY OSCILLATIONS

THE problem of the behaviour of a nozzle working in the supercritical range in oscillatory conditions was first treated by H. S. TSIEN[24]. He investigated the case in which the oscillations in the incoming flow are isothermal, and therefore non-isentropic, and determined the departures from the steady state behaviour in the range of very low frequencies, as well as the asymptotic response to very high frequencies. The treatment was extended by L. CROCCO[25] with the purpose of including the non-isothermal case and especially of determining the nozzle behaviour in the intermediate range of frequencies. In this appendix, account is given of these developments and of a few other unpublished results. It should be noted that all symbols in this appendix represent dimensional quantities unless otherwise stated.

B.01. THE EQUATIONS

Calling p, ρ and u the pressure, density and velocity in steady state, completely determined by the shape of the nozzle, and $p+p'$, $\rho+\rho'$ and $u+u'$, the corresponding values in unsteady conditions, and assuming the perturbations p', ρ' and u' to be small compared with the unperturbed quantities, Tsien has written the continuity and momentum equations in the following form, retaining only the first order terms in the perturbations:

$$\frac{\partial}{\partial t}\left(\frac{\rho'}{\rho}\right)+u\frac{\partial}{\partial x}\left(\frac{\rho'}{\rho}+\frac{u'}{u}\right)=0 \qquad \ldots.(B.01)$$

$$\frac{\partial}{\partial t}\left(\frac{u'}{u}\right)+\left(\frac{\rho'}{\rho}+2\frac{u'}{u}\right)\frac{\mathrm{d}u}{\mathrm{d}x}+u\frac{\partial}{\partial x}\left(\frac{u'}{u}\right)=\frac{p'}{p}\frac{\mathrm{d}u}{\mathrm{d}x}-\frac{p}{\rho u}\frac{\partial}{\partial x}\left(\frac{p'}{p}\right) \qquad \ldots.(B.02)$$

x being the distance along the nozzle and t the time. The third equation between the dependent variables p'/p, ρ'/ρ and u'/u is the energy equation or, more simply, the equation expressing the constancy of entropy of any fluid mass when we follow its motion:

$$\left(\frac{\partial}{\partial t}+u\frac{\partial}{\partial x}\right)\frac{S'}{c_v}=\left(\frac{\partial}{\partial t}+u\frac{\partial}{\partial x}\right)\left(\frac{p'}{p}-\gamma\frac{\rho'}{\rho}\right)=0 \qquad \ldots.(B.03)$$

where S' is the entropy perturbation, c_v is the constant volume specific heat, and γ the adiabatic index.

In these equations u, $\mathrm{d}u/\mathrm{d}x$ and $p/\rho u$ are to be considered known functions of x determined by the nozzle shape. Due to the linearity of the three equations above, the harmonic form of oscillatory time dependence can be chosen and, using the complex representation, the dependent variables can be written as:

$$p'/p=\varphi(x)\mathrm{e}^{i\omega t};\quad \rho'/\rho=\sigma(x)\mathrm{e}^{i\omega t};\quad u'/u=v(x)\mathrm{e}^{i\omega t} \qquad \ldots.(B.04)$$

where ω is the angular frequency of neutral oscillation and φ, σ and ν are complex functions of x alone†. At the nozzle entrance, $x = x_e$, the three functions have certain values φ_e, σ_e and ν_e. The problem in which we are interested is to find the distributions of φ, σ and ν along the nozzle, but especially to determine the relations between φ_e, σ_e and ν_e. These relations will in fact constitute the boundary conditions to be applied to the rest of the flow system as a result of the presence of the nozzle. Observe that if the quantities (B.04) are interpreted as rotating vectors of which only the projection on the real axis has a physical meaning, the quantities φ, σ and ν will represent fixed vectors, the magnitude of which is the amplitude of the oscillation of the corresponding quantities. The angle between any two such vectors represents the corresponding phase shift.

Equation (B.03) is immediately integrated as

$$\frac{S'}{c_v} = \frac{p'}{p} - \gamma \frac{\rho'}{\rho} = \mathrm{f}\left(t - \int_{x_e}^{x} \frac{\mathrm{d}x}{u}\right)$$

the arbitrary function f being in general determined by the known time dependence of the entropy at $x = x_e$. For the exponential time dependence assumed in equations (B.04) we obtain

$$\varphi(x) - \gamma\sigma(x) = \varepsilon \exp\left(-i\omega \int_{x_e}^{x} \frac{\mathrm{d}x}{u}\right) \qquad \ldots\ldots(\mathrm{B.05})$$

where the constant ε represents the amplitude of the entropy oscillation divided by c_e. With the assumption (B.04) and the relation (B.05) equations (B.01) and (B.02) are reduced to the following system of ordinary differential equations in ν and σ:

$$\left.\begin{aligned} u\frac{\mathrm{d}\nu}{\mathrm{d}x} + u\frac{\mathrm{d}\sigma}{\mathrm{d}x} + i\omega\sigma &= 0 \\ u\frac{\mathrm{d}\nu}{\mathrm{d}x} + \frac{c^2}{u}\frac{\mathrm{d}\sigma}{\mathrm{d}x} + \left(2\frac{\mathrm{d}u}{\mathrm{d}x} + i\omega\right)\nu - (\gamma - 1)\frac{\mathrm{d}u}{\mathrm{d}x}\sigma & \\ = \varepsilon\left(\frac{\mathrm{d}u}{\mathrm{d}x} + i\omega\frac{c^2}{\gamma u^2}\right)\exp\left(-i\omega\int_{x_e}^{x}\frac{\mathrm{d}x}{u}\right) & \end{aligned}\right\} \ldots\ldots(\mathrm{B.06})$$

in which c is the velocity of sound. It is easily seen that these equations present a singularity at $u = c$, that is, at the sonic throat, where therefore only one family of solutions remains regular.

Equations (B.06) could be solved numerically for any specified nozzle shape. However, an analytical solution can be obtained if, following Tsien, we confine our attention to nozzles in which u increases linearly with x in the subsonic portion of the nozzle. This condition is not too restrictive, since many actual nozzles have practically a linear velocity

† The definition of these quantities is somewhat different from that of the same symbols in Chapter 3. The difference is especially important for ν.

distribution near the sonic throat which is the region where an analytical solution is particularly useful†. We take therefore:

$$\frac{\mathrm{d}u}{\mathrm{d}x} = \frac{u}{x} = \frac{c_*}{x_*} = \frac{c_* - u_e}{l_{sub} \cdot L} \qquad \ldots\ldots(B.07)$$

in which c_* represents the so-called critical sound speed attained at the throat where $x = x_*$, $l_{sub} = (x_* - x_e)/L$ represents the ratio of the length of the subsonic portion of the nozzle to the chamber length L. The subscript $_*$ is used to denote conditions at the nozzle throat.

Moreover, we take, with Tsien, a new independent variable:

$$z = (x/x_*)^2 = (u/c_*)^2 \qquad \ldots\ldots(B.08)$$

in terms of which we have:

$$\left.\begin{aligned} c^2 &= c_*^2\{\tfrac{1}{2}(\gamma+1) - \tfrac{1}{2}(\gamma-1)z\} \\ \int_{x_e}^{z} \frac{\mathrm{d}x}{u} &= \frac{x_*}{2c_*} \log \frac{z}{z_e} \end{aligned}\right\} \ldots\ldots(B.09)$$

where z_e represents the assigned value of z at the nozzle entrance; and we define a reduced angular frequency:

$$\beta = \frac{x_*\omega}{c_*} = \frac{\omega l_{sub} \cdot L}{c_* - u_e} \qquad \ldots\ldots(B.10)$$

Introducing equations (B.07) and (B.10) into equations (B.06) and eliminating $\mathrm{d}v/\mathrm{d}x$, we find

$$\begin{aligned}(2 + i\beta)v = (\gamma - 1 + i\beta)\sigma - (\gamma+1)(1-z)\frac{\mathrm{d}\sigma}{\mathrm{d}z} \\ + \varepsilon\left(\frac{z}{z_e}\right)^{-i\beta/2}[1 - i\beta/2\gamma \cdot (\gamma-1) + i\beta/2\gamma \cdot (\gamma+1) \cdot 1/z] \ldots\ldots(B.11)\end{aligned}$$

and by eliminating v with the help of (B.11) from one of the equations (B.06) we obtain

$$\begin{aligned}z(1-z)\frac{\mathrm{d}^2\sigma}{\mathrm{d}z^2} - \left(2 + \frac{2i\beta}{\gamma+1}\right) z\frac{\mathrm{d}\sigma}{\mathrm{d}z} - \frac{i\beta(2+i\beta)}{2(\gamma+1)}\sigma \\ = -i\beta\varepsilon\left(\frac{z}{z_e}\right)^{-i\beta/2}\left[\frac{1 - i\beta(\gamma-1)/2\gamma}{2(\gamma+1)} + \frac{2+i\beta}{4\gamma}\frac{1}{z}\right] \qquad \ldots\ldots(B.12)\end{aligned}$$

Equation (B.12) is a non-homogeneous complex hypergeometric equation, with singularities at $z = 0$, $z = 1$, and $z = \infty$. Of these singularities, only the one at $z = 1$ is important for our problem, since the others are out of the range of interest in the variable z, which must be contained between a non-vanishing minimum at the entrance of the nozzle and a finite maximum at its exit.

† If u_e is not too small, the generatrix of a nozzle with such a linear distribution is nearly an arc of a circle.

B.02. The Condition at the Sonic Throat

Tsien has observed that since the motion is supersonic in the divergent part of the nozzle no wave can be transmitted backwards to the throat, and therefore the propagation of the oscillations must always take place in the downstream direction. He has therefore used the condition that the propagation velocity $U(x)$ must always be positive. If U is defined by the formula

$$\frac{\partial}{\partial t}\left(\frac{\rho'}{\rho}\right) + U\frac{\partial}{\partial x}\left(\frac{\rho'}{\rho}\right) = 0$$

substituting from (B.04) we have $U = -i\omega\sigma/(d\sigma/dx)$. The condition that U must remain of the same sign throughout the nozzle means that it must never vanish, and therefore $(d\sigma/dx)/\sigma$ must remain finite. This condition is not satisfied if the solution is singular, with the important consequence that only a solution which is regular is compatible with the condition of downstream propagation. This conclusion, which is true for the most general case considered in equations (B.06), allows a more concise and mathematically more definite expression of the condition at the throat. The same result is obtained on a more physical basis by considering that a wave of finite amplitude at the sonic throat cannot send any but infinitesimal waves upstream, since the upstream propagation velocity is zero, and therefore only waves of infinite amplitude at the sonic throat can send finite waves upstream. The absence of upstream-moving waves is therefore connected with the suppression of all singularities at the sonic throat.

B.03. Solution for Low Frequencies in the Non-isothermal Case

Tsien has treated the case of isothermal oscillations. His treatment is immediately extended to the non-isothermal case. Assuming a prescribed temperature oscillation at the entrance of the nozzle

$$(T'/\bar{T})_{x=x_e} = \theta e^{i\omega t} \qquad \ldots.(B.13)$$

we have the relation

$$\varphi_e - \sigma_e = \theta \qquad \ldots.(B.14)$$

between φ_e and σ_e.

On the other hand equation (B.05) gives

$$\varphi_e - \gamma\sigma_e = \varepsilon \qquad \ldots.(B.15)$$

and therefore we obtain the relation

$$\sigma_e = (\theta - \varepsilon)/(\gamma - 1) \qquad \ldots.(B.16)$$

which determines the amplitude of the density oscillation at the entrance of the nozzle when θ and ε are assigned. Of course, instead of prescribing arbitrary values of θ and ε, one could prescribe arbitrary values of φ_e and σ_e and determine the corresponding values of θ and ε. In Tsien's case $C = 0$.

At low frequencies, we can expand all quantities in powers of $i\beta$, since equations (B.11) and (B.12) contain only this combination of i and β.

We take therefore

$$\sigma(z, \beta) = \sigma^{(0)}(z) + i\beta\sigma^{(1)}(z) + \dots \qquad \dots.(B.17)$$

$$\nu(z, \beta) = \nu^{(0)}(z) + i\beta\nu^{(1)}(z) + \dots \qquad \dots.(B.18)$$

Substituting equation (B.17) into equation (B.12) and equating the coefficients of the same powers of $i\beta$, the resulting equation breaks up into:

$$z(1-z)\frac{d^2\sigma^{(0)}}{dz^2} - 2z\frac{d\sigma^{(0)}}{dz} = 0 \qquad \dots.(B.19)$$

$$z(1-z)\frac{d^2\sigma^{(1)}}{dz^2} - 2z\frac{d\sigma^{(1)}}{dz} = \frac{2}{\gamma+1}z\frac{d\sigma^{(0)}}{dz}$$

$$+\frac{1}{\gamma+1}\sigma^{(0)} - \frac{\varepsilon}{2}\left(\frac{1}{\gamma+1} + \frac{1}{\gamma z}\right) \qquad \dots.(B.20)$$

The solution of (B.19) which is non-singular at $z = 1$ is $\sigma^{(0)} = \text{const.}$, and therefore, since the solution (B.17) must hold at $\beta = 0$, we obtain from relation (B.16)

$$\sigma^{(0)} = (\theta - \varepsilon)/(\gamma - 1) \qquad \dots.(B.21)$$

Introducing this value into equation (B.20), and integrating the first order equation in $d\sigma^{(1)}/dz$ we obtain the expression

$$(1-z)^2\frac{d\sigma^{(1)}}{dz} = \frac{\theta}{\gamma^2-1}(\log z - z)$$

$$-\frac{\varepsilon}{2}\left[\frac{1}{\gamma(\gamma-1)}\log z - \frac{1}{\gamma-1}z - \frac{1}{\gamma}\frac{1}{z}\right] + C \qquad \dots.(B.22)$$

where the integration constant C has to be determined in such a way that the right hand side of equation (B.22) vanishes at $z = 1$, so that $d\sigma^{(1)}/dz$ may remain finite at this point. We obtain

$$\frac{d\sigma^{(1)}}{dz} = \frac{\theta}{\gamma^2-1}\frac{\log z + 1 - z}{(1-z)^2}$$

$$-\frac{\varepsilon}{2\gamma(\gamma-1)}\left[\frac{\log z + 1 - z}{(1-z)^2} - \frac{\gamma-1}{z}\right] \qquad \dots.(B.23)$$

It can be immediately checked that this expression is regular at $z = 1$. An additional integration, with the condition following from relations (B.16) and (B.21),

$$\sigma_e^{(1)} = 0 \qquad \dots.(B.24)$$

would give the (non-singular) expression for $\sigma^{(1)}(z)$.

Now introducing equations (B.17) and (B.18) into equation (B.11) and again equating the coefficients of like powers of $i\beta$ one obtains, using equations (B.21), (B.23) and (B.24),

$$\left.\begin{aligned} v^{(0)} &= v_e^{(0)} = \theta/2 \\ v_e^{(1)} &= -\frac{\theta}{4}\left(\frac{2}{\gamma-1}\frac{\log z_e}{1-z_e}+1\right)+\frac{\varepsilon}{4\gamma}\left(\frac{\gamma+1}{\gamma-1}\frac{\log z_e}{1-z_e}+1\right) \end{aligned}\right\} \quad \ldots.(B.25)$$

and therefore, recalling relations (B.17) and (B.18):

$$\begin{aligned} \alpha = \frac{v_e}{\sigma_e} &= \frac{v_e^{(0)} + i\beta v_e^{(1)} + \ldots}{\sigma_e^{(0)} + i\beta\sigma_e^{(1)} + \ldots} \\ &= \frac{\gamma-1}{2}\frac{\theta}{\theta-\varepsilon} + \frac{\gamma-1}{\theta-\varepsilon} v_e^{(1)} \cdot i\beta + \ldots \qquad (\beta \ll 1) \qquad \ldots.(B.26) \end{aligned}$$

This quantity, representing the complex ratio between the fractional variations of velocity and density at the entrance of the nozzle, and analogous to the specific admittance ratio of acoustics, can be used as a boundary condition for the rest of the flow system in an oscillatory state. We see that equation (B.26) depends only on β, z and the ratio θ/ε. The first term of the series (B.26) applies to the steady state and contains the isothermal case $\theta = 0$ where the velocity cannot change ($v_e = 0$), the isentropic case $\varepsilon = 0$, $v_e/\sigma_e = \frac{1}{2}(\gamma - 1)$, and the isopyknic case $\theta = \varepsilon$, $\sigma = 0$ as particular cases. Equation (B.26) shows that even for moderate β, the boundary condition imposed by the nozzle can change considerably since both the phase and the amplitude ratio between velocity and density fluctuations are affected considerably.

The same procedure can be used, without substantial difficulty, to compute higher order terms in $i\beta$.

B.04. Solution for High Frequencies in the Non-isothermal Case

Following a procedure similar to the one used by Tsien we first determine the particular solution σ_p of equation (B.12)

$$\sigma_p = Z(z)\,(z/z_e)^{-i\beta/2}$$

and substitute it into equation (B.12). An equation for $Z(z)$ is obtained which can be solved by taking the series

$$Z(z) = Z^{(0)}(z) + (1/i\beta)Z^{(1)}(z) + \ldots$$

and equating the coefficients of like powers of $i\beta$. The result is

$$\sigma_p = -\frac{\varepsilon}{\gamma}\left(\frac{z}{z_e}\right)^{-i\beta/2}\left(1 + \frac{1}{i\beta}\frac{1}{\dfrac{\gamma+1}{2}\dfrac{1}{z} - \dfrac{\gamma-1}{2}} + \ldots\right) \quad \ldots.(B.27)$$

Replacing result (B.27) in equation (B.11), the corresponding value of v is found to be zero; by pushing the expansions to higher powers it is actually found that the first non-vanishing term in the series for v corresponding to the particular solution (B.27) is the term in $(i\beta)^{-2}$. Thus σ_p

fulfils the condition of regularity at $z = 1$, but not the condition (B.16) at $z = z_e$.

Therefore a solution of the homogeneous equation corresponding to (B.12) must be determined. If we take $\sigma = \exp[i\beta\lambda(z)]$ and introduce it into this homogeneous equation, we find that the derivative $d\lambda/dz = y(z)$ satisfies the Riccati equation

$$z(1-z)\frac{dy}{dz} = \frac{2+i\beta}{2(\gamma+1)} + 2\left(1+\frac{i\beta}{\gamma+1}\right)zy - i\beta z(1-z)y^2$$

Introducing in this equation the series

$$y(z) = y^{(0)}(z) + \frac{1}{i\beta}y^{(1)}(z) + \dots$$

and equating the terms with equal powers of $i\beta$ we obtain

$$y^{(0)} = -\frac{1}{(\gamma+1)(1-z)}\left(\sqrt{1+\frac{\gamma+1}{2}\frac{1-z}{z}} - 1\right) \qquad \dots.(B.28)$$

$$y^{(1)} = \frac{\gamma+1}{2\{1+\frac{1}{2}(\gamma+1)(1-z)/z\}^{\frac{1}{2}}}\left[(1-z)\frac{dy^{(0)}}{dz} - 2y^{(0)} - \frac{1}{\gamma+1}\frac{1}{z}\right] \qquad \dots.(B.29)$$

where only the solutions remaining regular at $z = 1$ have been considered. The solution of equation (B.12) can now be put in the form

$$\sigma = C\exp\left[i\beta\int_{z_e}^{z} y^{(0)}\,dz + \int_{z_e}^{z} y^{(1)}\,dz + \dots\right] + \sigma_p \qquad \dots.(B.30)$$

where the constant C is determined by the condition (B.16) at $z = z_e$ and is expressed by

$$C = \frac{1}{\gamma-1}\left(\theta - \frac{\varepsilon}{\gamma}\right) + \frac{1}{i\beta}\frac{\varepsilon}{\gamma}\frac{1}{\frac{\gamma+1}{2}\frac{1}{z_e} - \frac{\gamma-1}{2}} + \dots \qquad \dots.(B.31)$$

Coming now to equation (B.11) and recalling that σ_p does not contribute to ν up to terms of order $(i\beta)^{-2}$, up to this order we can express ν as

$$\nu = \left(\eta^{(0)} + \frac{1}{i\beta}\eta^{(1)} + \dots\right)C\exp\left(i\beta\int_{z}^{z} y^{(0)}\,dz + \int_{z_e}^{z} y^{(1)}\,dz + \dots\right) \qquad \dots.(B.32)$$

and, after substitution into equation (B.11) and comparison of terms with like powers of $i\beta$, we find

$$\left.\begin{aligned}\eta^{(0)} &= \{1+\tfrac{1}{2}(\gamma+1)(1-z)/z\}^{\frac{1}{2}}\\ \eta^{(1)} &= \gamma - 1 - 2\eta^{(0)} - (\gamma+1)(1-z)y^{(1)}\end{aligned}\right\} \qquad \dots.(B.33)$$

$y^{(1)}$ being given by equations (B.28) and (B.29).

Finally computing ν at $z = z_e$ from equation (B.32) and recalling the condition (B.16) we find

$$\frac{\nu_e}{\sigma_e} = \frac{\theta - \varepsilon/\gamma}{\theta - \varepsilon}\,\eta_e^{(0)} + \frac{1}{i\beta}\left(\frac{\gamma-1}{\gamma}\,\frac{\varepsilon}{\theta-\varepsilon}\,\frac{\eta_e^{(0)}}{\dfrac{\gamma+1}{2}\,\dfrac{1}{z_e} - \dfrac{\gamma-1}{2}} + \frac{\theta - \varepsilon/\gamma}{\theta-\varepsilon}\,\eta_e^{(1)}\right) + \ldots \quad (\beta \gg 1) \qquad \ldots.(B.34)$$

with $\eta_e^{(0)}$, $\eta_e^{(1)}$ given by equations (B.33), (B.28) and (B.29) at $z = z_e$.

Higher order terms in the expansions (B.27), (B.30), (B.32) and (B.34) can easily be computed. Again we see that ν_e/σ_e depends only on β, z and θ/ε. For $\theta = 0$ and $\beta \to \infty$, equation (B.34) gives Tsien's result.

B.05. Solutions for All Frequencies in the Isentropic Case

It is possible to take advantage of the analytical properties of equation (B.12) to extend the computations to the whole range of frequencies. In order to avoid the complication connected with the determination of the particular solution of equations (B.12), we shall consider here only the isentropic case. With $\varepsilon = 0$ equation (B.12) is reduced to a homogeneous hypergeometric equation, of which the solution remaining non-singular at $z = 1$ is given by the known hypergeometric series in powers of $1 - z$

$$F(a, b, c; 1 - z) = 1 + \frac{ab}{c}(1 - z) + \frac{a(a+1)\,b(b+1)}{c(c+1)}\,\frac{(1-z)^2}{2!} + \ldots \qquad \ldots.(B.35)$$

with a, b and c given by:

$$\left.\begin{aligned} c &= a + b + 1 = 2\left(1 + \frac{i\beta}{\gamma+1}\right) \\ ab &= \frac{i\beta}{\gamma+1}\left(1 + \frac{i\beta}{2}\right) \end{aligned}\right\} \ldots.(B.36)$$

In principle, therefore, our problem is solved by taking

$$\sigma = C \,.\, F(a, b, c; 1 - z) \qquad \ldots.(B.37)$$

and computing ν from equation (B.11) with $\varepsilon = 0$ and with dF/dz obtained from the differentiation of the series (B.35). The ratio ν_e/σ_e is therefore determined and is independent of C.

However, this procedure cannot be followed in practical cases since z_e is generally quite small[24] and $1 - z_e$ is close to one, in a region where the convergence of the series (B.35) is too poor. The difficulty can be overcome with the help of the properties of the solutions of hypergeometric equations.

Simpler developments are obtained by using a series proportional to (B.35)

$$\mathrm{f}(a, b, c; 1-z) \equiv \frac{\Gamma(a)\Gamma(b)}{\Gamma(c)} F(a, b, c; 1-z)$$
$$= \sum_{s=0}^{\infty} (1-z)^s \frac{\Gamma(s+a)\Gamma(s+b)}{\Gamma(s+1)\Gamma(s+c)} \quad \ldots.(B.38)$$

where $\Gamma(x)$ represents the gamma function of argument x. This non-singular solution around $z = 1$ can be expressed as a linear combination of the fundamental system of the hypergeometric equation around $z = 0$.

One such relationship, particularly useful in the present case, is[36]

$$\mathrm{f}(a, b, c; 1-z)$$
$$= z^{c-a-b} \frac{\mathrm{g}(c-a, c-b, 1+c-a-b; z)}{\Gamma(c-a)\Gamma(c-b)\cos(c-a-b)\pi} \quad \ldots.(B.39)$$

where

$$\mathrm{g}(a', b', c'; z) = -\pi \cot(c'\pi)[\mathrm{f}(a', b', c'; z)$$
$$-z^{1-c'}\mathrm{f}(a'+1-c', b'+1-c', 2-c'; z)] \quad \ldots.(B.40)$$

the two functions f being given by the corresponding series (B.38). With the particular value (B.36) of c, the value of c' to be used in relation (B.40) is given, following (B.39), by $c' = 2$. When c' is an integer n, the quantity in the brackets of equation (B.40) vanishes, and the factor preceding the brackets becomes infinite. The corresponding value of g can be found through a limiting process to be[36], for $n > 1$,

$$\mathrm{g}(a', b', n; z)$$
$$= -\mathrm{f}(a', b', n; z)\log z + \sum_{s=-1}^{s=-(n-1)} (-z)^s \frac{\Gamma(-s)\Gamma(s+a')\Gamma(s+b')}{\Gamma(s+n)}$$
$$- \sum_{s=0}^{\infty} z^s \frac{\Gamma(s+a')\Gamma(s+b')}{\Gamma(s+1)\Gamma(s+n)} [\psi(s+a') + \psi(s+b')$$
$$- \psi(s+1) - \psi(s+n)] \quad \ldots.(B.41)$$

where $\psi(x)$ represents, as usual, the logarithmic derivative of the gamma function with respect to the argument x.

Finally from equations (B.38), (B.39) and (B.41), with a, b and c given by equations (B.36), and therefore $n = 2$, we find

$$\mathrm{f}(a, b, c; 1-z) = \log z \sum_{s=1}^{\infty} A_s z^s$$
$$+ \sum_{s=1}^{\infty} A_s D_s z^s + \frac{2(\gamma+1)}{i\beta(2+i\beta)} \quad \ldots.(B.42)$$

with the coefficients A_s given by the recurrence relation

$$\frac{A_{s+1}}{A_s} = 1 - \frac{\beta^2}{2(\gamma+1)s(s+1)} + i\beta \frac{2s+1}{(\gamma+1)s(s+1)}; \quad A_1 = 1$$

and with

$$D_s = \psi(s+a) + \psi(s+b) - \psi(s) - \psi(s+1) \quad \ldots.(B.43)$$

The computation of D_s can be performed with the help of the series expression of $\psi(x)$

$$\psi(x) = \log x - \frac{1}{2x} + \frac{1}{2}\sum_{r=1}^{\infty} \frac{(-1)^r B_r}{r x^{2r}}$$

where $B_1 = 1/6$, $B_2 = 1/30, \ldots$ are the Bernoulli numbers.

We obtain

$$D_s = \log \frac{A_{s+1}}{A_s} + \frac{1}{2}\left[\frac{1}{s} + \frac{1}{s+1} - \frac{2s+1+2i\beta/(\gamma+1)}{s(s+1)} \frac{A_s}{A_{s+1}}\right] + \sum_{r=1}^{\infty} (-1)^r \frac{B_r}{2r}[(s+a)^{-2r} + (s+b)^{-2r} - s^{-2r} - (s+1)^{-2r}] \quad \ldots.(B.44)$$

The convergence of the last series is very fast for high values of s. D_s has therefore been computed for this series (B.44) only for the highest value of s needed in the evaluation of relation (B.42), and for the other values of D_s from the recurrence relation

$$D_{s+1} - D_s = \frac{1}{s+a} + \frac{1}{s+b} - \frac{1}{s} - \frac{1}{s+1}$$

The solution (B.37) can be expressed as

$$\sigma = C' f(a, b, c; 1-z)$$

with the constants C' and C connected through equation (B.38); and the expression (B.42) provides the series expansion suited for computations at $z = z_e$. Actually to determine the downstream boundary condition of the chamber, equivalent to the presence of the nozzle, we need only calculate v/σ at $z = z_e$ which may be determined from series (B.42) using equation (B.11). The quantity $(1/f)\,(df/dz) = (1/F)\,(dF/dz)$ is independent of the values of the integration constants C or C' and can be used in evaluating v/σ. The real and the imaginary part of this quantity, the first divided by β^2 and the second by β for convenience of scale, are given for $\gamma = 1{\cdot}2$ in *Figures 57* and *58*. The number of terms used in the computation was sufficient to give very accurate values up to $z = 0{\cdot}2$ for series (B.42) and reasonably accurate data up to $z = 0{\cdot}3$; the corresponding limits for the series (B.35) are $z = 0{\cdot}8$ and $z = 0{\cdot}7$. Between $0{\cdot}3$ and $0{\cdot}7$ the dotted curve is only interpolated. The lines for $\beta = 0$ are entirely computed from the equations:

$$\lim_{\beta\to 0}\left[\frac{1}{\beta^2}\mathrm{R.P.}\left(\frac{1}{\sigma}\frac{d\sigma}{dz}\right)\right] = -\frac{1}{(\gamma+1)^2(1-z)^2}\cdot\left[2\int_1^z \frac{\log z}{1-z}\,dz + \frac{\gamma-1}{2}(1-z) + \left(z + \frac{\gamma+1}{2}\right)\log z - \frac{z\log z(\log z + 1 - z)}{1-z}\right]$$

$$\lim_{\beta\to 0}\left[\frac{1}{\beta}\mathrm{I.P.}\left(\frac{1}{\sigma}\frac{d\sigma}{dz}\right)\right] = \frac{\log z + 1 - z}{(\gamma+1)\,(1-z)^2}$$

which can be derived with the procedure used previously for small β.

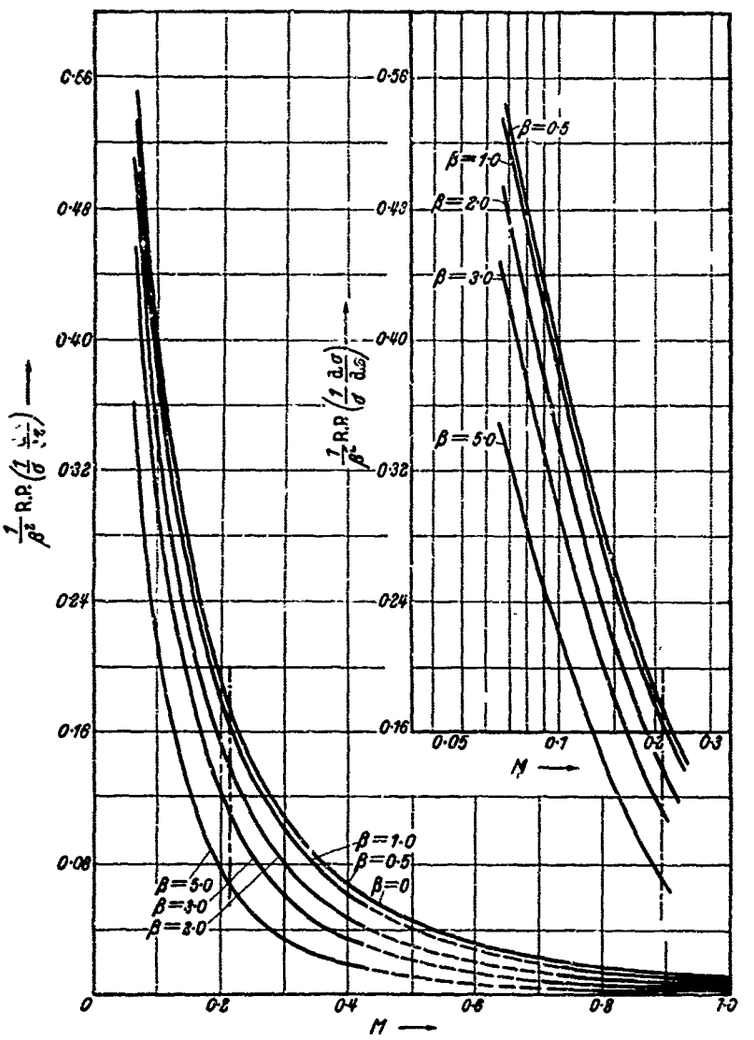

Figure 57. $1/\beta^2$ *times the real part of* $(d\sigma/dz)/\sigma$ *as a function of local steady state flow Mach number* M *for isentropic oscillations of the reduced frequency* β *in the nozzle. Calculation is based on the series* (B.35) *and* (B.42). σ *is the amplitude of density oscillation.* (*By courtesy of* L'Aerotecnica, Roma)

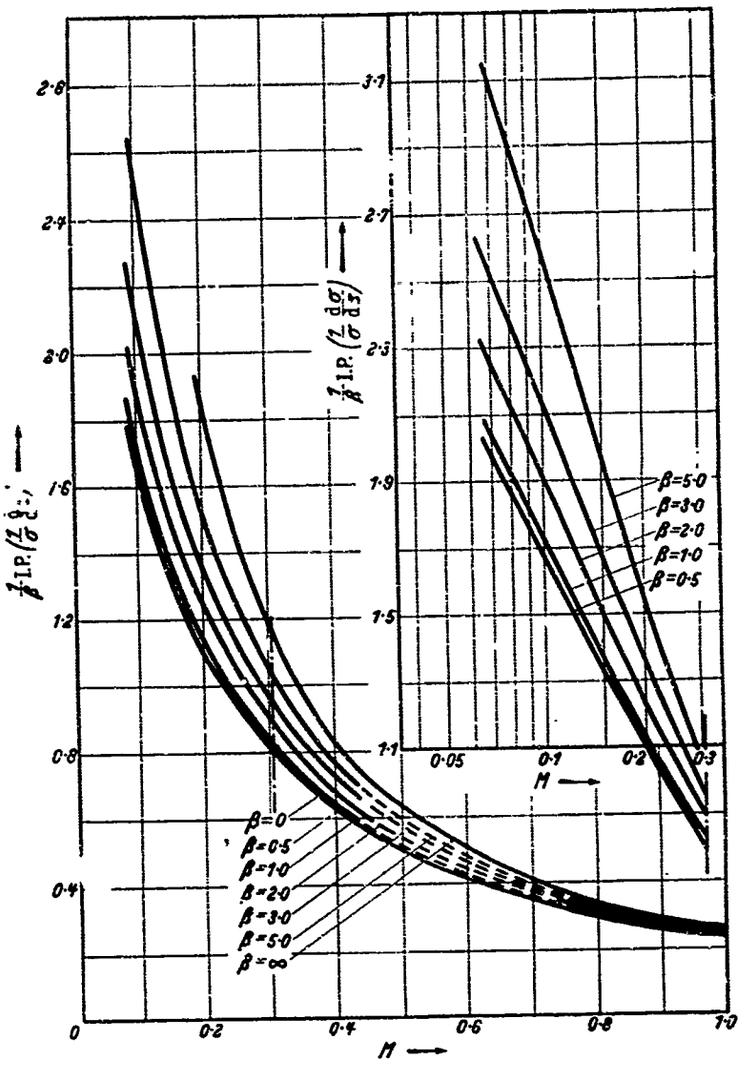

Figure 58. $1/\beta$ *times the imaginary part of* $(d\sigma/dz)/\sigma$ *as a function of local steady state flow Mach number* M *for isentropic oscillations of the reduced frequency* β *in the nozzle. Calculation is based on the series (B.35) and (B.42).* σ *is the amplitude of density oscillation.* (*By courtesy of* L'Aerotecnica, Roma)

NOTE: In the figures on the following pages, and throughout the text of Appendix B, it should be observed that the subscript $_e$ denotes conditions at the nozzle entrance and is used interchangeably with the subscript $_1$, e.g. $\bar{u}_1 = \bar{u}_e = u_e/c_e = [2z_e/(\gamma + 1)]^{1/2}$.

For $\beta \to \infty$ the first of the two quantities goes to zero, but the second one takes the expression

$$\lim_{\beta\to\infty}\left[\frac{1}{\beta}\,\mathrm{I}\,.\,\mathrm{P}\,.\left(\frac{1}{\sigma}\frac{\mathrm{d}\sigma}{\mathrm{d}z}\right)\right] = y^{(0)}$$

$y^{(0)}$ being given by equation (B.28). Both quantities tend logarithmically to infinity at $z = 0$, a value which can never occur in practice.

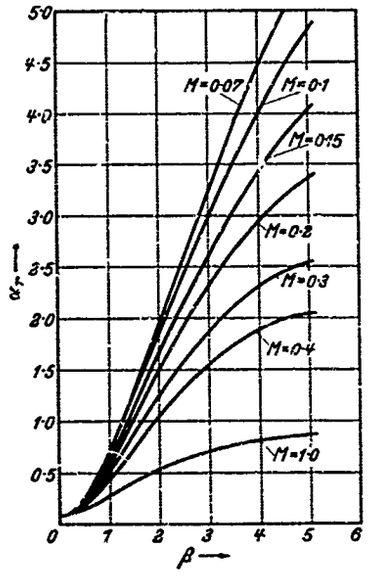

Figure 59

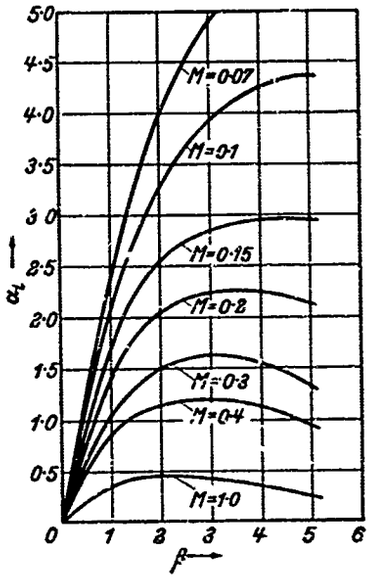

Figure 60

Figure 59. The real part α_r of the specific admittance ratio α as a function of the reduced frequency β of the isentropic oscillation in the nozzle at different flow Mach numbers. (*By courtesy of* L'Aerotecnica, Roma)

Figure 60. The imaginary part α_i of the specific admittance ratio α as a function of the reduced frequency β of the isentropic oscillation in the nozzle at different flow Mach numbers. (*By courtesy of* L'Aerotecnica, Roma)

From $(1/\sigma)\,(\mathrm{d}\sigma/\mathrm{d}z)_e$ and equation (B.11) the quantity $\alpha = \nu_e/\sigma_e$ has been computed. *Figures 59* and *60* show the real and the imaginary part of α as a function of β. The Mach number of the mean flow entering the nozzle is used instead of z_e in these figures where

$$z_e = \tfrac{1}{2}(\gamma+1)\bar{u}_e^2 = \tfrac{1}{2}(\gamma+1)\,(u_e/c_s)^2 = \tfrac{1}{2}(\gamma+1)M^2/[1+\tfrac{1}{2}(\gamma-1)M^2] \quad \ldots.(\mathrm{B.45})$$

c_s representing here the stagnation sound velocity. *Figure 61* gives a representation of α in the complex plane, from which the phase and amplitude relations between the velocity and density fractional fluctuations are immediately deduced. For a given Mach number at the nozzle entrance the ratio of the amplitudes increases steadily with increasing frequencies, while the phase goes from zero to a maximum which is always an important fraction of $\pi/2$ and then decreases back to zero.

Finally in *Figures 62* and *63* the real and imaginary parts of $\alpha\bar{u}_e$, with $\bar{u}_e$ given by condition (B.45), are plotted against β for various values of M. The knowledge of these two quantities is sufficient to represent completely the effect of a supercritical nozzle on the behaviour of a system when the

oscillations are isentropic and the velocity distribution is linear. If the last condition is still true but the entropy oscillates, the solution of equation

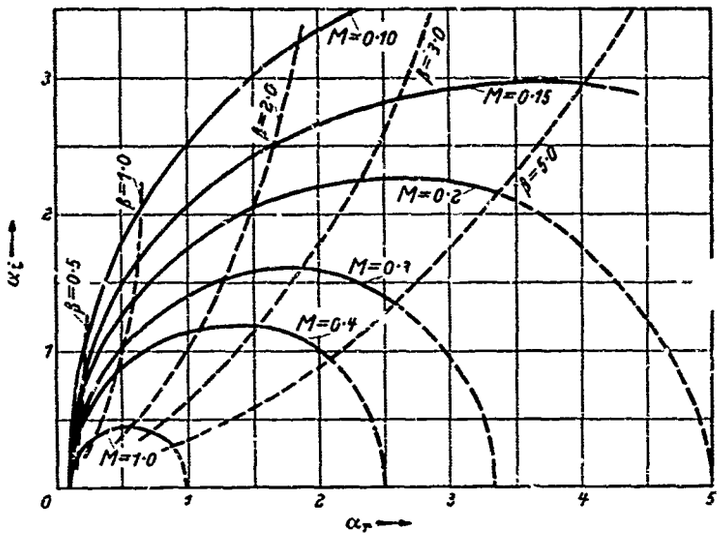

Figure 61. Polar plot of the specific admittance ratio $\alpha = \alpha_r + i\alpha_i$ for isentropic oscillations in the nozzle. (By courtesy of L'Aerotecnica, Roma)

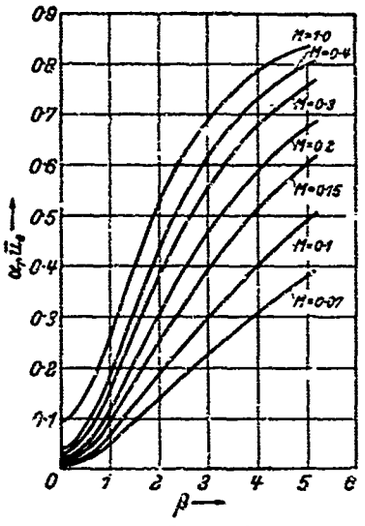

Figure 62

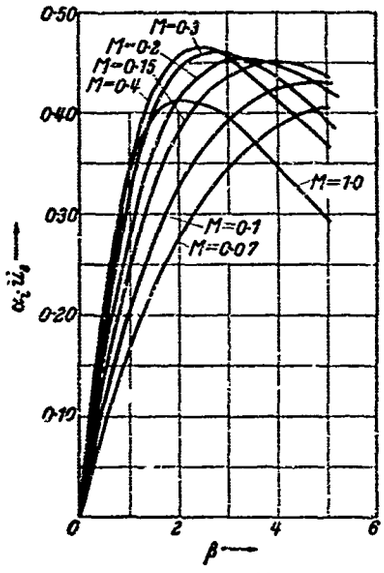

Figure 63

Figure 62. $\alpha_r \bar{u}_e$ as a function of the reduced frequency β of isentropic oscillations in the nozzle at different flow Mach numbers M corresponding to the different values of the dimensionless velocity $\bar{u}_e$ as defined in Chapter 3

Figure 63. $\alpha_i \bar{u}_e$ as a function of the reduced frequency β of isentropic oscillations in the nozzle at different flow Mach numbers M corresponding to the different values of the dimensionless velocity $\bar{u}_e$ as defined in Chapter 3

(B.12) can be obtained as the sum of the calculated homogeneous solution and a particular solution of the non-homogeneous equation. This particular solution can be obtained without fundamental difficulties from the

homogeneous solution. It only involves a certain amount of numerical computation. The case of a non-linear velocity distribution is, however, more involved and is briefly discussed next.

B.06. Non-linear Velocity Distribution

For a general velocity distribution the system (B.06) can be non-dimensionalized relating, for instance, the velocities to the critical sound velocity c_* and the lengths to $l_{sub} \cdot L$. If we take

$$x/l_{sub} \cdot L = \xi, \quad (0 \leqslant \xi \leqslant 1); \qquad u/c_* = w(\xi), \quad (w_e \leqslant w \leqslant 1)$$

where w is considered an arbitrary, monotonically increasing function of ξ, with $w(1) = 1$, and if the entropy oscillation is zero, the system of equations (B.06) is transformed into the following:

$$w\frac{\mathrm{d}v}{\mathrm{d}\xi} + w\frac{\mathrm{d}\sigma}{\mathrm{d}\xi} + i\beta\sigma = 0 \qquad \ldots\ldots(\text{B.46})$$

$$w\frac{\mathrm{d}v}{\mathrm{d}\xi} + \left(\frac{\gamma+1}{2w} - \frac{\gamma-1}{2}w\right)\frac{\mathrm{d}\sigma}{\mathrm{d}\xi} + \left(2\frac{\mathrm{d}w}{\mathrm{d}\xi} + i\beta\right)v - (\gamma-1)\frac{\mathrm{d}w}{\mathrm{d}\xi}\sigma = 0 \qquad \ldots\ldots(\text{B.47})$$

where $\beta = \omega l_{sub} \cdot L/c_*$† and where use has been made of the relation

$$(c/c_*)^2 = \tfrac{1}{2}(\gamma+1) - \tfrac{1}{2}(\gamma-1)\,w^2$$

Eliminating $\mathrm{d}v/\mathrm{d}\xi$ from equations (B.46) and (B.47) one obtains the equation

$$\frac{\gamma+1}{2}\frac{1-w^2}{w}\frac{\mathrm{d}\sigma}{\mathrm{d}\xi} + \left(2\frac{\mathrm{d}w}{\mathrm{d}\xi} + i\beta\right)v - \left[(\gamma-1)\frac{\mathrm{d}w}{\mathrm{d}\xi} + i\beta\right]\sigma = 0 \qquad \ldots\ldots(\text{B.48})$$

For general $w(\xi)$, no analytical treatment of the system is possible; one can, however, determine a series solution in the vicinity of $\xi = 1$ which will satisfy the condition of regularity. This series will give a sufficiently accurate value down to a certain $\xi < 1$; from there on, one has to proceed with numerical integration. From equation (B.48) we find at $w = 1$ and for non-singular $\mathrm{d}\sigma/\mathrm{d}\xi$

$$\left(\frac{v}{\sigma}\right)_* = \frac{(\gamma-1)\,(\mathrm{d}w/\mathrm{d}\xi)_* + i\beta}{2(\mathrm{d}w/\mathrm{d}\xi)_* + i\beta}$$

no matter what the nozzle shape is. The oscillation of the Mach number at the throat is thus given by

$$\sigma_*\left[\left(\frac{v}{\sigma}\right)_* - \frac{\gamma-1}{2}\right] = \sigma_*\frac{(3-\gamma)i\beta}{2[2(\mathrm{d}w/\mathrm{d}\xi)_* + i\beta)]}$$

and is therefore non-vanishing for $\beta \neq 0$. Thus the sonic line oscillates around the throat, and the amplitude of the oscillations could be related to that of the other quantities.

† Note that the definition of β in this section differs slightly from that given in equation (B.10).

For very low and very high frequencies and a general velocity distribution it is possible to find, as in the case of a linear distribution, series expansions in positive or negative powers of $i\beta$. Here we shall only determine the series expansion for small frequencies which is particularly useful for the problem of low frequency instability. Introducing into equations (B.46) and (B.48) the series

$$\sigma = \sum_{h=0}^{\infty} \sigma^{(h)}(i\beta)^h; \qquad v = \sum_{h=0}^{\infty} v^{(h)}(i\beta)^h$$

and equating the coefficients of $(i\beta)^h$ to zero, we obtain the following recurrence relations

$$w\left(\frac{\mathrm{d}\sigma^{(h)}}{\mathrm{d}\xi} + \frac{\mathrm{d}v^{(h)}}{\mathrm{d}\xi}\right) = -\sigma^{(h-1)} \qquad \ldots.(B.49)$$

$$\frac{\gamma+1}{2}\frac{1-w^2}{w}\frac{\mathrm{d}\sigma^{(h)}}{\mathrm{d}\xi} + 2\frac{\mathrm{d}w}{\mathrm{d}\xi}v^{(h)} - (\gamma-1)\frac{\mathrm{d}w}{\mathrm{d}\xi}\sigma^{(h)} = \sigma^{(h-1)} - v^{(h-1)} \qquad \ldots.(B.50)$$

For $h = 0$ the right hand members of these equations must be taken as zero. In the same way as for the linear velocity distribution it can be found that the only regular solution for $h = 0$ is with $v^{(0)}$ and $\sigma^{(0)}$ constants and related by

$$v^{(0)} = \tfrac{1}{2}(\gamma-1)\sigma^{(0)} = \tfrac{1}{2}\theta = \text{const.} \qquad \ldots.(B.51)$$

This relation simply expresses the fact that for quasi-steady solutions the Mach number variations at each section of the duct must be zero, because the Mach number at each section in quasi-steady state is determined only by the ratio of the area of the section to the section of the throat. Since at the entrance section equation (B.16) still applies, we see that again the boundary condition (B.24) holds for arbitrary k

$$\sigma_e^{(h)} = 0 \qquad (h = 1, 2 \ldots) \qquad \ldots.(B.52)$$

Now integrating equation (B.49), we obtain

$$v^{(h)} = -\sigma^{(h)} - \int_1^{\xi} \frac{\sigma^{(h-1)}}{w}\,\mathrm{d}\xi + C \qquad \ldots.(B.53)$$

where C is an arbitrary constant to be determined. Replacing this value of $v^{(h)}$ in equation (B.50) we find

$$\frac{\gamma+1}{2}\left[(1-w^2)\frac{\mathrm{d}\sigma^{(h)}}{\mathrm{d}\xi} - \frac{\mathrm{d}w^2}{\mathrm{d}\xi}\sigma^{(h)}\right]$$

$$= w[\sigma^{(h-1)} - v^{(h-1)}] + \frac{\mathrm{d}w^2}{\mathrm{d}\xi}\left(\int_1^{\xi}\frac{\sigma^{(h-1)}}{w}\,\mathrm{d}\xi - C\right)$$

which can be integrated immediately and, after integration by parts, gives

$$\frac{\gamma+1}{2}(1-w^2)\sigma^{(h)}$$

$$= \int_{\xi}^{1} wv^{(h-1)}\,\mathrm{d}\xi - \int_{\xi}^{1}\frac{\sigma^{(h-1)}}{w}\,\mathrm{d}\xi - (1-w^2)\left(\int_1^{\xi}\frac{\sigma^{(h-1)}}{w}\,\mathrm{d}\xi - C\right) \qquad \ldots.(B.54)$$

Here the new integration constant has been determined in such a way as to make the right hand member vanish at $w = 1$, in order that σ_h may remain regular. The constant C is obtained by applying the boundary condition (B.52) at $\xi = \xi_e$. This gives:

$$(1 - w_e^2)\left(\int_1^{\xi_e} \frac{\sigma^{(h-1)}}{w}\,d\xi - C\right) = \int_{\xi_e}^1 w\nu^{(h-1)}\,d\xi - \int_{\xi_e}^1 \frac{\sigma^{(h-1)}}{w}\,d\xi$$
$$= -(1 - w_e^2)\nu_e^{(h)} \qquad \ldots.(B.55)$$

the last equality being the consequence of equations (B.52) and (B.53). With the help of equation (B.55), equation (B.54) can be written as

$$\frac{\gamma+1}{2}(1 - w^2)\sigma^{(h)} = \int_\xi^1 w\nu^{(h-1)}\,d\xi - \int_\xi^1 \frac{\sigma^{(h-1)}}{w}\,d\xi$$
$$- (1 - w^2)\left[\int_{\xi_e}^{\xi} \frac{\sigma^{(h-1)}}{w}\,d\xi - \nu_e^{(h)}\right] \qquad \ldots.(B.56)$$

where the value of $\nu_e^{(h)}$ is determined in terms of the $(h-1)$th quantities by equation (B.55). From equation (B.53) one obtains then

$$\frac{\gamma+1}{2}(1 - w^2)\nu^{(h)} = -\int_\xi^1 w\nu^{(h-1)}\,d\xi$$
$$+ \int_\xi^1 \frac{\sigma^{(h-1)}}{w}\,d\xi - \frac{\gamma-1}{2}(1 - w^2)\left[\int_{\xi_e}^{\xi} \frac{\sigma^{(h-1)}}{w}\,d\xi - \nu_e^{(h)}\right] \qquad \ldots.(B.57)$$

The recurrence relations (B.56) and (B.57) allow calculation of all the functions $\sigma^{(h)}$, $\nu^{(h)}$ starting from the values (B.51). For the determination of $\alpha = \nu_e/\sigma_e$ only the quantities $\nu_e^{(h)}$ are required, because $\sigma_e^{(h)}$ are given by condition (B.52). The first two values are given by:

$$\frac{\nu_e^{(1}}{\sigma^{(0)}} = \frac{1}{1 - u_e^2}\int_{\xi_e}^1 \left(\frac{1}{w} - \frac{\gamma-1}{2}w\right)d\xi$$

$$\frac{\nu_e^{(2)}}{\sigma^{(0)}} = \frac{2}{\gamma+1}\left[\left(\frac{\nu_e^{(1)}}{\sigma^{(0)}}\right)^2 - \frac{2}{1 - w_e^2}\int_{\xi_e}^1 \frac{d\xi}{w(1 - w^2)}\int_\xi^1 \left(\frac{1}{w} - \frac{\gamma-1}{2}w\right)d\xi'\right]$$

Further terms can be found without fundamental difficulty.

Up to the second term of the expansion $(\nu_e^{(1)}/\sigma^{(0)})$ the specific admittance ratio $\alpha = \nu_e/\sigma_e$ of the nozzle expressed in terms of the original physical variables is given by

$$\alpha = \tfrac{1}{2}(\gamma - 1) + i\Omega^* k \qquad \ldots.(B.58)$$

where the quantity k coincides with the quantity introduced in equation (2.01.08) and is explicitly given by

$$k = \frac{c_*}{c_*^2 - u_e^2}\int\left(\frac{c_*}{u} - \frac{\gamma-1}{2}\frac{u}{c^*}\right)dx \qquad \ldots.(B.59)$$

the integration being performed on the whole convergent portion of the nozzle. This constant k represents the effect of the inertia of the gas in the

convergent portion of the nozzle in causing a phase difference between the oscillations of velocity and pressure of the gas entering the nozzle for low frequencies. From the quantity k one can determine the quantity b of equation (2.01.09). If the reduced frequency is defined through the corrected gas residence time $\theta_r = \theta_g(1 + b)$, so that

$$\omega/\Omega^* = \theta_g(1 + b)$$

b is given by the solution of the equation

$$b(1 + b) = k/\gamma\theta_g \qquad \ldots.(B.60)$$

In practical cases b is sufficiently smaller than unity so that its value is approximately given by the right hand side of equation (B.60). It has been explained in Section 2.03 that the net effect of the presence of this phase lead component of the nozzle transfer function is to modify the reference time characteristic of the low frequency oscillation from the gas residence time in the chamber, i.e.

$\theta_g = \bar{M}_g/\bar{m}$ = mass in the chamber/mass outflow rate to new reference time

$$(1 + b)\theta_g = (1 + b)\bar{M}_g/\bar{m}$$

This indicates that, so far as the analysis of the stability of the low frequency oscillations is concerned, the effective inertia of the gas in the convergent portion of the nozzle is equal to b times the inertia of the gas in the chamber. The following question naturally arises as to how this effective inertia bM compares with the actual inertia of the gas in the subsonic portion of the nozzle. But owing to the varying density of the gas in the nozzle and to the engineering practice of defining the gas residence time in terms of the chamber volume, V_c, we would rather compare the volume V_n of the subsonic portion of the nozzle with the effective volume bV_c. In other words, we would rather, following the conventions in acoustics, determine the end correction of the supercritical nozzle in terms of the additional length of the chamber (corresponding to the additional length of the organ pipe in acoustics). Thus let χ denote the end correction of the chamber volume per unit volume of the convergent section of the nozzle. Then

$$\chi = bV_c/V_n = b\theta_g/V_n \cdot \bar{m}/\rho_0$$

where $\bar{m}$ is the mass outflow rate which can be evaluated at the sonic throat and ρ_0 is the stagnation density of the gas as an approximation to the chamber condition. V_n can be obtained by integrating the sectional area of the nozzle over the entire length of the convergent portion. Thus, with $b\theta_g$ given approximately by k/γ and k given by equation (B.59), one obtains after some manipulation the following

$$\chi = \frac{1}{\gamma}\frac{1}{1 - w_c^2}\frac{\displaystyle\int_0^1\left[\frac{1}{w(\xi)} - \frac{\gamma - 1}{2}w(\xi)\right]d\xi}{\displaystyle\int_0^1\left[1 - \frac{\gamma - 1}{\gamma + 1}w(\xi)^2\right]^{-\frac{1}{\gamma-1}}\frac{1}{w(\xi)}d\xi} \qquad \ldots.(B.61)$$

The integrals can be evaluated at least numerically or graphically when

$w(\xi)$ is known. For a given type of $w(\xi)$ this factor χ depends only on the entering velocity w_e, and the adiabatic index γ of the gas. For a given value of γ, $w_e = u_e/c_*$ is a function only of the contraction ratio of the nozzle A_*/A_e. Thus, this correction factor χ is a function of the geometry of the nozzle or $w(\xi)$ alone.

The value of w_e for conventional rocket motors is usually of the order of 0.1 (except for throatless rockets) and w increases monotonically toward the maximum value of unity at $\xi = 1$. Conventional nozzles are usually constructed with a surface of revolution generated by a circular arc near the sonic throat and preceded by a tangent cone. Thus $w(\xi)$ increases from w_e rather slowly in the conical region and then increases almost linearly toward the throat. As a result $w(\xi)$ remains small of $O(w_e)$ for a considerable range of ξ, the more considerable if the convergent angle of the conical part becomes smaller. If one writes equation (B.61) as

$$\chi = \frac{1}{\gamma}\frac{1}{1-w_e^2} \cdot \frac{1-\frac{1}{2}(\gamma-1)E_1}{1+\frac{1}{\gamma+1}E_1+\frac{2\gamma-1}{2!(\gamma+1)^2}E_3+\frac{(2\gamma-1)(3\gamma-2)}{3!(\gamma+1)^3}E_5+\ldots} \quad \ldots\ldots(B.62)$$

where $$E_j = \int_0^1 w^j(\xi)\,d\xi \Big/ \int_0^1 \frac{d\xi}{w(\xi)}$$

one easily observes that $0 < E_{j+1} < E_j < 1$ ($j = 1, 2, 3$, etc.) and that all E_j's with $j \geqslant 1$ become smaller when the value of $w(\xi)$ becomes smaller for given ξ. It is also clear that the ratio of the two integrals in equation (B.61) is less than unity and therefore

$$\chi < \frac{1}{\gamma}\frac{1}{1-w_e^2} \simeq \frac{1}{\gamma}$$

Sample calculations based on equation (B.61) for a conventional nozzle with $w(\xi)$ given as

$$w(\xi) = \frac{4w_1^3}{(1-\lambda-3w_1)^2} \qquad \text{for } w < w_1$$

$$w(\xi) = 1-\lambda \qquad \text{for } w > w_1$$

with λ indicating the following dimensionless distance from the sonic throat

$$\lambda = 1/C_* \cdot (du/dx)_*(l_{sub} \cdot L - x)$$

where $(du/dx)_*$ is the dimensional velocity gradient at the throat, indicate that the ratio of these two integrals is very close to unity. For the case with $w_e = 0{\cdot}1$ and $w_1^2 = 0{\cdot}3$ the ratio of the two integrals is 0·96. Calculated results show that for a given value of w_e the ratio of the two integrals slowly decreases with increasing w_1; the effect is, however, rather insignificant. For a given value of w_1, if we decrease the entering velocity w_e, the ratio of the two integrals also decreases, and the effect of decreasing w_e is considerably larger than that of decreasing w_1. But in any practical case, the ratio of the two integrals will remain in the range of 0·9–1·0 and a good average value would be 0·95 for the type of nozzle discussed previously. This qualitative result can be expected as a result of investigating the

expanded form of the two integrals as given in equation (B.57). Thus the end correction factor χ is in most of the practical cases given approximately by

$$\chi = 0{\cdot}95/\gamma \qquad \ldots.(B.63)$$

and the factor $1 - w_e^2$ is relatively insignificant. For combustion gases with γ of the order of 1·2–1·25, one should therefore add 75–80 per cent of the nozzle volume to the combustion chamber volume in calculating the corrected residence time.

It should be noticed, however, that the previous result is for the case of isentropic oscillations which can at its best be roughly correct for cases in which entropy oscillations are not too large. When the entropy oscillation is taken into account, the solution of equation (B.12) should be used in obtaining the factor b from which the factor χ can be determined without difficulty.

APPENDIX C

DISCUSSION OF EQUATION (2.04.09)

In the plane (ω^2, Ψ^2) the left hand side of equation (2.04.09) represents a hyperbola with centre at the point $(0, -2J/E)$ and a vertical asymptote coinciding with the axis of the ordinates and the second asymptote with slope J^2, as shown in *Figure 64*. The only branch of the hyperbola with a physical meaning is the upper branch, tangent to the axis $\Psi^2 = 0$ at the point $(1/EJ, 0)$.

The right hand side of equation (2.04.09) represents a rectangular hyperbola with a horizontal asymptote at $\Psi^2 = -1$ and a vertical asymptote

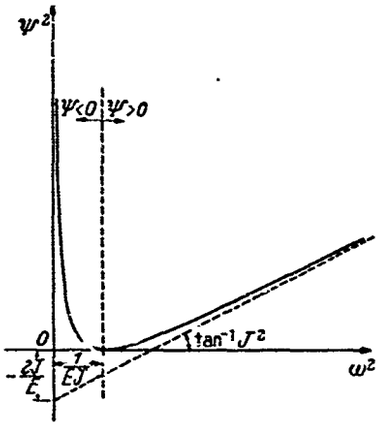

Figure 64. Schematic plot of Ψ^2 as expressed by the left hand side of equation (2.04.09)

at $\omega^2 = 2n - 1$. Thus for $n < \frac{1}{2}$ the vertical asymptote lies in the region of negative ω^2; for $n > \frac{1}{2}$, in the region of positive ω^2; and for $n = \frac{1}{2}$, it coincides with the axis $\omega^2 = 0$. The solutions of equation (2.04.09) are given by the intersections of the hyperbola of *Figure 64* with those of *Figure 65*. Only those intersections that lie in the first quadrant with positive ω^2 and Ψ^2 correspond to real solutions of ω and Ψ. A simple inspection of *Figures 64* and *65*(a) shows that if $n < \frac{1}{2}$ there are two such intersections when P is sufficiently large and there are no such intersections when P is small enough. For $n > \frac{1}{2}$ *Figures 64* and *65* show clearly that there is one, and only one, intersection no matter how large P is. The border case $n = \frac{1}{2}$ presents the behaviour of both cases, $n > \frac{1}{2}$ and $n < \frac{1}{2}$. In this case equation (2.04.09) becomes one of second degree and can be solved explicitly

$$2J^2\omega^2 = \frac{2J}{E} - 1 \pm \left[\left(\frac{2J}{E} - 1\right)^2 + 4J\left\{P(P+1) - \frac{1}{E^2}\right\}\right]^{\frac{1}{2}} \quad \ldots\ldots(C.01)$$

The following results are then obtained:

(*a*) if $P(P+1) > 1/E^2$ there is one, and only one, positive root ω^2. The behaviour is the same as that for $n > \frac{1}{2}$.

(*b*) if $1/E^2 > P(P+1) > (1/J)\,(1/E - 1/4J)$, there are two positive roots or none, depending upon $2J \gtrless E$.

(*c*) if finally $P(P+1) < (1/J)\,(1/E - 1/4J)$, there is no real root. Cases *b* and *c* show a behaviour similar to the case $n < \frac{1}{2}$.

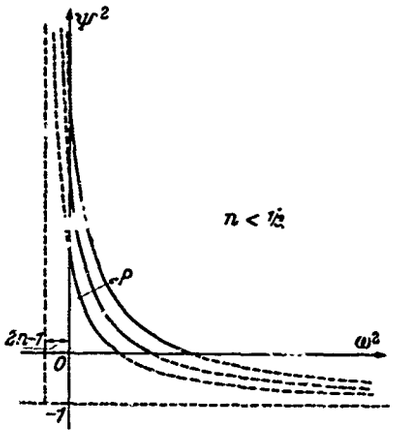

Figure 65(a)

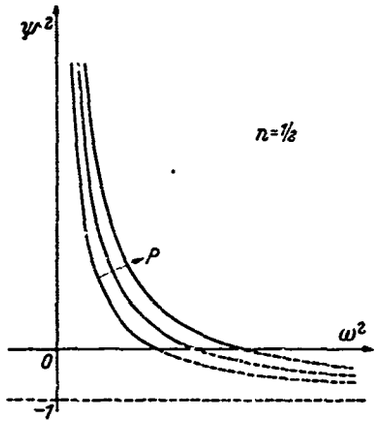

Figure 65(b)

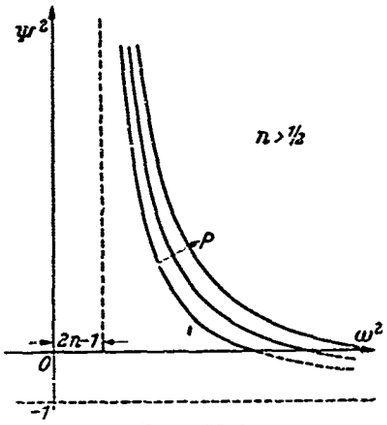

Figure 65(c)

Figure 65 (a), (b), (c). *Schematic plot of* Ψ^2 *as expressed by the right hand side of equation* (2.04.09) *for:* (a) $n < \frac{1}{2}$, (b) $n = \frac{1}{2}$, (c) $n > \frac{1}{2}$

For given values of n, P, E and J, once the corresponding real values of ω, if any, are found from equation (2.04.09), and the corresponding sign of Ψ is determined, then equation (2.04.06) gives a corresponding set of values for δ. From observation of *Figures 8, 9* and *10* we see that when there are two roots for ω, the larger root corresponds to the smaller values of δ and vice versa. If δ takes one of these values, an oscillation with $\Lambda = 0$ and $\Omega = \omega$ is possible, that is, we are on the stability boundary. If, without any change in n, P, E and J, the time lag is changed, then Λ must be different from zero. It will be larger than zero on one side of the boundary, corresponding to instability, and smaller than zero on the other side, where

the combustion is stable. It is important to determine, in addition to the stability boundary, the stable and the unstable sides. This can be done in the easiest way by differentiating equation (2.04.03) with respect to $\bar{\tau}$, for constant n, P, E and J, with $s = \Lambda + i\Omega$ and deriving the value of $d\Lambda/d\bar{\tau}$ on the stability boundary. After manipulation it is found that $(d\Lambda/d\bar{\tau})_{\Lambda=0}$ is equal to an essentially positive quantity times the expression

$$(2n - 1)\,[(P + n)^2 - n^2] + (\omega^2 + 1 - 2n)^2(2J^2\omega^2 + 1 - 2J/E)$$

Hence $(d\Lambda/d\bar{\tau})_{\Lambda=0}$ has the same sign as this expression or, in the particular case $n = \frac{1}{2}$, as the quantity $2J^2\omega^2 + 1 - 2J/E$.

Let us discuss in detail this particular case $n = \frac{1}{2}$. Suppose first the conditions are such that the solutions (C.01) are both positive. Then Λ goes through zero as an increasing function of $\bar{\tau}$ for the larger root ω_2 (corresponding to the smaller δ, as already noticed), and as a decreasing function of $\bar{\tau}$ for the smaller root ω_1 (corresponding to the larger δ). We conclude that when there are two real roots ω of equation (2.04.09) Λ is positive for $\bar{\tau}$ lying between the two critical values δ corresponding to the two roots of ω. Taking into account the fact that δ is multivalued, we find that the behaviour of Λ as a function of $\bar{\tau}$ for fixed values of n, P, E and J is schematically shown in *Figure 66*(a). The points A_1, A_2, A_3 are the values of δ corresponding to the larger root, ω_2; they correspond to the intersections of the vertical line through $\omega = \omega_2$ with the proper branch of the successive loops of *Figure 9*. Similarly the points B_1, B_2, B_3 correspond to the smaller root ω_1. We see that for each value of h there is a well determined range of instability. If one takes into account all the possible values of h, the combustion is stable when τ is below the value corresponding to A_1, or when it is contained in the range B_1A_2. For the example of *Figure 66*(a), there is only one such range of stability in addition to OA_1. However, it is clear that for other numerical conditions there can be more than one such range (however, always a discrete number); or there can be none. It is interesting to stress the fact that no matter what the magnitude of the time lag and the order of the unstable range, the frequencies are within the same range, between ω_1 and ω_2. What changes is only the number of periods of oscillation h contained in the time lag. In *Figure 66*(a) we have represented the case $n = \frac{1}{2}$ with two roots of ω. By changing the operating or the design conditions (for instance decreasing the pressure drop parameter P, which means increasing the pressure drop), one can always reduce the interval between ω_1 and ω_2, until the two roots come together [when the hyperbolae of *Figures 64* and *65*(b) are tangential to each other]. The corresponding ranges of instability A_1B_1, A_2B_2, etc. are then reduced to zero. If from now on we continue the change of conditions in the same direction we find the case in which equation (2.04.09) has no real roots. The corresponding distribution of Λ is schematically represented in *Figure 66*(b). Λ is now negative for all values of the time lag, and the combustion is always stable. If the change in conditions from those corresponding to *Figure 66*(a) to those corresponding to *Figure 66*(b) is gradual, the decrease of the unstable ranges will correspond to an increase in the width and the number of the ranges of stability such as B_1A_2; until eventually all the stability ranges together will spread over all the possible values

of $\bar{\tau}$, and the condition of *Figure 66*(b) will be reached. When the values of the parameters n, P, E and J of a given system are such that the situation of *Figure 66*(b) occurs, the system is always stable for arbitrary values of τ. We denote such systems as unconditionally stable. When the values of n, P, E and J are such that the situation of *Figure 66*(a) occurs, the system is stable only when the value of $\bar{\tau}$ is confined in a certain discrete number of

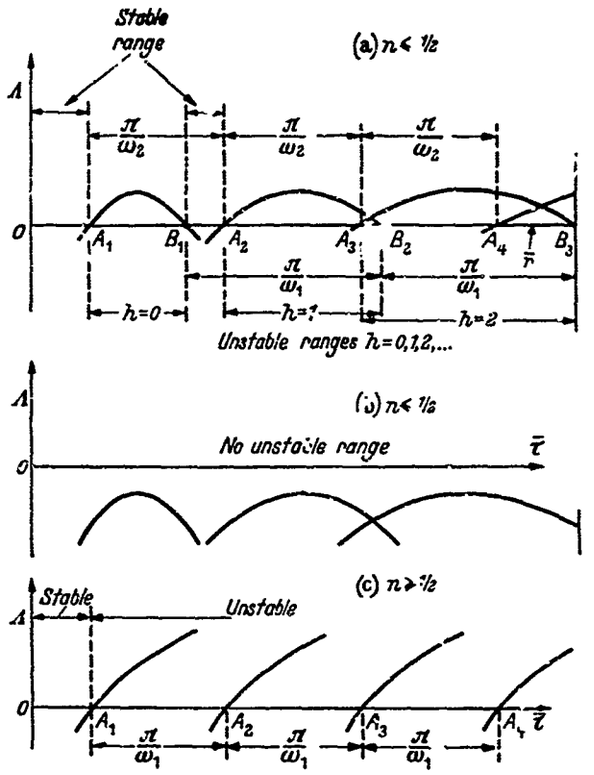

Figure 66. Qualitative diagram of the amplification coefficient A as a function of the sensitive time lag $\bar{\tau}$ of a liquid propellant rocket with constant rate feed

ranges of values. We designate such systems as conditionally stable. When a system is unconditionally stable, the hyperbolae of *Figures 64* and *65* do not intersect. Any change in the parameters of the system, which brings the two hyperbolae together to be tangential to each other and eventually to intersect, tends to decrease the 'unconditional stability' and vice versa.

The preceding discussion shows that in the case $n = \frac{1}{2}$, it is always possible to change the situation of *Figure 66*(a) to the one of *Figure 66*(b) by decreasing the value of P so that the hyperbola of *Figure 65*(b) is shifted sufficiently to the left so as not to touch the hyperbola of *Figure 64*. It is also clear that without any change in P, thus leaving the hyperbola of *Figure 65*(b) unchanged, the same results can be achieved by changing the feeding system parameters E and J through the displacement of the hyperbola of *Figure 64*. For instance, a decrease in the value of E displaces the point of tangency of the hyperbola with the axis of the abscissa to the right without changing

the slope of the asymptote. Thus, decreasing E has a stabilizing effect. The same is true for decreasing J. Therefore, if a system is unconditionally stable, the unconditional stability is improved by decreasing E, J or P. On the contrary, either when P increases, or when E or J or both increase, the system can become marginally unconditionally stable when the two hyperbolae become tangential to each other. Any further small change of the parameters in this direction will lead the hyperbolae to intersect and to define a number of discrete ranges of the values of $\bar{\tau}$ corresponding to unstable operation of the system. This system is conditionally stable. It will still remain stable if its time lag $\bar{\tau}$ is in the stable range but it will become unstable if the time lag $\bar{\tau}$ of the system falls in the unstable ranges.

Let us consider the conditionally stable configuration. If E and J are kept constant while P increases further (pressure drop decreases), the discrete unstable ranges of $\bar{\tau}$ grow in size, and gradually overlap each other till all the discrete stable ranges disappear except the lowest stable range OA_1 as shown in *Figure 66*(a). This lowest stable range OA_1 is kept decreasing in size while P increases even when $P(P+1)$ becomes greater than $1/E^2$ corresponding to the situation of *Figure 66*(c). On the other hand decreasing P tends to increase the stable ranges of $\bar{\tau}$ until the situation corresponding to *Figure 66*(b) occurs. Alternatively if we keep P constant and let E or J increase, each discrete unstable range of $\bar{\tau}$ like A_2B_2 in *Figure 66*(a) is shifted towards larger values of $\bar{\tau}$ and each discrete range like A_2B_2 grows in size with B_2 shifted more than A_2. As a result, while the discrete stable ranges disappear in succession as E or J increases, the lowest stable range OA_1 increases in extent with A_1 moving towards larger $\bar{\tau}$ in contrast with the situation of increasing P. Thus, if E or J increases from the value corresponding to a marginally unconditionally stable configuration, discrete unstable ranges of $\bar{\tau}$ appear and increase in extent with increasing E or J. But after a certain critical magnitude of E or J is reached before all the discrete stable ranges disappear, the total extent of the unstable range of $\bar{\tau}$ will decrease with further increase of E or J.

Now consider an unstable system with given P. If there is no discrete stable range of $\bar{\tau}$ except OA_1 for the given value of P, then conditional stability can be obtained only by a sufficiently large increase of E or J. If there is a discrete stable range like B_1A_2 and if the time lag $\bar{\tau}$ of the system lies in A_1B_1 then conditional stability can be obtained either by a sufficiently large increase of E or J to make $\bar{\tau}$ lie in OA_1 or by a proper decrease of E or J to make $\bar{\tau}$ lie in A_1B_2. If the decrease of E or J is too big, the system may become unstable again. If there are more than one discrete stable ranges like B_1A_2, B_2A_3, etc., the time lag of the unstable system may lie in the unstable range A_2B_2. In this case, with a gradual increase of E and/or J, the system will become stable at first and then become unstable with further increase of E and/or J and ultimately with sufficiently large increase of E and/or J the system will become stable again. From *Figures 9*, *64* and *65*(b), it can be observed that with $n = \frac{1}{2}$, the stable range OA_1 of the values of $\bar{\tau}$ can be made indefinitely large by indefinitely increasing E and J, even when the condition $P(P+1) > 1/E^2$ is reached corresponding to the situation of *Figure 66*(c). Therefore, for the cases with $n = \frac{1}{2}$ and a given value of P (corresponding to a given pressure drop Δp across the feed

system) it is always possible to obtain stability by a sufficiently large increase of E and J to enlarge the stable range OA_1 so as to include the time lag $\bar{\tau}$ of the system. But by sufficiently decreasing E and J, unconditional stability can also be obtained.

We have thus far discussed the case $n = \frac{1}{2}$ when the conditions are such that there are two real roots of equation (2.04.09) or more. It has been remarked that as under such circumstances the case $n = \frac{1}{2}$ has a similar behaviour to the case $n < \frac{1}{2}$, one can extend all the results of the previous discussion simply by continuity argument to the more general case of $n < \frac{1}{2}$. It can be observed, however, from *Figures 64* and *65*(a) or from equation (2.04.09) that for $n < \frac{1}{2}$ there are either two solutions of ω or none, no matter what the value of P is. Therefore a condition like $P(P+1) < 1/E^2$ for the existence of two real solutions of ω will not appear when $n < \frac{1}{2}$.

Let us now discuss the remaining possibility for $n = \frac{1}{2}$ quoted under item *a* in the discussion following equation (2.04.10); that is, the case where there is only one positive solution for ω^2 of equation (2.04.10) or one real root ω of equation (2.04.09). The real root of ω clearly corresponds to the upper sign of equation (2.04.10) in which case, the expression $2J^2\omega^2 + 1 - 2J/E$ is positive and therefore $(d\Lambda/d\bar{\tau})_{\Lambda=0} > 0$. Hence Λ goes through a single zero as an increasing function of $\bar{\tau}$ and the corresponding schematic representation is as shown in *Figure 66*(c). It is clear that the only stable range of $\bar{\tau}$ is OA_1 and that out of this range the oscillation is always unstable. From *Figures 64* and *65*(c) we find that when $n > \frac{1}{2}$ this is the only possible behaviour for any values of P and E while for the case $n = \frac{1}{2}$ this behaviour occurs only when $P(P+1) > 1/E^2$. Thus, for these cases, the only interesting critical value δ is the lowest one corresponding to $h = 0$, and the only interesting loop of *Figure 10* for $n > \frac{1}{2}$ is the lowest one. Unconditional stability is therefore no longer possible for $n > \frac{1}{2}$. We observe that this behaviour is qualitatively very similar to the one found for the case of intrinsic instability corresponding also to $n > \frac{1}{2}$. This is not surprising because the case with constant injection rate where the intrinsic instability is found, is included as the particular case $E = 0$ in the more general case discussed in this section. The corresponding value of Ψ is $-\infty$, which corresponds to the lower limit of the inequality (2.04.08), $\omega = (2n-1)^{\frac{1}{2}}$; that is, the point of minimum ω in *Figure 10*.

We shall thus concentrate our discussion on the lowest loop only in *Figure 10*. The upper branch and the lower branch of this loop correspond to different values of the system parameters E and J. For a given value of P and J if the elasticity parameter E increases from zero, Ψ increases algebraically but remains negative, and the value of δ moves from the value $[\pi - \tan^{-1}\{(2n-1)^{\frac{1}{2}}/(1-n)\}]/(2n-1)^{\frac{1}{2}}$ at the minimum value of $\omega = (2n-1)^{\frac{1}{2}}$ along the upper branch, as illustrated in *Figure 10*, towards larger values of ω. Thus a small increase of E from $E = 0$ is stabilizing. But if E is kept increasing, δ decreases after passing the maximum and a further increase of E is destabilizing till the value of $E = J[P^2 + 2nP + 2n - 1]$ is reached where $\Psi = 0$, and ω is at its maximum value. If E still increases from this value, the point δ begins to move along the lower branch of the loop toward smaller values of ω. Thus δ increases with increasing E; that

is, the effect of increasing E is again stabilizing. This qualitative trend persists all the way for E approaching ∞, that is, when χ is infinite [equation (2.02.09)] or p_1 is constant [equation (2.02.02)]. This is a particular case of the more general constant pressure system discussed in another section. The value of Ψ for $E = \infty$ is given by $J\omega$ which is always positive lying on the lower branch with its actual position determined by the value of n, P and J It is only when $J \to \infty$ that this end point coincides with the point of minimum ω.

The effect of increasing J from 0 to ∞ for given values of P and E is similar except that when $J = 0$ the critical value of $\bar{\tau}$ is somewhere on the upper branch with $\omega > (2n - 1)^{\frac{1}{2}}$ the value being again determined by the magnitudes of n, P and E.

For given values of E and J, the effect of increasing P or decreasing the pressure drop across the feeding system can be investigated in a similar way and is found to be in general destabilizing except when E is very small so that Ψ is large but negative.

It should be observed that for given values of $n > \frac{1}{2}$ and a given value of P, there is a maximum value of δ, as illustrated in *Figure 10*, corresponding to a small value of E. If the value of $\bar{\tau}$ of the system is bigger than this maximum value of δ, the system is definitely unstable. Stability cannot be achieved by any variations of E, or J, or both, but can only be achieved by increasing the parameter P through the reduction of the actual pressure drop in combination with proper changes in E and J. Or a different propellant with smaller values of n and $\bar{\tau}$ must be used under such circumstances. From another point of view, for a system with given values of P and $n > \frac{1}{2}$, the optimum combination of the elasticity and inertia of the feeding system is to have the system operating at this point of maximum δ, corresponding to a certain small value of E. Any changes of E or J from this condition make the system less stable.

Finally let us observe that when $n < \frac{1}{2}$ it is always possible to make a system unconditionally stable with a sufficiently small value of P, that is, a sufficiently large pressure drop $\Delta\bar{p}$ across the feeding system. In fact the inequality (2.04.08) shows that if $P \leqslant 1 - 2n$ no real value of ω can exist, and therefore we are certainly in the case of *Figure 66*(b). Hence $\Delta\bar{p}/\bar{p} \geqslant \frac{1}{2} \cdot 1/(1 - 2n)$ represents a sufficient stability criterion when $n < \frac{1}{2}$. However, we see immediately that when n approaches $\frac{1}{2}$ it becomes more and more difficult to satisfy this condition because of the exceedingly large values of $\Delta\bar{p}$ required. When $n > \frac{1}{2}$ no such sufficient stability criterion can be found. In fact we have seen that systems with $n > \frac{1}{2}$ will become unstable if the time lag $\bar{\tau}$ of the system is above a certain finite value of δ for given pressure drop $\Delta\bar{p}$ of the system no matter how large the pressure may be.

APPENDIX D

DISCUSSION OF EQUATION (2.05.07)

THE left hand side of equation (2.05.07) can be represented as a hyperbola in the (Φ^2, ω^2) plane, as shown in *Figure 67* and the right hand side by rectangular hyperbolae schematically represented in *Figures 68*(a), (b) and (c) for the three cases $n < \frac{1}{2}$, $n = \frac{1}{2}$, $n > \frac{1}{2}$. From the comparison of *Figures 67* and *68*(a) we see that when $n < \frac{1}{2}$ there is always a real root ω of equation (2.05.07) in the region where $\Phi < 0$, and there can be two

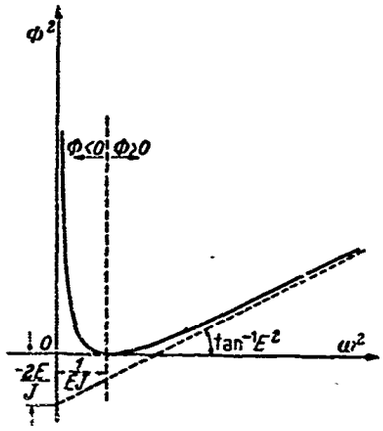

Figure 67. Schematic plot of Φ^2 as expressed by the left hand side of equation (2.05.07)

additional real roots or none in the region $\Phi > 0$, the appearance of these two roots being favoured by a large value of P and by large values of E and J. The same behaviour is found for $n = \frac{1}{2}$ from the comparison of *Figures 67* and *68*(b). Finally for $n > \frac{1}{2}$ comparing *Figures 67* and *68*(c) we see that here, too, one can find one or three roots ω. However, when there is one, this root is not necessarily on the side $\Phi < 0$. Moreover, there can be three roots for only some intermediate values of P, E and J. For sufficiently small or large values of the three parameters there is only one root. Following a method similar to the one used in the Appendix C one can show that $(\mathrm{d}\Lambda/\mathrm{d}\bar{\tau})_{\Lambda=0}$ is positive for the smallest and largest roots, and negative for the middle root when there are three roots, and that it is always positive when there is a single root. This result, when transferred to the $(\Lambda, \bar{\tau})$ plane, gives the behaviour shown in *Figures 69*(a), (b) and (c) where, however, the curves corresponding to $h = 1, 2, 3$, etc., have not been shown in order not to complicate the figure. Here again the larger root ω corresponds to the smaller value of δ and vice versa. Curve *69*(a) shows the behaviour of $\Lambda(\bar{\tau})$ when there are three real roots to equation (2.05.07). This behaviour can be found for all values of n, but more commonly for $n < \frac{1}{2}$. There are two ranges of stability OA_1 and B_1C_1 for $h = 0$. From the combination of these ranges with those pertaining to the higher integral values of h, it is seen that the stability range OA_1 is

left unchanged but the other range B_1C_1 may be reduced or suppressed by the unstable ranges pertaining to higher values of h. When $n \leqslant \frac{1}{2}$ it is possible to change from the condition corresponding to *Figure 69*(a) to the situation of *Figure 69*(b) by decreasing P (that is, increasing $\Delta\bar{p}$) or E or J. The unstable range A_1B_1 between the two larger roots ω is

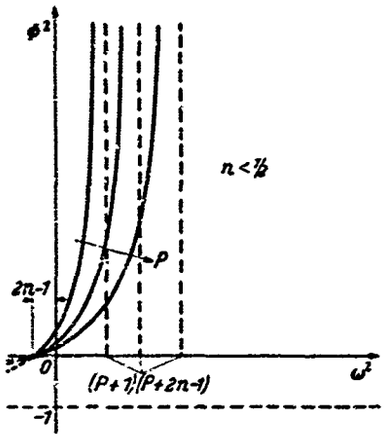

Figure 68(a)

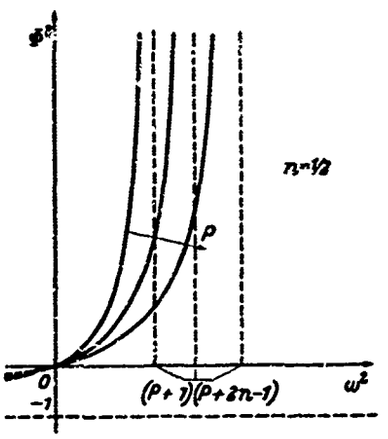

Figure 68(b)

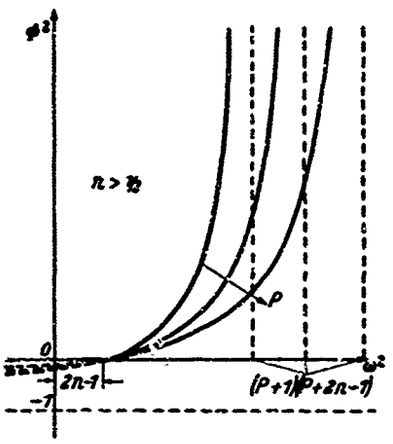

Figure 68(c)

Figure 68. Schematic plot of Φ^2 as expressed by the right hand side of equation (2.05.07) (a) $n < \frac{1}{2}$, (b) $n = \frac{1}{2}$, (c) $n > \frac{1}{2}$

now suppressed, and there is left only the instability range to the right of C_2. In this case, the unstable ranges corresponding to higher values of h are unimportant. When $n > \frac{1}{2}$ a switch from the situation of *Figure 69*(a) to that of *Figure 69*(b) is also possible; however, it requires generally a smaller value of P, E and J than that required in the previous case. On the other hand when P, E and J are increased above certain values, the situation of *Figure 69*(c) becomes possible, with the complete disappearance of the stability range B_1C_1, all the points to the right of the point A_2 being now unstable. We see from the preceding discussion that the distinction between the case $n < \frac{1}{2}$ and the case $n > \frac{1}{2}$ is less clear than in systems with a constant rate of supply. However, a neat distinction can be found when, for particular values of the parameters, a given physical configuration can be

considered as belonging both to the constant pressure and to the constant rate system. For instance, when we take $J = \infty$ in a system with constant pressure feed, the resulting formulae coincide exactly with those obtained for $J = 0$ in the constant rate case. The infinite length of the feed lines is

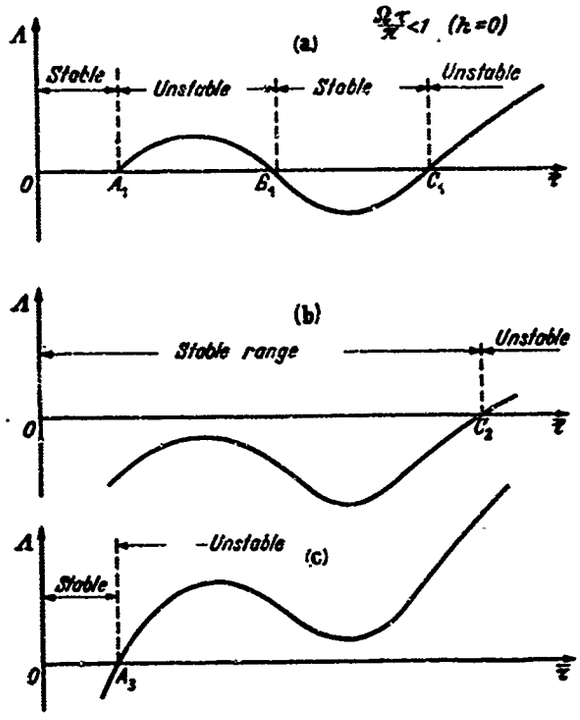

Figure 69. Qualitative diagram of the amplification coefficient Λ as a function of the sensitive time lag $\bar{\tau}$ of a liquid propellant rocket with constant pressure feed

sufficient to produce a constant rate of supply to the capacitance as in an earlier section. With $J = \infty$ the hyperbola of *Figure 67* degenerates into two straight lines and we see immediately that while the smaller root ω for $n \leqslant \frac{1}{2}$ goes to zero with the corresponding δ approaching ∞, there are only two significant real roots or none; and for $n > \frac{1}{2}$ one and only one root is always present.

Similarly the case $E = 0$ of the constant pressure system is identical with the case $E = \infty$ of the constant rate system, discussed at the end of Appendix C, and it is immediately checked that no matter what the value of n, there is only one real root of ω. It is clear that the constant pressure case with $J = \infty$ is represented for various E by the upper parts of *Figures 11, 12* and *13*, and with $E = 0$ for various J by the lower parts of these figures.

Finally we observe that the inequality (2.04.08) holds also for the constant pressure case, and again the sufficient criterion of unconditional stability $\Delta\bar{p}/\bar{p} = \frac{1}{2} \cdot 1/(1 - 2n)$ holds for $n < \frac{1}{2}$. We observe also that when $n > \frac{1}{2}$ we may obtain the best conditions of stability by making Φ positive and of such magnitude that the representative point on the loop $P =$ constant of *Figure 10* lies near the point of maximum δ. In this range the effect of increasing $\Delta\bar{p}$ is reversed, like the constant rate system as analysed in Appendix C.

REFERENCES

[1] 'On Sound Generated Aerodynamically' by M. J. LIGHTHILL, *Proc. Roy. Soc. A* 211 (1952) 564.

[2] 'Combustion Instability in Liquid Propellant Rocket Motors—A Survey' by C. C. Ross and P. P. DATNER, AGARD, NATO, Dec. 1953.

[3] 'The Ignition of Gas Mixtures by Impulsive Pressures' by W. C. F. SHEPHERD, *Third Symposium on Combustion*, p301, Williams & Wilkins Co., Baltimore, 1949.

[4] 'Some Experiments on the Initiation of Detonation in $2H_2$-O_2 Mixtures by Uniform Shock Waves' by J. A. FAYS, *Fourth Symposium on Combustion*, p501, Williams & Wilkins Co, Baltimore, 1953.

[5] 'Stability of Flow in a Rocket Motor' by D. F. GUNDER and D. R. FRIANT, *J. appl. Mech.* 17 (1950) 327.

[6] Discussion of Reference 1 by M. YACHTER and WALDINGER, *ibid* 18 (1951) 114.

[7] 'A Theory of Unstable Combustion in Liquid Propellant Rocket Motors' by M. SUMMERFIELD, *J. Amer. Rocket Soc.* 21 (1951) 108.

[8] 'Aspects of Combustion Instability in Liquid Propellant Rocket Motors' by L. CROCCO, Part I: *ibid* 21 (1951) 163; Part II: 22 (1952) 7.

[9] 'Servo-stabilization of Combustion in Rocket Motors' by H. S. TSIEN, *ibid* 22 (1952) 256.

[10] 'Servo-stabilization of Low Frequency Oscillations in a Liquid Bipropellant Rocket Motor' by F. E. MARBLE and D. W. COX, Jr, *ibid* 23 (1953) 63.

[10a] *Theory of Sound* by Lord RAYLEIGH, Vol. II, p227.

[11] 'High Frequency Combustion Instability in Rockets with Concentrated Combustion' by L. CROCCO and SIN-I CHENG, presented at *Eighth int. Congr. appl. Mech., Istanbul*, Aug. 1952. Published also in *J. Amer. Rocket Soc.* 23 (1953) 301.

[12] 'High Frequency Combustion Instability in Rockets with Distributed Combustion', *Fourth Symposium on Combustion*, p865, Williams & Wilkins Co., Baltimore, 1953.

[13] 'Versuche mit einer elektrischen Pfeife' by H. PFLAUM, *Dissertation*, Universität Rostock, 1909.

[14] 'Flow Stability in Small Orifices' by R. P. NORTHUP, *J. Amer. Rocket Soc.* (1951) Reprint No. 49–51.

[15] 'Fluctuations in a Spray Formed by Two Impinging Jets' by M. F. HEIDMANN and J. C. HUMPHREY, *ibid* 22 (1952) 127.

[16] 'Effect of Wave Propagation in Feed Lines on Low Frequency Rocket Instability' by R. H. SABERSKY, *Jet Propulsion* 24 (1954) 172.

[16a] 'Rocket Motor Instability Studies' by K. BERMAN and S. H. CHENEY, Jr, *ibid* 25 (1955) 513.

[17] 'Preliminary Measurements of the Combustion Time Lag in a Monopropellant Rocket Motor' by L. CROCCO, J. GREY and G. B. MATTHEWS, *Fifth International Symposium on Combustion*, p164. Reinhold Publishing Co., New York, 1955.

[18] 'Burning Velocity Measurements in a Spherical Vessel with Central Ignition' by J. MANTON, G. VON ELBE and B. LEWIS *Fourth Symposium on Combustion*, p358, Williams & Wilkins Co., Baltimore, 1953.

[19] 'Combustion in Vitiated Atmospheres, II: Effect of Oxygen Concentration on Induction Period' by B. P. MULLINS, *Fuel, Lond.* 28 (1949) 205.

[20] 'Low Frequency Combustion Stability of Liquid Propellant Rocket Motor with Different Nozzles' by SIN-I CHENG, *Jet Propulsion* 25 (1955) 163.

[21] 'Aerodynamic Stability and Automatic Control' by W. BOLLAY, *J. aero Sci.* 18 (1951).

[22] 'Unconditional Stability of Low Frequency Oscillations in Liquid Propellant Rockets' by SIN-I CHENG, *Jet Propulsion* 24 (1954) 310.

[23] 'High Frequency Combustion Instability in Liquid Propellant Rockets with Concentrated Combustion and Distributed Time Lag' by SIN-I CHENG. *Rep. Princeton Univ. Dept. aero. Engng No. 246* (1953).

[24] 'The transfer Functions of Rocket Nozzles' by H. S. TSIEN, *J. Amer. Rocket Soc.* 22 (1952) 139, 162.

[25] 'Supercritical Gaseous Discharge with High Frequency Oscillations' by L. CROCCO, *Aerotecnica, Roma* 33 (1953) 46. [English text.]

[26] 'Combustion Studies in Rocket Motors' by K. BERMAN and S. H. CHENEY, Jr, *J. Amer. Rocket Soc.* 23 (1953) 89.

[27] 'Experimental Investigation of Combustion Instability in Rocket Motors' by H. ELLIS, I. ODGERS, A. J. STOSICH, N. VANDE VERG and R. S. WICK, *Fourth Symposium on Combustion*, p860, Williams & Wilkins Co., Baltimore, 1953.

[28] 'Longitudinal Vibrations of Gas at Ambient Pressure in a Rocket Thrust Chamber' by I. ELIAS and R. GORDON, *J. Amer. Rocket Soc.* 22 (1952) 263.

[29] 'Self-excited Oscillations in Dynamical Systems Possessing Retarded Action' by N. MINORSKY, *J. appl. Mech.* 9 (1942) A65.

[30] 'Stability of Linear Oscillation Systems with Constant Time Lag' by H. I. ANSOFF, *ibid* 16 (1949) 158.

[31] 'Discussion on Reference 30' by M. SATCHE, *ibid* 16 (1949) 418.

[32] 'Rocket Applications of the Cavitating Venturi' by L. N. RANDALL, presented at the joint A.S.M.E. and A.R.S. midseason session, Toronto, Canada, July 1951.

[33] 'High Frequency Combustion Instability in Solid Propellant Rockets' by SIN-I CHENG, Part I: *ibid* 24 (1954) 27; Part II: 24 (1954) 102.

[34] 'Les Instabilités de Basse Fréquence dans un Moteur-fusée' by M. BARRERE and A. MOUTET, *Rech. aéro.* 44 (1955) 29.

[35] 'Combustion Instability in an Acid–Heptane Rocket with a Pressurized-gas Propellant Pumping System' by A. O. TISCHLER and D. R. BELLMAN, *Nat. adv. Comm. Aero. tech. Note No. 2936* (1953).

[36] 'The Hypergeometric and Legendre Functions with Applications to Integral Equations of Potential Theory' by C. SNOW, *Appl. Math. Ser. U.S. Bur. Stand. No. 19.*